CAPITAL UNIVERSITY OF SCIENCE AND TECHNOLOGY, ISLAMABAD

A Specific Study of Heat and Mass Transportation of Casson and Carreau Nanofluids

by

Areej Fatima

A dissertation submitted in partial fulfillment for the degree of Doctor of Philosophy

in the

Faculty of Computing
Department of Mathematics

2025

A Specific Study of Heat and Mass Transportation of Casson and Carreau Nanofluids

By
Areej Fatima
DMT193002

Dr. Fatma Ibrahim, Associate Professor
Technische universität Dortmund, Dortmund, Germany
(Foreign Evaluator 1)

Dr. Hakan Öztop, Professor
Firat University, Elazig, Türkiye
(Foreign Evaluator 2)

Dr. Muhammad Sagheer
(Research Supervisor)

Dr. Muhammad Sagheer
(Head, Department of Mathematics)

Dr. Muhammad Abdul Qadir
(Dean, Faculty of Computing)

DEPARTMENT OF MATHEMATICS
CAPITAL UNIVERSITY OF SCIENCE AND TECHNOLOGY
ISLAMABAD
2025

Dedicated to my cherished Parents, esteemed Teachers and Siblings, who have instilled in me the value of hard work in pursuit of my aspirations and beloved husband, whose unwavering support, patience, and encouragement have been my steadfast companions throughout this journey.

CAPITAL UNIVERSITY OF SCIENCE & TECHNOLOGY
ISLAMABAD
Expressway, Kahuta Road, Zone-V, Islamabad
Phone:+92-51-111-555-666 Fax: +92-51-4486705
Email: info@cust.edu.pk Website: https://www.cust.edu.pk

CERTIFICATE OF APPROVAL

This is to certify that the research work presented in the dissertation, entitled "**A Specific Study of Heat and Mass Transportation of Casson and Carreau Nanofluids**" was conducted under the supervision of **Dr. Muhammad Sagheer**. No part of this dissertation has been submitted anywhere else for any other degree. This dissertation is submitted to the **Department of Mathematics, Capital University of Science and Technology** in partial fulfillment of the requirements for the degree of Doctor in Philosophy in the field of **Mathematics.** The open defence of the dissertation was conducted on **April 04, 2025**.

Student Name : Areej Fatima (DMT193002)

The Examination Committee unanimously agrees to award PhD degree in the mentioned field.

Examination Committee :

(a)	External Examiner 1:	Dr. Rashid Mahmood Professor Namal University, Mianwali	
(b)	External Examiner 2:	Dr. Muhammad Kamran Professor CUI, Wah Cantt Campus	
(c)	Internal Examiner :	Dr. Rashid Ali Professor CUST, Islamabad	

Supervisor Name : Dr. Muhammad Sagheer
Professor
CUST, Islamabad

Name of HoD : Dr. Muhammad Sagheer
Professor
CUST, Islamabad

Name of Dean : Dr. Muhammad Abdul Qadir
Professor
CUST, Islamabad

AUTHOR'S DECLARATION

I, **Areej Fatima** (Registration No. **DMT193002**), hereby state that my dissertation titled, "**A Specific Study of Heat and Mass Transportation of Casson and Carreau Nanofluids**" is my own work and has not been submitted previously by me for taking any degree from Capital University of Science and Technology, Islamabad or anywhere else in the country/ world.

At any time, if my statement is found to be incorrect even after my graduation, the University has the right to withdraw my PhD Degree.

Areej Fatima

(**Areej Fatima**)

Registration No : DMT193002

Dated: 04 April, 2025

PLAGIARISM UNDERTAKING

I solemnly declare that research work presented in the dissertation titled "**A Specific Study of Heat and Mass Transportation of Casson and Carreau Nanofluids**" is solely my research work with no significant contribution from any other person. Small contribution/ help wherever taken has been duly acknowledged and that complete dissertation has been written by me.

I understand the zero-tolerance policy of the HEC and Capital University of Science and Technology towards plagiarism. Therefore, I as an author of the above titled dissertation declare that no portion of my dissertation has been plagiarized and any material used as reference is properly referred/ cited.

I undertake that if I am found guilty of any formal plagiarism in the above titled dissertation even after award of PhD Degree, the University reserves the right to withdraw/ revoke my PhD degree and that HEC and the University have the right to publish my name on the HEC/ University Website on which names of students are placed who submitted plagiarized dissertation.

(**Areej Fatima**)

Dated: 04 April, 2025

Registration No : DMT193002

List of Publications

It is certified that following publication has been made out of the research work that has been carried out for this dissertation:-

1. **A. Fatima**, M. Sagheer, and S. Hussain, "A study of inclined magnetically driven Casson nanofluid using the Cattaneo-Christov heat flux model with multiple slips towards a chemically reacting radially stretching sheet," *Journal of Central South University*, vol. 30, pp. 3721-3736, 2023.

Areej Fatima

Registration No: DMT193002

Acknowledgement

First and foremost, I would like to express my gratitude to Almighty Allah for bestowing upon me the gift of knowledge and facilitating my pursuit of PhD studies.

I am profoundly and sincerely grateful to my esteemed research supervisor and mentor, Dr. Muhammad Sagheer, for his unwavering support throughout this research. I wish to express my deepest appreciation for his invaluable suggestions that have significantly enhanced the quality of this dissertation. Under his guidance, I have gained not only technical knowledge but also valuable lessons on being a good human being. I also thank him for always making time for discussions on this thesis, despite his extremely busy schedule.

My heartfelt and sincere gratitude goes to my Parents, Siblings and in-laws, whose love and guidance support me in all my endeavors.

I want to express my heartfelt gratitude to my dear husband. His steadfast support and constant encouragement have been crucial throughout this journey.

I am deeply thankful to my teachers at Capital University of Science and Technology, Dr. Rashid Ali, Dr. Abdul Rehman Kashif, Dr. Samina Rashid, Dr. Muhammad Sabeel khan, Dr. Muhammad Afzal and Dr. Dur e Shehwar. Their exceptional teaching has greatly enriched my learning experience throughout my PhD studies.

I would also like to extend my gratitude to Capital University of Science and Technology for providing the scholarship during my PhD studies. Additionally, I acknowledge the senior management of Capital University of Science and Technology for their commitment to maintaining high educational standards.

I am thankful to my fellow researchers at Capital University of Science and

Technology for their insightful discussions on this research. Working alongside them in such a supportive and enjoyable environment has been a pleasure.

Areej Fatima

Abstract

This dissertation presents the numerical investigation of the transportation of thermal and mass exchange by incorporating Casson and Carreau nanofluids over a radially stretching sheet and bi-directional surface stretched in both the x and y directions. Heat conduction is modeled using the advanced Cattaneo-Christov heat flux model, while mass transport is described using a generalized mass flux model. The study considers the effects of magnetohydrodynamic 3D flow under a variable magnetic field across a stretching sheet. The boundary layer theory is applied to present the proposed flow model under specific assumptions. The remarkable characteristics of the various flows considered in the thesis are intended to be investigated in the light of heat generation/ absorption, Brownian motion, thermophoresis and thermal radiation. Additionally, the resulting ordinary differential equations, derived through appropriate similarity variables, are solved numerically using the shooting method. The shooting method is used to solved the BVPs. The convergence criterion is satisfied when the discrepancy between the computed solution and the prescribed boundary condition falls below 10^{12}. The accuracy of the computational code is validated through comparative analysis. The numerical results of every flow problem are illustrated through graphs and tables, highlighting the impact of key flow parameters on velocity, concentration, and temperature profiles. Furthermore, the Sherwood number, skin-friction coefficient, and Nusselt number reveal important physical characteristics of the proposed flow model. It has been noted that irrespective of the choice of geometry and nanofluid considered, the temperature profile upsurges significantly for the higher values of the Brownian motion parameter whereas an opposite trend has been sighted by taking into account the heat generation or absorption parameter. Furthermore, for the larger values of the thermal Grashof number, the magnitude of Sherwood number eascalates significantly.

Contents

List of Figures

List of Tables

Abbreviations

BVP	Boundary Value Problem
IVP	Initial Value Problem
MHD	Magnetohydrodynamics
ODE	Ordinary Differential Equation
PDE	Partial Differential Equation

Symbols

a	Constant
ρ	Fluid Density
A	Velocity Ratio Parameter
T_f	Convective Fluid Temperature
k	Thermal Conductivity
σ	Electrical Conductivity
Bi_1	Thermal Biot Number
T_∞	Ambient Temperature
Bi_2	Concentration Biot Number
U_e	Free Stream Velocity for u-component
V_e	Free Stream Velocity for v-component
C_f	Concentration at the Surface
U_w	Radial Stretching Velocity
C_∞	Ambient Concentration
k^*	Absorption Coefficient
c_p	Specific Heat
β	Casson Fluid Parameter
D_T	Thermophoresis Diffusion Coefficient
$\theta(\eta)$	Dimensionless Temperature
D_B	Brownian Diffusion Coefficient
$\phi(\eta)$	Dimensionless Concentration
Ec	Eckert Number
$f'(\eta)$	Dimensionless Velocity
$g'(\eta)$	Dimensionless Velocity

M	Magnetic Parameter
Nt	Thermophoresis Parameter
Pr	Prandtl Number
α_f	Thermal Diffusivity of Fluid
Nb	Brownian Motion Parameter
Rd	Thermal Radiation Parameter
η	Dimensionless Variable
$(\rho c_p)_p$	Effective Heat Capacity of the Nanoparticles
γ	Chemical Reaction Parameter
We	Weissenberg Number
k_f	Thermal Conductivity of Fluid
ρ_p	Nanoparticle Mass Density
h_h	Heat Transfer Coefficient
ρ_f	Fluid Density
Q_0	Rate of Heat Generation/Absorption
$(\rho c_p)_f$	Heat Capacity of the Fluid
q_r	Radiative Heat Flux
K'	concentration slip factor
S'	thermal slip factor
K	permeability parameter
Gr	thermal Grashof number
Gc	solutal Grashof number
ω	thermal slip/jump parameter
χ	mass slip parameter
α	angle of inclination of magnetic field
L	velocity slip length
S	suction/injection parameter
δ	velocity slip parameter
Γ	Deborah number
Sc	Schmidt number

Chapter 1

Introduction

Fluids are fundamental to life, and their significance in both natural and technological processes has driven extensive scientific exploration into the behavior of fluid flow. Fluid dynamics, the analysis of the behavior of fluid's motion and the factors influencing it, is key to understanding a broad spectrum of phenomena, from the evolution of stars and weather patterns to ocean currents and blood circulation. The field traces its origins back to Archimedes, an ancient Greek mathematician who first investigated the principles of fluid statics and buoyancy, formulating the renowned Archimedes' principle. Significant advancements in fluid dynamics began in earnest in the fifteenth century. Today, fluid dynamics plays a critical role in various engineering applications, including oil transport pipelines, rocket thrusters, air conditioning units, and windmills. Over the past few years, prompt research has been pulled off by disparate scholars on non-Newtonian fluids owing to its tremendous applications in the scientific and engineering fields. Major applications of non-Newtonian fluids comprise of chemical solutions, food production, medicines, paints, detergents and natural substances [1]. The mathematical modeling of such fluids involves intricate rheological variables with more than one fluid model which makes their study more complex as compared to other fluids. Casson fluid was introduced in 1995 as a type of non-Newtonian fluid. The structure version is characterized by the interrelation of the liquid and solid subject to the availability of stress. If the viscosity of the fluid is greater than stress, the fluid functions as a solid whereas, for higher stress and lesser viscosity, the fluid behaves like a liquid. Casson fluid is a fundamental part of a lot of edibles like fruit juices, jams, raw honey and tomato paste. Furthermore, it has a wide range of application spectrum in tumor treatment, blood circulation and refinement of crude oil [2–4]. Kumar et al. [5] studied the thermal effects of flow of Casson fluid past an exponentially curved sheet. The study demonstrated that the Casson parameter tends to repress the magnitude of momentum. The detailed investigation of heat and mass transfer of Casson fluids using different numerical methods was studied by Verma et al. [6] with a finding that the shooting method, Keller Box method and Runge–Kutta technique are more stable among the other numerical techniques used by the scholars. Moreover, myriad experts have played a vital role in contributing to the literature by incorporating Casson fluid [7–17]. In the class of non-Newtonian fluids, lies the power law Carreau fluid model. It has numerous applications in the chemical industry and is suitable for viscous flows subject to the availability of higher shear stress. Gayatri et al. [18] examined the slip flow under the influence of Joule heating by using Carreau fluid past a slendering stretching sheet. They concluded that the velocity configuration slows down for the higher velocity slip parameter. Furthermore, Salahuddin et al. [19] explored the variable fluid properties of Carreau fluid flow near the boundary layer region and revealed that the concentration distribution magnifies by increasing the activation energy. Since the Carreau fluid has countless uses in the engineering process, multitudinous scholars have shed light on its significant features [20–28].

The technological advancement of nanoparticles has gained considerable interest among various scientists due to their tremendous features. This happens because nanoparticles manifest astonishingly remarkable conductive and electrical properties. This is the reason why nanoparticles have a comprehensive range of applications in tomography, thermolysis, microchip technology, ecological and medical arena. The setting up of nanoparticles is primarily executed by employing carbides, oxides, metals and non-metals. Nanofluids are generally processed by diffusing nanoparticles in the base fluid. In comparison with standard thermal conductive fluids, nanofluids exhibit a more rapid pace of heat transfer. Under their efficacious properties, nanofluids are comprehensively employed in auto production, refrigerating system, drug industry, atomic power plants and so much more. Ali et al. [29] investigated the flow characteristics of MHD Casson-Carreau nanofluid in the presence of activation energy and reached the conclusion that the temperature escalates by lifting the magnetic force. In addition to this, Shaw et al. [30] studied the MHD flow of non-linear microrotation of Casson-Carreau nanomaterials using Thomson and Trion slip conditions and figured out that the velocity profile diminishes for the higher Weissenberg number and Casson parameter. Due to the extraordinary behavior of nanofluids in heat transfer, countless scientists have shed light on the studies incorporating different nanofluids and brought forth fruitful outcomes [31–37].

The scrutinization of flows involving mass and heat exchange over a stretching sheet has a critical role to play in the arena of metallurgy and the chemical industry. In history the analysis of characteristics of heat transfer by Fourier [38] marks the initial instance. In like manner, modification in his research was done by Cattaneo [39]. Furthermore, Christov [40] amended the concepts of the later studies. Due to the colossal significance of the Cattaneo-Christov heat flux model in examining heat transfer, innumerable researchers have provided insight into the conclusions in this regard [41–49].

Scholars have focused extensively on exploring the boundary layer flows by using stretching sheets and incorporating Casson and Carreau fluid due to their wide ranging applications in the realm of science and technology. The flows past the shrinking/expanding sheets have a comprehensive application spectrum in the production of plastic, solar energy generation, glass fabrication, and polymer chemical engineering facilities [50]. Crane's initial study focused on the flow problem involving a stretching sheet [51]. Furthermore, the heat analysis of MHD Carreau fluid flow past a radially stretching sheet was studied by Qayyum et al. [52] and concluded that the velocity escalates for the higher Weissenberg number past the stretching sheet. Moreover, Sobamowo explored the flow characteristics of Casson-Carreau nanofluid over a stretching sheet by using the effects of MHD and internal heat [32]. In addition to this, owing to the remarkable and significant properties in the field of fluid dynamics, the study of stretching sheet flows has attracted numerous scholars contributing to the valuable insights [53–60].

Based on the previous findings related to both non-Newtonian and Newtonian fluids, the research has been carried out on MHD flow at stagnation points using the Casson and Carreau nanofluids by incorporating the effects of inclined magnetic field, thermal radiation, chemical reaction and heat generation absorption in the light of multiple slip boundary conditions. The heat transfer has been studied using the Cattaneo-Christov heat flux model. Moreover, the flow characteristics of Brownian motion, thermophoresis and viscous dissipation have been factored in. The PDEs were transformed into a set of ODEs using appropriate similarity transformations, and the numerical results obtained using the shooting method have been presented using the tables and graphs. For this purpose, The MATLAB version $R2017a$ has been utilized. For the flow problem discussed in Chapter 3, the MATLAB code was prepared from scratch. However, for the rest of the problems discussed in the later chapters, the initial code was modified.

Layout of Dissertation:

A brief overview of the dissertation contents is given below.

Chapter 2 includes fundamental definitions and terminology, which will assist in comprehending the concepts covered later.

Chapter 3 presents the proposed MHD inclined magnetic field stagnation point flow using the Casson nanofluid over the stretching sheet. The computed outcomes of the governing flow equations are obtained using the shooting technique.

Chapter 4 expands the suggested flow examined in Chapter 3 by employing the Carreau nanofluid in place of the Casson fluid.

Chapter 5 extends the proposed flow discussed in Chapter 3 and Chapter 4 by utilizing the Casson-Carreau nanofluid.

Chapter 6 modifies the proposed flow discussed in the previous chapters by studying the three dimensional flow of Casson-Carreau nanofluid.

Chapter 7 delivers the closing comments of the dissertation.

The references cited in the dissertation are listed in the **Bibliography**.

Chapter 2

Basic Definitions and Governing Equations

The forthcoming chapter will introduce essential definitions, fundamental laws, and terminologies that will be referenced in subsequent chapters.

2.1 Important Definitions

Definition 2.1 (Fluid)**.** [61]
"A substance exists in three primary phases: solid, liquid, and gas. (At very high temperatures, it also exists as plasma.) A substance in the liquid or gas phase is referred to as a fluid. Distinction between a solid and a fluid is made on the basis of the substance's ability to resist an applied shear (or tangential) stress that tends to change its shape. A solid can resist an applied shear stress by deforming, whereas a fluid deforms continuously under the influence of shear stress, no matter how small. In solids stress is proportional to strain, but in fluids stress is proportional to strain rate. When a constant shear force is applied, a solid eventually stops deforming, at some fixed strain angle, whereas a fluid never stops deforming and approaches a certain rate of strain."

Definition 2.2 (Nanofluid). [62]

"A nanofluid is a fluid containing nanometer-sized particles, called nanoparticles. These fluids are engineered colloidal suspensions of nanoparticles in a base fluid. The nanoparticles used in nanofluids are typically made of metals, oxides, carbides, or carbon nanotubes. Common base fluids include water, ethylene glycol and oil."

Definition 2.3 (Fluid Mechanics). [61]

"Fluid mechanics is defined as the science that deals with the behavior of fluids at rest (fluid statics) or in motion (fluid dynamics) and the interaction of fluids with solid or other fluids at the boundaries."

Definition 2.4 (Fluid dynamics). [61]

"It is the study of the motion of liquids, gases and plasmas from one place to another. Fluid dynamics has a wide range of applications like calculating force and moments on aircraft, mass flow rate of petroleum passing through pipelines, prediction of weather, etc."

Definition 2.5 (Hydrodynamics). [62]

"The study of the motion of fluids that are practically incompressible such as liquids, especially water and gases at low speeds is usually referred to as hydrodynamics."

Definition 2.6 (Magnetohydrodynamics). [62]

"Magnetohydrodynamics (MHD) is concerned with the flow of electrically conducting fluids in the presence of magnetic fields, either externally applied or generated within the fluid by inductive action."

Definition 2.7 (No-Slip Condition and Boundary Layer). [61]

"Consider the flow of a fluid in a stationary pipe or over a solid surface that is nonporous (i.e., impermeable to the fluid). All experimental observations indicate that a fluid in motion comes to a complete stop at the surface and assumes a zero velocity relative to the surface. That is, a fluid in direct contact with a solid "sticks" to the surface, and there is no slip. This is known as the no-slip condition. The fluid property responsible for the no-slip condition and the development of the boundary layer is viscosity. The no-slip condition is responsible for the development of the velocity profile. The flow region adjacent to the wall in which the viscous effects (and thus the velocity gradients) are significant is called the boundary layer. Another consequence of the no-slip condition is the surface drag, or skin friction drag, which is the force a fluid exerts on a surface in the flow direction."

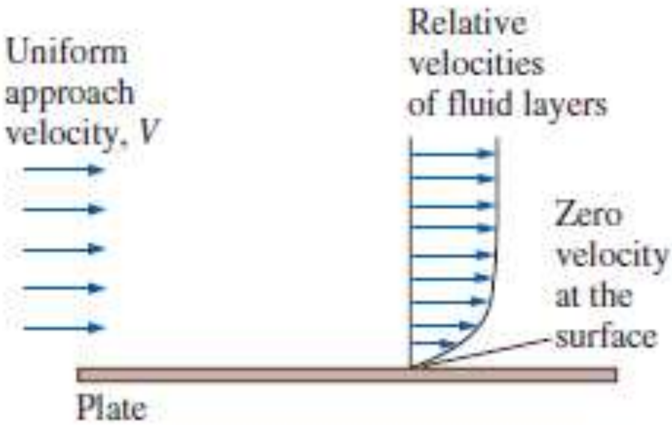

FIGURE 2.1: A fluid flowing over a stationary surface comes to a complete stop at the surface because of the no-slip condition.

2.2 Types of Flow

Definition 2.8 (Compressible and Incompressible Flows)**.** [61]
"A flow is classified as being compressible or incompressible, depending on the level of variation of density during flow. Incompressibility is an approximation, and a flow is said to be incompressible if the density remains nearly constant throughout. Therefore, the volume of every portion of fluid remains unchanged over the course of its motion when the flow (or the fluid) is incompressible. The densities of liquids are essentially constant, and thus the flow of liquids is typically incompressible. Therefore, liquids are usually referred to as incompressible substances. A pressure of 210 atm, for example, causes the density of liquid water at 1 atm to change by just 1%. Gases, on the other hand, are highly compressible. A pressure change of

just 0.01 atm, for example, causes a change of 1% in the density of atmospheric air."

Definition 2.9 (Laminar and Turbulent Flow)**.** [61]
"Some flows are smooth and orderly while others are rather chaotic. The highly ordered fluid motion characterized by smooth layers of fluid is called laminar. The word laminar comes from the movement of adjacent fluid particles together in laminates. The flow of high-viscosity fluids such as oils at low velocities is typically laminar. The highly disordered fluid motion that typically occurs at high velocities and is characterized by velocity fluctuations is called turbulent. The flow of low-viscosity fluids such as air at high velocities is typically turbulent. The flow regime greatly influences the required power for pumping. A flow that alternates between being laminar and turbulent is called transitional."

Definition 2.10 (Viscous and Inviscid Flows)**.** [61]
"There is no fluid with zero viscosity, and thus all fluid flows involve viscous effects to some degree. Flows in which the frictional effects are significant are called viscous flows. However, in many flows of practical interest, there are regions (typically regions not close to solid surfaces) where viscous forces are negligibly small compared to inertial or pressure forces. Neglecting the viscous terms in such inviscid flow regions greatly simplifies the analysis without much loss in accuracy."

Definition 2.11 (Steady and Unsteady Flow)**.** [61]
"The terms steady and uniform are used frequently in engineering, and thus it is important to have a clear understanding of their meanings. The term steady implies no change at a point with time. The opposite of steady is unsteady. The term uniform implies no change with location over a specified region. The terms unsteady and transient are often used interchangeably, but these terms are not synonyms. In fluid mechanics, unsteady is the most general term that applies to any flow that is not steady, but transient is typically used for developing flows."

Definition 2.12 (One-, Two-, and Three-Dimensional Flows)**.** [61]
"A flow field is best characterized by its velocity distribution, and thus a flow is said to be one-, two-, or three-dimensional if the flow velocity varies in one, two, or three

primary dimensions, respectively. A typical fluid flow involves a three-dimensional geometry, and the velocity may vary in all three dimensions, rendering the flow three-dimensional [$V(x, y, z)$ in rectangular or $V(r, \theta, z)$ in cylindrical coordinates]."

2.3 Fluid Properties

Definition 2.13 (Density)**.** [61]

"Density is defined as mass per unit volume, that is,

$$\rho = \frac{m}{v} \ \left(kg/m^3\right).'' \tag{2.1}$$

Definition 2.14 (Energy)**.** [61]

"Energy can exist in numerous forms such as thermal, mechanical, kinetic, potential, electrical, magnetic, chemical, and nuclear and their sum constitutes the total energy E of a system. The forms of energy related to the molecular structure of a system and the degree of the molecular activity are referred to as the microscopic energy. The sum of all microscopic forms of energy is called the internal energy of a system, and is denoted by U. The macroscopic energy of a system is related to motion and the influence of some external effects such as gravity, magnetism, electricity, and surface tension. The energy that a system possesses as a result of its motion is called kinetic energy. The energy that a system possesses as a result of its elevation in a gravitational field is called potential energy."

Definition 2.15 (Stress, Normal Stress, Shear Stress, Pressure)**.** [61]

"Stress is defined as force per unit area and is determined by dividing the force by the area upon which it acts. The normal component of a force acting on a surface per unit area is called the normal stress, and the tangential component of a force acting on a surface per unit area is called shear stress. In a fluid at rest, the normal stress is called pressure. A fluid at rest is at a state of zero shear stress. When the walls are removed or a liquid container is tilted, a shear develops as the liquid moves to re-establish a horizontal free surface."

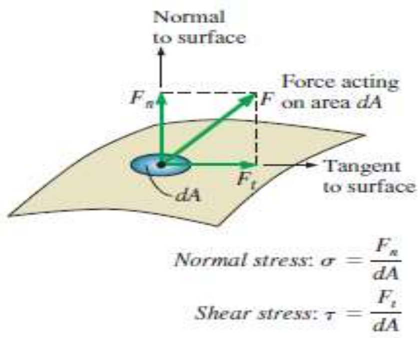

FIGURE 2.2: The normal stress and shear stress at the surface of a fluid element [61].

Definition 2.16 (Viscosity and Drag Force)**.** [61]
"The property that represents the internal resistance of a fluid to motion or the "fluidity," is the viscosity. The force a flowing fluid exerts on a body in the flow direction is called the drag force, and the magnitude of this force depends, in part, on viscosity. The fluid in contact with the upper plate sticks to the plate surface and moves with it at the same speed, and the shear stress τ acting on this fluid layer is:

$$\tau = \frac{F}{A} \ \left(N/m^2\right) . \text{''} \tag{2.2}$$

Definition 2.17 (Newtonian and Non-Newtonian Fluids)**.** [61]
"Fluids for which the rate of deformation is linearly proportional to the shear stress are called Newtonian fluids after Sir Isaac Newton, who expressed it first in 1687. Most common fluids such as water, air, gasoline, and oils are Newtonian fluids. Blood and liquid plastics are examples of non-Newtonian fluids. In the one-dimensional shear flow of Newtonian fluids, shear stress can be expressed by the linear relationship. Fluids for which the rate of deformation is linearly proportional to the shear stress are called Newtonian fluids after Sir Isaac Newton, who expressed it first in 1687. Most common fluids such as water, air, gasoline, and oils are Newtonian fluids. Blood and liquid plastics are examples of non-Newtonian fluids. In one-dimensional shear flow of Newtonian fluids, shear stress can be expressed by the linear relationship.

$$\tau = \mu \frac{du}{dy} \ \left(N/m^2\right), \tag{2.3}$$

where the constant of proportionality μ is called the coefficient of viscosity or the dynamic (or absolute) viscosity of the fluid."

2.4 Conservation Laws [61]

2.4.1 Conservation of Mass

"The conservation of mass relation for a closed system undergoing a change is expressed as $m_{sys} =$ constant or $dm_{sys}/dt = 0$, which is a statement of the obvious that the mass of the system remains constant during a process. For a control volume (CV), mass balance is expressed in the rate form as

$$m_{in} - m_{out} = \frac{dm_{CV}}{dt},$$

where m_{in} and m_{out} are the total rates of mass flow into and out of the control volume, respectively, and dm_{CV}/dt is the rate of change of mass within the control volume boundaries. In fluid mechanics, the conservation of mass relation written for a differential control volume is usually called the continuity equation."

2.4.2 Conservation of Momentum

"The product of the mass and the velocity of a body is called the linear momentum or just the momentum of the body, and the momentum of a rigid body of mass m moving with a velocity $\overrightarrow{V}$ is $m\overrightarrow{V}$. Newton's second law states that the acceleration of a body is proportional to the net force acting on it and is inversely proportional to its mass, and that the rate of change of the momentum of a body is equal to the net force acting on the body. Therefore, the momentum of a system remains constant when the net force acting on it is zero, and thus the momentum of such systems is conserved. This is known as the conservation of momentum principle."

2.4.3 Conservation of Energy

"Energy can be transferred to or from a closed system by heat or work, and the conservation of energy principle requires that the net energy transfer to or from a system during a process be equal to the change in energy content of the system. Control volumes involve energy transfer via mass flow also, and the conservation of energy principle, also called the energy balance, is expressed as

$$E_{in} - E_{out} = \frac{dE_{cv}}{dt},$$

where E_{in} and E_{out} are the total rates of energy transfer into and out of the control volume, respectively, and dE_{CV}/dt is the rate of change of energy within the control volume boundaries."

2.5 Dimensional Analysis [61]

Dimensional analysis serves as an essential method for researchers, enabling the transformation of dimensional and non-dimensional quantities, along with physical constants, into non-dimensional groups that simplify a problem by minimizing the number of independent variables involved.

2.5.1 Dimensions and Units

"A dimension is the measure of a physical quantity (without numerical values), while a unit is a way to assign a number to that dimension. For example, length is a dimension that is measured in units such as microns (μm), feet (ft), centimeters (cm), meters (m), kilometers (km), etc. Further, force has the same dimensions as mass times acceleration (by Newtons's second law). Thus, in terms of primary dimensions, dimensions of force:

2.5.2 Dimensional Homogeneity

"The law of dimensional homogeneity, stated as

Every additive term in an equation must have the same dimensions.

Consider, for example, the change in total energy of a simple compressible closed system from one state and/or time(1) to another (2). The change in total energy of the system E is given by

$$\Delta E = \Delta U + \Delta KE + \Delta PE, \tag{2.4}$$

where E has three components: internal energy (U), kinetic energy (KE), and potential energy (PE). These components can be written in terms of the system mass (m); measurable quantities and thermodynamic properties at each of the two states, such as speed (V), elevation (z), specific internal energy (u) and the known gravitational acceleration constant (g).

$$\begin{aligned}
\Delta U &= m(u_2 - u_1), \\
\Delta KE &= \frac{1}{2} m(V_2^2 - V_1^2), \\
\Delta PE &= mg(Z_2 - Z_1).
\end{aligned}$$

It is straightforward to verify that the left side of Eq. (2.4) and all three additive terms on the right side of above equations have the same dimensions—energy. Using the definitions of above equations, we write the primary dimensions of each term,

$$\{\Delta E\} = \{Energy\} = \{Force.Length\} \rightarrow \{\Delta E\} = \left[\frac{mL^2}{t^2}\right],$$
$$\{\Delta U\} = \{Mass\frac{Energy}{Mass}\} = \{Energy\} \rightarrow \{\Delta U\} = \left[\frac{mL^2}{t^2}\right],$$
$$\{\Delta KE\} = \{Mass\frac{Length^2}{time^2}\} \rightarrow \{\Delta KE\} = \left[\frac{mL^2}{t^2}\right],$$
$$\{\Delta PE\} = \{Mass\frac{Length^2}{time}Length\} \rightarrow \{\Delta PE\} = \left[\frac{mL^2}{t^2}\right].$$

In addition to dimensional homogeneity, calculations are valid only when the units are also homogeneous in each additive term."

2.5.3 Non-Dimensionalization of Equations

The principle of dimensional consistency requires that all terms combined through addition possess identical dimensional units.

2.6 Dimensionless Parameters

Definition 2.18 (Skin-Friction Coefficient)**.** [63]
"It is a dimensionless number and is defined as

$$C_f = \frac{\tau_w}{2Qw_\infty{}^2},$$

where τ_w is the local wall shear stress, ρ is the fluid density and U_e is the free stream velocity (usually taken outside of the boundary layer or at the inlet). It expresses the dynamic friction resistance originating in viscous fluid flow around a fixed wall."

Definition 2.19 (Nusselt Number)**.** [63]
"It is a dimensionless number, first introduced by a German engineer Ernst Kraft Wilhelm Nusselt and is defined as

$$Nu = \frac{\alpha L}{k},$$

where where α represents the heat transfer coefficient, L denotes the characteristic length and k is the thermal conductivity. It expresses the ratio of the total heat transfer in a system to the heat transfer by conduction. In characterizes the heat transfer by convection between a fluid and the environment close to it or, alternatively, the connection between the heat transfer intensity and the temperature field in a flow boundary layer. It expresses the dimensionless thermal transference. The physical significance is based on the idea of a fluid boundary layer in which the heat is transferred by conduction."

Definition 2.20 (Sherwood Number)**.** [63]
"The Sherwood number was first introduced by an American chemical engineer, Thomas Kilgore Sherwood and is defined as

$$Sh = \frac{BL}{D},$$

where B is the mass transfer coefficient, L denotes the characteristic length and D stands for molecular diffusivity.It expresses the ratio of the heat transfer to the molecular diffusion. It characterizes the mass transfer intensity at the interface of phases."

Definition 2.21 (Eckert Number)**.** [63]
"The Eckert number (Ec) is a dimensionless number used in the continuum mechanics. It expresses the relationship between a flow's kinetic energy and enthalpy, and is used to characterize the dissipation. It is defined as

$$Ec = \frac{u^2}{C_p \Delta T},$$

where u (ms^{-1}) fluid flow velocity far from body, C_p is the constant pressure local specific heat of continuum, ΔT is temperature difference.

It expresses the ratio of kinetic energy to a thermal energy change."

Definition 2.22 (Prandtl Number)**.** [63]
"The Prandtl number which is a dimensionless number, named after the German physicist Ludwig Prandtl, is defined as

$$Pr = \frac{\nu}{\alpha},$$

where ν stands for the kinematic viscosity and α denotes the thermal diffusivity. This number expresses the ratio of the momentum diffusivity (viscosity) to the thermal diffusivity. It characterizes the physical properties of a fluid with convective and diffusive heat transfers. It describes, for example, the phenomena connected with the energy transfer in a boundary layer. It expresses the degree of similarity between velocity and diffusive thermal fields or, alternatively, between hydrodynamic and thermal boundary layers."

Definition 2.23 (Schmidt Number)**.** [63]
"The Schmidt number is defined as

$$Sc = \frac{\mu}{\rho D_m} = \frac{\nu}{D_m},$$

where ν is the kinematic viscosity, D_m is mass diffusivity, μ is the dynamic viscosity of the fluid and ρ is the density of the fluid.

This number expresses the ratio of the kinematic viscosity, or momentum transfer by internal friction, to the molecular diffusivity. It characterizes the relation between the material and momentum transfers in mass transfer. It provides the similarity of velocity and concentration fields in mass transfer. For example, molten materials with an equal Schmidt number have similar velocity and concentration fields. Higher Sc number values characterize slower mass exchange and higher values of dividing coefficients. This leads to higher mixing and a tendency to crack in a solidified casting. The criterion was first introduced by Schmidt in 1929."

Definition 2.24 (Weissenberg Number)**.** [63]
"The dimensionless Weissenberg number, formulated by German physicist Karl Weissenberg, is defined as

$$We = \frac{\rho u^2}{\tau},$$

where ρ is the fluid density, u denotes the flow velocity and τ stands for the shear stress. This number expresses the characteristic material time (relaxation time) and the shear velocity. It characterizes the velocity and time relations in rheological processes in viscoelastic shear flow. Furthermore, it also expresses the ratio of the dynamic viscoelastic force to the viscous force."

Definition 2.25 (Biot Number)**.** [63]
"The Biot number is defined as

$$Bi = \frac{h_h L}{k},$$

where h_h represents the heat transfer coefficient, L denotes the characteristic length and k is the thermal conductivity. This number expresses the ratio of the heat flow transferred by convection on a body surface to the heat flow transferred by conduction in a body. The criterion was first introduced by French physicist, Jean-Baptiste Biot."

Definition 2.26 (Radiation Parameter)**.** [63]
"The dimensionless Radiation parameter is defined as

$$Rd = \frac{\epsilon \sigma^* T^3 L_h}{\lambda},$$

where ϵ is the emissivity of inner channel wall, σ^* represents the Stefan Boltzmann constant, L_h stands for the hydraulic diameter, T_f denotes the temperature of the fluid and k is the thermal conductivity. This parameter expresses the ratio of the heat transferred by radiation in a passageway to that transferred by conduction in a channel wall. It characterizes the relation between the radiation and conduction heat transfers in passageways. Alternatively, it expresses the influence of the radiation on the convective transfer."

Definition 2.27 (Grashof Heat Number)**.** [63]
"The dimensionless Grashof heat number is defined as

$$Gr = \frac{L^3 g \Delta T}{\nu^2 T},$$

where L is the characteristic length dimension, g is the gravitational acceleration, ΔT is the temperature change, ν is the kinematic viscosity. It expresses the buoyancy-to-viscous forces ratio and its action on a fluid. It characterizes the free non-isothermal convection of the fluid due to the density difference caused by the temperature gradient in the fluid."

Definition 2.28 (Hartmann Number)**.** [63]
"The dimensionless Hartmann number is defined as

$$Ha = \mu H L \sqrt{\frac{\gamma}{\eta}},$$

where μ is the permeability, H is the magnetic field intensity , L is the characteristic length, γ is the specific electrical conductance and η is the dynamic viscosity. It is an important criterion of magneto-hydrodynamics. It expresses the ratio of the induced electrodynamic (magnetic) force to the hydrodynamic force of the viscosity or, alternatively, the ratio of the ponderomotive force (the electromagnetic volume force by means of which the magnetic field acts on a conductor through which electric current flows, which causes magnetic pressure) to the molecular friction force. It characterizes the magnetic field influence on the flow of viscous, electrically conducting fluid. With small Ha values, the motion proceeds as if no magnetic field were acting. With great Ha values, the viscosity forces act only on a thin layer of the electrically conducting fluid (ionized gas) which adheres closely to a by-passed wall surface.”

Chapter 3

Inclined Magnetically driven Casson Nanofluid using the Cattaneo-Christov Heat Flux Model

3.1 Introduction

A numerical investigation is carried out by taking into consideration a two-dimensional inclined magnetically driven Casson nanofluid near a stagnation point flowing past a chemically reacting radially stretching sheet to scrutinize the phenomena of conduction, heat radiation, thermal emission and absorption in the light of multiple slips. For the purpose of investigating the characteristics of heat transfer conscientiously, the frequently cited Cattaneo-Christov heat flux model has been factored in. The mathematical formulation of the current flow problem has been described by employing the Buongiorno nanofluid model to explore the impact of Brownian motion, thermophoresis and thermal and mass slip conditions. A set of some appropriate similarity transformations has been incorporated for converting highly non-linear PDEs characterizing the designed flow model to a system of ODEs.

The computational handling of the proposed flow equations utilizes the shooting method. Tables and graphs are employed to analyze how pertinent flow parameters affect velocity, concentration, and temperature configurations. The pivotal aspect of this research validates that the derived numerical outcomes demonstrate strong concordance with those from existing literature.

3.2 Mathematical Modeling

The present study is centered on exploring the steady, incompressible, laminar flow of a Casson nanofluid around a radially stretching sheet in close proximity to a stagnation location. The flow and heat transfer characteristics are investigated under the thermal radiation and heat generation/absorption conditions. The coordinate system is established such that the $r-$ axis aligns with the flow direction, and the $z-$ axis is oriented perpendicular to the flow.

The velocity of the external flow is designated as U_e. Additionally, the uniform magnetic field's direction is oriented such that it is perpendicular to the surface of the fluid flow. The influences of Brownian motion and thermophoresis have been explained thoroughly. Furthermore, the analysis of the convective surface conditions has been included in the study.

The following equations represent the constitutive model of the Casson nanofluid [64, 65]:

$$\frac{\partial u}{\partial r}+\frac{u}{r}+\frac{\partial w}{\partial z}=0, \tag{3.1}$$

$$u\frac{\partial u}{\partial r}+w\frac{\partial u}{\partial z}=\nu_f\left(1+\frac{1}{\beta}\right)\frac{\partial^2 u}{\partial z^2}+U_e\frac{dU_e}{dr}+g\beta_T(T-T_\infty)-\frac{\nu_f u}{k'}$$
$$-\frac{\sigma B_0^2(u-U_e)\sin^2\alpha}{\rho_f}+g\beta_c(C-C_\infty), \tag{3.2}$$

$$u\frac{\partial T}{\partial r}+w\frac{\partial T}{\partial z}+\lambda\Bigg[w^2\frac{\partial^2 T}{\partial z^2}+w\frac{\partial w}{\partial z}\frac{\partial T}{\partial z}+w\frac{\partial u}{\partial z}\frac{\partial T}{\partial r}+u\frac{\partial u}{\partial r}\frac{\partial T}{\partial r}+u^2\frac{\partial^2 T}{\partial r^2}+u\frac{\partial w}{\partial r}\frac{\partial T}{\partial z}$$
$$+2uw\frac{\partial^2 T}{\partial r\partial z}\Bigg]=\alpha_f\frac{\partial^2 T}{\partial z^2}+\tau\left[D_B\frac{\partial C}{\partial z}\frac{\partial T}{\partial z}+\frac{D_T}{T_\infty}\left(\frac{\partial T}{\partial z}\right)^2\right]+\frac{\sigma B_0^2\,(u-U_e)^2\sin^2\!\alpha}{(\rho c_p)_f}$$

$$+\frac{\nu_f}{c_p}\left(1+\frac{1}{\beta}\right)\left(\frac{\partial u}{\partial z}\right)^2+\frac{Q_0\left(T-T_\infty\right)}{(\rho c_p)_f}-\frac{1}{(\rho c_p)_f}\frac{\partial q_r}{\partial z}, \tag{3.3}$$

$$u\frac{\partial C}{\partial r}+w\frac{\partial C}{\partial z}=D_B\frac{\partial^2 C}{\partial z^2}+\frac{D_T}{T_\infty}\frac{\partial^2 T}{\partial z^2}-C_r\left(C-C_\infty\right). \tag{3.4}$$

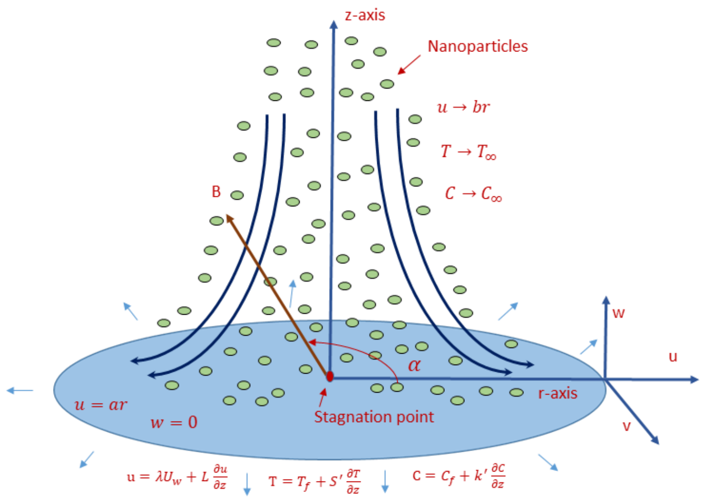

FIGURE 3.1: Schematic physical model

The subsequent explanation delineates the roles of the terms presented in the preceding equation:

- $\nu_f\left(1+\frac{1}{\beta}\right)\frac{\partial^2 u}{\partial z^2}$: Effect of Casson nanofluid.
- $U_e\frac{dU_e}{dr}$: Stretching sheet's velocity effect.
- $g\beta_T(T-T_\infty)$: Effect of thermal expansion coefficient.
- $\frac{\sigma B_0^2(u-U_e)\sin^2\alpha}{\rho_f}$: Effect exerted by inclined magnetic field.
- $g\beta_c(C-C_\infty)$: Influence of concentration expansion coefficient.
- $\alpha_f\frac{\partial^2 T}{\partial z^2}$: Impact of thermal diffusivity.
- $D_B\frac{\partial C}{\partial z}\frac{\partial T}{\partial z}$: Influence of Brownian motion.
- $\frac{D_T}{T_\infty}\frac{\partial T}{\partial z}$: Thermophoretic effect.

- $\frac{Q_0(T-T_\infty)}{(\rho c_p)_f}$: Impact of heat generation/ absorption.
- $\frac{1}{(\rho c_p)_f}\frac{\partial q_r}{\partial z}$: Influence of thermal radiation.
- $C_r\left(C-C_\infty\right)$: Chemical raction effect.

The radiative flux in the light of Rosseland approximation for radiation is as follows:

$$\frac{\partial q_r}{\partial z} = -\frac{16\sigma^* T_\infty^3}{3k^*}\frac{\partial^2 T}{\partial z^2}. \tag{3.5}$$

The boundary surface conditions are given by [66]:

$$\begin{aligned} &w = w_0, \quad u = \lambda U_w + L\frac{\partial u}{\partial z}, \quad T = T_f + S'\frac{\partial T}{\partial z}, \quad C = C_f + K'\frac{\partial C}{\partial z} \ \text{ when } z = 0, \\ &u \to U_e = br, \quad C \to C_\infty, \quad T \to T_\infty, \quad \text{as} \quad z \to \infty. \end{aligned} \tag{3.6}$$

The following similarity transformations are successfully used for the conversion of the governing PDEs to the corresponding ODEs [64, 65]:

$$\begin{aligned} &u = arf'\left(\eta\right), \ w = -2\sqrt{a\nu_f}f\left(\eta\right), \ \eta = \sqrt{\frac{a}{\nu_f}}z, \\ &\phi\left(\eta\right) = \frac{C-C_\infty}{C_f-C_\infty}, \ \theta\left(\eta\right) = \frac{T-T_\infty}{T_f-T_\infty}. \end{aligned} \tag{3.7}$$

After utilizing the above similarity transformations, the resulting ODEs are:

$$\left(1+\frac{1}{\beta}\right)f''' + 2ff'' - Kf' - f'^2 + Gr\theta + Gc\phi - M^2\left(f'-A\right)\sin^2\alpha + A^2 = 0, \tag{3.8}$$

$$\left(1+\frac{4}{3}Rd - 4\Gamma f^2\right)\theta'' + PrNb\theta'\phi' + PrNt\theta'^2 + 2Prf\theta' + \left(1+\frac{1}{\beta}\right)PrEcf''^2$$
$$+ PrQ\theta - 4\Gamma ff'\theta' + PrEcM^2\left(f'-A\right)^2\ \sin^2\alpha = 0, \tag{3.9}$$

$$\phi'' + Sc\left(2f\phi' - \gamma\phi\right) + \frac{Nt}{Nb}\theta'' = 0. \tag{3.10}$$

The corresponding boundary conditions get the following dimensionless form:

$$f(0)=S,\ f'(0)=\lambda+\delta f''(0),\ \theta(0)=1+\omega\theta'(0),\ \phi(0)=1+\chi\phi'(0),$$
$$f'\to A,\ \phi\to 0,\ \theta\to 0\ \text{ as }\ \eta\to\infty. \tag{3.11}$$

The dimensionless quantities used in the above equations are formulated as:

$$\begin{aligned}
&Nb=\frac{\tau D_B(C_f-C_\infty)}{\nu_f},\ Pr=\frac{\nu_f}{\alpha_f},\ Nt=\frac{\tau D_T(T_f-T_\infty)}{\nu_f T_\infty},\ M^2=\frac{\sigma B_0^2}{\rho_f a},\\
&Q=\frac{Q_0}{\rho_f c_p a},\ Rd=\frac{4T_\infty\sigma^*}{k^*(\alpha_f\rho_f c_p)},\ \ Ec=\frac{a^2r^2}{\alpha_f c_p(T_f-T_\infty)},\ A=\frac{b}{a},\ Sc=\frac{\nu_f}{D_B},\\
&Gr=\frac{g\beta_T(T_f-T_\infty)}{a^2r},\ \ Gc=\frac{g\beta_c(C_f-C_\infty)}{a^2r},\ S=-\frac{w_0}{\sqrt{a\nu_f}},\ \ \gamma=\frac{C_r}{a},\\
&\omega=\sqrt{\frac{a}{\nu_f}}S',\ \chi=\sqrt{\frac{a}{\nu_f}}K',\ \delta=\sqrt{\frac{a}{\nu_f}}L,\ K=\frac{\nu_f}{k'a},\ \Gamma=\lambda a.
\end{aligned}$$

The skin-friction coefficient, Sherwood number and Nusselt number in the original form are formulated as follows:

$$C_f=\frac{\tau_w}{\rho_f U_w^2},\ Nu=\frac{rq_w}{k_f(T_f-T_\infty)},\ Sh=\frac{rq_m}{D_B(C_f-C_\infty)}. \tag{3.12}$$

Given below are the formulae for τ_w, q_w and q_m.

$$\begin{aligned}
&\tau_w=\mu\left(1+\frac{1}{\beta}\right)\left(\frac{\partial u}{\partial z}\right)_{z=0},\quad q_w=-k_f\left[\left(\frac{\partial T}{\partial z}\right)-\frac{q_r}{k_f}\right]_{z=0},\\
&q_m=-D_B\left(\frac{\partial C}{\partial z}\right)_{z=0}.
\end{aligned} \tag{3.13}$$

The dimensionless form of the quantities of physical interest mention in (3.12), achieved through the similarity transformation, is as follows:

$$Re^{\frac{1}{2}}C_f=\left(1+\frac{1}{\beta}\right)f''(0),\ Re^{-\frac{1}{2}}Sh=-\phi'(0),\ Re^{-\frac{1}{2}}Nu=-\left(1+\frac{4}{3}Rd\right)\theta'(0), \tag{3.14}$$

where $Re=\dfrac{rU_w}{\nu_f}$ elucidates the local Reynolds number.

3.3 Solution Methodology

For solving the system of ODEs (3.8)-(3.11) numerically along with the boundary conditions, the shooting method has been incorporated. The non-existing initial conditions $f''(0)$, $\theta(0)$ and $\phi(0)$ have been represented by s, l and m, respectively. For the implementation of the shooting technique, the following notations have been introduced:

$$\begin{aligned}
&f = y_1, f' = y_2, f'' = y_3, \theta = y_4, \theta' = y_5, \phi = y_6, \phi' = y_7, \frac{\partial f}{\partial s} = y_8, \frac{\partial f'}{\partial s} = y_9,\\
&\frac{\partial f''}{\partial s} = y_{10}, \frac{\partial \theta}{\partial s} = y_{11}, \frac{\partial \theta'}{\partial s} = y_{12}, \frac{\partial \phi}{\partial s} = y_{13}, \frac{\partial \phi'}{\partial s} = y_{14}, \frac{\partial f}{\partial l} = y_{15}, \frac{\partial f'}{\partial l} = y_{16},\\
&\frac{\partial f''}{\partial l} = y_{17}, \frac{\partial \theta}{\partial l} = y_{18}, \frac{\partial \theta'}{\partial l} = y_{19}, \frac{\partial \phi}{\partial l} = y_{20}, \frac{\partial \phi'}{\partial l} = y_{21}, \frac{\partial f}{\partial m} = y_{22}, \frac{\partial f'}{\partial m} = y_{23},\\
&\frac{\partial f''}{\partial m} = y_{24}, \frac{\partial \theta}{\partial m} = y_{25}, \frac{\partial \theta'}{\partial m} = y_{26}, \frac{\partial \phi}{\partial m} = y_{27}, \frac{\partial \phi'}{\partial m} = y_{28}.
\end{aligned} \tag{3.15}$$

Using the above notations, equations (3.8)-(3.10) yield the following system of twenty eight ODEs:

$$\begin{aligned}
y_1' &= y_2, && y_1(0) = S,\\
y_2' &= y_3, && y_2(0) = \lambda + \delta s,\\
y_3' &= \frac{y_2^2 + Ky_2 + M^2 \sin^2\alpha\,(y_2 - A) - 2y_1y_3 - A^2 - Gry_4 - Gcy_6}{\left(1 + \frac{1}{\beta}\right)}, && y_3(0) = s,\\
y_4' &= y_5, && y_4(0) = 1 + \omega l,\\
y_5' &= \frac{-1}{\left(1 + \frac{4}{3}Rd - 4\gamma y_1^2\right)} + [PrNby_5y_7 + PrNty_5^2 + 2Pry_1y_5 + PrQy_4\\
&\quad + \left(1 + \frac{1}{\beta}\right) PrEcy_3^2 + PrEcM^2(y_2 - A)^2 \sin^2\alpha - 4\Gamma y_1y_2y_5\Big], && y_5(0) = l,\\
y_6' &= y_7, && y_6(0) = 1 + \chi m,\\
y_7' &= -\left(\frac{Nt}{Nb}\right) y_5' - Sc\,(2y_1y_7 - \gamma y_6)\,, && y_7(0) = m,\\
y_8' &= y_9, && y_8(0) = 0,\\
y_9' &= y_{10}, && y_9(0) = \delta,\\
y_{10}' &= \frac{\left(2y_2 + K + M^2 \sin^2\alpha\right) y_9 - 2(y_3y_8 + y_1y_{10}) - Gry_{11} - Gcy_{13}}{\left(1 + \frac{1}{\beta}\right)}, && y_{10}(0) = 1,
\end{aligned}$$

$$y_{11}' = y_{12} \qquad y_{11}(0) = 0,$$

$$\begin{aligned} y_{12}' = \frac{-1}{\left(1+\frac{4}{3}Rd - 4\Gamma y_1^2\right)^2}\Bigg[&\left(1+\tfrac{4}{3}Rd - 4\Gamma y_1^2\right)\Big(\big(PrNby_7 + 2PrNty_5 \\ &+ 2Pry_1 - 4\Gamma y_1 y_2\big)y_{12} + Pr\left(Nby_5y_{14} + Qy_{11} + 2\left(1+\tfrac{1}{\beta}\right)Ecy_3y_{10}\right) \\ &+ 2Pry_5y_8 + \big(2PrEcM^2(y_2 - A)sin^2\alpha - 4\Gamma y_1y_5\big)y_9 - 4\Gamma y_2y_5y_8\Big) \\ &+ 8\Big((\Gamma y_1 y_8)\big(PrNby_5y_7 + PrNty_5^2 + 2Pry_1y_5 + PrQy_4 \\ &+ \left(1+\tfrac{1}{\beta}\right)PrEcy_3^2 + PrEcM^2(y_2 - A)^2\sin^2\alpha - 4\Gamma y_1y_2y_5\big)\Big)\Bigg], \quad y_{12}(0) = 0, \end{aligned}$$

$$y_{13}' = y_{14}, \qquad y_{13}(0) = 0,$$

$$y_{14}' = -\left(\tfrac{Nt}{Nb}\right)y_{12}' - 2Sc\big(y_1y_{14} + y_7y_8\big) + Sc\gamma y_{13}, \qquad y_{14}(0) = 0,$$

$$y_{15}' = y_{16}, \qquad y_{15}(0) = 0,$$

$$y_{16}' = y_{17}, \qquad y_{16}(0) = 0,$$

$$y_{17}' = \frac{\left(2y_2 + K + M^2\sin^2\alpha\right)y_{16} - 2(y_3y_{15} + y_1y_{17}) - Gry_{17} - Gcy_{20}}{\left(1+\frac{1}{\beta}\right)}, \quad y_{17}(0) = 0,$$

$$y_{18}' = y_{19} \qquad y_{18}(0) = \omega,$$

$$\begin{aligned} y_{19}' = \frac{-1}{\left(1+\frac{4}{3}Rd - 4\Gamma y_1^2\right)^2}\Bigg[&\left(1+\tfrac{4}{3}Rd - 4\Gamma y_1^2\right)\Big(\big(PrNby_7 + 2PrNty_5 \\ &+ 2Pry_1 - 4\Gamma y_1 y_2\big)y_{19} + Pr\left(Nby_5y_{21} + Qy_{18} + 2\left(1+\tfrac{1}{\beta}\right)Ecy_3y_{17}\right) \\ &+ 2Pry_5y_{15} + \big(2PrEcM^2(y_2 - A)sin^2\alpha - 4\Gamma y_1y_5\big)y_{16} - 4\Gamma y_2y_5y_{15}\Big) \\ &+ 8\Big((\Gamma y_1 y_{15})\big(PrNby_5y_7 + PrNty_5^2 + 2Pry_1y_5 + PrQy_4 \\ &+ \left(1+\tfrac{1}{\beta}\right)PrEcy_3^2 + PrEcM^2(y_2 - A)^2\sin^2\alpha - 4\Gamma y_1y_2y_5\big)\Big)\Bigg], y_{19}(0) = 1, \end{aligned}$$

$$y_{20}' = y_{21}, \qquad y_{20}(0) = 0,$$

$$y_{21}' = -\left(\tfrac{Nt}{Nb}\right)y_{19}' - 2Sc\big(y_1y_{21} + y_7y_{15}\big) + Sc\gamma y_{20}, \qquad y_{21}(0) = 0,$$

$$y_{22}' = y_{23}, \qquad y_{22}(0) = 0,$$

$$]y_{23}' = y_{24}, \qquad y_{23}(0) = 0,$$

$$y_{24}' = \frac{\left(2y_2 + K + M^2\sin^2\alpha\right)y_{23} - 2(y_3y_{22} + y_1y_{24}) - Gry_{24} - Gcy_{27}}{\left(1+\frac{1}{\beta}\right)}, y_{24}(0) = 0,$$

$$y_{25}' = y_{26} \qquad y_{25}(0) = 0,$$

$$y_{26}' = \frac{-1}{\left(1+\frac{4}{3}Rd - 4\Gamma y_1^2\right)^2}\Bigg[\left(1+\tfrac{4}{3}Rd - 4\Gamma y_1^2\right)\Big(\big(PrNby_7 + 2PrNty_5$$

$$
\begin{aligned}
&+2Pry_1-4\Gamma y_1y_2\big)y_{26}+Pr\left(Nby_5y_{28}+Qy_{25}+2\left(1+\tfrac{1}{\beta}\right)Ecy_3y_{24}\right)\\
&+2Pry_5y_{22}+\big(2PrEcM^2(y_2-A)sin^2\alpha-4\Gamma y_1y_5\big)y_{23}-4\Gamma y_2y_5y_{22}\big)\\
&+8\big(\,(\Gamma y_1y_{22})\,\big(PrNby_5y_7+PrNty_5^2+2Pry_1y_5+PrQy_4\\
&+\left(1+\tfrac{1}{\beta}\right)PrEcy_3^2+PrEcM^2(y_2-A)^2\sin^2\alpha-4\Gamma y_1y_2y_5\big)\big)\Big],\quad y_{26}(0)=0,
\end{aligned}
$$

$$y'_{27}=y_{28}, \qquad y_{27}(0)=\chi,$$

$$y'_{28}=-\left(\tfrac{Nt}{Nb}\right)y'_{26}-2Sc\big(y_1y_{28}+y_7y_{22}\big)+Sc\gamma y_{27}, \qquad y_{28}(0)=1.$$

For the sake of solving the above initial value problem, the RK-4 method has been employed. In pursuance of the numerical results, the problem's domain is set as $[0,\eta_\infty]$, where η_∞ is selected to be a positive real number in a manner that for $\eta>\eta_\infty$, no significant variation in the solution is noticed. Moreover, the missing initial conditions are selected in order to ensure that

$$y_2\,(s,l,m)=A,\qquad y_4(s,l,m)=0,\qquad y_6(s,l,m)=0. \tag{3.16}$$

The Newton's iterative scheme has been employed for solving the above algebraic equations, in the following sense:

$$
\begin{bmatrix} s^{(k+1)}\\ l^{(k+1)}\\ m^{(k+1)}\end{bmatrix}=\begin{bmatrix} s^{(k)}\\ l^{(k)}\\ m^{(k)}\end{bmatrix}-\left(\begin{bmatrix}\frac{\partial y_2}{\partial s} & \frac{\partial y_2}{\partial l} & \frac{\partial y_2}{\partial m}\\ \frac{\partial y_4}{\partial s} & \frac{\partial y_4}{\partial l} & \frac{\partial y_4}{\partial m}\\ \frac{\partial y_6}{\partial s} & \frac{\partial y_6}{\partial l} & \frac{\partial y_6}{\partial m}\end{bmatrix}^{-1}\begin{bmatrix} y_2-A\\ y_4\\ y_6\end{bmatrix}\right)_{\left(s^{(k)},\ l^{(k)},\ m^{(k)}\right)}.
$$

$$
\Rightarrow\begin{bmatrix} s^{(k+1)}\\ l^{(k+1)}\\ m^{(k+1)}\end{bmatrix}=\begin{bmatrix} s^{(k)}\\ l^{(k)}\\ m^{(k)}\end{bmatrix}-\left(\begin{bmatrix} y_9 & y_{16} & y_{23}\\ y_{11} & y_{18} & y_{25}\\ y_{13} & y_{20} & y_{27}\end{bmatrix}^{-1}\begin{bmatrix} y_2-A\\ y_4\\ y_6\end{bmatrix}\right)_{\left(s^{(k)},\ l^{(k)},\ m^{(k)}\right)},
$$

where k represents the k^{th} iterations.

In order to terminate the numerical procedure and obtain the numerical solution, the stopping criteria has been set as:

$$max\{(|y_2(\eta_\infty) - A|,\ \ |y_4(\eta_\infty)|, |y_6(\eta_\infty)|)\} < \epsilon, \tag{3.17}$$

where ϵ has been chosen as 10^{-12}. For all numerical results presented in the present model, $\eta_\infty = 7$ is observed as an appropriate replacement of ∞.

3.4 Results with Discussion

In the said section, the numerical solutions of the described model for various choices of the values of some important pertinent flow parameters have been computed and discussed. The significant numerical results of some parameters of interest are illustrated in the tabular form, as well.

3.4.1 Skin-friction Coefficient, Nusselt and Sherwood Numbers

To validate the MATLAB code for the shooting method, the values of $-\theta'(0)$ are replicated for the problem addressed by Khan and Pop [67], Arulmozhi et al. [68] and Noeiaghdam et al. [69].

Table 3.1: Comparison of the present results of local Nusselt number with those published in the literature.

		$-\theta'(0)$ with $Pr = 10$			
Nb	Nt	Khan and Pop [67]	Arulmozhi et al. [68]	Noeiaghdam et al. [69]	Present
0.1	0.1	2.1294	2.1294	2.1294	2.129346
0.2	0.1	2.2740	2.2740	2.2740	2.273857
0.3	0.1	2.5286	2.5286	2.5286	2.528362
0.4	0.1	2.7952	2.7952	2.7952	2.794799

Table 3.1 reflects a great settlement between the numerical values obtained by the present code and those already existing in the above mentioned articles.

Tables 3.2-3.4 disclose the computed values of the skin-friction coefficient, along with the Nusselt and Sherwood numbers, for the model under consideration by varying different parameters like β, Pr, M, A, Nb, K, α, Gr, Ec, Gc, λ, S, δ, Rd, Q, Nt, γ, ω, Γ, Sc and χ. In these tables, c_1 and c_2 have been used to denote $(1+\frac{1}{\beta})$ and $(1+\frac{4}{3}Rd)$, respectively.

TABLE 3.2: The computed results of skin-friction coefficient, Nusselt and Sherwood numbers for $Rd = Pr = Q = Ec = Sc = \gamma = \Gamma = \omega = \chi = \delta = 0.1,\ Nb = Nt = 0.5, S = 0.2$.

β	M	A	K	α	Gr	Gc	λ	$c_1 f''(0)$	$-c_2\theta'(0)$	$-\phi'(0)$
0.5	1	0.1	0.10	0.1	2.0	1.0	1.0	7.137509	-0.049569	0.443023
5.0								3.919429	0.202223	0.203195
10								3.705960	0.208801	0.194452
	2							7.143034	-0.048568	0.441440
	3							7.153131	-0.046991	0.438882
		0.2						7.199230	-0.052690	0.455493
		0.3						7.304999	-0.059659	0.472074
			0.12					7.170019	-0.117796	0.500933
			1.14					7.202880	-0.187092	0.559735
				0.2				7.142958	-0.048581	0.441461
				0.3				7.152626	-0.047063	0.439002
					3.0			9.032205	-0.192861	0.583438
					4.0			10.865648	-0.361764	0.740824
						2.0		8.773996	-0.175495	0.580361
						3.0		10.180833	-0.304880	0.709926
							1.5	5.022552	-0.015530	0.378087
							2.0	-3.359565	0.061521	-1.130882

It has been remarked that by taking into account the larger values of A, K, Gr, Gc, S, Pr, ω and Γ, the magnitude of the skin-friction coefficient along with the mass transfer rate climb marginally whereas a diminution in the heat transfer rate has been seen.

It has been sighted that as the values of β, λ, Rd and χ go up, the skin-friction coefficient and Sherwood number depreciate while the Nusselt number escalates significantly. An escalation has been observed in the heat and mass transfer rates as Q and γ assume the higher values, whereas the magnitude of the skin-friction coefficient declines remarkably.

TABLE 3.3: The computed results of skin-friction coefficient, Nusselt and Sherwood numbers for $M = Gc = 1,\ A = K = \alpha = \delta = \chi = \Gamma = 0.1,\ S = 0.2,\ \lambda = 1,\ \beta = 0.5$.

Rd	Pr	Q	Nb	Nt	Ec	Sc	γ	ω	$c_1 f''(0)$	$-c_2\theta'(0)$	$-\phi'(0)$
0.1	0.1	0.1	0.5	0.5	0.1	0.1	0.1	0.1	7.137509	-0.049569	0.443023
0.2									7.011342	1.532161	0.208155
0.3									7.001480	3.135451	0.189926
	0.5								7.210993	-0.908215	1.224026
	1.0								7.528930	-2.251737	2.412752
		0.2							6.938789	-0.003572	0.521921
		0.3							6.824714	0.014398	0.586091
			5.0						7.173127	-0.080883	0.289679
			10						7.292440	-0.148627	0.287447
				1.0					7.111343	-0.105493	0.695248
				2.0					7.096359	-0.178978	1.270402
					0.2				7.123904	-0.034203	0.430949
					0.3				7.110563	-0.019112	0.419074
						0.2			7.138603	-0.043605	0.434486
						0.3			7.138834	-0.038299	0.426577
							0.2		7.110128	-0.042745	0.456648
							0.3		7.084463	-0.036599	0.469936
								0.2	7.154268	-0.049695	0.443887
								0.3	7.171101	-0.049826	0.444758

The skin-friction coefficient, Sherwood and Nusselt numbers are magnified for the higher estimation of M. On the contrary, as Ec and δ attain the larger values, the skin-friction coefficient, heat and mass transfer rates are observed to fall moderately.

The skin-friction coefficient shows an increasing behavior whereas an opposite trend has been observed in the magnitude of Sherwood number with the rise of Nb and Sc.

Table 3.4: The computed results of skin-friction coefficient, Nusselt and Sherwood numbers for $Rd = Pr = Q = Ec = Sc = \gamma = \Gamma = \omega = A = K = \alpha = 0.1,\ Nb = Nt = 0.5,\ M = Gc = 1,\ \lambda = 1,\ \beta = 0.5$.

S	δ	Γ	χ	$c_1 f''(0)$	$-c_2\theta'(0)$	$-\phi'(0)$
0.2	0.1	0.1	0.1	7.137509	-0.049569	0.443023
1.0				26.724105	-1.968488	2.1641677
1.5				55.542392	-8.772177	8.0310438
	0.05			7.071766	-0.025425	0.437019
	0.2			5.205177	-0.020618	0.385569
		0.2		7.331324	-0.206812	0.553291
		0.3		7.527138	-0.350740	0.647269
			0.2	7.057073	-0.040312	0.422880
			0.3	6.983258	-0.031997	0.404645

3.4.2 The Velocity, Temperature and Concentration Profiles

Figures 3.2-3.4 highlight the effect of M on the velocity, temperature and concentration profiles. A sudden escalation has been sighted in the concentration and temperature profiles whereas the velocity drops subsequently by applying a higher magnetic field. This happens due to the fact that the applied magnetic field encounters an opposing force generally referred to as the Lorentz force, is originated consequently which brings down the motion of the fluid leading to a drastic fall in the momentum boundary layer thickness and a marginal hike in the thermal and concentration boundary layer thickness.

The impact of A on the velocity and temperature distributions has been presented in Figures 3.5-3.6. By taking into account the values of A larger than 1, an increment has been seen in the velocity. Contrariwise, the flow velocity reduces for $A < 1$. Moreover, the temperature profile is noticed to de-escalate for the higher estimation of A. This stems from the fact that the transfer of thermal energy from the surface to the fluid tends to decline as the value of A escalates and therefore, the temperature drops and the related thermal boundary layer thickness is shrinked.

Figure 3.7 illustrates the influence of Casson parameter on the flow velocity. An increasing behaviour is observed in the velocity by escalating the values of β. Moreover, a decrement is experienced by the velocity boundary layer thickness with a rise in β. The reason for this lies in the fact that for the smaller values of β, the plasticity of the Casson fluid climbs which results in an enlargement in the corresponding momentum boundary layer thickness.

The dynamics of the velocity and temperature distributions by incorporating diverse values of Ec have been illustrated through Figures 3.8-3.9. In the physical sense, the ratio of the fluid particles' kinetic energy and enthalpy is characterized by the Eckert number. An escalation in the kinetic energy of the fluid is observed by rising the values of Ec. Therefore, the temperature and velocity go up exhibit an augmentation which results in an enhancement in the thickness of the momentum and thermal boundary layer.

Figure 3.10 depicts the impact of γ on the concentration configuration. It has been seen that the higher estimation of γ leads to a depreciation in the chemical molecular diffusion and thereby the fluid's concentration drops marginally and a decrement has been noted in the associated concentration boundary layer thickness.

The effect of the Brownian motion parameter on the temperature and concentration profiles are displayed through Figures 3.11-3.12. The temperature profile upsurges significantly by considering higher Nb. This happens due to the fact that the rising values of Nb cause a notable elevation in the nanoparticles' motion which catalyzes the nanoparticles' kinetic energy. This leads to an increment in the temperature and the thermal boundary layer thickness. However, the concentration of the fluid falls down as the values of Nb are allowed to rise up. This cause a natural reduction in concentration boundary layer thickness.

Figures 3.13-3.14 are delineated to display the influence of the thermophoresis parameter on the temperature and concentration configurations. Both the temperature and concentration go up by increasing the magnitude of Nt. On top of that, an escalation in the associated thermal and concentration boundary layer thickness has been observed.

Figures 3.15-3.16 are drawn to portray the impact of Pr on the temperature and concentration configurations. Physically, Pr is defined to be proportionate between the viscous diffusion rate and thermal diffusivity. As the magnitude of Pr heightens, the thermal diffusion rate undergoes a curtailment and eventually the fluid's temperature depresses considerably. Therefore, a diminution has been noted in the thermal boundary layer thickness. Meanwhile, for the higher assumption of Pr, the fluid's concentration is noticed to escalate. Apart from this, a sudden upsurge can be noted in the thickness of the concentration boundary layer.

The impact of the heat generation or absorption parameter on the temperature profile is elucidated in Figure 3.17. The larger the magnitude of Q, the more the heat is generated, which allows the temperature and the thermal boundary layer thickness to climb significantly. However, a drop in the magnitude of Q results in higher heat absorption which cools down the temperature and as a result, the associated thermal boundary layer thickness undergoes a decrement.

Figures 3.18-3.19 illustrate the effect of Sc and Rd on the concentration fields. The fluid's concentration is reduced for taking into account larger Sc. This happens owing to the fact that the relation between Schmidt number and mass diffusion rate is inversely proportional, that is why, as Sc rises, the phenomenon of mass diffusion happens more slowly and hence results in a sudden drop in the concentration and the thickness of concentration boundary layer is decreased. On the other hand, the radiation parameter affects the concentration distribution, the other way round. The larger the values of Rd, the higher the concentration, which further magnifies the associated concentration boundary layer thickness.

Figure 3.20 is sketched to delineate the influence of M and β on the skin-friction coefficient. It is remarked from the figure that as the values of β and M escalate, the shearing stress of the surface approaches an alleviation. Figure 3.21 represents the effect of Rd and Ec on the Nusselt number. Notably, the magnitude of the heat transfer gradient increases marginally by assuming the higher values of Rd and Ec into account.

The impact of Pr and γ on the Sherwood number is depicted in Figure 3.22. Evidently, it is apparent that as the values of Pr and γ escalate, the mass transfer gradient exhibits an increment in magnitude.

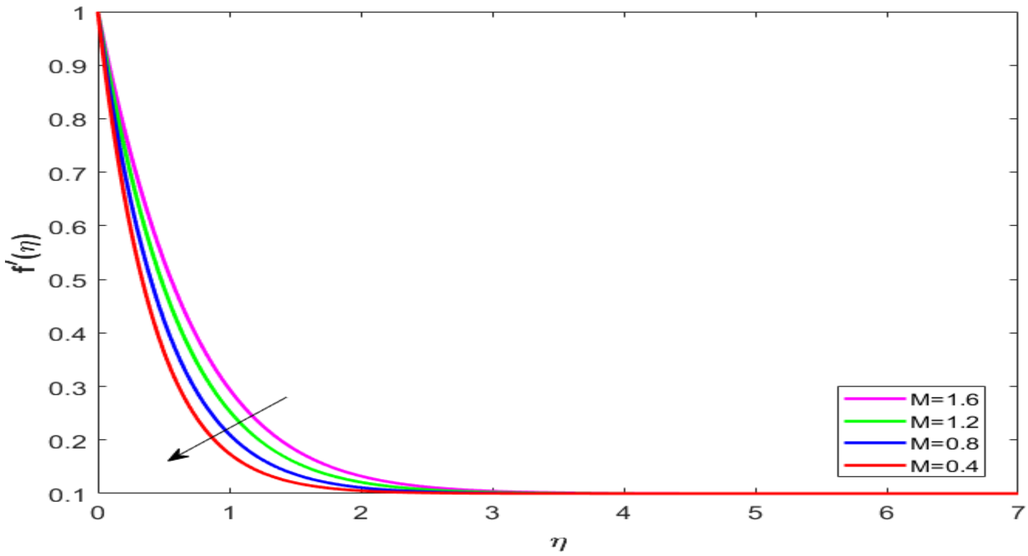

FIGURE 3.2: Effect of M on $f'(\eta)$ when $K = \omega = \delta = A = Q = Ec = \alpha = \Gamma = \chi = Sc = 0.1$ $\beta = Nt = Nb = 0.5,\ Rd = Pr = \gamma = Gc = 1,\ Gr = 2,\ \lambda = -1,\ S = 0.2$

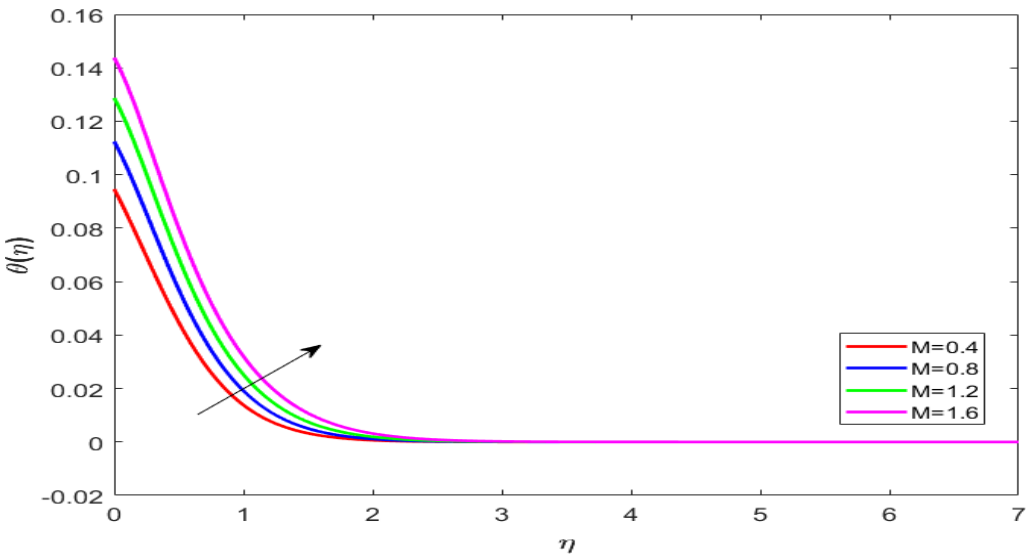

FIGURE 3.3: Effect of M on $\theta(\eta)$ when $K = \omega = \delta = A = Q = Ec = \alpha = \Gamma = \chi = Sc = 0.1,\ \beta = Nt = Nb = 0.5,\ Rd = Pr = \gamma = Gc = 1,\ Gr = 2, \lambda = -1,\ S = 0.2$

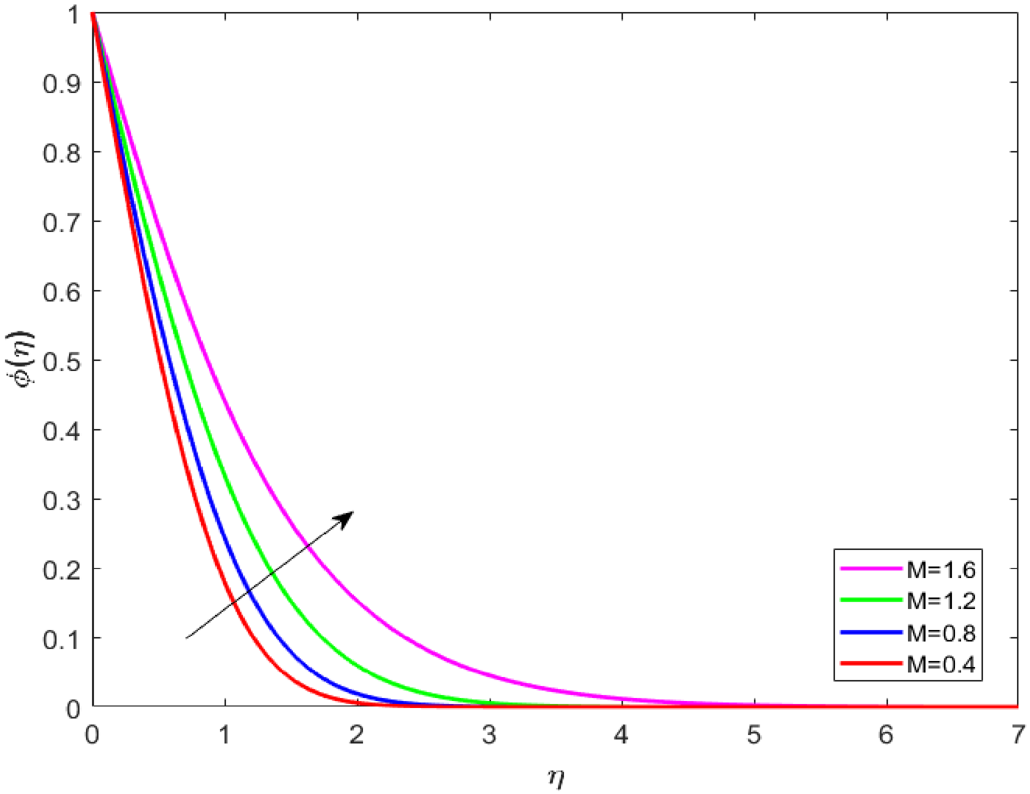

FIGURE 3.4: Effect of M on $\phi(\eta)$ when $K = \omega = \delta = A = Q = Ec = \alpha = \Gamma = \chi = Sc = 0.1,\ \beta = Nt = Nb = 0.5,\ Rd = Pr = \gamma = Gc = 1,\ Gr = 2, \lambda = -1,\ S = 0.2$

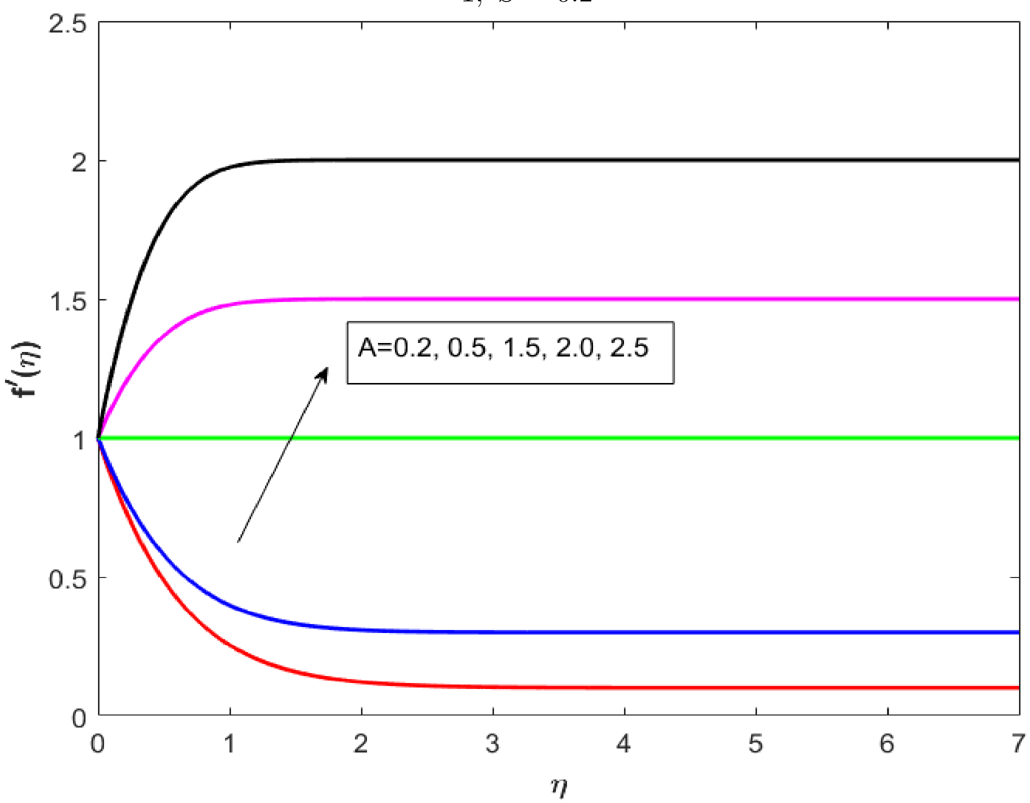

FIGURE 3.5: Effect of A on $f'(\eta)$ when $K = \omega = \delta = Q = Ec = \alpha = \Gamma = \chi = Sc = 0.1,\ \beta = Nt = Nb = 0.5,\ M = Rd = Pr = \gamma = Gc = 1,\ Gr = 2,\ \lambda = -1,\ S = 0.2$

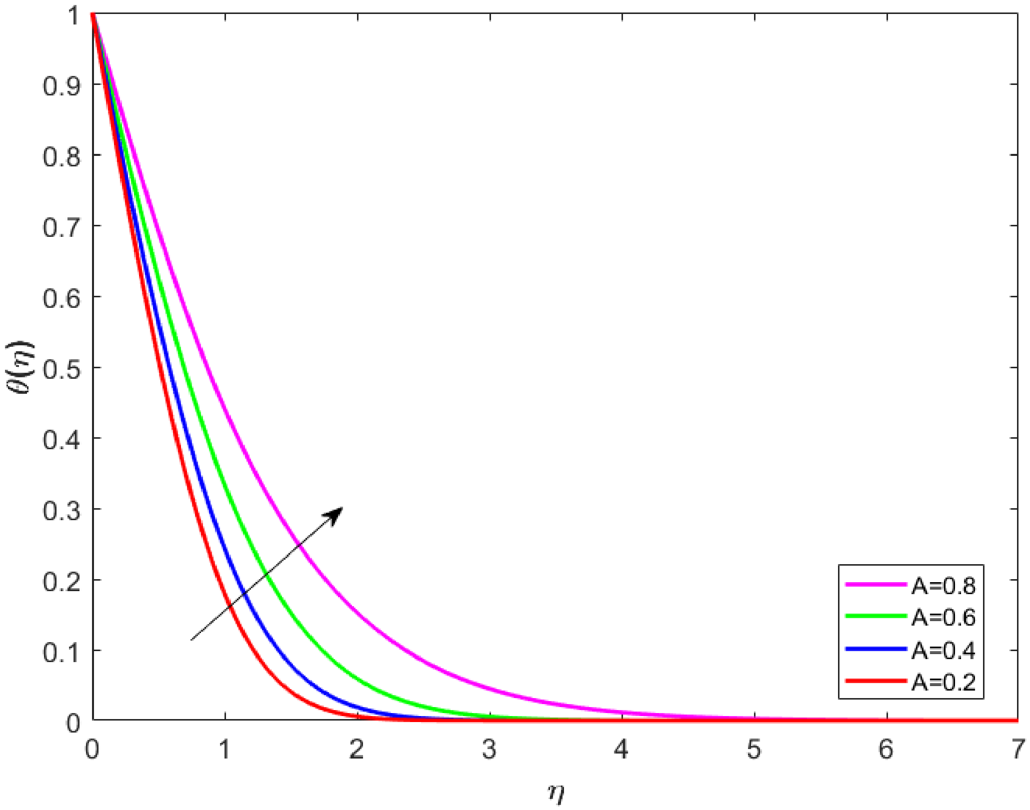

FIGURE 3.6: Effect of A on θ when $K = \omega = \delta = Q = Ec = \alpha = \Gamma = \chi = Sc = 0.1$ $\beta = Nt = Nb = 0.5, M = Rd = Pr = \gamma = Gc = 1, Gr = 2, \lambda = -1, S = 0.2$

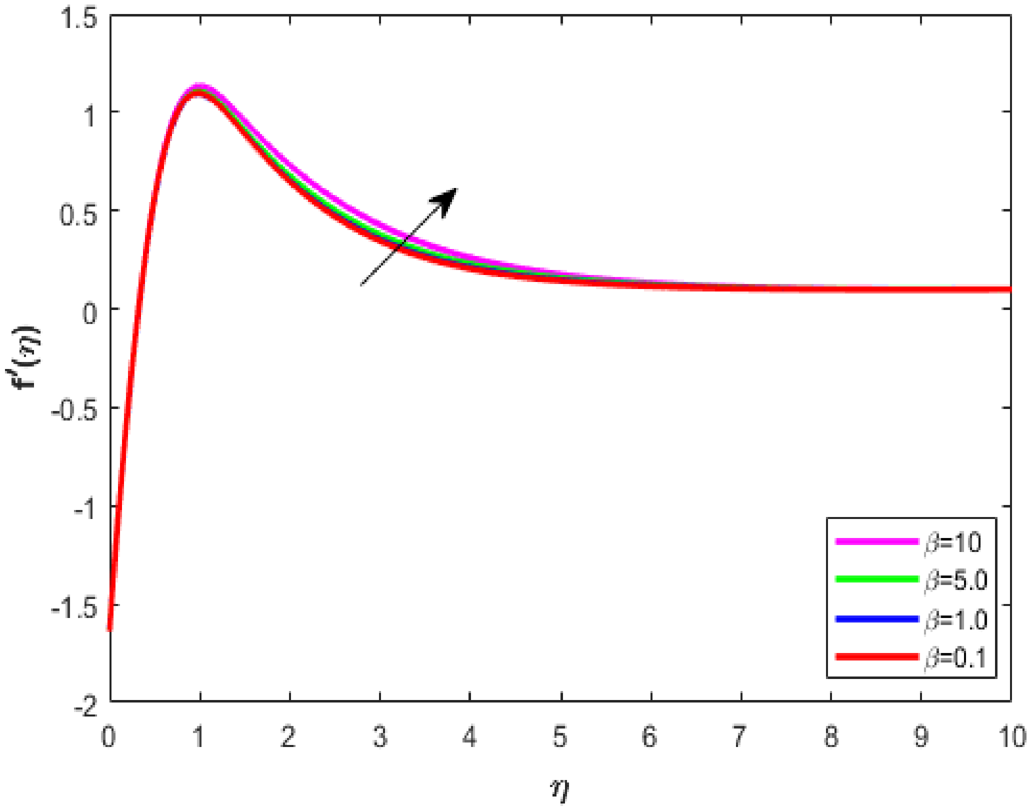

FIGURE 3.7: Effect of β on $f'(\eta)$ when $K = \omega = \delta = A = Q = Ec = \alpha = \Gamma = \chi = Sc = 0.1$ $Nt = Nb = 0.5, M = Rd = Pr = \gamma = Gc = 1, Gr = 2, \lambda = -1, S = 0.2$

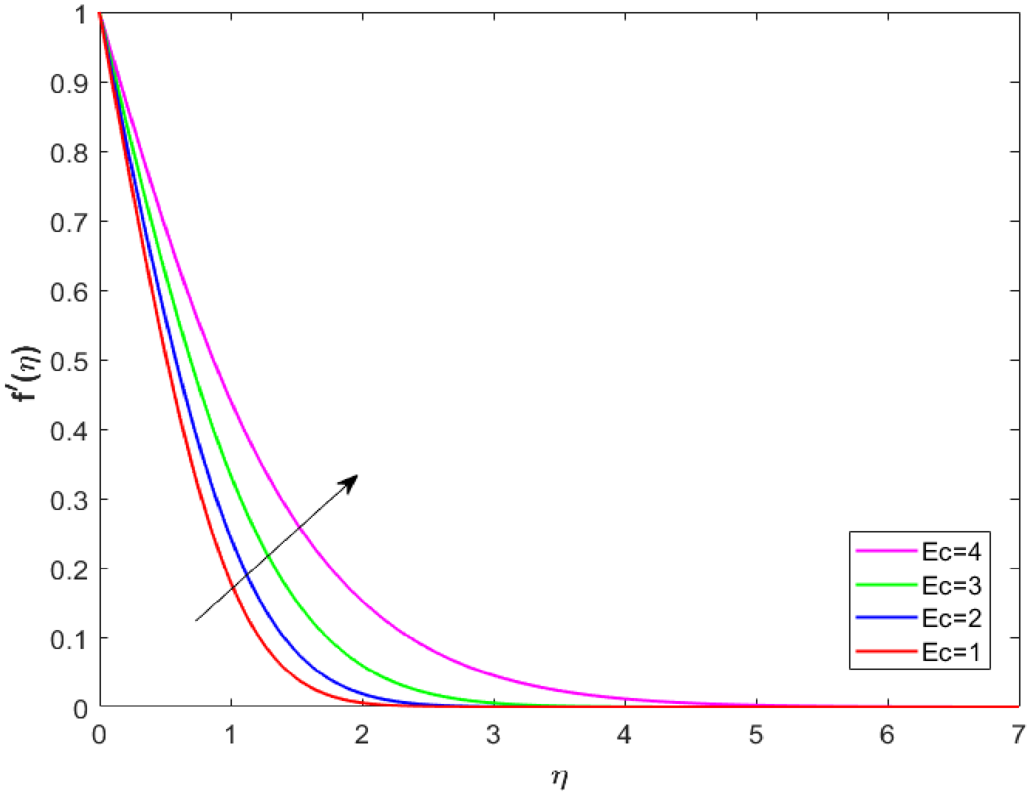

FIGURE 3.8: Effect of Ec on $f'(\eta)$ when $K = \omega = \delta = A = Q = \alpha = \Gamma = \chi = Sc = 0.1,\ \beta = Nt = Nb = 0.5,\ M = Rd = Pr = \gamma = Gc = 1,\ Gr = 2,\ \lambda = -1,\ S = 0.2$

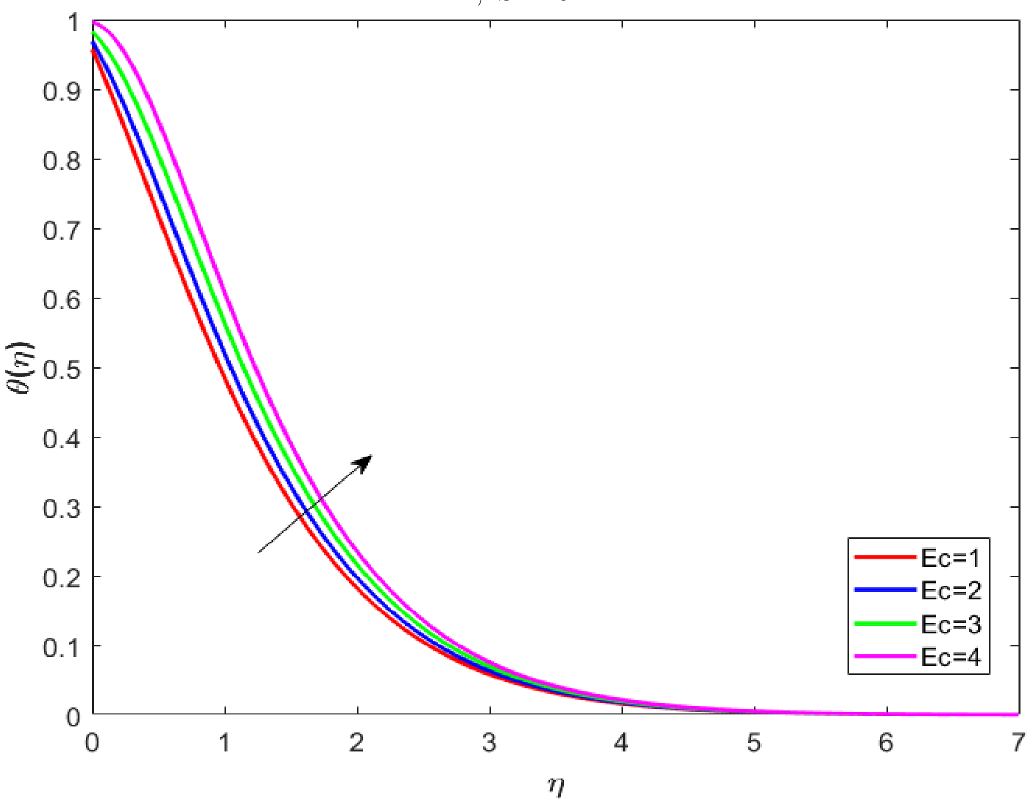

FIGURE 3.9: Effect of Ec on $\theta(\eta)$ when $K = \omega = \delta = A = Q = \alpha = \Gamma = \chi = Sc = 0.1,\ \beta = Nt = Nb = 0.5,\ M = Rd = Pr = \gamma = Gc = 1,\ Gr = 2,\ \lambda = -1,\ S = 0.2$

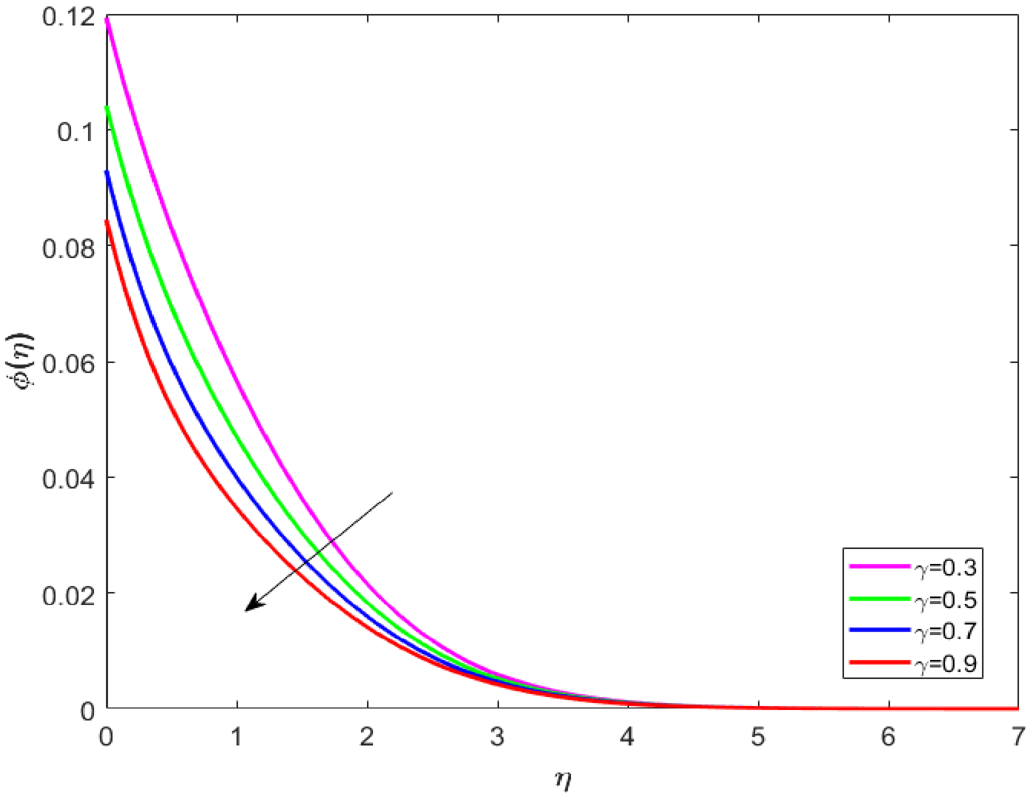

FIGURE 3.10: Effect of γ on $\phi(\eta)$ when $K = \omega = \delta = A = Q = Ec = \alpha = \Gamma = \chi = Sc = 0.1,\ \ \beta = Nt = Nb = 0.5,\ M = Rd = Pr = Gc = 1,\ Gr = 2,\ \lambda = -1,\ S = 0.2$

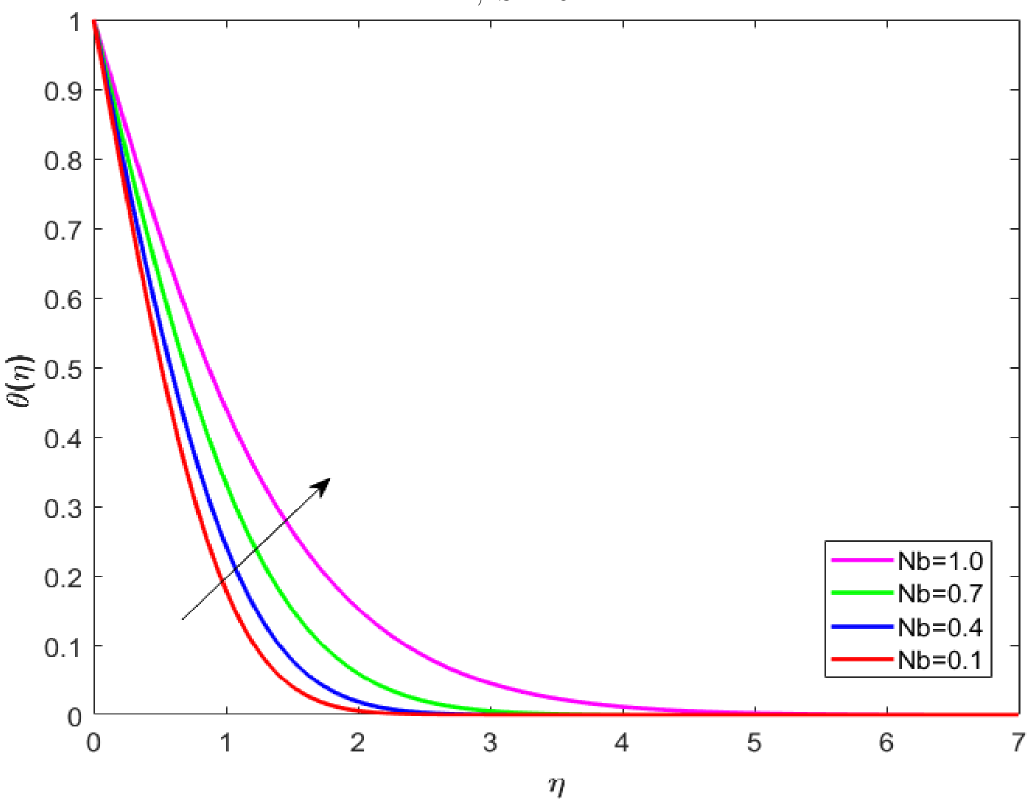

FIGURE 3.11: Effect of Nb on $\theta(\eta)$ when $K = \omega = \delta = A = Q = Ec = \alpha = \Gamma = \chi = Sc = 0.1,\ \ \beta = Nt = 0.5,\ M = Rd = Pr = \gamma = Gc = 1,\ Gr = 2,\ \lambda = -1,\ S = 0.2$

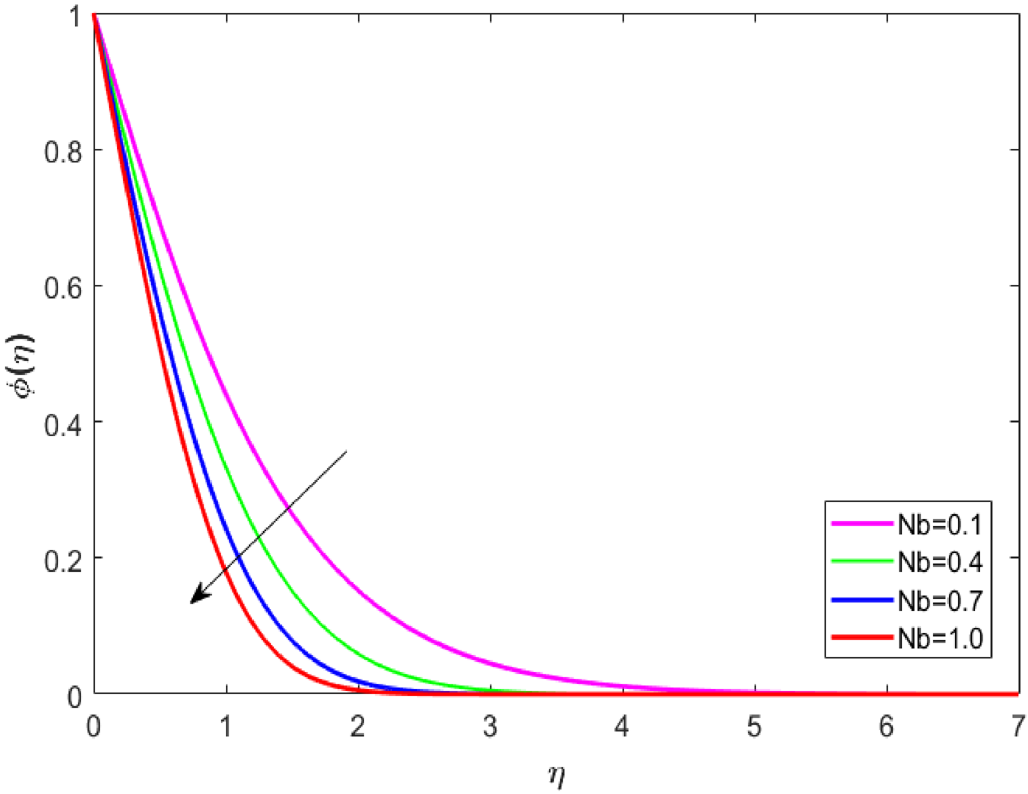

FIGURE 3.12: Effect of Nb on $\phi(\eta)$ when $K = \omega = \delta = A = Q = Ec = \alpha = \Gamma = \chi = Sc = 0.1,\ \beta = Nt = 0.5,\ M = Rd = Pr = \gamma = Gc = 1,\ Gr = 2,\ \lambda = -1,\ S = 0.2$

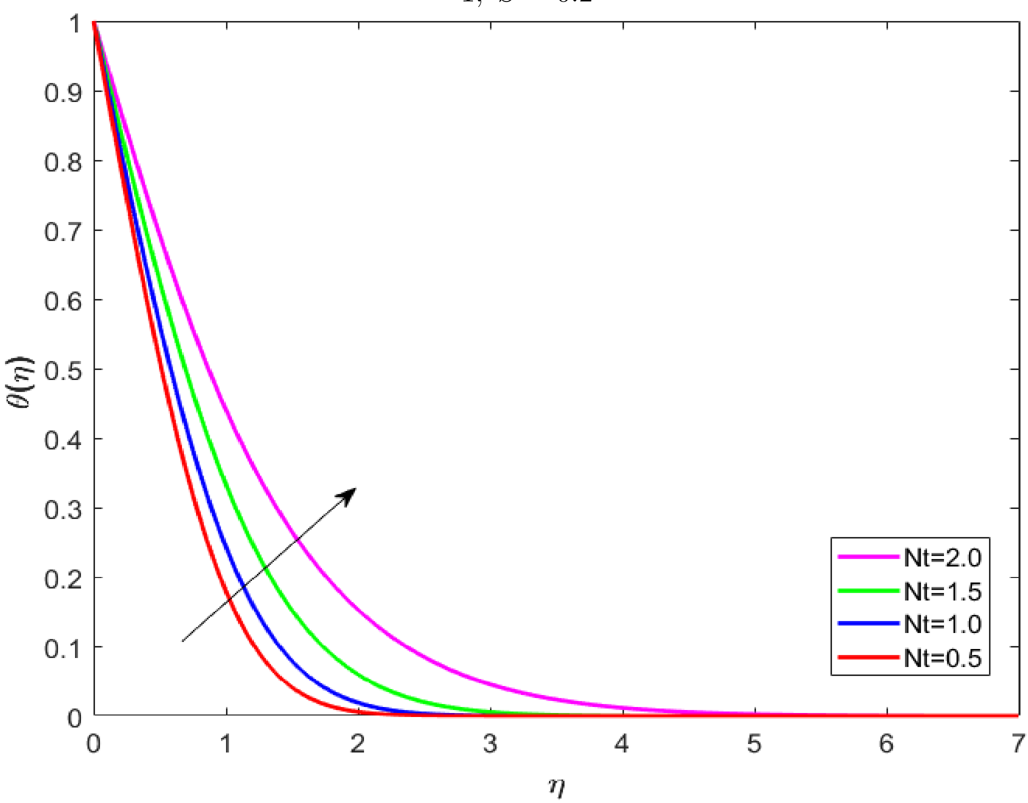

FIGURE 3.13: Effect of Nt on $\theta(\eta)$ when $K = \omega = \delta = A = Q = Ec = \alpha = \Gamma = \chi = Sc = 0.1,\ \beta = Nb = 0.5,\ M = Rd = Pr = \gamma = Gc = 1,\ Gr = 2,\ \lambda = -1,\ S = 0.2$

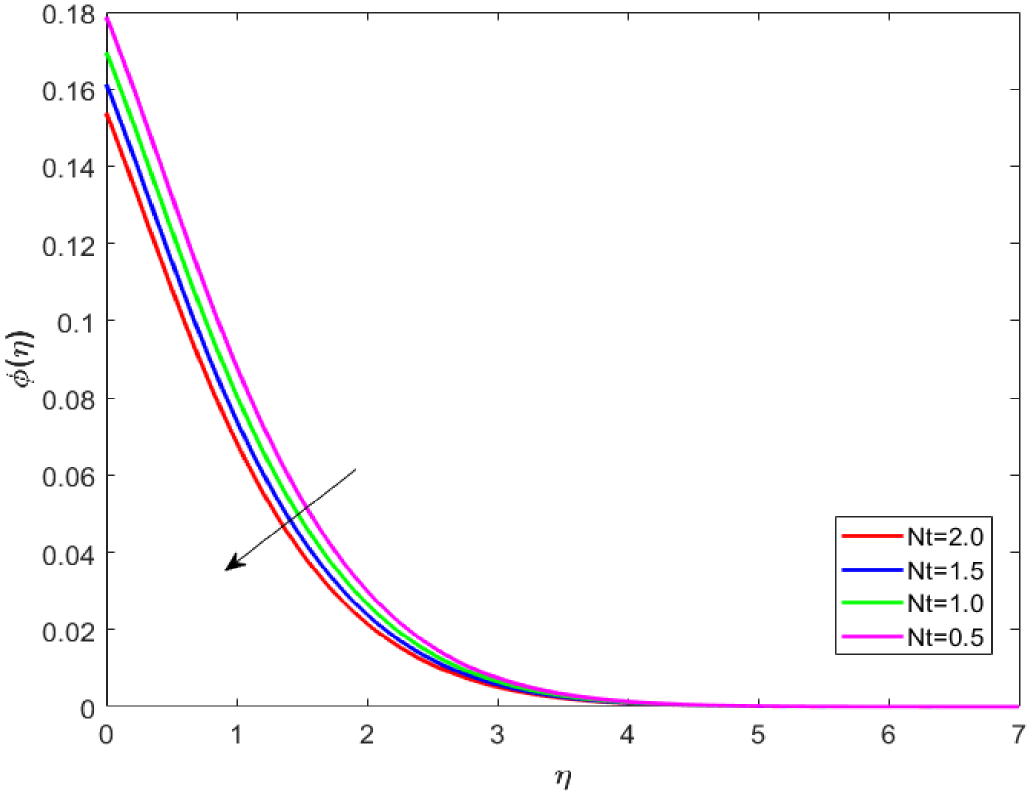

FIGURE 3.14: Effect of Nt on $\phi(\eta)$ when $K = \omega = \delta = A = Q = Ec = \alpha = \Gamma = \chi = Sc = 0.1,\ \beta = Nb = 0.5,\ M = Rd = Pr = \gamma = Gc = 1,\ Gr = 2,\ \lambda = -1,\ S = 0.2$

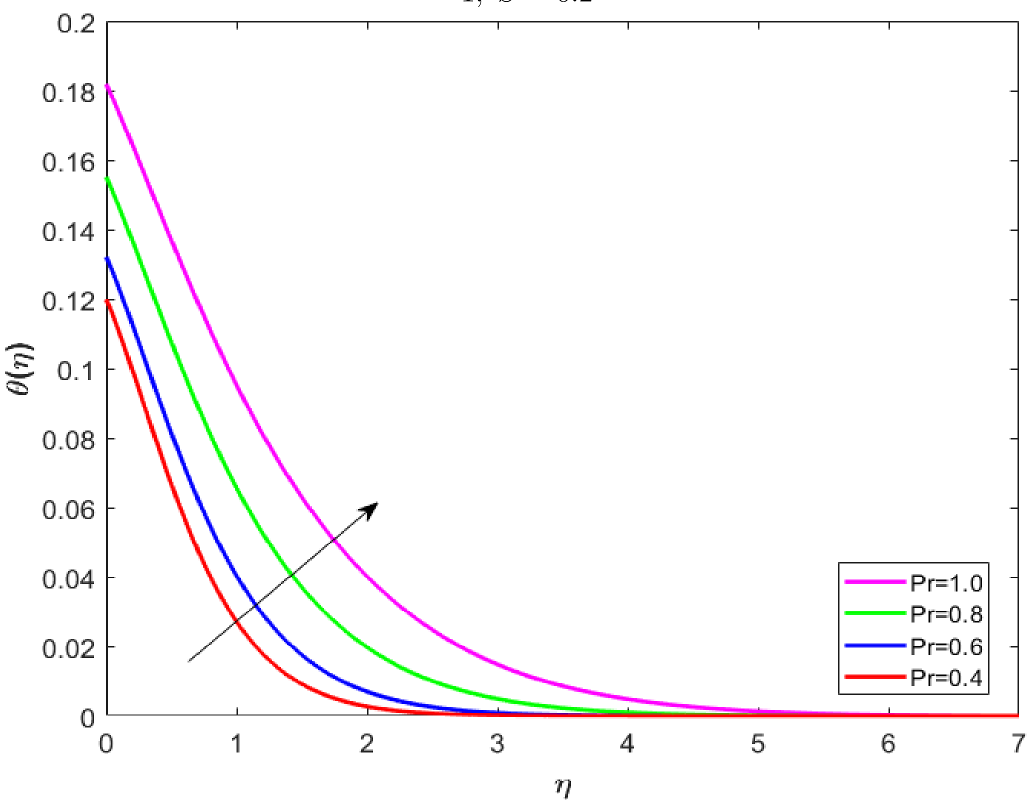

FIGURE 3.15: Effect of Pr on $\theta(\eta)$ when $K = \omega = \delta = A = Q = Ec = \alpha = \Gamma = \chi = Sc = 0.1,\ \beta = Nt = Nb = 0.5,\ M = Rd = \gamma = Gc = 1,\ Gr = 2,\ \lambda = -1,\ S = 0.2$

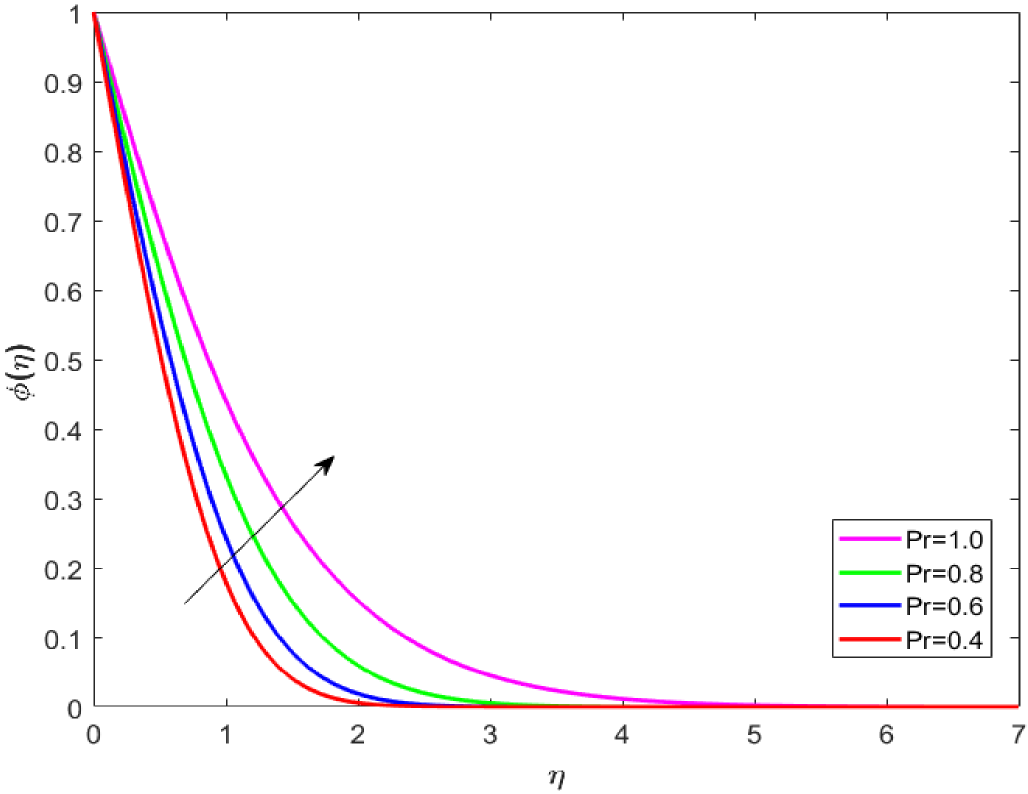

FIGURE 3.16: Effect of Pr on $\phi(\eta)$ when $K = \omega = \delta = A = Q = Ec = \alpha = \Gamma = \chi = Sc = 0.1,\ \beta = Nt = Nb = 0.5,\ M = Rd = \gamma = Gc = 1,\ Gr = 2,\ \lambda = -1,\ S = 0.2$

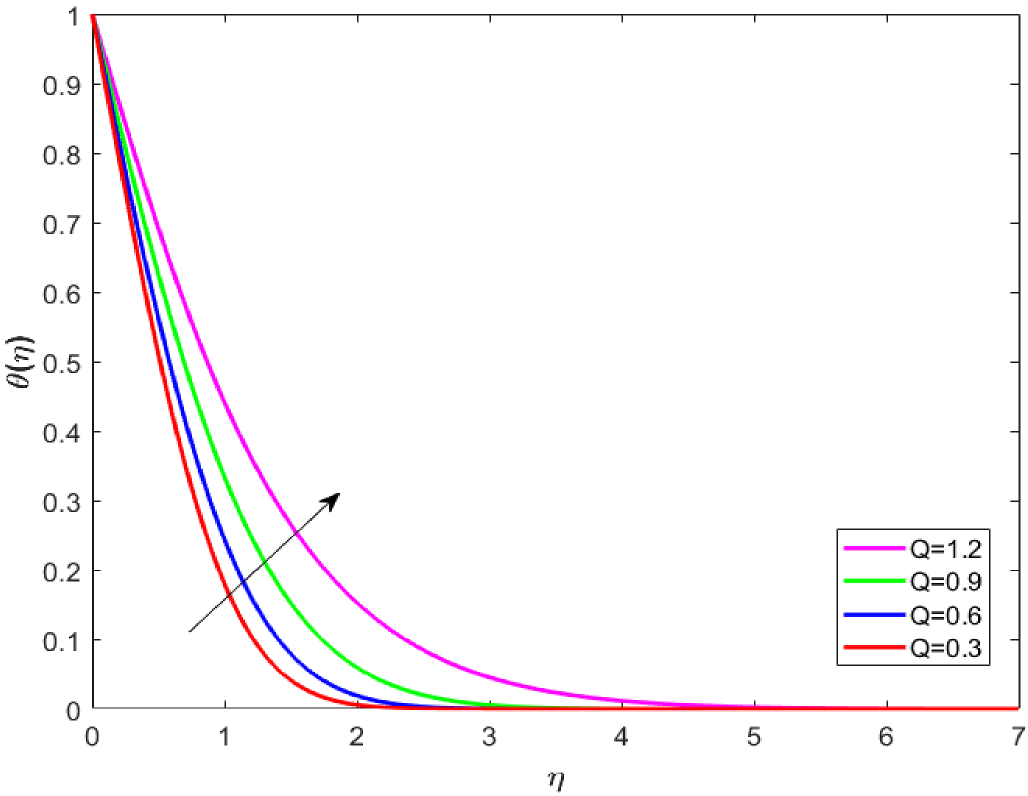

FIGURE 3.17: Effect of Q on $\theta(\eta)$ $K = \omega = \delta = A = Ec = \alpha = \Gamma = \chi = Sc = 0.1,\ \beta = Nt = Nb = 0.5,\ M = Rd = Pr = \gamma = Gc = 1,\ Gr = 2,\ \lambda = -1,\ S = 0.2$

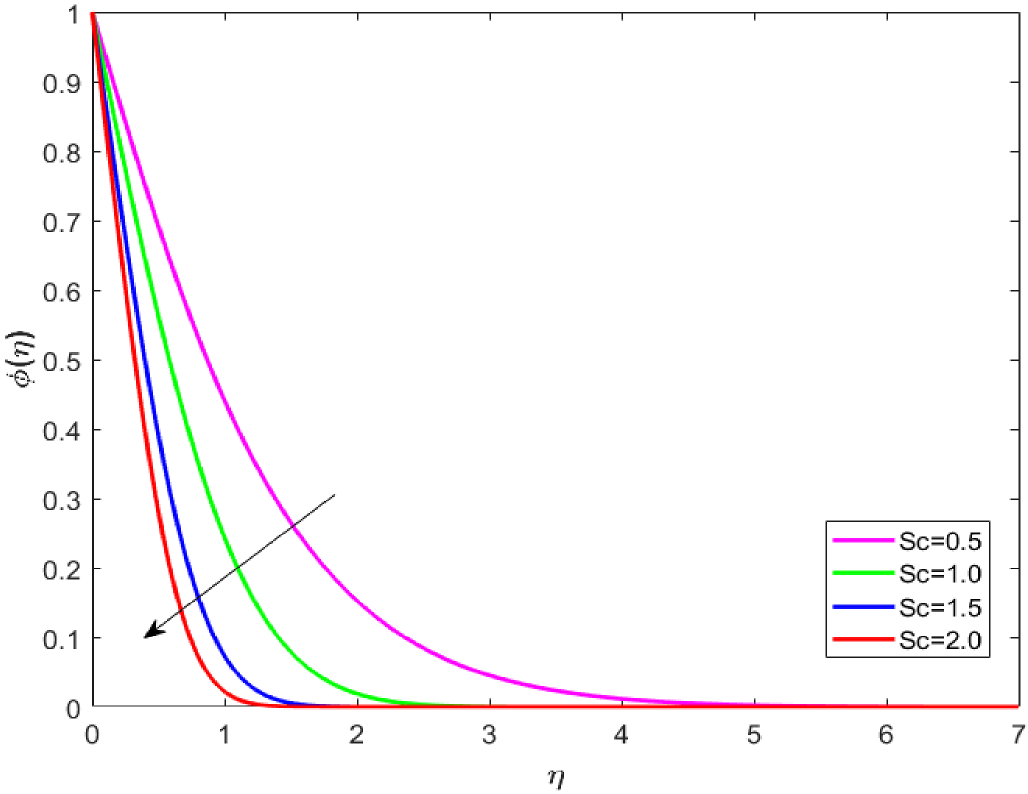

FIGURE 3.18: Effect of Sc on $\phi(\eta)$ when $K = \omega = \delta = A = Q = Ec = \alpha = \Gamma = \chi = 0.1,\ \ \beta = Nt = Nb = 0.5,\ \ M = Rd = Pr = \gamma = Gc = 1,\ Gr = 2,\ \lambda = -1,\ S = 0.2$

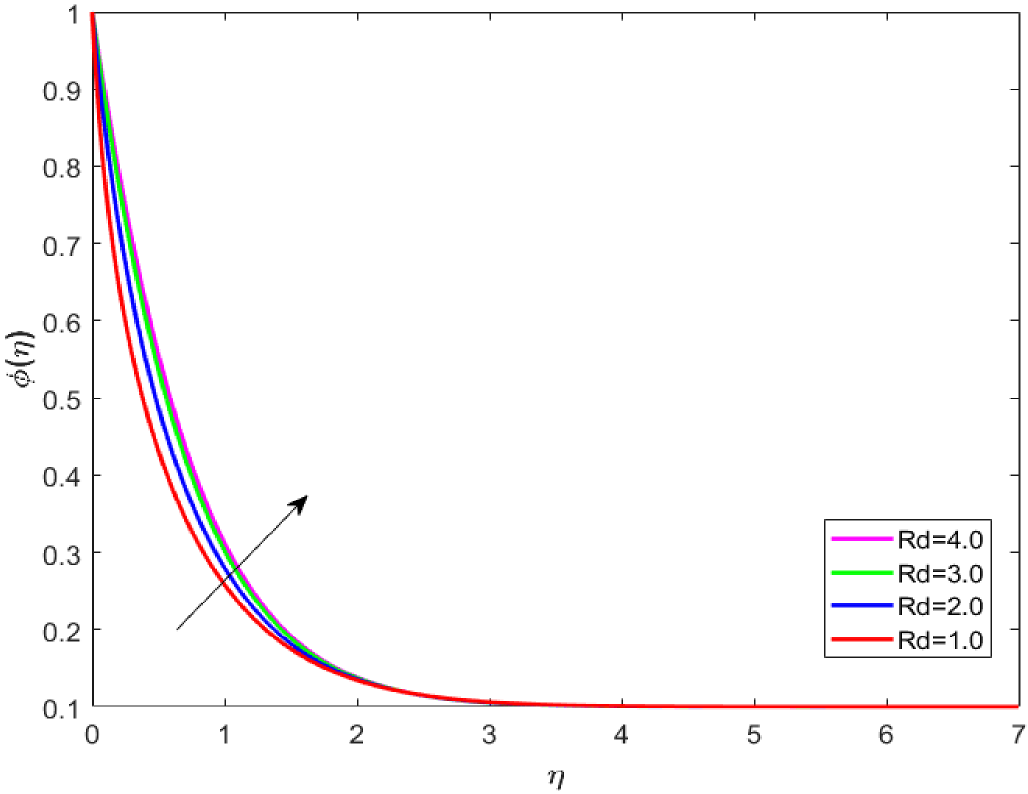

FIGURE 3.19: Effect of Rd on $\phi(\eta)$ when $K = \omega = \delta = A = Q = Ec = \alpha = \Gamma = \chi = Sc = 0.1,\ \beta = Nt = Nb = 0.5,\ M = Pr = \gamma = Gc = 1,\ Gr = 2,\ \lambda = -1,\ S = 0.2$

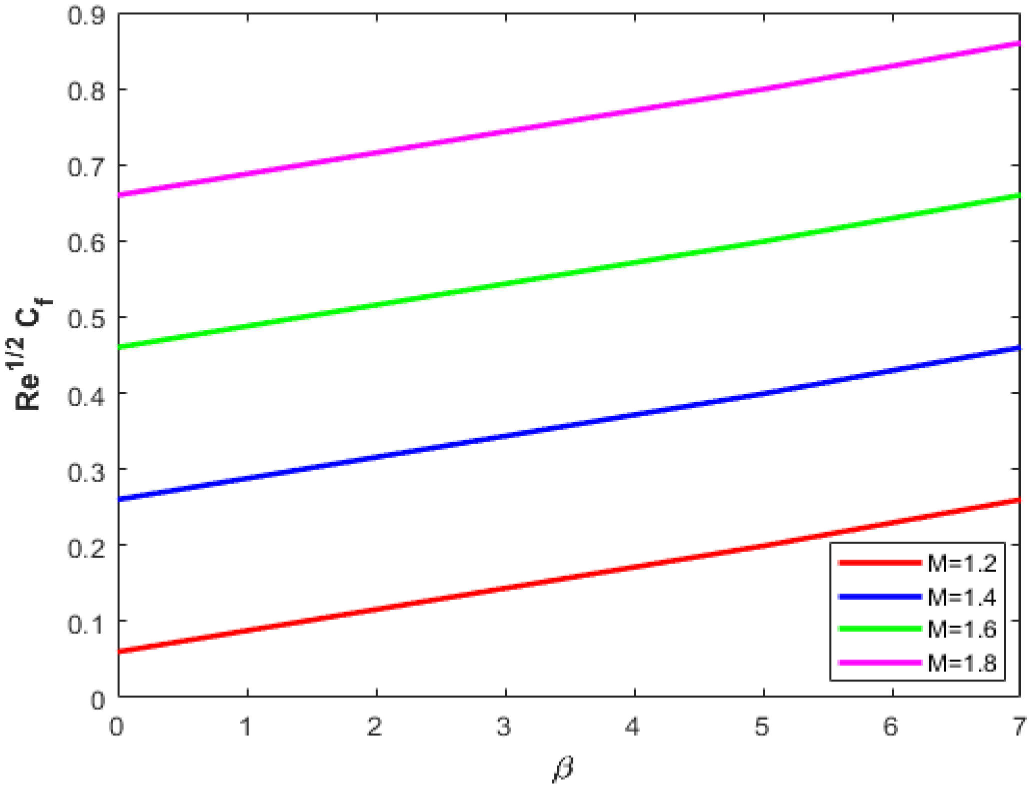

FIGURE 3.20: Effect of M and β on $Re^{\frac{1}{2}}C_f$ when $K = \omega = \delta = n = A = Q = Ec = \alpha = \Gamma = \chi = Sc = 0.1$, $Nt = Nb = 0.5$, $M = Rd = Pr = \gamma = Gc = 1$, $Gr = 2$, $\lambda = -1$, $S = 0.2$

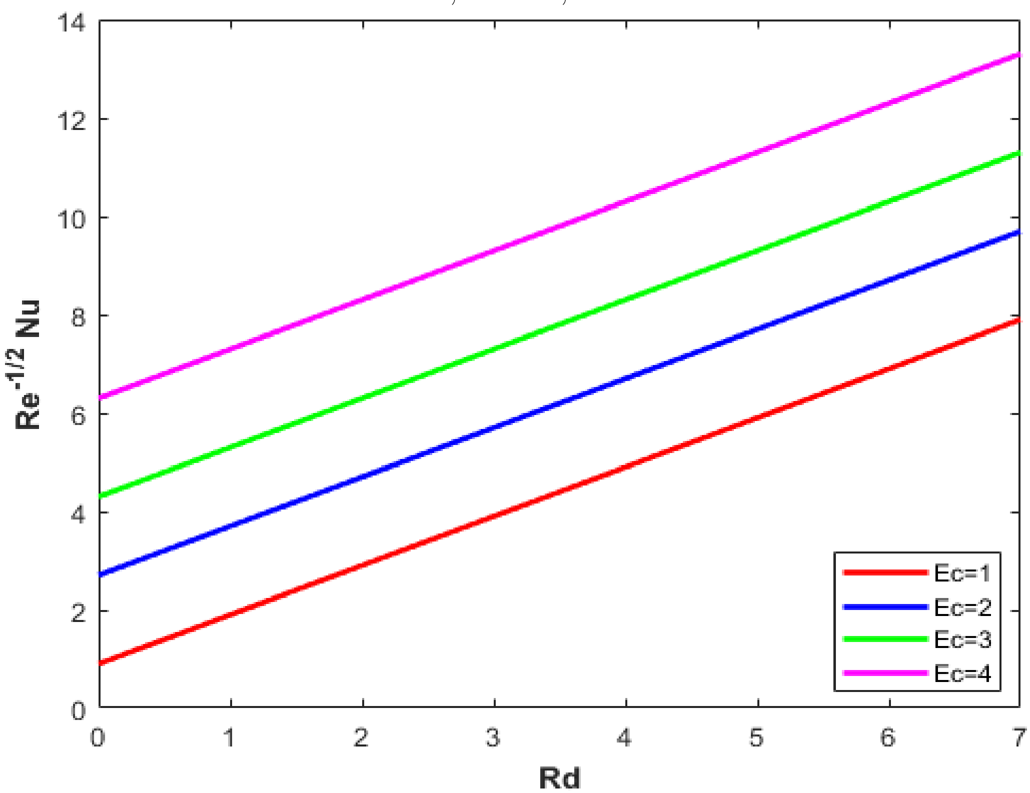

FIGURE 3.21: Effect of Rd and Ec on $Re^{-\frac{1}{2}}Nu$ when when $K = \omega = \delta = n = A = Q = Ec = \alpha = \Gamma = \chi = Sc = 0.1$, $Nt = Nb = 0.5$, $M = Rd = Pr = \gamma = Gc = 1$, $Gr = 2$, $\lambda = -1$, $S = 0.2$

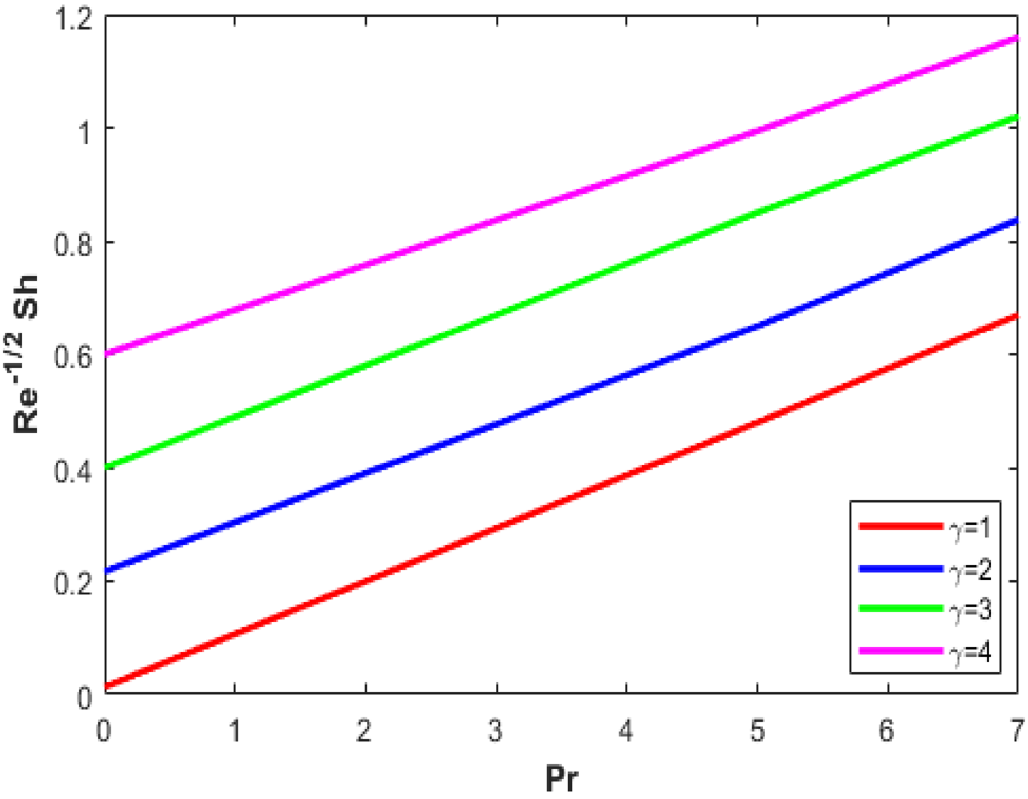

FIGURE 3.22: Effect of Pr and γ on Re∧-∧1∧/∧2 Sh when $K = \omega = \delta = n = A = Q = Ec = \alpha = \Gamma = \chi = Sc = 0.1$, $Nt = Nb = 0.5$, $M = Rd = Pr = \gamma = Gc = 1$, $Gr = 2$, $\lambda = -1$, $S = 0.2$

Chapter 4

Inclined Magnetically driven Carreau Nanofluid using the Cattaneo-Christov Heat Flux Model

4.1 Introduction

The numerical study of the flow of Carreau nanofluid subject to the availability of an inclined magnetic field, using the Cattaneo-Christov heat flux across a radially stretching sheet in the neighborhood of a stagnation point has been taken into consideration. Besides this, the impact of Brownian motion and thermal radiation are also analyzed. Furthermore, the impact of multiple slips and the permeability of the porous medium is studied in detail. A group of suitable similarity variables has been brought in for the reformation of non-linear PDEs defining the proposed flow model into a system of ODEs. For the extraction of the numerical results of the ODEs describing the proposed flow problem, the advantage of the efficiency of the shooting method has been taken. The concentration, velocity and temperature profiles have been investigated against diverse values of the significant flow parameters.

4.2 Mathematical Modeling

An analysis of a steady and laminar flow using incompressible Carreau nanofluid in the vicinity of a stagnation point past a chemically reacting radially stretched surface by incorporating Cattaneo-Christov model has been considered. Considering an inclined magnetic field and multiple slips, the fundamental characteristics of the flow will be analyzed. Moreover, the coordinate system is chosen in an appropriate fashion that the $r-$axis is taken in the direction of flow while $z-$axis normal to the flow. The velocity of the stretching sheet is assumed to be λU_w with $\lambda > 0$ and $U_w = ar$. Furthermore, the influence of Brownian movement and thermophoresis phenomena has been taken into account.

The problem describing the flow takes the following form[70, 71]:

$$\frac{\partial u}{\partial r} + \frac{u}{r} + \frac{\partial w}{\partial z} = 0, \tag{4.1}$$

$$u\frac{\partial C}{\partial r} + w\frac{\partial C}{\partial z} = D_B\frac{\partial^2 C}{\partial z^2} + \frac{D_T}{T_\infty}\frac{\partial^2 T}{\partial z^2} - C_r\left(C - C_\infty\right), \tag{4.2}$$

$$\begin{aligned} u\frac{\partial u}{\partial r} + w\frac{\partial u}{\partial z} = {} & \nu_f\frac{\partial^2 u}{\partial z^2}\left[1 + \Gamma^2\left(\frac{\partial u}{\partial z}\right)^2\right]^{\frac{n-1}{2}} + U_e\frac{dU_e}{dr} + g\beta_T(T - T_\infty) - \frac{\nu_f u}{k'} \\ & + \nu_f\left(n-1\right)\Gamma^2\frac{\partial^2 u}{\partial z^2}\left(\frac{\partial u}{\partial z}\right)^2\left[1 + \tau^2\left(\frac{\partial u}{\partial z}\right)^2\right]^{\frac{n-3}{2}} + g\beta_c(C - C_\infty) \\ & - \frac{\sigma B_0^2(u - U_e)\sin^2\alpha}{\rho_f}, \end{aligned} \tag{4.3}$$

$$\begin{aligned} & u\frac{\partial T}{\partial r} + w\frac{\partial T}{\partial z} + \lambda\left[u\frac{\partial u}{\partial r}\frac{\partial T}{\partial r} + w\frac{\partial w}{\partial z}\frac{\partial T}{\partial z} + u\frac{\partial w}{\partial r}\frac{\partial T}{\partial z} + w\frac{\partial u}{\partial z}\frac{\partial T}{\partial r} + u^2\frac{\partial^2 T}{\partial r^2} + w^2\frac{\partial^2 T}{\partial z^2}\right. \\ & \left. + 2uw\frac{\partial^2 T}{\partial r\partial z}\right] = \alpha_f\frac{\partial^2 T}{\partial z^2} + \tau\left[D_B\frac{\partial C}{\partial z}\frac{\partial T}{\partial z} + \frac{D_T}{T_\infty}\left(\frac{\partial T}{\partial z}\right)^2\right] + \frac{\sigma B_0^2\left(u - U_e\right)^2\sin^2\alpha}{(\rho c_p)_f} \\ & \qquad + \frac{Q_0\left(T - T_\infty\right)}{(\rho c_p)_f} - \frac{1}{(\rho c_p)_f}\frac{\partial q_r}{\partial z}. \end{aligned} \tag{4.4}$$

While several terms correspond to those discussed in the mathematical modeling section of Chapter 3, the remaining terms are delineated in detail below.

- $\left[1+\Gamma^2\left(\frac{\partial u}{\partial z}\right)^2\right]^{\frac{n-1}{2}}, \Gamma^2\left(\frac{\partial u}{\partial z}\right)^2\left[1+\tau^2\left(\frac{\partial u}{\partial z}\right)^2\right]^{\frac{n-3}{2}}$: Effects of Carreau nanofluid.

The radiative heat flux in the light of the Rosseland approximation can be formulated as

$$\frac{\partial q_r}{\partial z} = -\frac{16\sigma^* T_\infty^3}{3k^*}\frac{\partial^2 T}{\partial z^2}. \tag{4.5}$$

The surface conditions at the boundary are introduced in the following manner [72].

$$\begin{aligned} &w = w_0, \quad u = \lambda U_w + L\frac{\partial u}{\partial z}, \quad T = T_f + S'\frac{\partial T}{\partial z}, \quad C = C_f + k'\frac{\partial C}{\partial z} \quad \text{when } z = 0, \\ &u \to U_e = br, \quad C \to C_\infty, \quad T \to T_\infty \quad \text{as} \quad z \to \infty. \end{aligned} \tag{4.6}$$

A set of similarity variables is incorporated in the following form [70]:

$$\begin{aligned} &u = arf'(\eta), \quad \eta = \sqrt{\frac{a}{\nu_f}}\,z, \quad w = -2\sqrt{a\nu_f}\,f(\eta), \\ &\theta(\eta) = \frac{T - T_\infty}{T_f - T_\infty}, \qquad \phi(\eta) = \frac{C - C_\infty}{C_f - C_\infty}. \end{aligned} \tag{4.7}$$

By incorporating the similarity transformations in equations (4.1)-(4.4), the continuity equation is satisfied and the rest of the PDEs assume the following form.

$$\begin{aligned} &\left[1 + nWe^2 (f'')^2\right]\left[1 + We^2 (f'')^2\right]^{\frac{n-3}{2}} f''' + 2ff'' - Kf' + Gr\theta - f'^2 + A^2 + Gc\phi \\ &- M^2 (f' - A)\sin^2\alpha = 0, \end{aligned} \tag{4.8}$$

$$\begin{aligned} &\left(1 + \frac{4}{3}Rd - 4\zeta f^2\right)\theta'' + PrNb\theta'\phi' + PrNt\theta'^2 + 2Prf\theta' + PrQ\theta - 4\zeta ff'\theta' \\ &+ PrEcM^2 (f' - A)^2\, sin^2\alpha = 0, \end{aligned} \tag{4.9}$$

$$\phi'' + \frac{Nt}{Nb}\theta'' + Sc\,(2f\phi' - \gamma\phi) = 0. \tag{4.10}$$

The corresponding conditions at the boundary are given by

$$\begin{aligned} & f(0)=S,\ f'(0)=\lambda+\delta f''(0),\ f'\to A, \quad \text{as} \quad \eta\to\infty, \\ & \theta(0)=1+\omega\theta'(0),\ \phi(0)=1+\chi\phi'(0),\ \theta\to 0,\ \phi\to 0 \ \text{ as } \ \eta\to\infty. \end{aligned} \tag{4.11}$$

The formulae of the dimensionless parameters incorporated in the above equations are listed below.

$$\begin{aligned} & Nb=\frac{\tau D_B\left(C_f-C_\infty\right)}{\nu_f},\ Pr=\frac{\nu_f}{\alpha},\ Nt=\frac{\tau D_T\left(T_f-T_\infty\right)}{\nu_f T_\infty},\ M^2=\frac{\sigma B_0^2}{\rho a}, \\ & Q=\frac{Q_0}{\rho c_p a},\ Rd=\frac{4T_\infty\sigma^*}{k^*\left(\alpha\rho c_p\right)},\quad Ec=\frac{a^2r^2}{\alpha c_p\left(T_f-T_\infty\right)},\ A=\frac{b}{a},\ Sc=\frac{\nu_f}{D_B}, \\ & Gr=\frac{g\beta_T\left(T_f-T_\infty\right)}{a^2r},\quad Gc=\frac{g\beta_c\left(C_f-C_\infty\right)}{a^2r},\ S=-\frac{w_o}{\sqrt{a\nu_f}},\quad \gamma=\frac{C_r}{a}, \\ & \omega=\sqrt{\frac{a}{\nu}}S',\ \chi=\sqrt{\frac{a}{\nu}}K',\ \delta=\sqrt{\frac{a}{\nu}}L,\ K=\frac{\nu}{k'a},\ \zeta=\lambda a,\ We^2=\frac{\Gamma^2a^3r^2}{\nu_f}. \end{aligned} \tag{4.12}$$

The skin-friction coefficient, Nusselt number and Sherwood number in the dimensional form are formulated as follows:

$$C_f=\frac{\tau_w}{\rho_f U_w^2},\ Nu=\frac{rq_w}{k_f\left(T_f-T_\infty\right)},\ Sh=\frac{rq_m}{D_B\left(C_f-C_\infty\right)}. \tag{4.13}$$

Given below are the formulae for τ_w, q_w and q_m.

$$\begin{aligned} & \tau_w=\mu\left(\frac{\partial u}{\partial z}\right)_{z=0}\left[1+\Gamma^2\left(\frac{\partial u}{\partial z}\right)^2\right]_{z=0}^{\frac{n-1}{2}},\quad q_w=-k_f\left[\left(\frac{\partial T}{\partial z}\right)-\frac{q_r}{k_f}\right]_{z=0}, \\ & q_m=-D_B\left(\frac{\partial C}{\partial z}\right)_{z=0}. \end{aligned} \tag{4.14}$$

The dimensionless form of skin-friction coefficient, Nusselt number and Sherwood number achieved through the similarity transformation is as follows.

$$\begin{aligned} & Re^{\frac{1}{2}}C_f=f''(0)\left[1+We^2f''^2(0)\right]^{\frac{n-1}{2}},\quad Re^{-\frac{1}{2}}Nu=-\left[1+\frac{4}{3}Rd\right]\theta'(0), \\ & Re^{-\frac{1}{2}}Sh=-\phi'(0), \end{aligned} \tag{4.15}$$

where $Re = \dfrac{rU_w}{\nu_f}$ elucidates the local Reynolds number.

4.3 Method of Solution

For the numerical treatment of ODEs together with the boundary conditions (4.8)-(4.11), the shooting method has been opted. The missing initial conditions $f''(0)$, $\theta(0)$ and $\phi(0)$ have been denoted as s, l and q, respectively. As a procedural requirement, the following notations have also been introduced.

$$
\begin{aligned}
&f = y_1, f' = y_2, f'' = y_3, \theta = y_4, \theta' = y_5, \phi = y_6, \phi' = y_7, \frac{\partial f}{\partial s} = y_8, \frac{\partial f'}{\partial s} = y_9,\\
&\frac{\partial f''}{\partial s} = y_{10}, \frac{\partial \theta}{\partial s} = y_{11}, \frac{\partial \theta'}{\partial s} = y_{12}, \frac{\partial \phi}{\partial s} = y_{13}, \frac{\partial \phi'}{\partial s} = y_{14}, \frac{\partial f}{\partial l} = y_{15}, \frac{\partial f'}{\partial l} = y_{16},\\
&\frac{\partial f''}{\partial l} = y_{17}, \frac{\partial \theta}{\partial l} = y_{18}, \frac{\partial \theta'}{\partial l} = y_{19}, \frac{\partial \phi}{\partial l} = y_{20}, \frac{\partial \phi'}{\partial l} = y_{21}, \frac{\partial f}{\partial q} = y_{22}, \frac{\partial f'}{\partial q} = y_{23},\\
&\frac{\partial f''}{\partial q} = y_{24}, \frac{\partial \theta}{\partial q} = y_{25}, \frac{\partial \theta'}{\partial q} = y_{26}, \frac{\partial \phi}{\partial q} = y_{27}, \frac{\partial \phi'}{\partial q} = y_{28}.
\end{aligned} \tag{4.16}
$$

Using the above notations, equations (4.8)-(4.10) are transformed into the following first order ODEs. Furthermore, the differentiation of these first seven ODEs w.r.t s, l and q, respectively, yields the remaining twenty one ODEs.

$$
\begin{aligned}
&y_1' = y_2, && y_1(0) = S,\\
&y_2' = y_3, && y_2(0) = \lambda + \delta s,\\
&y_3' = \frac{y_2^2 + Ky_2 + M^2 sin^2\alpha\,(y_2 - A) - 2y_1y_3 - A^2 - Gry_4 - Gcy_6}{(1 + nWe^2y_3^2)\,(1 + We^2y_3^2)^{\frac{n-3}{2}}}, && y_3(0) = s,\\
&y_4' = y_5, && y_4(0) = 1 + \omega l,\\
&y_5' = \frac{-1}{\left(1 + \frac{4}{3}Rd - 4\zeta y_1^2\right)}\Big[PrNby_5y_7 + PrNty_5^2 + 2Pry_1y_5 + PrQy_4 &&\\
&\quad + PrEcM^2(y_2 - A)^2 sin^2\alpha - 4\zeta y_1y_2y_5\Big] && y_6(0) = l,\\
&y_6' = y_7, && y_6(0) = 1 + \chi q,\\
&y_7' = -\left(\tfrac{Nt}{Nb}\right) y_5' - Sc\,(2y_1y_7 - \gamma y_6)\,, && y_7(0) = q,\\
&y_8' = y_9, && y_8(0) = 0,
\end{aligned}
$$

$$
\begin{aligned}
y_9' &= y_{10}, && y_9(0)=\delta,\\
y_{10}' &= \frac{1}{\left(1+nWe^2y_3^2\right)^2\left(1+We^2y_3^2\right)^{n-3}}\\
&\quad\Bigg[\Bigg(\left[1+nWe^2y_3^2\right]\left[1+We^2y_3^2\right]^{\frac{n-3}{2}}\left[\,\left(2y_2+M^2\sin^2\alpha+K\right)y_9\right.\\
&\quad\left.-Gry_{11}-Gcy_{13}-2\left(y_1y_{10}+y_3y_8\right)\right]\Bigg)-\Bigg(\Big(y_2^2+M^2(y_2-A)\sin^2\alpha\\
&\quad-2y_1y_3-A^2+Ky_2-Gry_4-Gcy_6\Big)\left[1+We^2y_3^2\right]^{\frac{n-5}{2}}\\
&\quad\left(2We^2y_3y_{10}\right)\left(\tfrac{n-3}{2}\left[1+nWe^2y_3^2\right]+n\left[1+We^2y_3^2\right]\right)\Bigg)\Bigg], && y_{10}(0)=1,\\
y_{11}' &= y_{12}, && y_{11}(0)=0,\\
y_{12}' &= \frac{-1}{\left(1+\frac{4}{3}Rd-4\zeta y_1^2\right)^2}\Bigg[\left(1+\tfrac{4}{3}Rd-4\zeta y_1^2\right)\Bigg\{\Big(PrNby_7+2PrNty_5\\
&\quad+2Pry_1-4\zeta y_1y_2\Big)y_{12}+Pr\left(Nby_5y_{14}+Qy_{11}+2y_5y_8\right)-4\zeta y_2y_5y_8\\
&\quad+\left(2PrEcM^2(y_2-A)\sin^2\alpha-4\zeta y_1y_5\right)y_9\Bigg\}+8\zeta y_1y_8\Big(PrNby_5y_7\\
&\quad+PrNty_5^2+2Pry_1y_5+PrQy_4+PrEcM^2(y_2-A)^2sin^2\alpha\\
&\quad-4\zeta y_1y_2y_5\Big)\Bigg] && y_{12}(0)=0,\\
y_{13}' &= y_{14}, && y_{13}(0)=0,\\
y_{14}' &= -\left(\tfrac{Nt}{Nb}\right)y_{12}'-2Sc\big(y_1y_{14}+y_7y_8\big)+Sc\gamma y_{13}, && y_{14}(0)=0,\\
y_{15}' &= y_{16}, && y_{15}(0)=0,\\
y_{16}' &= y_{17}, && y_{16}(0)=0,\\
y_{17}' &= \frac{1}{\left(1+nWe^2y_3^2\right)^2\left(1+We^2y_3^2\right)^{n-3}}\\
&\quad\Bigg[\Bigg(\left[1+nWe^2y_3^2\right]\left[1+We^2y_3^2\right]^{\frac{n-3}{2}}\left[\,\left(2y_2+M^2\sin^2\alpha+K\right)y_{16}\right.\\
&\quad\left.-Gry_{18}-Gcy_{20}-2\left(y_1y_{17}+y_3y_{15}\right)\right]\Bigg)-\Bigg(\Big(y_2^2+M^2(y_2-A)\sin^2\alpha\\
&\quad-2y_1y_3-A^2+Ky_2-Gry_4-Gcy_6\Big)\left[1+We^2y_3^2\right]^{\frac{n-5}{2}}\\
&\quad\left(2We^2y_3y_{17}\right)\left(\tfrac{n-3}{2}\left[1+nWe^2y_3^2\right]+n\left[1+We^2y_3^2\right]\right)\Bigg)\Bigg], && y_{17}(0)=0,\\
y_{18}' &= y_{19}, && y_{18}(0)=\omega,
\end{aligned}
$$

$$y'_{19} = \frac{-1}{\left(1+\frac{4}{3}Rd-4\zeta y_1^2\right)^2}\Bigg[\left(1+\tfrac{4}{3}Rd-4\zeta y_1^2\right)\Big\{\big(PrNby_7+2PrNty_5$$
$$+2Pry_1-4\zeta y_1y_2\big)y_{19}+Pr\left(Nby_5y_{21}+Qy_{18}+2y_5y_{15}\right)-4\zeta y_2y_5y_{15}$$
$$+\big(2PrEcM^2(y_2-A)\sin^2\alpha-4\zeta y_1y_5\big)y_{16}\Big\}+8\zeta y_1y_{15}\big(PrNby_5y_7$$
$$+PrNty_5^2+2Pry_1y_5+PrQy_4+PrEcM^2(y_2-A)^2sin^2\alpha$$
$$-4\zeta y_1y_2y_5\big)\Bigg] \qquad y_{19}(0)=0,$$

$$y'_{20} = y_{21}, \qquad y_{20}(0)=0,$$

$$y'_{21} = -\left(\tfrac{Nt}{Nb}\right)y'_{19}-2Sc\big(y_1y_{21}+y_7y_{15}\big)+Sc\gamma y_{20}, \qquad y_{21}(0)=0,$$

$$y'_{22} = y_{23}, \qquad y_{22}(0)=0,$$

$$y'_{23} = y_{24}, \qquad y_{23}(0)=0,$$

$$y'_{24} = \frac{1}{(1+nWe^2y_3^2)^2\,(1+We^2y_3^2)^{n-3}}$$
$$\Bigg[\Bigg(\left[1+nWe^2y_3^2\right]\left[1+We^2y_3^2\right]^{\frac{n-3}{2}}\Big[\left(2y_2+M^2\sin^2\alpha+K\right)y_{23}$$
$$-Gry_{25}-Gcy_{27}-2\left(y_1y_{24}+y_3y_{22}\right)\Big]\Bigg)-\Bigg(\Big(y_2^2+M^2(y_2$$
$$-A)\sin^2\alpha-2y_1y_3-A^2+Ky_2-Gry_4-Gcy_6\Big)\left[1+We^2y_3^2\right]^{\frac{n-5}{2}}$$
$$(2We^2y_3y_{24})\left(\tfrac{n-3}{2}\left[1+nWe^2y_3^2\right]+n\left[1+We^2y_3^2\right]\right)\Bigg)\Bigg], \qquad y_{24}(0)=0,$$

$$y'_{25} = y_{26} \qquad y_{25}(0)=0,$$

$$y'_{26} = \frac{-1}{\left(1+\frac{4}{3}Rd-4\zeta y_1^2\right)^2}\Bigg[\left(1+\tfrac{4}{3}Rd-4\zeta y_1^2\right)\Big\{\big(PrNby_7+2PrNty_5$$
$$+2Pry_1-4\zeta y_1y_2\big)y_{26}+Pr\left(Nby_5y_{28}+Qy_{25}+2y_5y_{22}\right)-4\zeta y_2y_5y_{22}$$
$$+\big(2PrEcM^2(y_2-A)\sin^2\alpha-4\zeta y_1y_5\big)y_{23}\Big\}+8\zeta y_1y_{22}\big(PrNby_5y_7$$
$$+PrNty_5^2+2Pry_1y_5+PrQy_4+PrEcM^2(y_2-A)^2sin^2\alpha$$
$$-4\zeta y_1y_2y_5\big)\Bigg] \qquad y_{26}(0)=0,$$

$$y'_{27} = y_{28}, \qquad y_{27}(0)=\chi,$$

$$y'_{28} = -\left(\tfrac{-Nt}{Nb}\right)y'_{26}-2Sc\big(y_1y_{28}+y_7y_{22}\big)+Sc\gamma y_{27}, \qquad y_{28}(0)=1.$$

With the aim of solving the above initial value problem, the RK-4 method has been employed. For the sake of numerical results, the domain of the problem is supposed to be bounded and considered as $[0, \eta_\infty]$. The value of η_∞ is selected to be a positive finite real number with the property that the increasing values of η_∞ do not cause influensive variations in the solution. For the system of equations mentioned above, the missing initial conditions are selected in order to ensure that

$$\left(y_2\left(s,l,q\right)\right)_{\eta=\eta_\infty} = A, \;\; \left(y_4(s,l,q)\right)_{\eta=\eta_\infty} = 0, \;\; \left(y_6(s,l,q)\right)_{\eta=\eta_\infty} = 0. \tag{4.17}$$

The Newton's iterative scheme has been employed for solving the above algebraic equations.

$$\begin{bmatrix} s^{(k+1)} \\ l^{(k+1)} \\ q^{(k+1)} \end{bmatrix} = \begin{bmatrix} s^{(k)} \\ l^{(k)} \\ q^{(k)} \end{bmatrix} - \left[\begin{bmatrix} \frac{\partial y_2(s,l,q)}{\partial s} & \frac{\partial y_2(s,l,q)}{\partial l} & \frac{\partial y_2(s,l,q)}{\partial q} \\ \frac{\partial y_4(s,l,q)}{\partial s} & \frac{\partial y_4(s,l,q)}{\partial l} & \frac{\partial y_4(s,l,q)}{\partial q} \\ \frac{\partial y_6(s,l,q)}{\partial s} & \frac{\partial y_6(s,l,q)}{\partial l} & \frac{\partial y_6(s,l,q)}{\partial q} \end{bmatrix}^{-1} \begin{bmatrix} y_2 - A \\ y_4 \\ y_6 \end{bmatrix}\right]_{\left(s^{(k)},\; l^{(k)},\; q^{(k)},\; \eta_\infty\right)},$$

$$\begin{bmatrix} s^{(k+1)} \\ l^{(k+1)} \\ q^{(k+1)} \end{bmatrix} = \begin{bmatrix} s^{(k)} \\ l^{(k)} \\ q^{(k)} \end{bmatrix} - \left[\begin{bmatrix} y_9 & y_{16} & y_{23} \\ y_{11} & y_{18} & y_{25} \\ y_{13} & y_{20} & y_{27} \end{bmatrix}^{-1} \begin{bmatrix} y_2 - A \\ y_4 \\ y_6 \end{bmatrix}\right]_{\left(s^{(k)},\; l^{(k)},\; q^{(k)},\; \eta_\infty\right)},$$

where k represents the iteration level of the scheme.

For the termination of the numerical procedure and to obtain the numerical solution, the stopping criteria has been set as:

$$max\{(|y_2(\eta_\infty) - A|, \; |y_4(\eta_\infty)|, |y_6(\eta_\infty)|)\} < \epsilon, \tag{4.18}$$

where ϵ has been chosen as 10^{-12}. During this analysis, η_∞ is selected as 7.

4.4 Results with Discussion

The numerical solutions of the proposed model for various choices of the values of some important pertinent flow parameters have been included in this segment. The significant numerical results of the skin-friction coefficient, Sherwood and Nusselt numbers are illustrated in the tabular form.

4.4.1 Skin-friction Coefficient, Nusselt and Sherwood Numbers

To validate the MATLAB code for the shooting method, the values of $-f''(0)$ are replicated for the problem addressed by Ramesh et al. [72] and Cortell [73].

TABLE 4.1: Comparison of the present results of $-f''(0)$ with those published in the literature, in the absence of irrelevant parameters.

	$-f''(0)$ for various values of M		
M	Ramesh et. al [72]	Cortell [73]	Present
0	1.00006	1.000	1.00006253
0.5	1.22475	1.224	1.22474606
1.0	1.41421	1.414	1.41421360
1.5	1.58114	1.581	1.58113883
2.0	1.73205	1.732	1.73205081

On the other hand, an escalation has been seen in the mass transfer rate as χ, Sc, Ec and Pr assume the higher values whereas the magnitude of the skin-friction coefficient and heat transfer rate declines remarkably. Furthermore, the skin-friction coefficient appears to be a decreasing function of S, Q and γ whereas an opposite trend has been remarked for the heat and mass transfer rates.

Table 4.1 reflects a great settlement between the numerical values obtained by the present code and those already existing in the mentioned articles. Tables 4.2-4.3

disclose the numerical results of skin-friction coefficient accompanied by Sherwood and Nusselt numbers by varying different parameters like We, M, A, K, α, Gr, Gc, λ, S, ζ, Rd, Pr, Q, Nb, Nt, Ec, Sc, γ, ω and χ, for the proposed model.

Table 4.2: The computed results of skin-friction coefficient, Nusselt and Sherwood numbers for $Rd = Pr = Q = Ec = Sc = \gamma = \omega = \chi = 0.1,\ Nb = Nt = 0.5$, where $b_1 = \left(1 + We^2 f''^2(0)\right)^{\frac{n-1}{2}}$ and $b_2 = \left(1 + \frac{4}{3}Rd\right)$.

We	M	A	α	K	Gc	S	Gr	ζ	λ	$b_1 f''(0)$	$-b_2\theta'(0)$	$-\phi'(0)$
0.1	1.0	0.1	0.1	0.1	1.0	0.2	2.0	0.1	1.0	0.28187	0.29346	0.21313
0.5										0.28820	0.29349	0.21301
0.9										0.39577	0.29376	0.20772
	1.5									0.28107	0.29342	0.21291
	2.0									0.27994	0.29335	0.21260
		1								0.34508	0.22828	0.37196
		2								0.41940	0.11283	0.53137
			0.5							0.26627	0.29268	0.20932
			0.9							0.22561	0.29126	0.20298
				1.1						0.28193	0.29216	0.21414
				2.1						0.38008	0.25467	0.15276
					1.4					0.30445	0.28659	0.23236
					1.8					0.32082	0.27906	0.24986
						0.8				0.25771	0.31217	0.24885
						1.4				-0.11737	0.34092	0.28098
							2.5			0.30582	0.28968	0.22278
							3.0			0.32348	0.28545	0.23228
								0.5		0.37958	0.28249	0.17039
								0.9		0.36975	0.23376	0.14340
									2.0	-0.36647	0.28271	0.25416
									3.0	-0.51143	0.25391	0.31231

The conclusions deduced from the numerical solutions indicate that the higher values of We and Rd escalate the magnitude of the skin-friction coefficient and heat transfer rate whereas a depreciation has been observed in the mass transfer rate.

Moreover, the magnitude of the skin-friction coefficient, Nusselt and Sherwood numbers falls off marginally as the values of M, α and ζ go up.

Table 4.3: The computed results of skin-friction coefficient, Nusselt and Sherwood numbers for $\lambda = M = Gc = 1, We = A = K = \alpha = \zeta = 0.1,\ S = 0.2,\ Gr = 2$, where $b_1 = \left(1 + We^2 f''^2(0)\right)^{\frac{n-1}{2}}$ and $b_2 = \left(1 + \frac{4}{3}Rd\right)$.

Rd	Q	Pr	Ec	Nt	Nb	γ	Sc	χ	ω	$b_1 f''(0)$	$-b_2\theta'(0)$	$-\phi'(0)$
0.1	0.1	0.1	0.1	0.5	0.5	0.1	0.1	0.1	0.1	0.28187	0.29346	0.21313
0.3										0.28192	0.36725	0.21004
0.5										0.28198	0.44099	0.20796
	0.4									0.23139	0.37734	0.60041
	0.7									0.19676	0.39392	0.88168
		1.1								0.21923	1.22344	-0.53731
		2.1								0.19262	1.66756	-0.91242
			0.3							0.28099	0.31419	0.19662
			0.5							0.28014	0.33439	0.18051
				1.5						0.30248	0.16737	0.23854
				2.5						0.30939	0.11328	0.30629
					1.5					0.26973	0.31788	0.28265
					2.5					0.26831	0.30672	0.30293
						0.4				0.27717	0.30933	0.25797
						0.7				0.27291	0.32161	0.29921
							0.2			0.27409	0.29466	0.20883
							0.3			0.26537	0.29573	0.20472
								0.3		0.27923	0.29979	0.19414
								0.5		0.27694	0.30506	0.17830
									0.4	0.27114	0.27779	0.21484
									0.3	0.25969	0.26277	0.21711

In addition to this, it has been sighted that by assuming the larger values of A, Gc, Gr and Nt into account, the skin-friction coefficient and mass transfer rate climb significantly while a declining behaviour has been observed in the case of Nusselt number. Besides, the higher assumption of λ, Nb and ω results in a decrement in the skin-friction coefficient and Nusselt number while Sherwood number escalates substantially. Furthermore, the skin-friction coefficient depicts an escalating demeanour whereas a declining effect has been observed in the magnitude of Sherwood and Nusselt numbers with the rise in the values of K.

4.4.2 The Velocity, Temperature and Concentration Profiles

Figures 4.2 and 4.3 are delineated to highlight the effect of n and We on the velocity distribution. It has been remarked that the velocity of the fluid can be observed to depress as n and We assume the higher values. Moreover, the associated momentum boundary layer thickness also experiences a significant decrement in the magnitude.

The impact of M on the velocity, concentration and temperature distributions has been illustrated through Figures 4.4-4.6. An abrupt growth has been seen in the concentration and temperature configurations while the velocity of the fluid drops subsequently in the presence of the higher magnetic field. This stems from the fact that the applied magnetic field generates an opposing force, commonly described as Lorentz force, which is the key ingredient behind the dramatic decline in the fluid's motion which further results in a decrement in the momentum boundary layer thickness whereas a substantial increment has been noticed in the concentration and thermal boundary layer thickness.

Figures 4.7-4.8 are sketched to emphasize the influence of A on the velocity and temperature profiles. By the inclusion of the values of A greater than 1, a sudden escalation has been observed in the velocity. Perversely, the flow velocity drops significantly by taking into account the values of A lesser than 1. Moreover, the temperature distribution de-escalates for the higher assumption of A. This reflects the fact that the heat exchange from the surface to the fluid becomes smaller as the value of A escalates and therefore, the temperature drops and the related thermal boundary layer thickness is shrinked.

The effect on the temperature and concentration configurations by incorporating various values of Pr has been depicted through Figures 4.9-4.10. By definition, Prandtl number delineates the relationship between the thermal diffusivity and viscous diffusion rate. For the higher assumption of Pr, the thermal diffusion rate experiences diminution and ultimately, the fluid's temperature goes down drastically. As a consequence, a curtailment has been noted in the thermal boundary layer thickness. Concurrently, the fluid's nanoparticle volume fraction reflects a sudden growth as the magnitude of Pr heightens and an abrupt expansion can be seen in the thickness of the concentration boundary layer.

The influence of K and ζ on the velocity profile has been outlined through Figures 4.11-4.12. It is worth noticing that the velocity of the fluid accelerates for the eminent values of K and henceforth, an augmentation in the thickness of the momentum boundary layer can be observed. On the other hand, quite an opposite trend has been inspected by taking higher values of ζ into account.

Figures 4.13-4.14 are epitomized to represent the effect of Nt on the temperature and concentration distributions. It can be seen that the temperature as well as the concentration of the fluid go up by assuming higher values of Nt and likewise, an elevation can be noticed in the thickness of thermal and concentration boundary layer.

The impact of Nb on the concentration and temperature profiles is elucidated through Figures 4.15-4.16. As the value of Nb goes up, the fluid's temperature rises owing to the reason that the motility of the nanoparticles increases considerably, accelerating the nanoparticles' kinetic energy which leads to a sudden rise in the temperature and the associated thermal boundary layer thickness.

Figures 4.17-4.18 manifest the influence of Ec on the velocity and temperature configurations. In view of the physical meaning, Eckert number intrinsically set forth the ratio of the enthalpy and kinetic energy of the fluid particles. A prompt escalation in the kinetic energy of the fluid is witnessed by rising the values of Ec. Henceforth, the fluid's velocity and temperature climb marginally and as a result, thickness of the momentum and thermal boundary layer are enhanced. The impact of Gr, Q and Rd on the temperature profile is elucidated through Figures 4.19-4.21. The larger the values of Q and Rd being considered, the more the heat is produced, which leads to a sudden rise in the temperature and a significant increment can be seen in the thermal boundary layer thickness. However, it can be remarked that Gr has an opposite effect on the temperature distribution.

Figures 4.22-4.24 illustrate the effect of Gc, Sc and γ on the concentration fields. The fluid's concentration falls substantially by taking into account the larger values of Gc, Sc and γ, which further magnifies the associated concentration boundary layer thickness. Figure 4.25 is sketched to portray the influence of We and M on the skin-friction coefficient. It can be remarked from the figure that as the values of M and We climb, the surface's shear stress experiences an elevation. Figure 4.26 epitomizes the effect of γ and Sc on the Sherwood number. Eminently, the thermal energy gradient climbs marginally by taking into consideration the higher values of γ and Sc. Moreover, the impact of Rd and Nb on the Nusselt number is pictured in Figure 4.27. Undoubtedly it can be observed that as the values of Rd and Nb rises, the mass transfer gradient observes an augmentation in the magnitude.

$K = \omega = \delta = We = n = A = Q = Ec = \alpha = \Gamma = \chi = Sc = 0.1$ $Nt = Nb = B_{i1} = B_{i2} = 0.5, M = Rd = Pr = \gamma = Gc = 1, Gr = 2, \lambda = -1, S = 0.2$

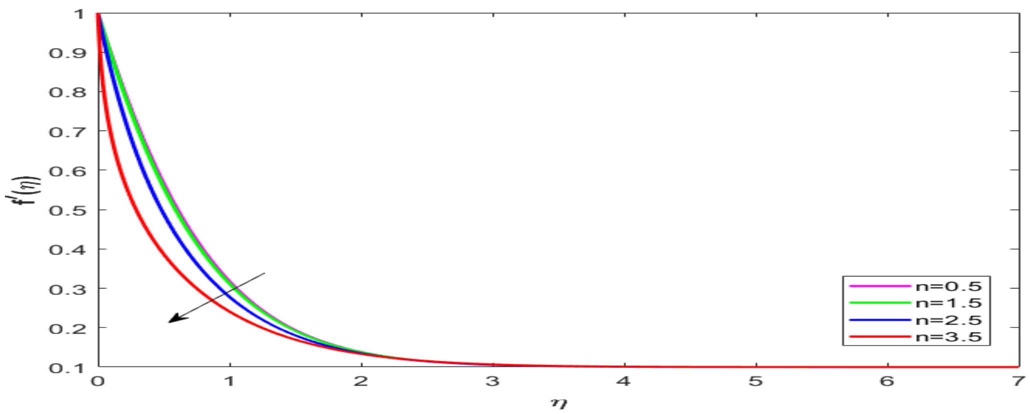

FIGURE 4.1: Effect of n on $f'(\eta)$ when $K = \omega = \delta = We = A = Q = Ec = \alpha = \Gamma = \chi = Sc = 0.1,\ Nt = Nb = 0.5,\ M = Rd = Pr = \gamma = Gc = 1,\ Gr = 2,\ \lambda = -1,\ S = 0.2$

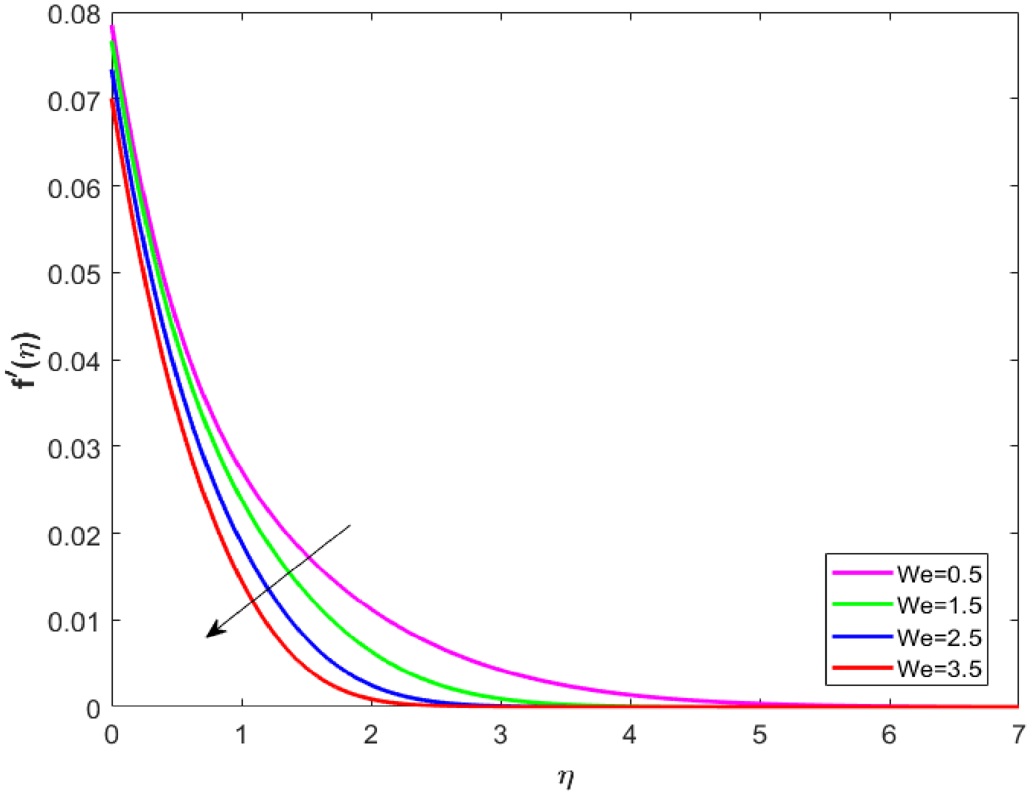

FIGURE 4.2: Effect of We on $f'(\eta)$ when $K = \omega = \delta = n = A = Q = Ec = \alpha = \Gamma = \chi = Sc = 0.1,\ Nt = Nb = 0.5,\ M = Rd = Pr = \gamma = Gc = 1,\ Gr = 2,\ \lambda = -1,\ S = 0.2$

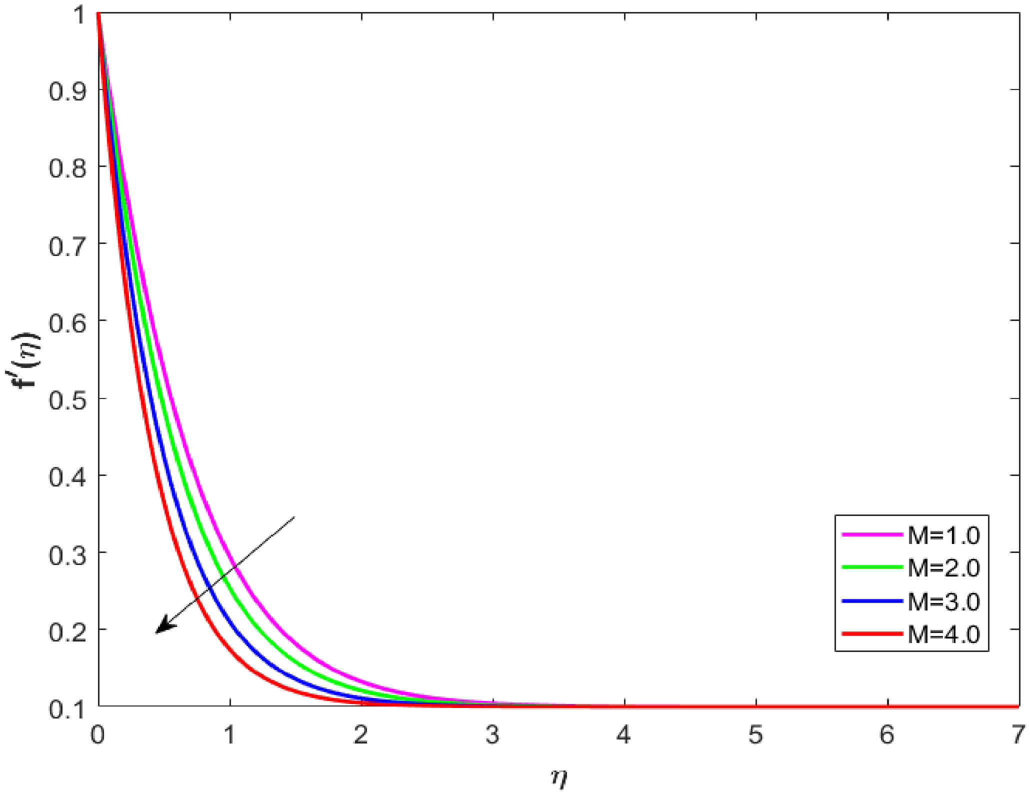

FIGURE 4.3: Effect of M on $f'(\eta)$ when $K = \omega = \delta = We = n = A = Q = Ec = \alpha = \Gamma = \chi = Sc = 0.1,\ Nt = Nb = 0.5,\ Rd = Pr = \gamma = Gc = 1,\ Gr = 2, \lambda = -1, S = 0.2$

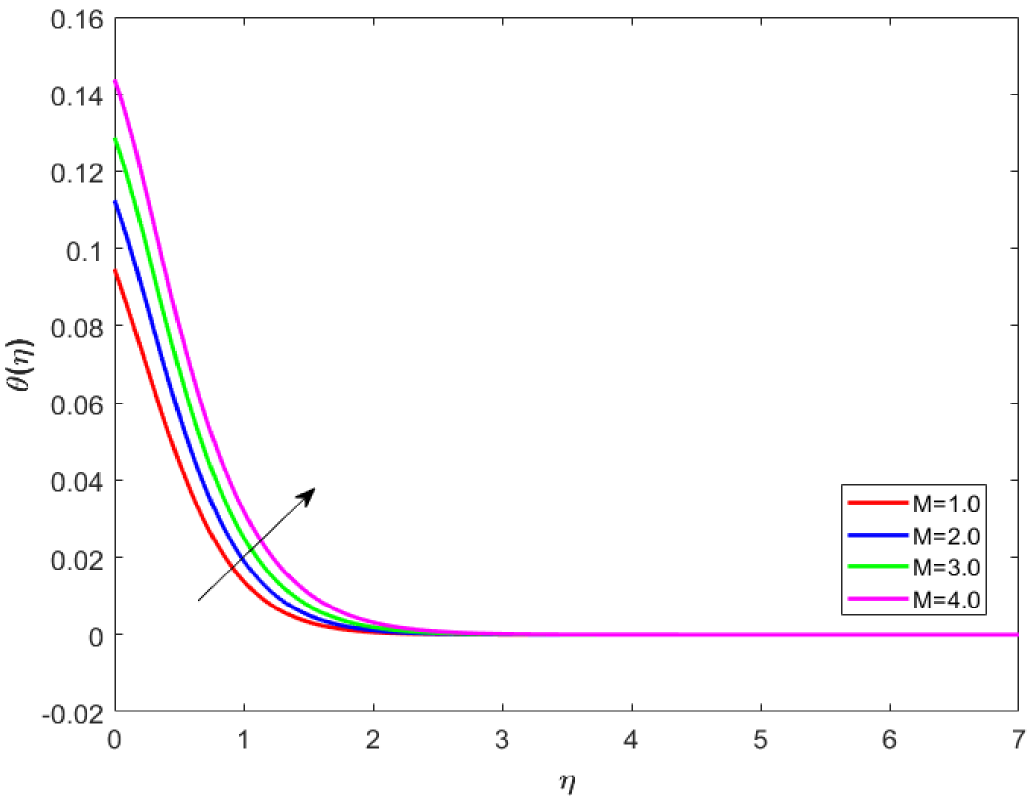

FIGURE 4.4: Effect of M on $\theta(\eta)$ when $K = \omega = \delta = We = n = A = Q = Ec = \alpha = \Gamma = \chi = Sc = 0.1,\ Nt = Nb = 0.5,\ Rd = Pr = \gamma = Gc = 1,\ Gr = 2,\ S = 0.2$

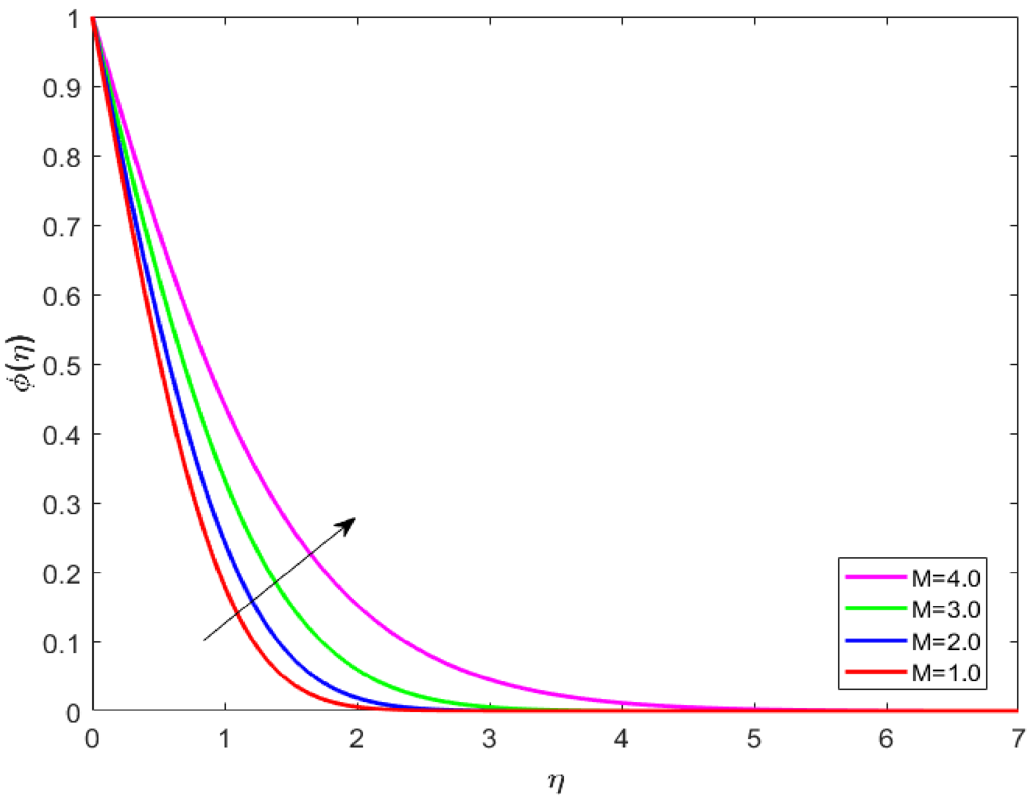

FIGURE 4.5: Effect of M on $\phi(\eta)$ $K = \omega = \delta = We = n = A = Q = Ec = \alpha = \Gamma = \chi = Sc = 0.1,\ Nt = Nb = 0.5,\ Rd = Pr = \gamma = Gc = 1,\ Gr = 2,\ \lambda = -1,\ S = 0.2$

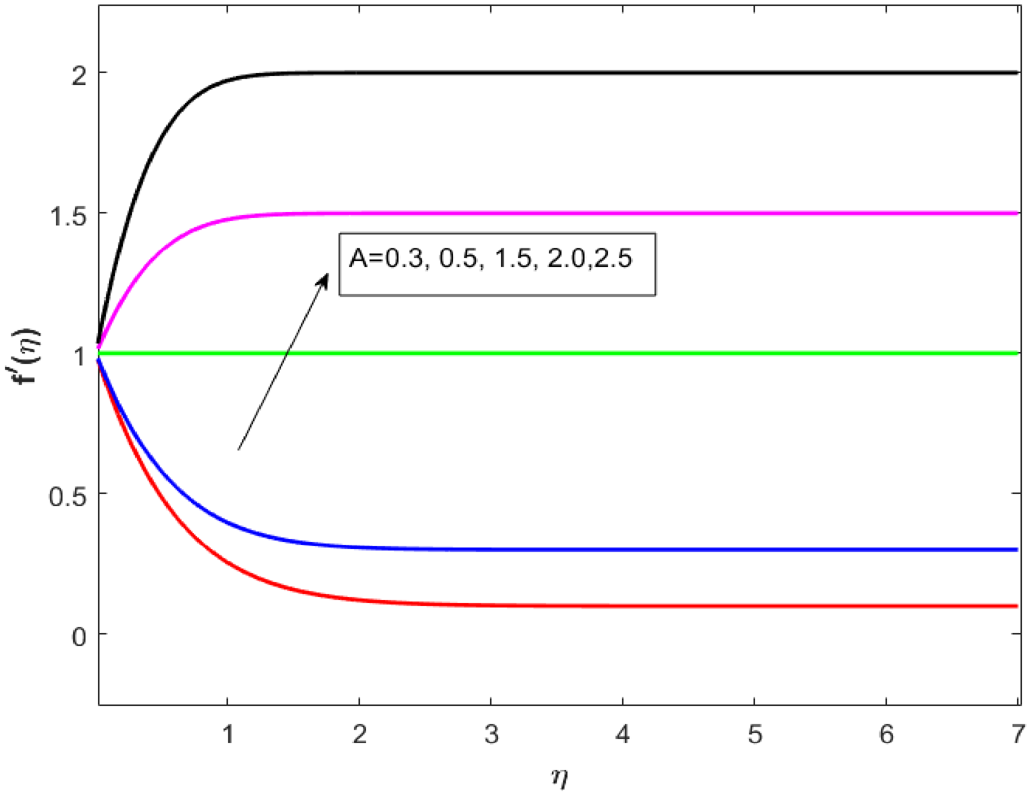

FIGURE 4.6: Effect of A on $f'(\eta)$ when $K = \omega = \delta = We = n = Q = Ec = \alpha = \Gamma = \chi = Sc = 0.1,\ Nt = Nb = 0.5,\ M = Rd = Pr = \gamma = Gc = 1,\ Gr = 2,\ \lambda = -1,\ S = 0.2$

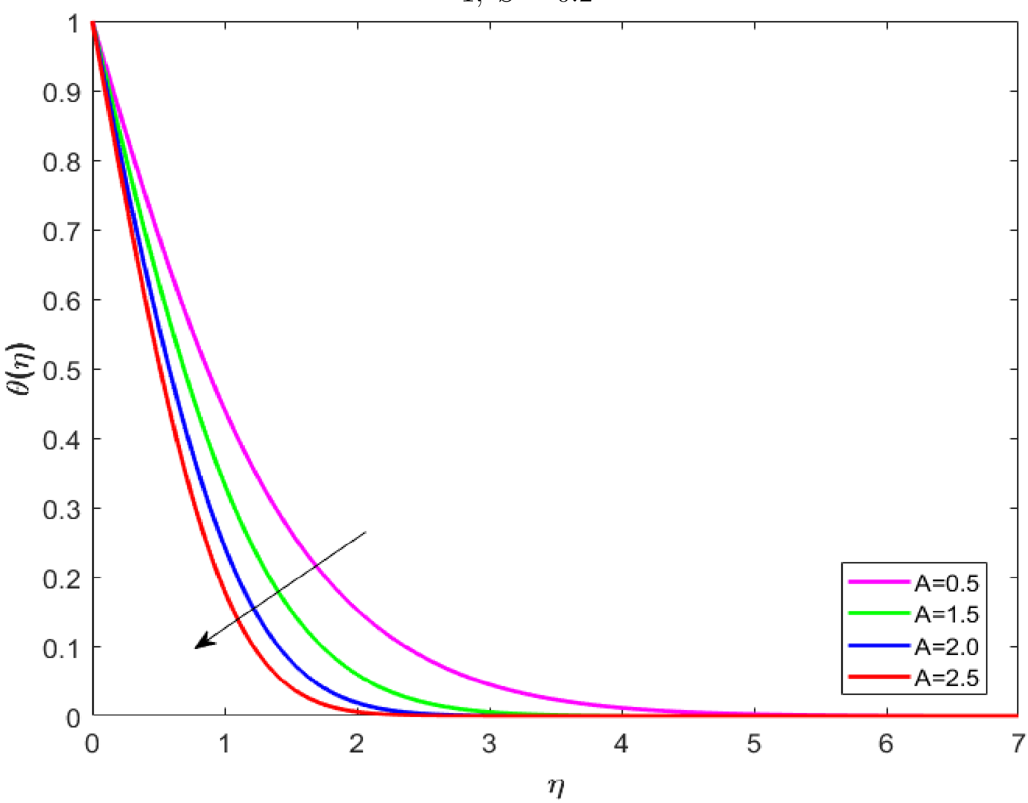

FIGURE 4.7: Effect of A on $\theta(\eta)$ when $K = \omega = \delta = We = n = Q = Ec = \alpha = \Gamma = \chi = Sc = 0.1,\ Nt = Nb = 0.5,\ M = Rd = Pr = \gamma = Gc = 1,\ Gr = 2,\ \lambda = -1,\ S = 0.2$

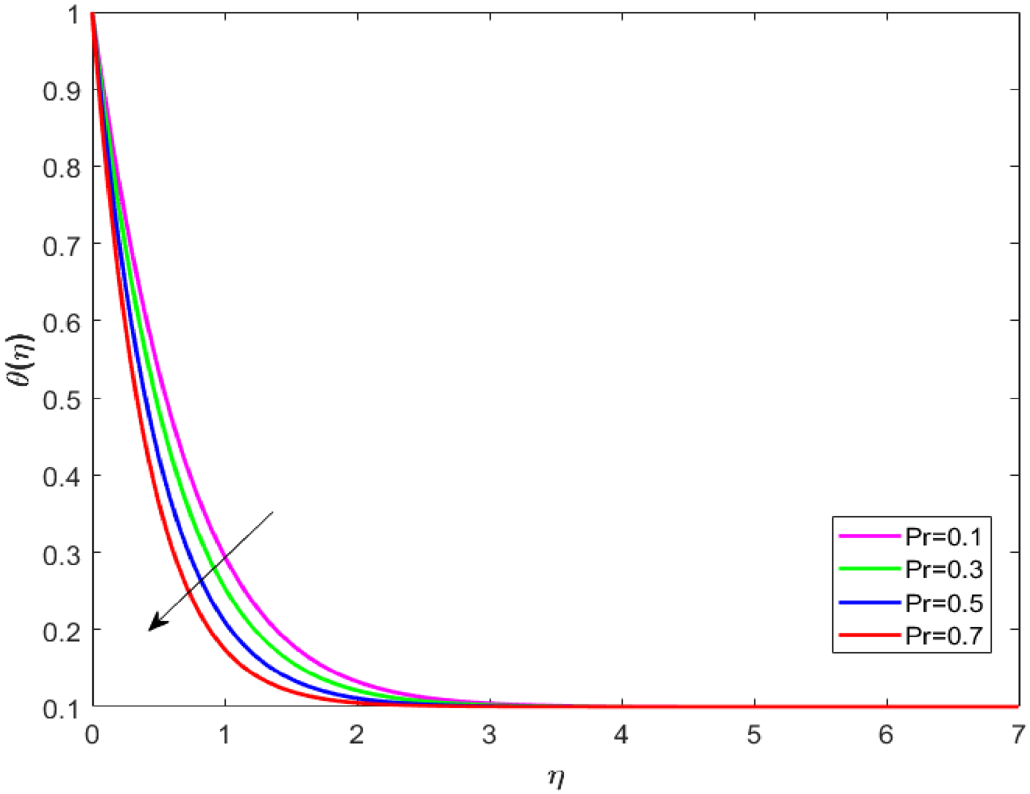

FIGURE 4.8: Effect of Pr on $\theta(\eta)$ when $K = \omega = \delta = We = n = A = Q = Ec = \alpha = \Gamma = \chi = Sc = 0.1,\ Nt = Nb = 0.5,\ M = Rd = \gamma = Gc = 1,\ Gr = 2,\ \lambda = -1,\ S = 0.2$

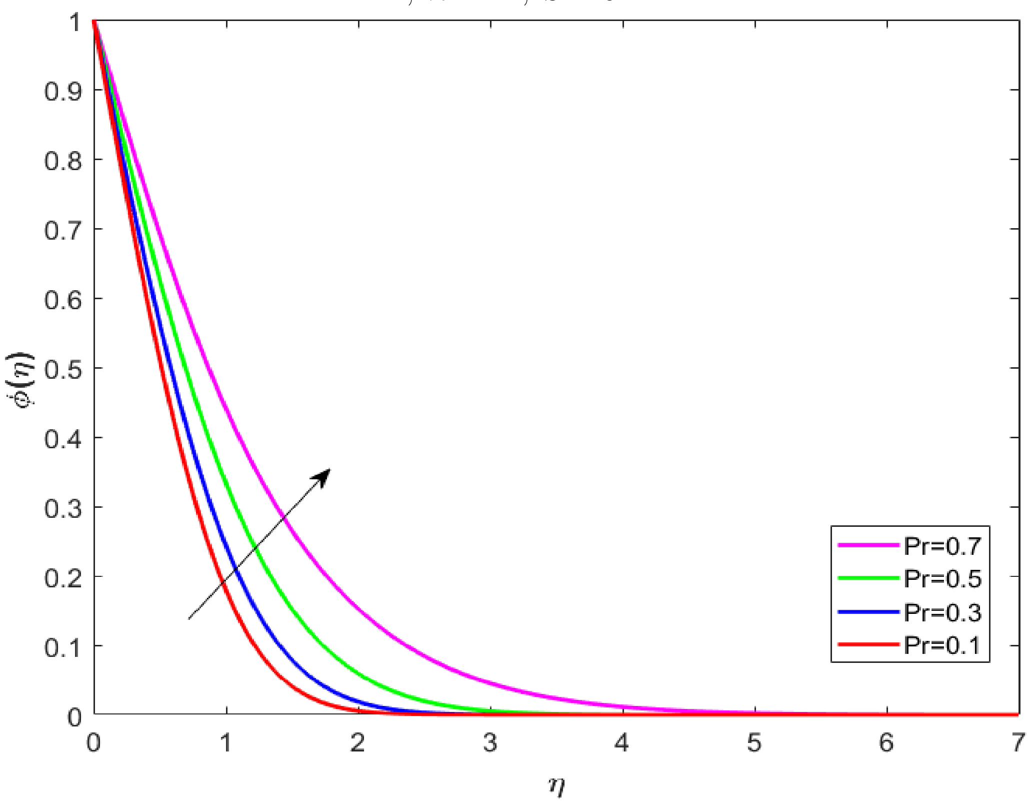

FIGURE 4.9: Effect of Pr on $\phi(\eta)$ when $K = \omega = \delta = We = n = A = Q = Ec = \alpha = \Gamma = \chi = Sc = 0.1,\ Nt = Nb = 0.5,\ M = Rd = \gamma = Gc = 1,\ Gr = 2,\ \lambda = -1,\ S = 0.2$

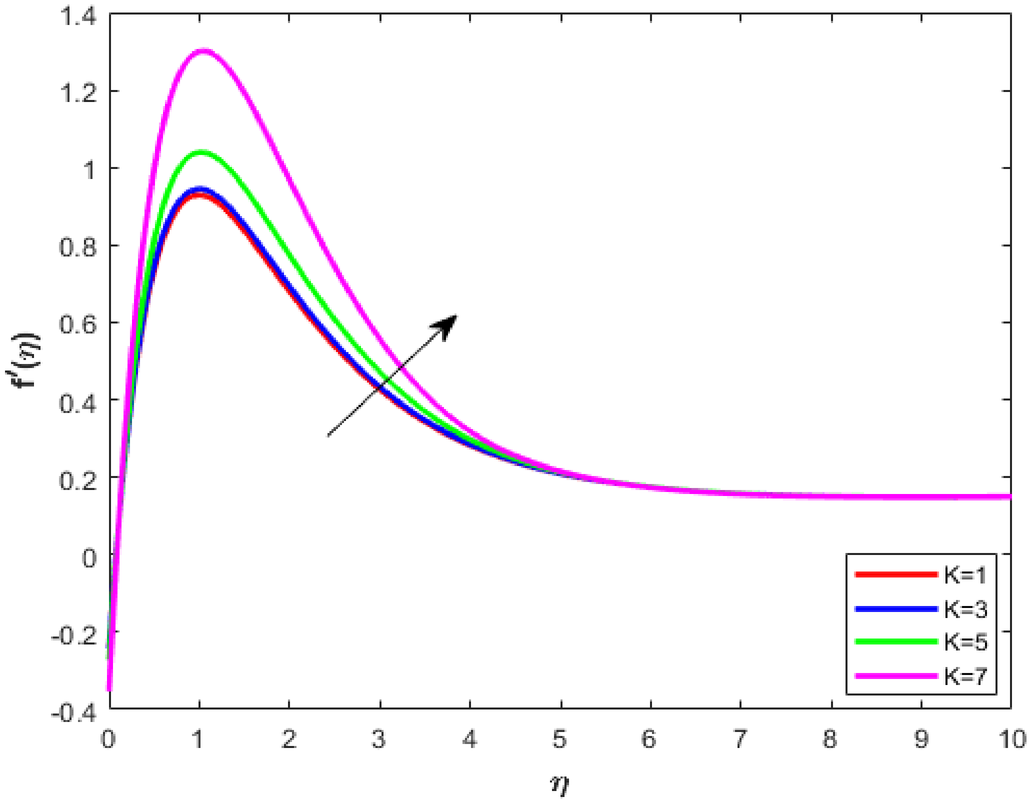

FIGURE 4.10: Effect of K on f' (β) when ω = δ = We=n=A=Q=Ec = α = γ = χ =Sc=0.1, Nt=Nb=0.5, M=Rd=Pr = γ = Gc=1, Gr=2, λ = c-1, S=0.2

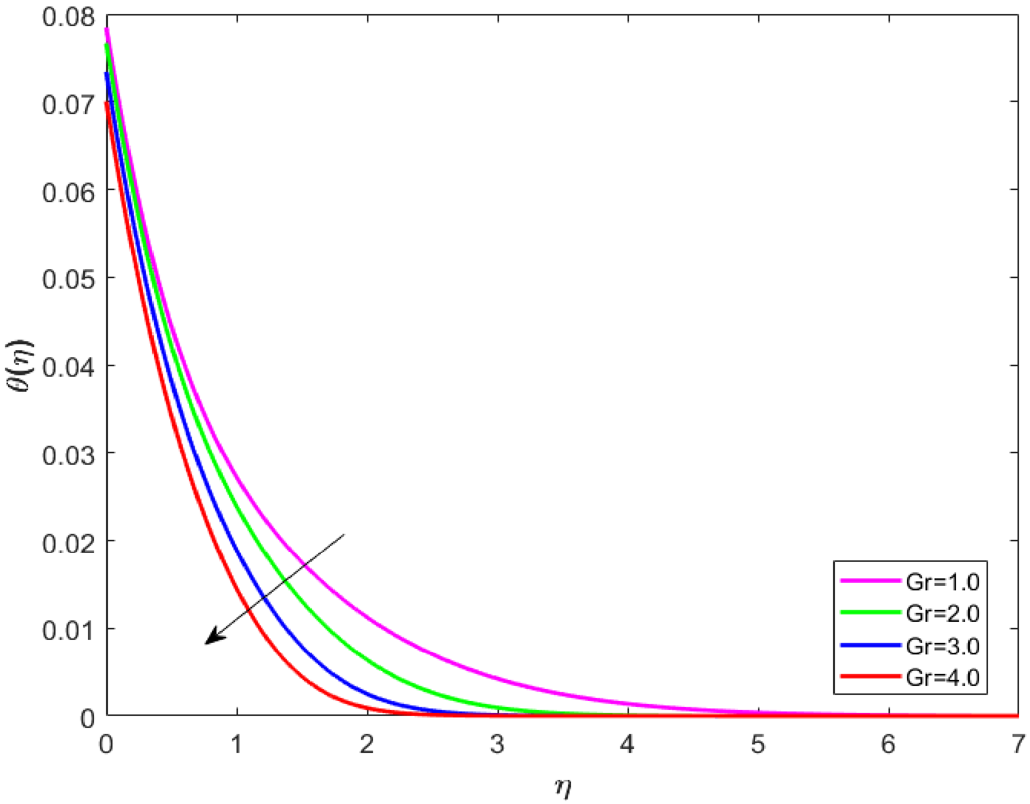

FIGURE 4.11: Effect of Gr on $\theta(\eta)$ when $K = \omega = \delta = We = n = A = Q = Ec = \alpha = \Gamma = \chi = Sc = 0.1,\ Nt = Nb = 0.5,\ M = Rd = Pr = \gamma = Gc = 1,\ \lambda = -1,\ S = 0.2$

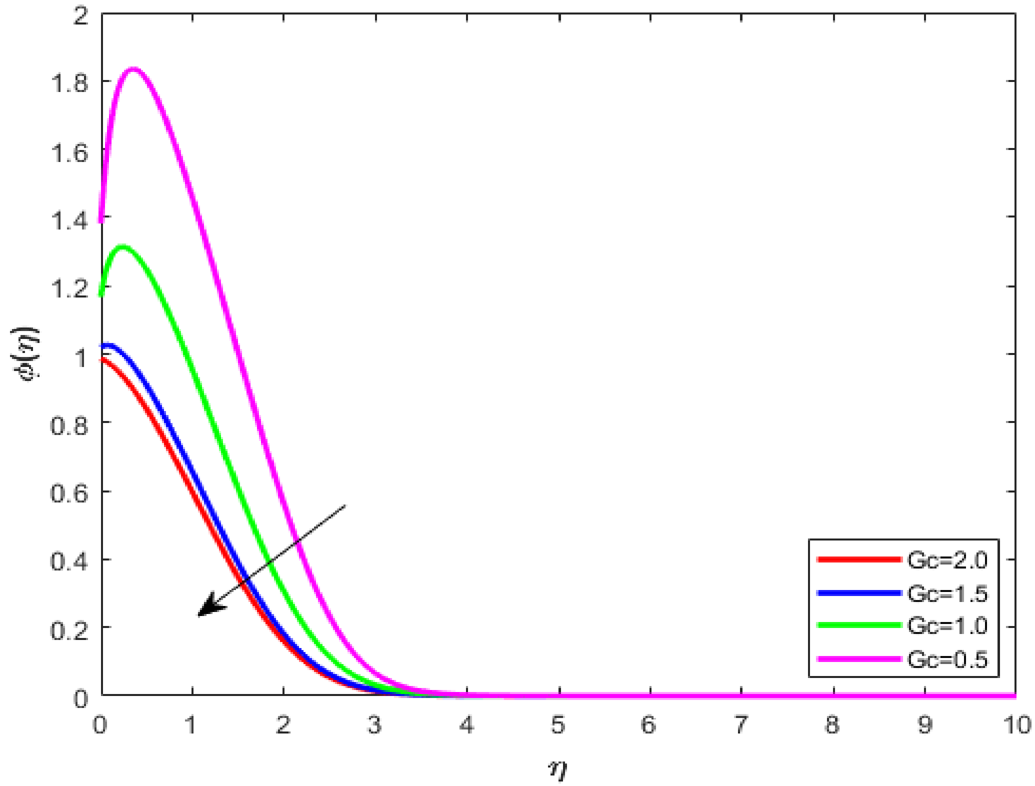

FIGURE 4.12: Effect of Gc on $\phi(\eta)$ when $K = \omega = \delta = We = n = A = Q = Ec = \alpha = \Gamma = \chi = Sc = 0.1,\ Nt = Nb = 0.5,\ M = Rd = Pr = \gamma = 1,\ Gr = 2,\ \lambda = -1,\ S = 0.2$

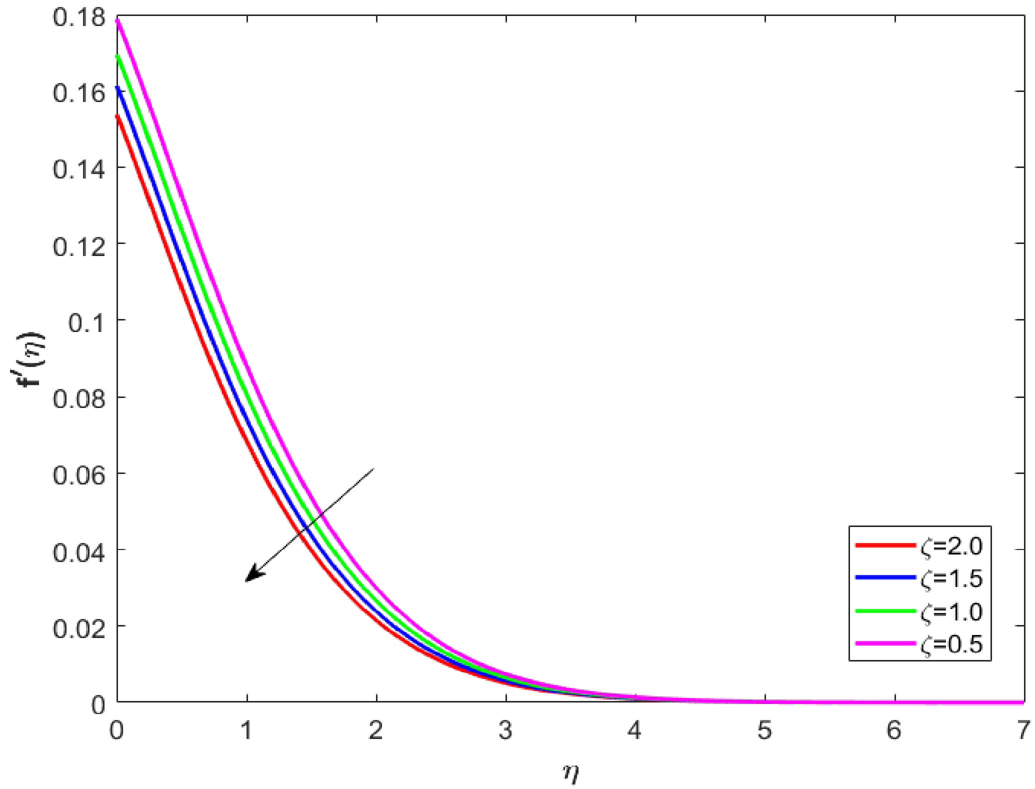

FIGURE 4.13: Effect of ζ on $f'(\eta)$ when $K = \omega = \delta = We = n = A = Q = Ec = \alpha = \Gamma = \chi = Sc = 0.1,\ Nt = Nb = 0.5,\ M = Rd = Pr = \gamma = Gc = 1,\ Gr = 2,\ \lambda = -1,\ S = 0.2$

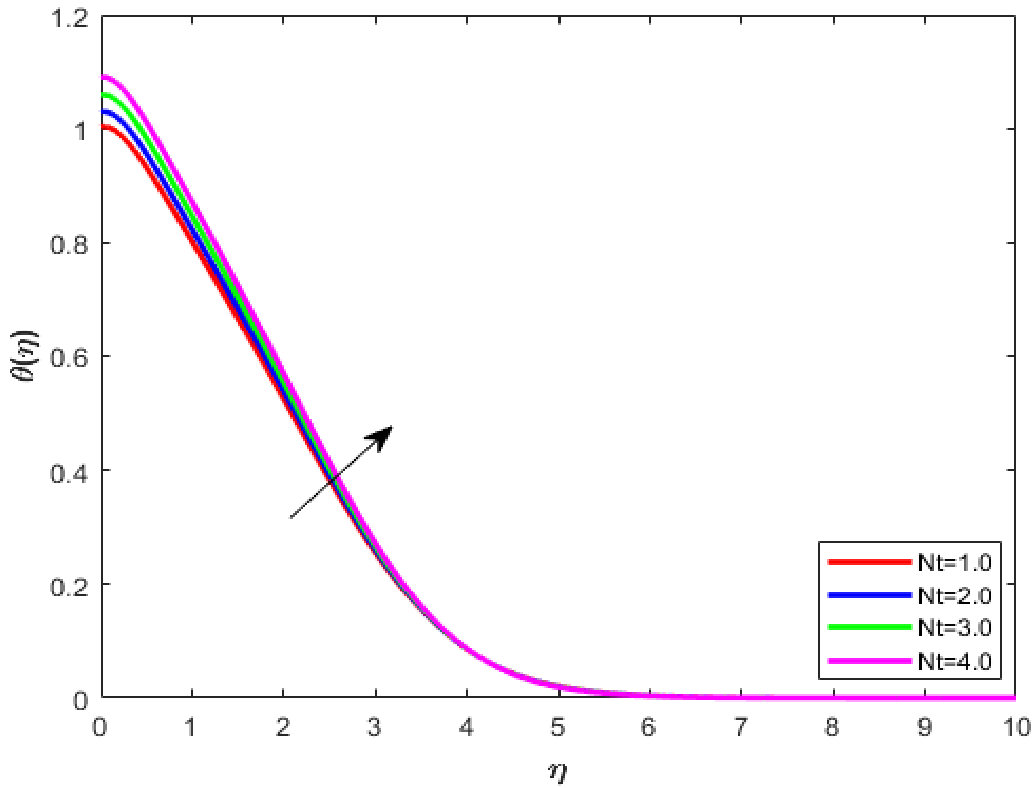

FIGURE 4.14: Effect of Nt on $\theta(\eta)$ when $K = \omega = \delta = We = n = A = Q = Ec = \alpha = \Gamma = \chi = Sc = 0.1,\ Nb = 0.5,\ M = Rd = Pr = \gamma = Gc = 1,\ Gr = 2,\ \lambda = -1,\ S = 0.2$

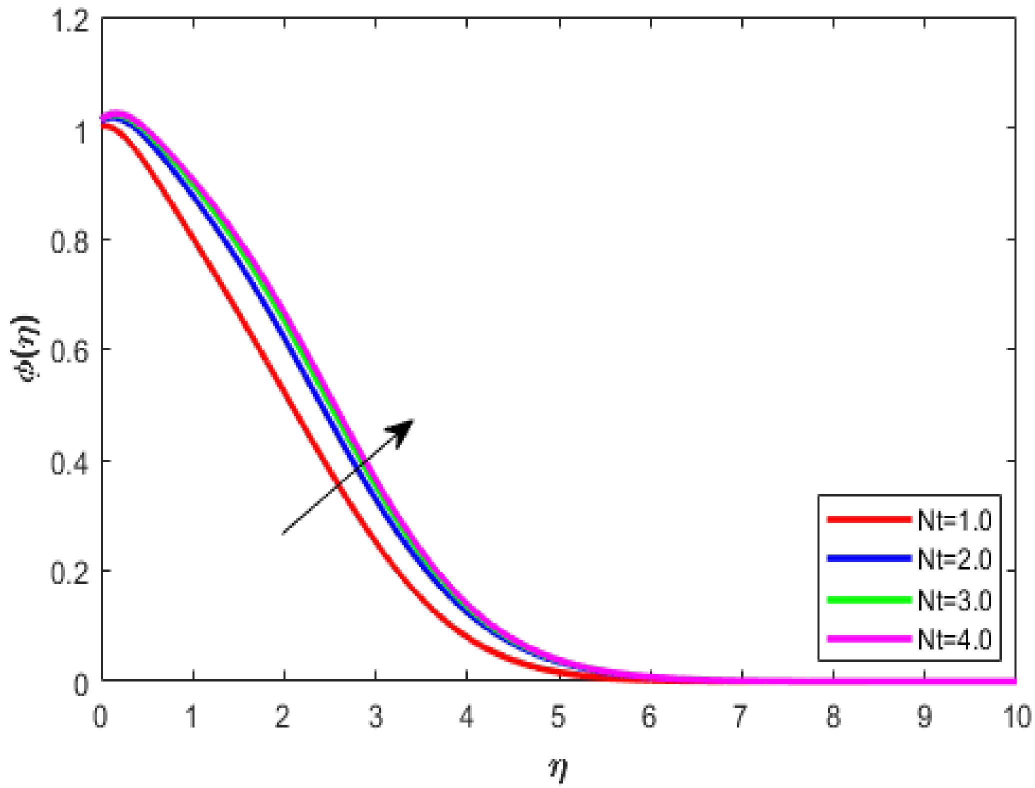

FIGURE 4.15: Effect of Nt on $\phi(\eta)$ when $K = \omega = \delta = We = n = A = Q = Ec = \alpha = \Gamma = \chi = Sc = 0.1,\ Nb = 0.5,\ M = Rd = Pr = \gamma = Gc = 1,\ Gr = 2,\ \lambda = -1,\ S = 0.2$

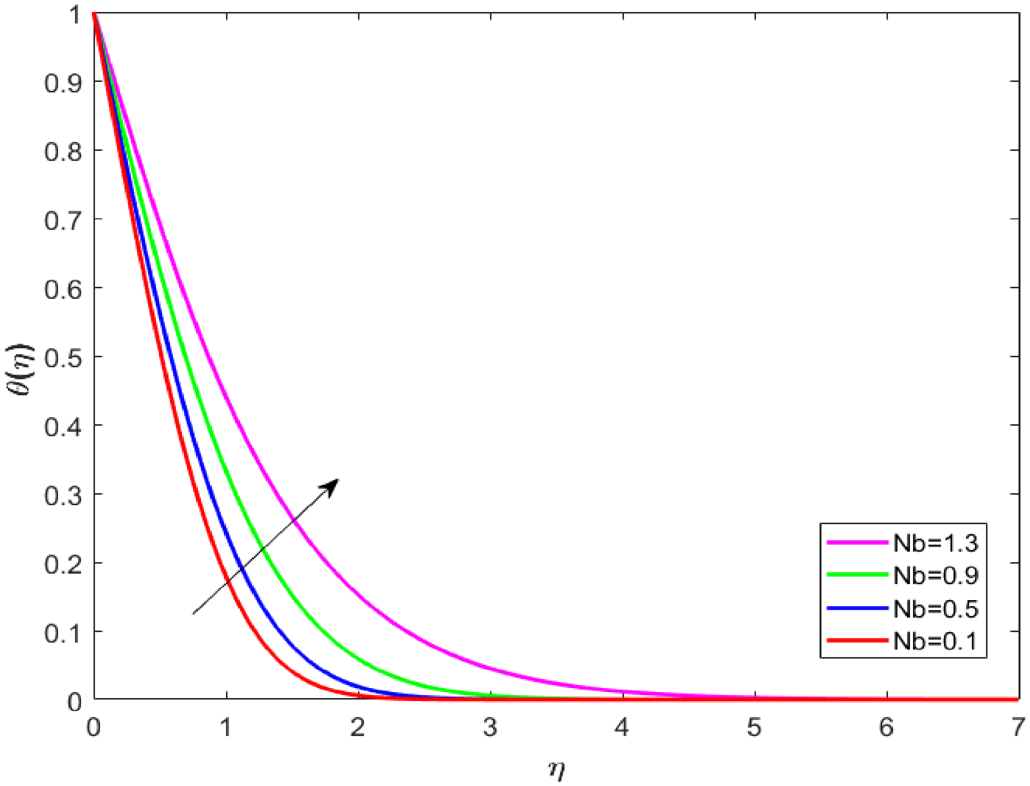

FIGURE 4.16: Effect of Nb on $\theta(\eta)$ when $K = \omega = \delta = We = n = A = Q = Ec = \alpha = \Gamma = \chi = Sc = 0.1,\ Nt = 0.5,\ M = Rd = Pr = \gamma = Gc = 1,\ Gr = 2,\ \lambda = -1,\ S = 0.2$

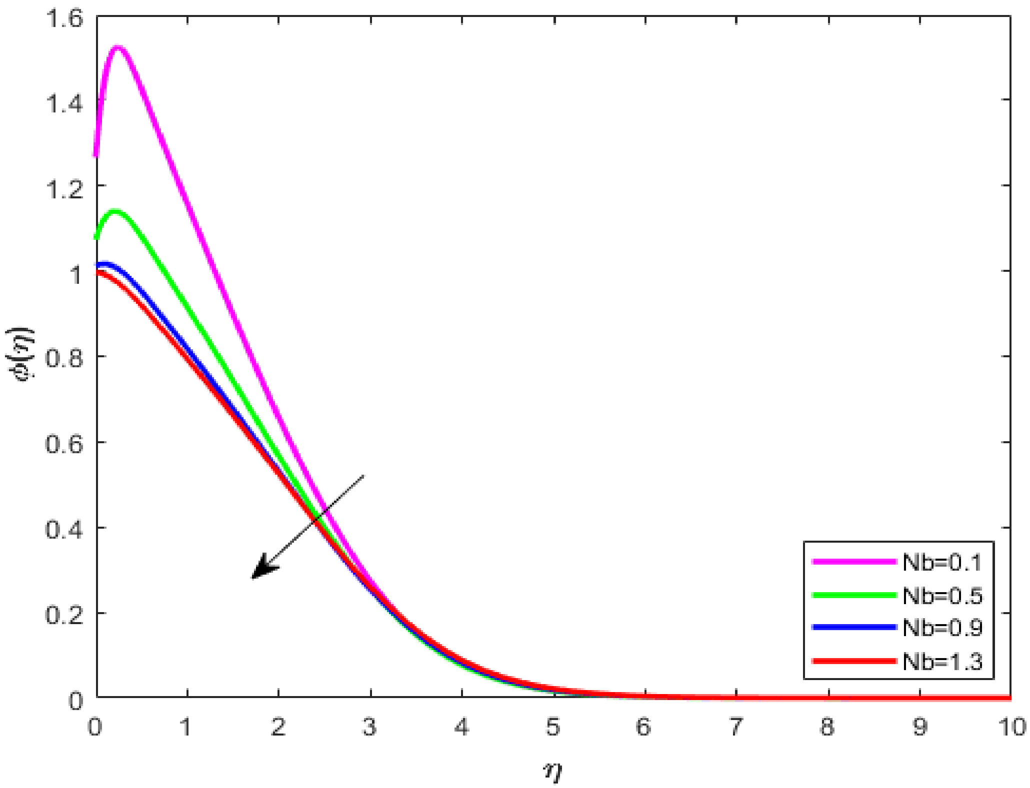

FIGURE 4.17: Effect of Nb on $\phi(\eta)$ when $K = \omega = \delta = We = n = A = Q = Ec = \alpha = \Gamma = \chi = Sc = 0.1,\ Nt = 0.5,\ M = Rd = Pr = \gamma = Gc = 1,\ Gr = 2,\ \lambda = -1,\ S = 0.2$

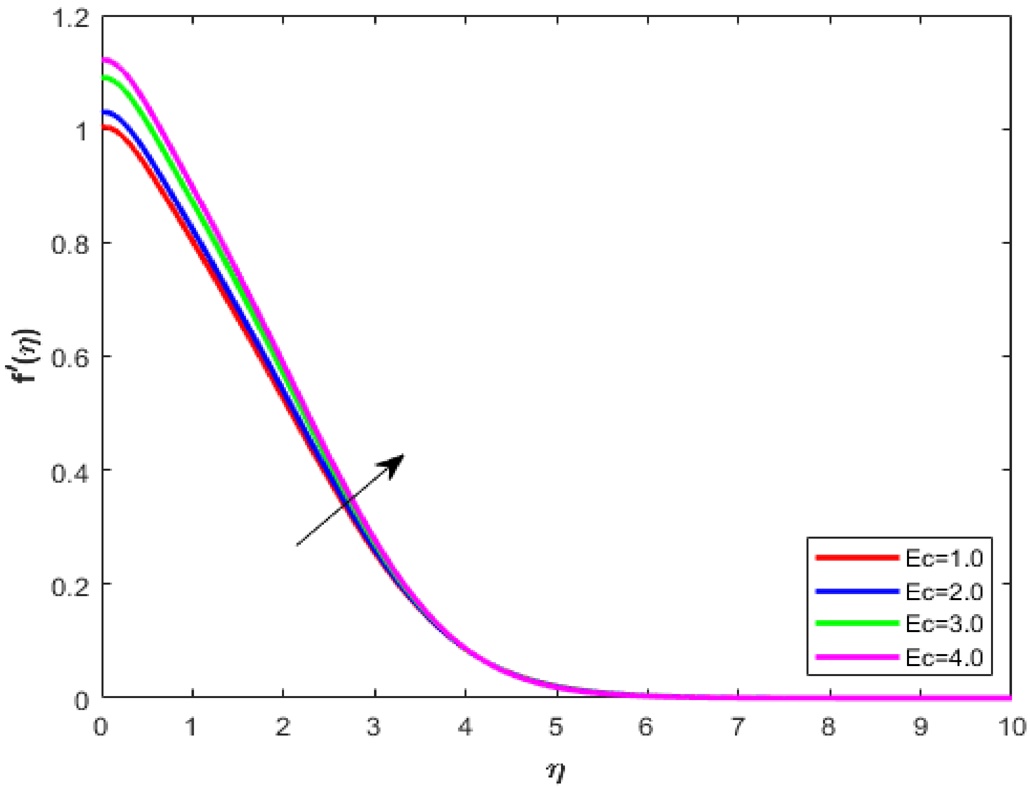

FIGURE 4.18: Effect of Ec on $f'(\eta)$ when $K = \omega = \delta = We = n = A = Q = \alpha = \Gamma = \chi = Sc = 0.1,\ Nt = Nb = 0.5,\ M = Rd = Pr = \gamma = Gc = 1,\ Gr = 2,\ \lambda = -1,\ S = 0.2$

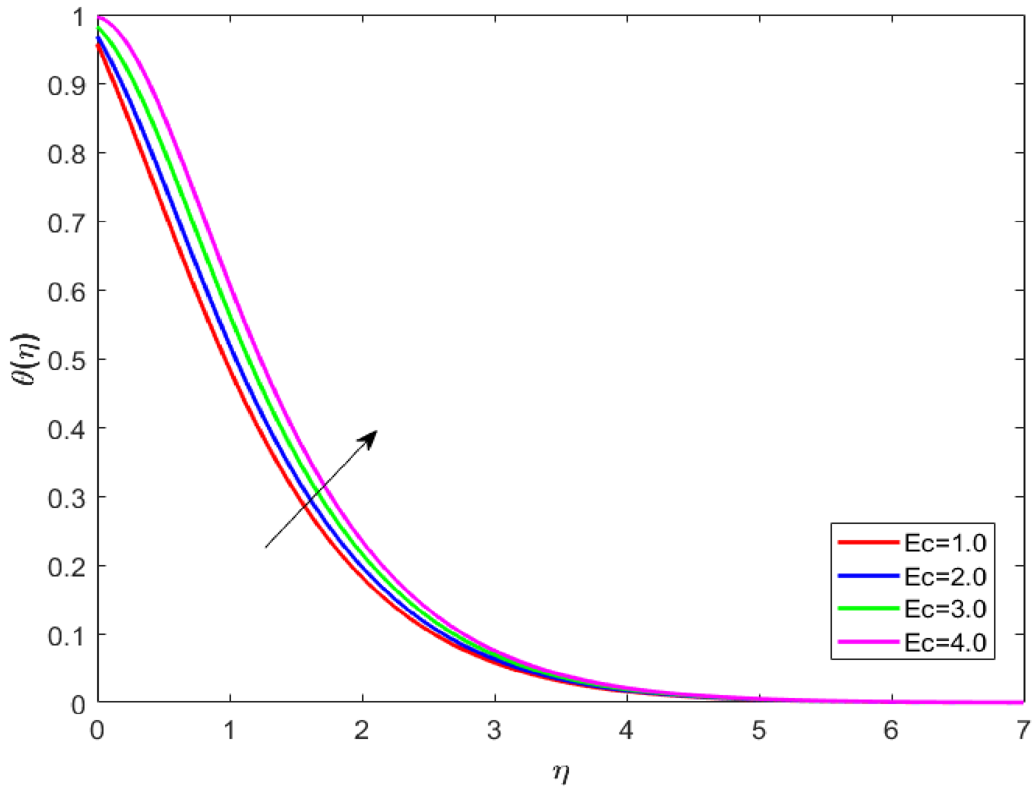

FIGURE 4.19: Effect of Ec on $\theta(\eta)$ when $K = \omega = \delta = We = n = A = Q = \alpha = \Gamma = \chi = Sc = 0.1,\ Nt = Nb = 0.5,\ M = Rd = Pr = \gamma = Gc = 1,\ Gr = 2,\ \lambda = -1,\ S = 0.2$

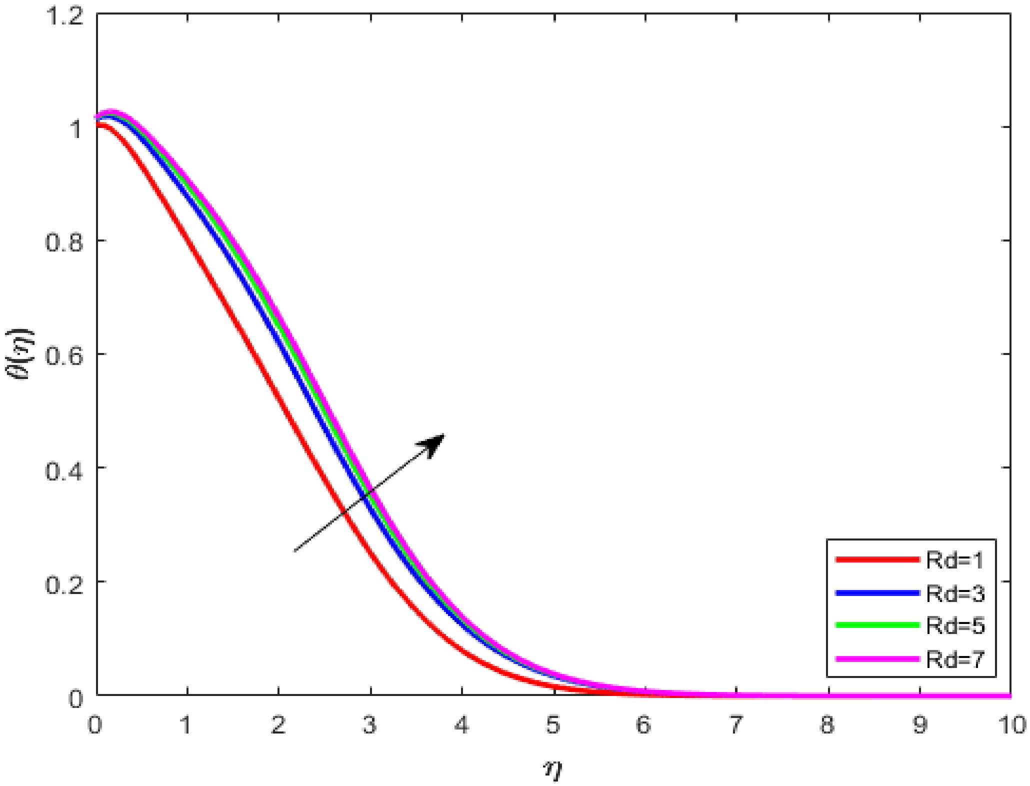

FIGURE 4.20: Effect of Rd on $\theta(\eta)$ when $K = \omega = \delta = We = n = A = Q = Ec = \alpha = \Gamma = \chi = Sc = 0.1,\ Nt = Nb = 0.5,\ M = Pr = \gamma = Gc = 1,\ Gr = 2,\ \lambda = -1,\ S = 0.2$

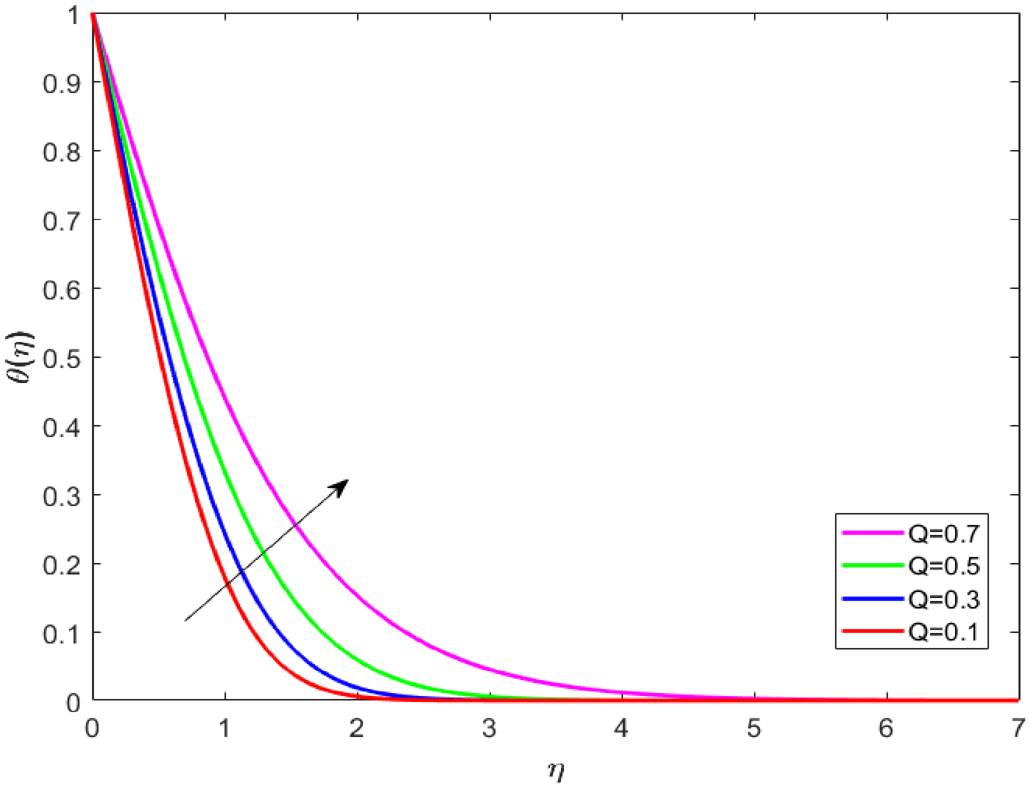

FIGURE 4.21: Effect of Q on $\theta(\eta)$ when $K = \omega = \delta = We = n = A = Ec = \alpha = \Gamma = \chi = Sc = 0.1,\ Nt = Nb = 0.5,\ M = Rd = Pr = \gamma = Gc = 1,\ Gr = 2,\ \lambda = -1,\ S = 0.2$

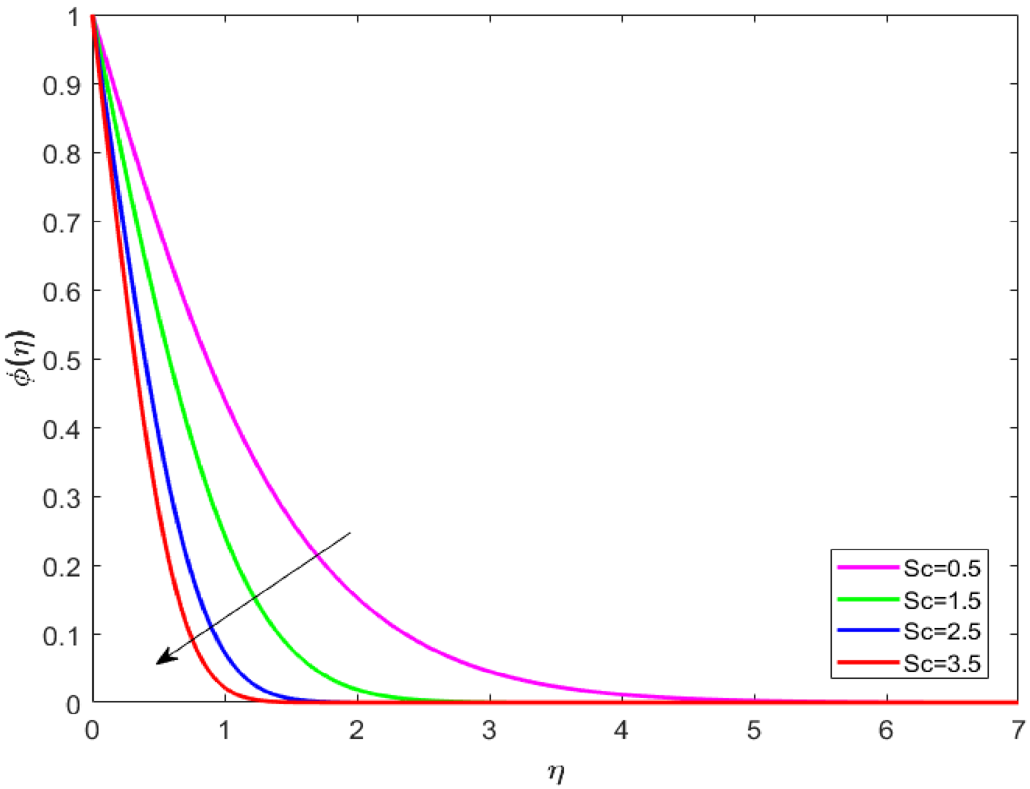

FIGURE 4.22: Effect of Sc on $\phi(\eta)$ when $K = \omega = \delta = We = n = A = Q = Ec = \alpha = \Gamma = \chi = 0.1,\ Nt = Nb = 0.5,\ M = Rd = Pr = \gamma = Gc = 1,\ Gr = 2,\ \lambda = -1,\ S = 0.2$

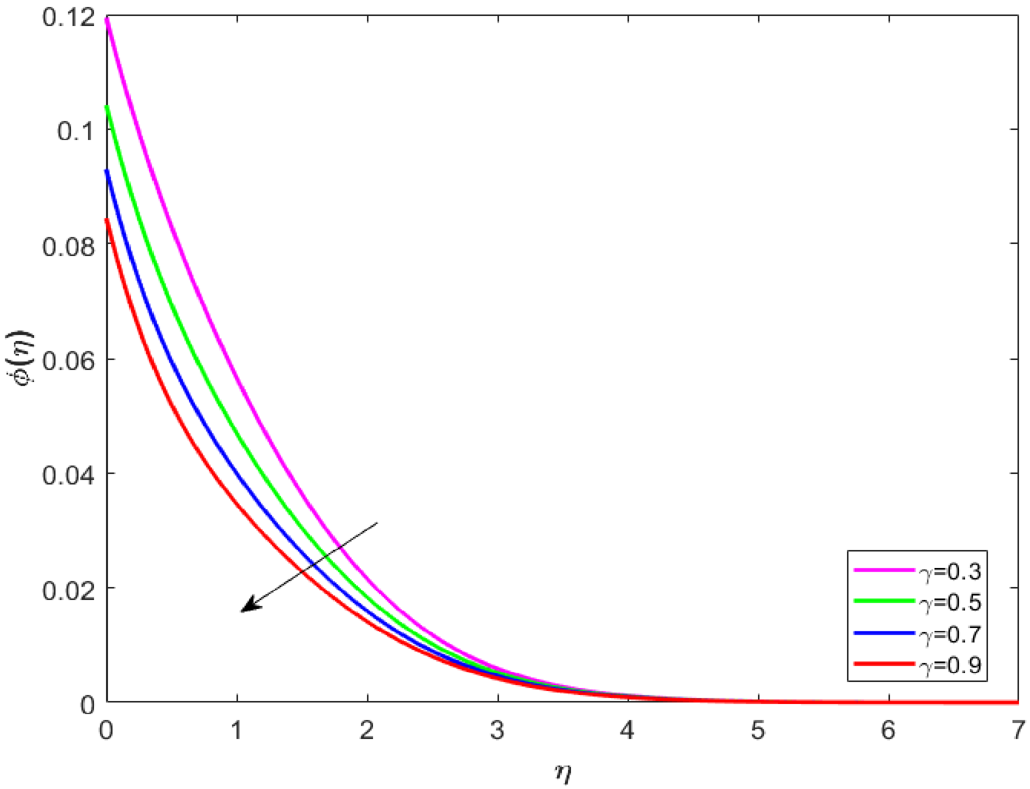

FIGURE 4.23: Effect of γ on $\phi(\eta)$ when $K = \omega = \delta = We = n = A = Q = Ec = \alpha = \Gamma = \chi = Sc = 0.1,\ Nt = Nb = 0.5,\ M = Rd = Pr = Gc = 1,\ Gr = 2,\ \lambda = -1,\ S = 0.2$

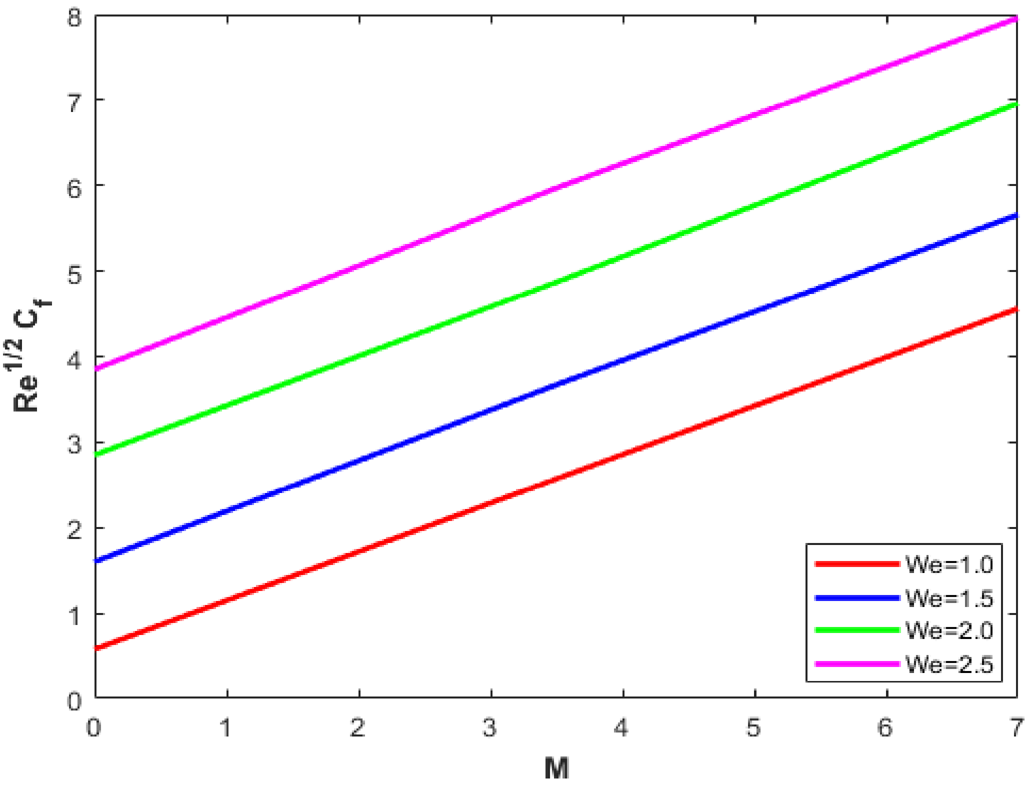

FIGURE 4.24: Effect ofWe and M on $Re^{\frac{1}{2}}\, C_f$ when $K = \omega = \delta = n = A = Q = Ec = \alpha = \Gamma = \chi = Sc = 0.1$, $Nt = Nb = 0.5$, $M = Rd = Pr = \gamma = Gc = 1$, $Gr = 2$, $\lambda = -1$, $S = 0.2$

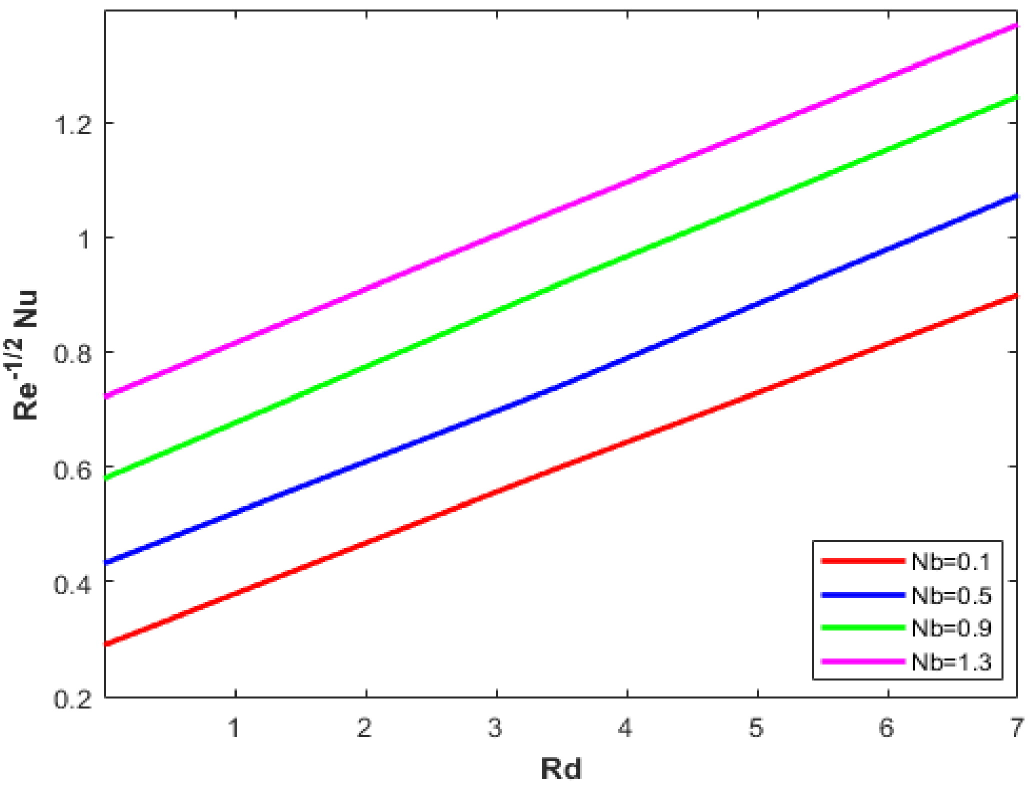

FIGURE 4.25: Effect of Rd and Nb on $Re^{-\frac{1}{2}}\, Nu$ when $K = \omega = \delta = n = A = Q = Ec = \alpha = \Gamma = \chi = Sc = 0.1$, $Nt = Nb = 0.5$, $M = Rd = Pr = \gamma = Gc = 1$, $Gr = 2$, $\lambda = -1$, $S = 0.2$

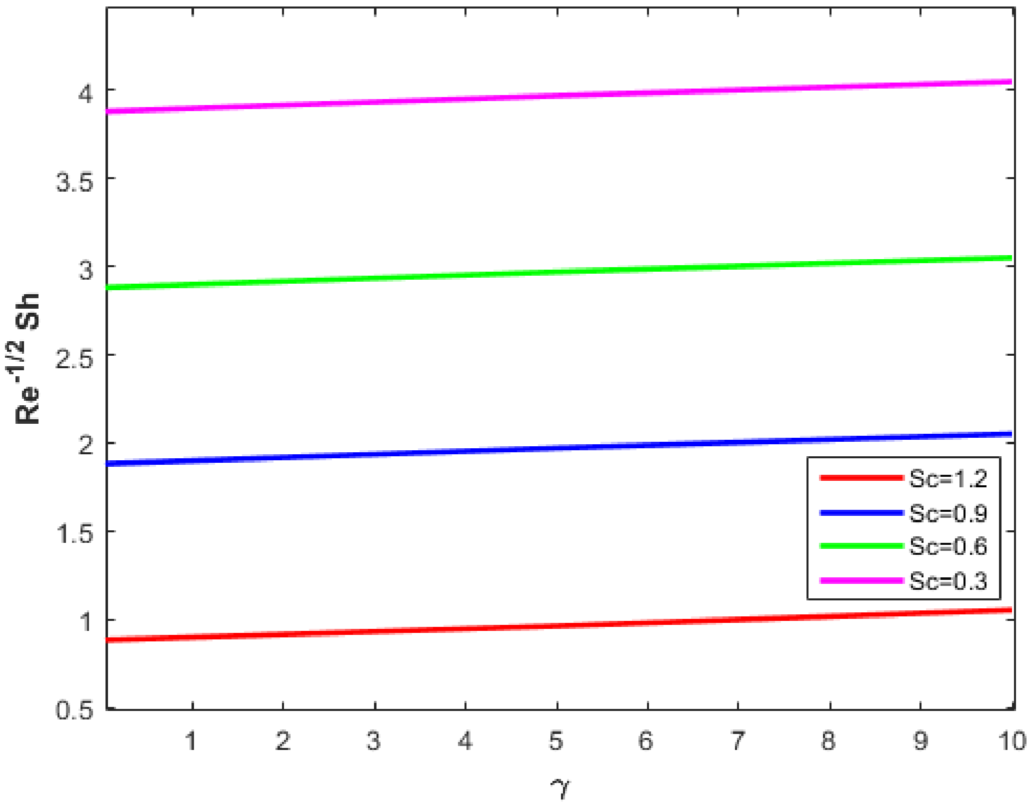

FIGURE 4.26: Effect of γ and Sc on $Re^{-\frac{1}{2}}\ Sh$ when $K = \omega = \delta = n = A = Q = Ec = \alpha = \Gamma = \chi = Sc = 0.1,\ Nt = Nb = 0.5,\ M = Rd = Pr = \gamma = Gc = 1,\ Gr = 2,\ \lambda = -1,\ S = 0.2$

Chapter 5

Inclined Magnetically driven Casson Carreau Nanofluid using the Cattaneo-Christov Heat Flux Model

5.1 Introduction

The numerical scrutinization of the Casson Carreau nanofluid flow by incorporating the heat flux model known as the Cattaneo-Christov model and multiple slip boundary conditions over a chemically reacting radially stretching sheet has been presented. Besides this, the Brownian movement, stagnation point and thermal radiation effects are added to the physical modeling. Furthermore, the influence of heat generation/absorption and inclined magnetic field are examined. A group of suitable similarity variables has opted for the adaptation of non-linear PDEs summing up the contemplate flow framework to a system of ODEs. To oversee the numerical solution of the proposed flow problem, the shooting method has been employed. The numerical solution has been presented through graphs and tables, illustrating the influence of relevant flow parameters on non-dimensional velocity, temperature, and concentration profiles. Additionally, physical characteristics of the flow model such as the Nusselt number, Sherwood number, and skin-friction coefficient have been evaluated.

5.2 Mathematical Modeling

Consider a steady and laminar flow of an incompressible Casson Carreau nanofluid in the neighborhood of a stagnation point past a chemically reacting radially stretching sheet along with multiple slips boundary conditions. The remarkable characteristics of the flow are intended to investigate in the light of inclined magnetic field, heat generation/ absorption and thermal radiation. Furthermore, the radial coordinates are chosen and frame of reference is selected in such a way that the flow is confined in the direction of $r-$axis. In addition to this, the velocity of the stretching sheet is chosen to be λU_w with $\lambda > 0$ restricted for the flow due to the stretching sheet. Moreover, the effect of Brownian motion, thermophoresis and viscous dissipation have been taken into consideration.

The mathematical form for the considered flow problem is presented by the following equations [74, 75].

$$\frac{\partial u}{\partial r} + \frac{u}{r} + \frac{\partial w}{\partial z} = 0, \tag{5.1}$$

$$\begin{aligned} u\frac{\partial u}{\partial r} + w\frac{\partial u}{\partial z} &= \nu_f \left[\left(1 + \tfrac{1}{\beta}\right) + \left(1 + \Gamma^2 \left(\frac{\partial u}{\partial z}\right)^2\right)^{\frac{n-1}{2}} \right] \frac{\partial^2 u}{\partial z^2} + g\beta_T (T - T_\infty) \\ &\quad + \nu_f \,(n-1)\, \Gamma^2 \frac{\partial^2 u}{\partial z^2} \left(\frac{\partial u}{\partial z}\right)^2 \left[1 + \tau^2 \left(\frac{\partial u}{\partial z}\right)^2\right]^{\frac{n-3}{2}} + U_e \frac{dU_e}{dr} \\ &\quad + g\beta_c (C - C_\infty) - \frac{\nu_f u}{k'} - \frac{\sigma B_0^2 (u - U_e) sin^2\alpha}{\rho_f}, \end{aligned} \tag{5.2}$$

$$\begin{aligned} u\frac{\partial T}{\partial r} + w\frac{\partial T}{\partial z} + \lambda \Bigg[& u\frac{\partial u}{\partial r}\frac{\partial T}{\partial r} + w\frac{\partial w}{\partial z}\frac{\partial T}{\partial z} + u\frac{\partial w}{\partial r}\frac{\partial T}{\partial z} + w\frac{\partial u}{\partial z}\frac{\partial T}{\partial r} + u^2\frac{\partial^2 T}{\partial r^2} + w^2\frac{\partial^2 T}{\partial z^2} \\ & + 2uw\frac{\partial^2 T}{\partial r \partial z} \Bigg] = \alpha_f \frac{\partial^2 T}{\partial z^2} + \tau \left[D_B \frac{\partial C}{\partial z}\frac{\partial T}{\partial z} + \frac{D_T}{T_\infty}\left(\frac{\partial T}{\partial z}\right)^2 \right] + \frac{\sigma B_0^2 \,(u - U_e)^2 \sin^2\alpha}{(\rho c_p)_f} \end{aligned}$$

$$+\frac{\nu_f}{c_p}\left(1+\tfrac{1}{\beta}\right)\left(\frac{\partial u}{\partial z}\right)^2+\frac{Q_0\left(T-T_\infty\right)}{\left(\rho c_p\right)_f}-\frac{1}{\left(\rho c_p\right)_f}\frac{\partial q_r}{\partial z}, \tag{5.3}$$

$$u\frac{\partial C}{\partial r}+w\frac{\partial C}{\partial z}=D_B\frac{\partial^2 C}{\partial z^2}+\frac{D_T}{T_\infty}\frac{\partial^2 T}{\partial z^2}-C_r\left(C-C_\infty\right). \tag{5.4}$$

For the heat radiation flux, the advantage of the Rosseland approximation has been taken.

$$\frac{\partial q_r}{\partial z}=-\frac{16\sigma^* T_\infty^3}{3k^*}\frac{\partial^2 T}{\partial z^2}. \tag{5.5}$$

The boundary conditions described at the surface are introduced in the following pattern [75].

$$\begin{aligned}
&w=w_0,\quad u=\lambda U_w+L\frac{\partial u}{\partial z},\quad T=T_f+S'\frac{\partial T}{\partial z},\quad C=C_f+K'\frac{\partial C}{\partial z}\ \text{ when } z=0,\\
&u\to U_e=br,\quad T\to T_\infty,\quad C\to C_\infty\quad \text{as}\quad z\to\infty.
\end{aligned} \tag{5.6}$$

The following type of transformation variables have been incorporated wisely for the proposed investigations [75].

$$\begin{aligned}
&\eta=\sqrt{\frac{a}{\nu_f}}\,z,\quad u=arf'\left(\eta\right),\quad w=-2\sqrt{a\nu_f}\,f\left(\eta\right),\\
&\theta\left(\eta\right)=\frac{T-T_\infty}{T_f-T_\infty},\quad \phi\left(\eta\right)=\frac{C-C_\infty}{C_f-C_\infty}.
\end{aligned} \tag{5.7}$$

After the inclusion of the above similarity transformations, the ODEs characterizing the proposed flow problem assume the following form.

$$\left[\left(1+nWe^2\left(f''\right)^2\right)\left(1+We^2\left(f''\right)^2\right)^{\frac{n-3}{2}}+\left(1+\tfrac{1}{\beta}\right)\right]f'''+2ff''-f'^2+A^2$$

$$+Gc\phi-M^2\left(f'-A\right)\sin^2\alpha-Kf'+Gr\theta=0, \tag{5.8}$$

$$\left(1+\frac{4}{3}Rd-4\zeta f^2\right)\theta''+PrNb\theta'\phi'+PrNt\theta'^2+2Prf\theta'+PrQ\theta-4\zeta ff'\theta'$$

$$+PrEcM^2\left(f'-A\right)^2 sin^2\alpha+\left(1+\tfrac{1}{\beta}\right)PrEcf''^2=0, \tag{5.9}$$

$$\phi''+\frac{Nt}{Nb}\theta''+Sc\left(2f\phi'-\gamma\phi\right)=0. \tag{5.10}$$

The corresponding conditions prescribed at the boundary are as follow.

$$f(0) = S,\ f'(0) = \lambda + \delta f''(0),\ \theta(0) = 1 + \omega\theta'(0),\ \phi(0) = 1 + \chi\phi'(0),$$
$$f' \to A,\ \phi \to 0,\ \theta \to 0 \ \text{ as } \ \eta \to \infty. \tag{5.11}$$

The formulation of the non-dimensional quantities incorporated in the above equations takes the following form.

$$Nb = \frac{\tau D_B (C_f - C_\infty)}{\nu_f},\ Pr = \frac{\nu_f}{\alpha_f},\ Nt = \frac{\tau D_T (T_f - T_\infty)}{\nu_f T_\infty},\ M^2 = \frac{\sigma B_0^2}{\rho_f a},$$
$$Q = \frac{Q_0}{\rho_f c_p a},\ Rd = \frac{4T_\infty \sigma^*}{k^* (\alpha_f \rho_f c_p)},\ \ Ec = \frac{a^2 r^2}{\alpha_f c_p (T_f - T_\infty)},\ A = \frac{b}{a},\ Sc = \frac{\nu_f}{D_B},$$
$$Gr = \frac{g\beta_T (T_f - T_\infty)}{a^2 r},\ \ Gc = \frac{g\beta_c (C_f - C_\infty)}{a^2 r},\ S = -\frac{w_0}{\sqrt{a\nu_f}},\ \ \gamma = \frac{C_r}{a},$$
$$\omega = \sqrt{\frac{a}{\nu_f}} S',\ \chi = \sqrt{\frac{a}{\nu_f}} K',\ \delta = \sqrt{\frac{a}{\nu_f}} L,\ K = \frac{\nu_f}{k' a},\ \zeta = \lambda a,\ We^2 = \frac{\Gamma^2 a^3 r^2}{\nu_f}.$$

Given below are the formulae for the skin-friction coefficient, Nusselt number and Sherwood number in the original form.

$$C_f = \frac{\tau_w}{\rho_f U_w^2},\ Nu = \frac{r q_w}{k_f (T_f - T_\infty)},\ Sh = \frac{r q_m}{D_B (C_f - C_\infty)}. \tag{5.12}$$

The formulation of τ_w, q_w and q_m are as follows:

$$\tau_w = \mu \left(\frac{\partial u}{\partial z}\right)_{z=0} \left[\left(1 + \tfrac{1}{\beta}\right) + \left[1 + \Gamma^2 \left(\frac{\partial u}{\partial z}\right)^2\right]_{z=0}^{\frac{n-1}{2}}\right],$$
$$q_w = -k_f \left[\left(\frac{\partial T}{\partial z}\right) - \frac{q_r}{k_f}\right]_{z=0},\ \ q_m = -D_B \left(\frac{\partial C}{\partial z}\right)_{z=0}. \tag{5.13}$$

The non-dimensional form of the skin-friction coefficient, Nusselt number and Sherwood number obtained by incorporating the similarity variables is given by:

$$Re^{\frac{1}{2}} C_f = \left[\left(1 + \tfrac{1}{\beta}\right) + \left(1 + We^2 f''^2(0)\right)^{\frac{n-1}{2}}\right] f''(0),$$
$$Re^{-\frac{1}{2}} Nu = -\left[1 + \frac{4}{3} Rd\right] \theta'(0),\ \ Re^{-\frac{1}{2}} Sh = -\phi'(0), \tag{5.14}$$

where $Re = \dfrac{rU_w}{\nu_f}$ elucidates the local Reynolds number.

5.3 Solution Methodology

For the sake of extracting the numerical solution of the system of ODEs (5.8)-(5.11) accompanied by boundary conditions, the benefit of shooting method has been considered. The missing initial conditions $f''(0)$, $\theta(0)$ and $\phi(0)$ have been denoted by s, l and m respectively. Before incorporating the shooting method approach, the following notations have been taken into consideration.

$$\begin{aligned}
&f = y_1, f' = y_2, f'' = y_3, \theta = z_4, \theta' = y_5, \phi = y_6, \phi' = y_7, \frac{\partial f}{\partial s} = y_8, \frac{\partial f'}{\partial s} = y_9,\\
&\frac{\partial f''}{\partial s} = y_{10}, \frac{\partial \theta}{\partial s} = y_{11}, \frac{\partial \theta'}{\partial s} = y_{12}, \frac{\partial \phi}{\partial s} = y_{13}, \frac{\partial \phi'}{\partial s} = y_{14}, \frac{\partial f}{\partial l} = y_{15}, \frac{\partial f'}{\partial l} = y_{16},\\
&\frac{\partial f''}{\partial l} = y_{17}, \frac{\partial \theta}{\partial l} = y_{18}, \frac{\partial \theta'}{\partial l} = y_{19}, \frac{\partial \phi}{\partial l} = y_{20}, \frac{\partial \phi'}{\partial l} = y_{21}, \frac{\partial f}{\partial m} = y_{22}, \frac{\partial f'}{\partial m} = y_{23},\\
&\frac{\partial f''}{\partial m} = y_{24}, \frac{\partial \theta}{\partial m} = y_{25}, \frac{\partial \theta'}{\partial m} = y_{26}, \frac{\partial \phi}{\partial m} = y_{27}, \frac{\partial \phi'}{\partial m} = y_{28}.
\end{aligned} \tag{5.15}$$

Using the above notations, equations (5.8)-(5.10) are transformed into a system of seven first order ODEs. Furthermore, the differentiation of these first seven ODEs w.r.t s, l and m, respectively, yields the remaining system of ODEs.

$$y_1' = y_2, \qquad y_1(0) = S,$$

$$y_2' = y_3, \qquad y_2(0) = \lambda + \delta s,$$

$$y_3' = \frac{y_2^2 + Ky_2 + M^2 \sin^2\alpha\,(y_2 - A) - 2y_1y_3 - A^2 - Gry_4 - Gcy_6}{\left[(1 + nWe^2y_3^2)\,(1 + We^2y_3^2)^{\frac{n-3}{2}} + \left(1 + \frac{1}{\beta}\right)\right]}, \qquad y_3(0) = s,$$

$$y_4' = y_5, \qquad y_4(0) = 1 + \omega l,$$

$$\begin{aligned}
y_5' = \frac{-1}{\left(1 + \frac{4}{3}Rd - 4\zeta y_1^2\right)} \Big[&PrNby_5y_7 + PrNty_5^2 + 2Pry_1y_5 + PrQy_4\\
&+ \left(1 + \tfrac{1}{\beta}\right) PrEcy_3^2 + PrEcM^2(y_2 - A)^2 \sin^2\alpha - 4\zeta y_1y_2y_5\Big],
\end{aligned} \qquad y_5(0) = l,$$

$$y_6' = y_7, \qquad y_6(0) = 1 + \chi m,$$

$$y_7' = -\left(\tfrac{Nt}{Nb}\right) y_5' - Sc\,(2y_1y_7 - \gamma y_6)\,, \qquad y_7(0) = m,$$

$$
\begin{aligned}
y_8' &= y_9, & y_8(0) &= 0,\\
y_9' &= y_{10}, & y_9(0) &= \delta,\\
y_{10}' &= \frac{1}{\left[(1+nWe^2y_3^2)\,(1+We^2y_3^2)^{\frac{n-3}{2}} + \left(1+\frac{1}{\beta}\right)\right]^2}\\
&\quad \left[\left(\left((1+nWe^2y_3^2)\,\left(1+We^2y_3^2\right)^{\frac{n-3}{2}} + \left(1+\frac{1}{\beta}\right)\right)\left[(2y_2 + M^2\sin^2\alpha\right.\right.\right.\\
&\quad \left.\left.+ K)y_9 - Gry_{11} - Gcy_{13} - 2\,(y_1y_{10} + y_3y_8)\,\right]\right) - \left(\left(y_2^2 - Gcy_6\right.\right.\\
&\quad \left.+ M^2(y_2 - A)\sin^2\alpha - 2y_1y_3 - A^2 + Ky_2 - Gry_4\right)\left[1 + We^2y_3^2\right]^{\frac{n-5}{2}}\\
&\quad \left.\left.(2We^2y_3y_{10})\left(\tfrac{n-3}{2}\left[1+nWe^2y_3^2\right] + n\left[1+We^2y_3^2\right]\right)\right)\right], & y_{10}(0) &= 1,\\
y_{11}' &= y_{12}, & y_{11}(0) &= 0,\\
y_{12}' &= \frac{-1}{\left(1+\frac{4}{3}Rd - 4\zeta y_1^2\right)^2}\left[\left(1+\tfrac{4}{3}Rd - 4\zeta y_1^2\right)\left(\left(PrNby_7 + 2PrNty_5 + 2Pry_1\right.\right.\right.\\
&\quad \left.- 4\zeta y_1y_2\right)y_{12} + Pr\left(Nby_5y_{14} + Qy_{11} + 2\left(1+\tfrac{1}{\beta}\right)Ecy_3y_{10}\right) + 2Pry_5y_8\\
&\quad + \left(2PrEcM^2(y_2-A)sin^2\alpha - 4\zeta y_1y_5\right)z_9 - 4\zeta y_2y_5y_8\big) + 8\big(\,(\zeta y_1y_8)\\
&\quad \big(PrNby_5y_7 + PrNty_5^2 + 2Pry_1y_5 + PrQy_4 + \left(1+\tfrac{1}{\beta}\right)PrEcy_3^2\\
&\quad \left.+ PrEcM^2(y_2-A)^2\sin^2\alpha - 4\zeta y_1y_2y_5)\big)\right], & y_{12}(0) &= 0,\\
y_{13}' &= y_{14}, & y_{13}(0) &= 0,\\
y_{14}' &= -\left(\tfrac{Nt}{Nb}\right)y_{12}' - 2Sc\big(y_1y_{14} + y_7y_8\big) + Sc\gamma y_{13}, & y_{14}(0) &= 0,\\
y_{15}' &= y_{16}, & y_{15}(0) &= 0,\\
y_{16}' &= y17, & y_{16}(0) &= 0,\\
y_{17}' &= \frac{\left(2y_2 + K + M^2\sin^2\alpha\right)y_{16} - 2(y_3y_{15} + y_1y_{17}) - Gry_{17} - Gcy_{20}}{\left(1+\frac{1}{\beta}\right)}, & y_{17}(0) &= 0,\\
y_{18}' &= y_{19}, & y_{18}(0) &= \omega,\\
y_{19}' &= \frac{-1}{\left(1+\frac{4}{3}Rd - 4\zeta y_1^2\right)^2}\left[\left(1+\tfrac{4}{3}Rd - 4\zeta y_1^2\right)\left(\left(PrNby_7 + 2PrNty_5 + 2Pry_1\right.\right.\right.\\
&\quad \left.- 4\zeta y_1y_2\right)y_{19} + Pr\left(Nby_5y_{21} + Qy_{18} + 2\left(1+\tfrac{1}{\beta}\right)Ecy_3y_{17}\right) + 2Pry_5y_{15}\\
&\quad + \left(2PrEcM^2(y_2-A)sin^2\alpha - 4\zeta y_1y_5\right)y_{16} - 4\zeta y_2y_5y_{15}\big) + 8\big(\,(\zeta y_1y_{15})\\
&\quad \big(PrNby_5y_7 + PrNty_5^2 + 2Pry_1y_5 + PrQy_4 + \left(1+\tfrac{1}{\beta}\right)PrEcy_3^2
\end{aligned}
$$

$$+ PrEcM^2(y_2 - A)^2\sin^2\alpha - 4\zeta y_1 y_2 y_5)\Big)\Big], \qquad y_{19}(0) = 0,$$

$$y'_{20} = y_{21}, \qquad y_{20}(0) = 0,$$

$$y'_{21} = -\left(\tfrac{Nt}{Nb}\right) y'_{19} - 2Sc\big(y_1 y_{21} + y_7 y_{15}\big) + Sc\gamma y_{20}, \qquad y_{21}(0) = 0,$$

$$y'_{22} = y_{23}, \qquad y_{22}(0) = 0,$$

$$y'_{23} = y_{24}, \qquad y_{23}(0) = 0,$$

$$y'_{24} = \frac{\big(2y_2 + K + M^2\sin^2\alpha\big)\, y_{23} - 2(y_3 y_{22} + y_1 y_{24}) - Gr y_{24} - Gc y_{27}}{\left(1 + \frac{1}{\beta}\right)}, \quad y_{24}(0) = 0,$$

$$y'_{25} = y_{26}, \qquad y_{25}(0) = 0,$$

$$y'_{26} = \frac{-1}{\left(1 + \frac{4}{3}Rd - 4\zeta y_1^2\right)^2}\Big[\left(1 + \tfrac{4}{3}Rd - 4\zeta y_1^2\right)\big(\big(PrNby_7 + 2PrNty_5 + 2Pry_1$$
$$- 4\zeta y_1 y_2\big) y_{26} + Pr\left(Nby_5 y_{28} + Qy_{25} + 2\left(1 + \tfrac{1}{\beta}\right) Ecy_3 y_{24}\right) + 2Pry_5 y_{22}$$
$$+ \big(2PrEcM^2(y_2 - A)sin^2\alpha - 4\zeta y_1 y_5\big) y_{23} - 4\zeta y_2 y_5 y_{22}\big) + 8\big(\,(\zeta y_1 y_{22})$$
$$\big(PrNby_5 y_7 + PrNty_5^2 + 2Pry_1 y_5 + PrQy_4 + \left(1 + \tfrac{1}{\beta}\right) PrEcy_3^2$$
$$+ PrEcM^2(y_2 - A)^2\sin^2\alpha - 4\zeta y_1 y_2 y_5)\big)\Big], \qquad y_{26}(0) = 0,$$

$$y'_{27} = y_{28}, \qquad y_{27}(0) = \chi,$$

$$y'_{28} = -\left(\tfrac{Nt}{Nb}\right) y'_{26} - 2Sc\big(y_1 y_{28} + y_7 y_{22}\big) + Sc\gamma y_{27}, \qquad y_{28}(0) = 1.$$

Rk-4 technique has been utilized in order to get the solution of the above IVP. In this context, the problem's domain is selected $[0, \eta_\infty)$, where $\eta_\infty > 0$ is such that the growing values of η_∞ have no influential impact on the solution.

The missing initial conditions for the system of equations mentioned above are chosen in such a way as to ensure that

$$y_2\,(s, l, m) = A, \quad y_4(s, l, m) = 0, \quad y_6(s, l, m) = 0. \tag{5.16}$$

The advantage of Newton's iterative numerical method has been taken for solving the above algebraic equations.

$$\begin{bmatrix} s^{(k+1)} \\ l^{(k+1)} \\ m^{(k+1)} \end{bmatrix} = \begin{bmatrix} s^{(k)} \\ l^{(k)} \\ m^{(k)} \end{bmatrix} - \left(\begin{bmatrix} \frac{\partial y_2}{\partial s} & \frac{\partial y_2}{\partial l} & \frac{\partial y_2}{\partial m} \\ \frac{\partial y_4}{\partial s} & \frac{\partial y_4}{\partial l} & \frac{\partial y_4}{\partial m} \\ \frac{\partial y_6}{\partial s} & \frac{\partial y_6}{\partial l} & \frac{\partial y_6}{\partial m} \end{bmatrix}^{-1} \begin{bmatrix} y_2 - A \\ y_4 \\ y_6 \end{bmatrix} \right)_{\left(s^{(k)},\ l^{(k)},\ m^{(k)}\right)},$$

$$\Rightarrow \begin{bmatrix} s^{(k+1)} \\ l^{(k+1)} \\ m^{(k+1)} \end{bmatrix} = \begin{bmatrix} s^{(k)} \\ l^{(k)} \\ m^{(k)} \end{bmatrix} - \left(\begin{bmatrix} y_9 & y_{16} & y_{23} \\ y_{11} & y_{18} & y_{25} \\ y_{13} & y_{20} & y_{27} \end{bmatrix}^{-1} \begin{bmatrix} y_2 - A \\ y_4 \\ y_6 \end{bmatrix} \right)_{\left(s^{(k)},\ l^{(k)},\ m^{(k)}\right)},$$

where k illustrates the scheme's iteration level.

With the aim of extracting the numerical solution, the termination criterion has been selected as

$$max\{(|y_2(\eta_\infty) - A|,\ \ |y_4(\eta_\infty)|, |_6(\eta_\infty)|)\} < \epsilon, \tag{5.17}$$

where ϵ has been chosen as 10^{-14}.

For all numerical results presented in the present article, $\eta_\infty = 10$ is found an appropriate choice.

5.4 Results with Discussion

In the present section, the numerical results of the proposed flow model have been depicted against several choices of the values of some apropos flow parameters. The remarkable numerical values of skin-friction coefficient, Sherwood and Nusselt numbers against salient parameters have been delineated in the tabular format.

5.4.1 Skin-friction Coefficient, Nusselt and Sherwood Numbers

With the aim of verifying the MATLAB code for the shooting method, the results for $-\left(1 + \frac{1}{\beta}\right) f''(0)$ are reproduced for the problem formulated by Nadeem et al.

[76].

TABLE 5.1: Comparison of the present results of $-\left(1+\frac{1}{\beta}\right)f''(0)$ with those published in the literature.

	$-\left(1+\frac{1}{\beta}\right)f''(0)$ with $M=\lambda=0$	
β	Nadeem et. al [76]	Present
1	1.4142	1.4142896
5	1.0954	1.0954345
∞	1.0042	1.0042235

The findings as seen in Table 5.1 indicate a significant settlement between the numerical results produced from the present code and already established research.

Tables 5.2-5.4 are delineated to throw light on the numerical values of the skin-friction coefficient along with the Nusselt and Sherwood numbers for the present model by fluctuating the values of various dimensionless parameters like n, We, β, M, A, K, α, Gr, Gc, λ, S, ζ, Rd, Pr, Q, Nb, Nt, Ec, Sc, γ, ω, δ and χ.

The numerical results reflect that the higher values of paramters like n, We, β, M, α, Pr, Sc, Ec and χ decrease the magnitude of the skin-friction coefficient and Sherwood number whereas a marginal magnification has been seen in the values of the Nusselt number. Moreover, with the rising values of Nb and γ, the heat and mass transfer rates climb significantly whereas the magnitude of the skin-friction coefficient goes down.

TABLE 5.2: The computed results of skin-friction coefficient, Nusselt and Sherwood numbers for $S=0.2$, $Nt=0.5$, $Gr=2$, $\zeta=Pr=\omega=Rd=Sc=Q=Ec=\gamma=\delta=\chi=0.1$, $\lambda=Nb=1$, where $c_1=\left[\left(1+\frac{1}{\beta}\right)+\left(1+We^2f''^2(0)\right)^{\frac{n-1}{2}}\right]$ and $c_2=\left(1+\frac{4}{3}Rd\right)$.

n	We	β	K	M	A	Gc	α	$c_1f''(0)$	$-c_2\theta'(0)$	$-\phi'(0)$
0.1	0.1	0.5	0.1	0.1	0.1	1.0	0.1	4.430660	2.129876	0.215984
5.0								4.421344	2.130063	0.215967

10								4.412477	2.130244	0.215951
	0.7							3.613556	2.135860	0.215424
	1.3							2.920442	2.141292	0.214810
		2.5						3.459476	2.183406	0.209910
		4.5						3.408249	2.189730	0.209252
			0.3					4.514544	1.895088	0.241119
			0.5					4.601060	1.649113	0.267429
				3.1				4.076599	2.147994	0.212089
				5.1				3.481249	2.176216	0.205763
					0.6			6.690888	1.673092	0.330634
					1.1			11.063065	0.800431	0.474012
						1.5		6.401721	1.878697	0.261301
						2.0		8.174677	1.628146	0.301983
							0.7	4.415589	2.130666	0.215816
							1.3	4.396495	2.131666	0.215604

It is further observed that the values of the skin-friction coefficient and Sherwood number boost up whereas the Nusselt number diminishes by considering the larger values of K, A, Gc, Gr, ζ, Nt and δ into account.

The higher estimation of λ and S escalates the mass transfer rate while the magnitude of the skin-friction coefficient and Nusselt number fall subsequently. In addition to this, the heat and mass transfer rates along with the skin-friction coefficient subside as the value of ω goes up.

TABLE 5.3: The computed results of skin-friction coefficient, Nusselt and Sherwood numbers for $n = We = K = M = A = \alpha = \gamma = \delta = \chi = 0.1$, $\beta = Nb = 0.5$, $Gc = 1$, $Gr = 2$, Ec=0.2, S=0.8 where $c_1 = \left[\left(1+\frac{1}{\beta}\right) + \left(1 + We^2 f''^2(0)\right)^{\frac{n-1}{2}}\right]$ and $c_2 = \left(1 + \frac{4}{3}Rd\right)$.

ζ	λ	Pr	ω	Nt	Rd	Sc	Q	$c_1 f''(0)$	$-c_2\theta'(0)$	$-\phi'(0)$
0.1	1.0	0.1	0.1	0.5	0.1	0.1	0.1	4.430660	2.129876	0.215984
0.5								6.345825	-0.107946	0.426874
0.9								6.635122	-0.156728	0.434971

1.4							-1.504224	2.034308	0.238104
1.8							-8.540752	1.608457	0.297288
	1.1						2.204186	9.829911	-0.632756
	2.1						1.799772	13.071638	-1.007239
		0.4					3.843585	2.063607	0.212256
		0.8					3.130832	1.958230	0.210187
			2.5				6.264730	0.560167	0.433549
			4.5				6.546410	0.402387	0.539571
				0.3			4.421392	2.179262	0.210557
				0.5			4.415011	2.213382	0.206807
					0.4		3.164843	2.238063	0.194086
					0.7		2.319665	2.319665	0.175824
						0.5	1.934986	3.255504	0.655651
						0.9	1.179433	3.411671	0.991044

TABLE 5.4: The computed results of skin-friction coefficient, Nusselt and Sherwood numbers for $n = We = K = M = A = \alpha = \gamma = \delta = \chi = \zeta = Pr = \omega = Rd = Sc = Q = Ec = 0.1,\ \beta = Nb = Nt = 0.5,\ Gc = \lambda = Nb = 1,\ Gr = 2,$ Ec=S=0.2, S=0.8 where $c_1 = \left[\left(1 + \frac{1}{\beta}\right) + \left(1 + We^2 f''^2(0)\right)^{\frac{n-1}{2}}\right]$ and $c_2 = \left(1 + \frac{4}{3}Rd\right)$.

Gr	Nb	Ec	S	$c_1 f''(0)$	$-c_2\theta'(0)$	$-\phi'(0)$
2.0				4.430660	2.129876	0.215984
3.0				7.729405	1.852347	0.257134
4.0				10.882892	1.498437	0.305297
	1.0			3.837804	2.489934	0.248401
	1.5			3.659156	2.528236	0.270574
		0.2		4.412897	2.196855	0.208657
		0.3		4.395323	2.263217	0.201393
			0.8	3.539966	2.109109	0.267938
			1.4	-0.759124	2.071294	0.327543

5.4.2 The Velocity, Temperature and Concentration Profiles

The influence of n, We and β on the velocity distribution has been delineated through figures 5.2-5.4. An increasing behavior is observed in the velocity by escalating the values of n, We and β. Moreover, a decrement is experienced by the velocity boundary layer thickness when higher values of n and β are taken into account whereas an enhancement has been observed in the case of larger We.

Figures 5.5-5.7 are drawn to highlight the effect of M on the velocity, temperature and concentration profiles. AS mentioned in the previous chapters, An escalation has been observed in the temperature and concentration profiles whereas the velocity drops subsequently by applying higher magnetic field.

Moreover, a drastic fall in the momentum boundary layer thickness and a marginal climb in the thermal and concentration boundary layer thickness has been recorded.

The impact of K, α and ζ on the velocity distribution has been depicted through figures 5.8-5.10. Clearly, it can be seen that the velocity of the fluid climbs marginally for the larger values of K, α and ζ. However, a decrement in the momentum boundary layer thickness has been noticed for the higher K whereas an opposite trend has been observed for α and ζ.

Figures 5.15-5.16 are drawn to portray the impact of Pr on the temperature and concentration configurations. Physically, Pr is defined to be proportionate between the viscous diffusion rate and thermal diffusivity. As the magnitude of Pr heightens, the thermal diffusion rate undergoes curtailment and eventually the fluid's temperature depresses considerably. Therefore, a diminution has been noted in the thermal boundary layer thickness. Meanwhile, for the higher assumption of Pr, the fluid's concentration is remarked to escalate. Apart from this, a sudden upsurge can be noted in the thickness of the concentration boundary layer.

The effect of Nt and Nb on the temperature distribution has been shown through figures 5.13-5.14. The temperature profile upsurges significantly by considering the higher values of Nb and Nt. Moreover, an increment in the associated thermal boundary layer thickness has been noticed.

The dynamics of the velocity and temperature profiles by incorporating various values of Ec have been illustrated through Figures 5.15-5.16. As stated in the previous chapters, an escalation in the kinetic energy of the fluid is observed by rising the values of Ec. Therefore, the velocity and temperature go up subsequently and hence, the thickness of momentum and thermal boundary layer is enhanced.

Figures 5.17-5.19 are sketched to highlight the impact of Gr, Q and Rd on the temperature distribution. For the larger the values of Q and Rd, the more heat is generated, which allows the temperature and the associated thermal boundary layer thickness to climb significantly. However, for the escalating values of Gr, the temperature suddenly drops and a decrement in the thermal boundary layer thickness has been seen.

The effect of Gc, Sc and γ on the concentration profile has been portrayed through figures 5.20-5.22. It has been seen that the higher estimation of γ leads to a depreciation in the chemical molecular diffusion and thereby the fluid's concentration drops marginally and a decrement has been noted in the associated concentration boundary layer thickness. Morever, a smiliar trend has been observed by taking higher values of Gc and Sc into account.

Figure 5.23 represents the effect of M and We on the Nusselt number. Notably, the magnitude of the heat transfer gradient increases marginally by assuming the higher values of M and We into account.

Furthermore, figure 5.24 is drawn to delineate the influence of Rd and Pr on the skin-friction coefficient. It is remarked from the figure that as the values of Rd and Pr escalate, the shearing stress of the surface approaches an alleviation.

The impact of γ and Ec on the Sherwood number is depicted through Figure 5.25. Evidently, it can be seen that as the values of γ and Ec escalate, the mass transfer gradient observes an increment in the magnitude.

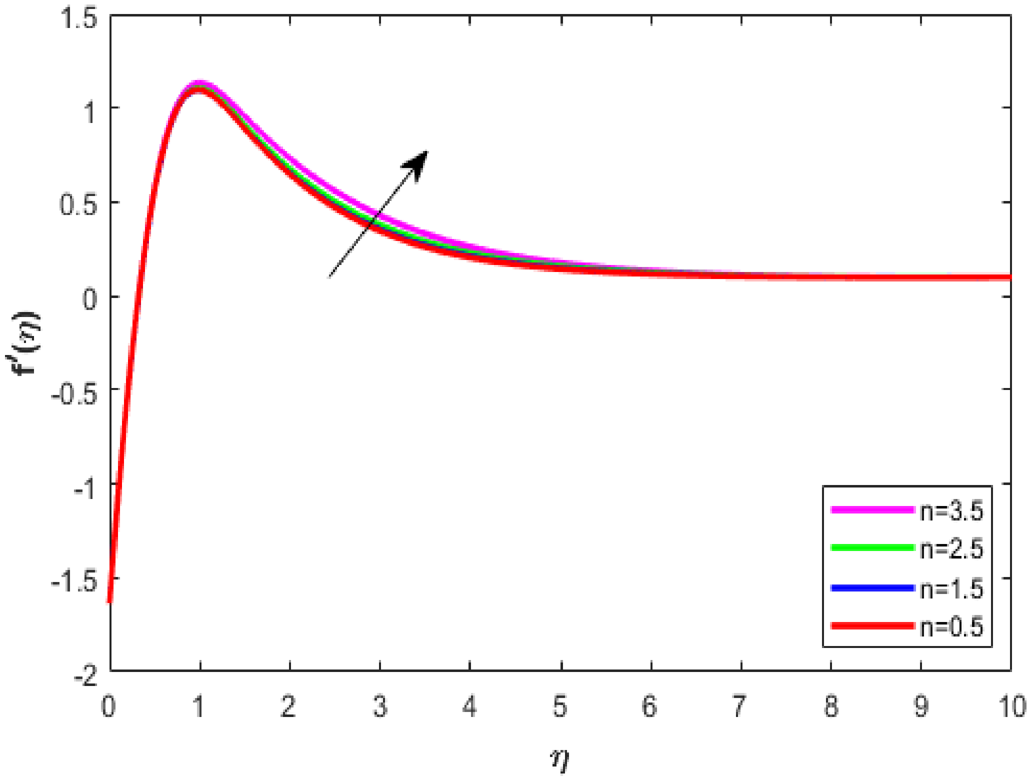

FIGURE 5.1: Effect of n on $f'(\eta)$ when $K = \omega = \delta = We = A = Q = Ec = \alpha = \Gamma = \chi = Sc = 0.1,\ \beta = Nt = Nb = 0.5,\ M = Rd = Pr = \gamma = Gc = 1,\ Gr = 2,\ \lambda = -1,\ S = 0.2$

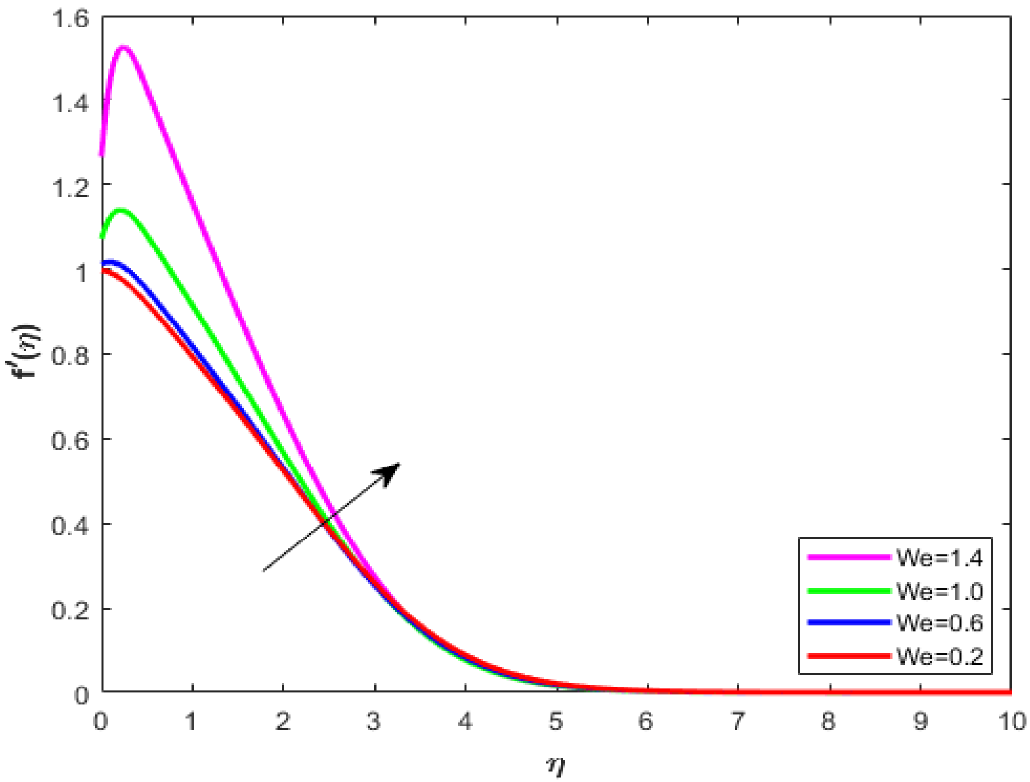

FIGURE 5.2: Effect of We on $f'(\eta)$ when $K = \omega = \delta = n = A = Q = Ec = \alpha = \Gamma = \chi = Sc = 0.1,\ \beta = Nt = Nb = 0.5,\ M = Rd = Pr = \gamma = Gc = 1,\ Gr = 2,\ \lambda = -1,\ S = 0.2$

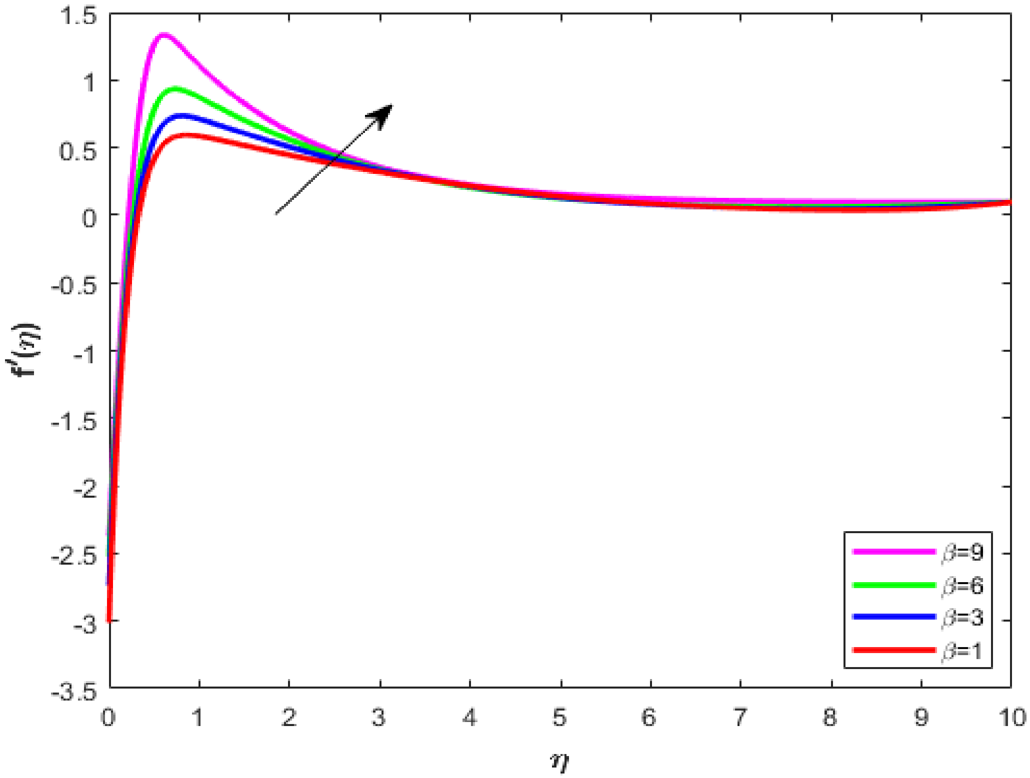

FIGURE 5.3: Effect of β on $f'(\eta)$ when $K = \omega = \delta = We = n = A = Q = Ec = \alpha = \Gamma = \chi = Sc = 0.1,\ Nt = Nb = 0.5,\ M = Rd = Pr = \gamma = Gc = 1,\ \lambda = -1,\ S = 0.2$

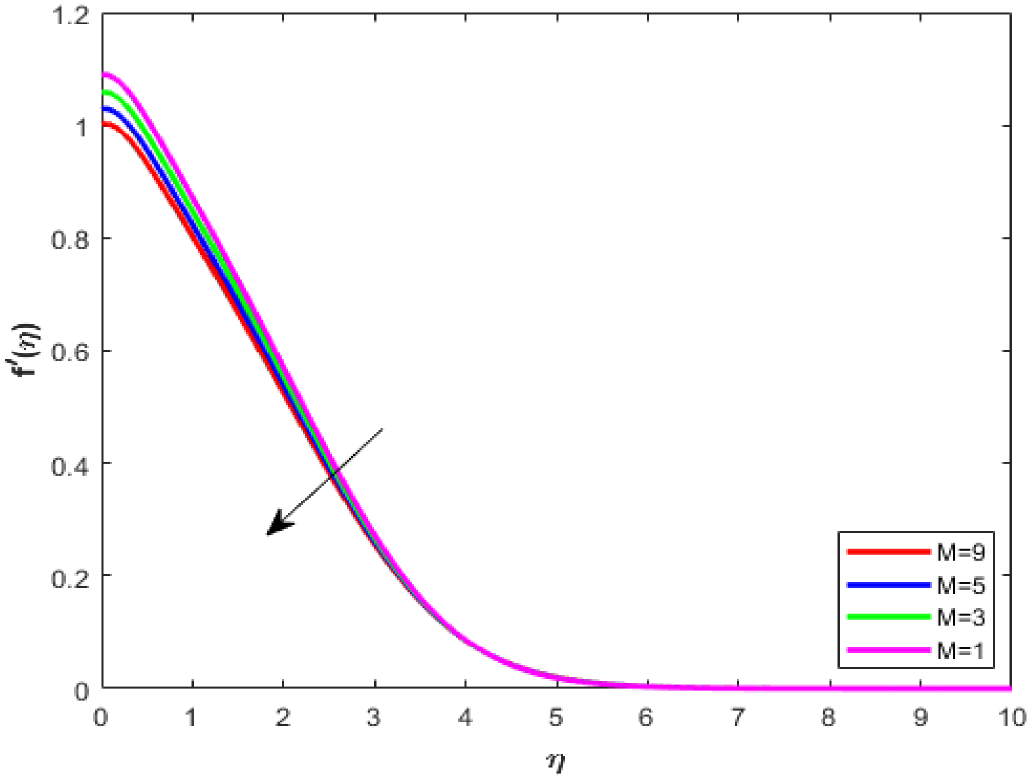

FIGURE 5.4: Effect of M on $f'(\eta)$ when $K = \omega = \delta = We = n = A = Q = Ec = \alpha = \Gamma = \chi = Sc = 0.1,\ \beta = Nt = Nb = 0.5,\ Rd = Pr = \gamma = Gc = 1,\ Gr = 2,\ \lambda = -1,\ S = 0.2$

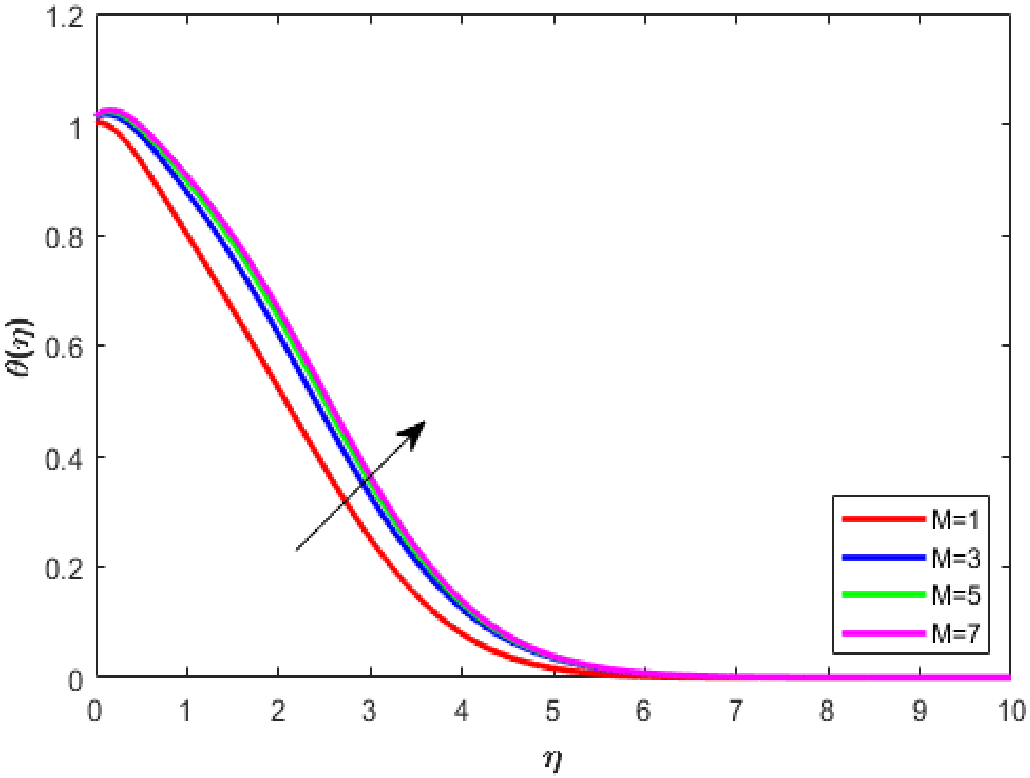

FIGURE 5.5: Effect of M on $\theta(\eta)$ when $K = \omega = \delta = We = n = A = Q = Ec = \alpha = \Gamma = \chi = Sc = 0.1,\ \beta = Nt = Nb = 0.5,\ Rd = Pr = \gamma = Gc = 1,\ Gr = 2,\ \lambda = -1,\ S = 0.2$

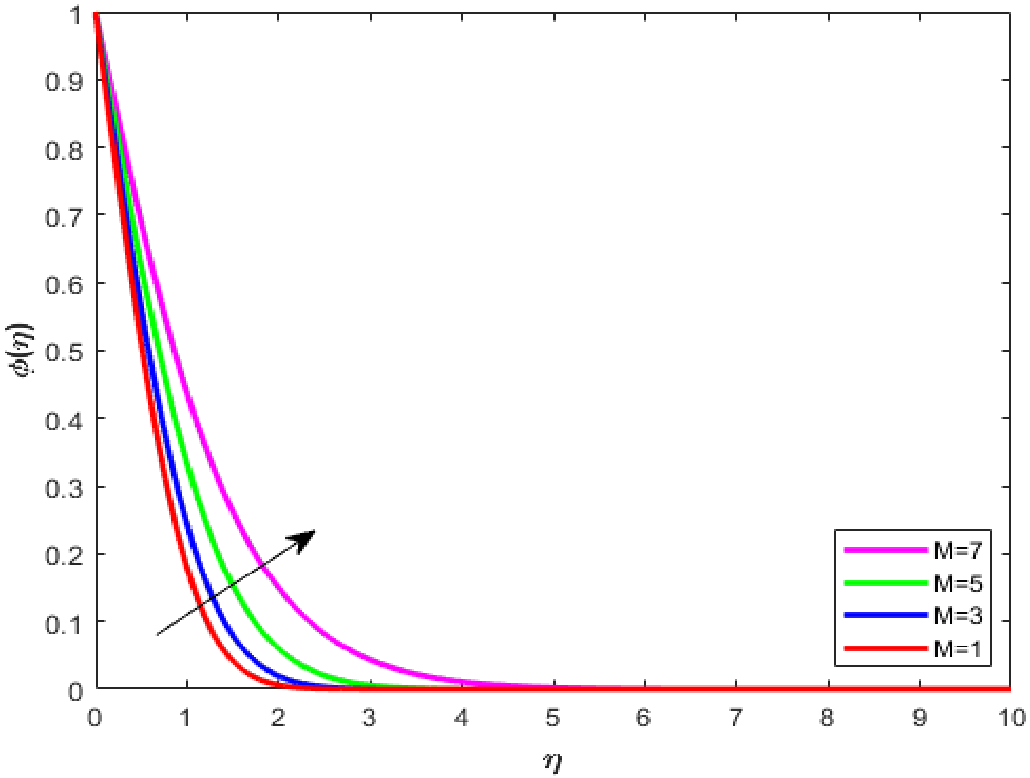

FIGURE 5.6: Effect of M on $\phi(\eta)$ when $K = \omega = \delta = We = n = A = Q = Ec = \alpha = \Gamma = \chi = Sc = 0.1,\ \beta = Nt = Nb = 0.5,\ Rd = Pr = \gamma = Gc = 1,\ Gr = 2,\ \lambda = -1,\ S = 0.2$

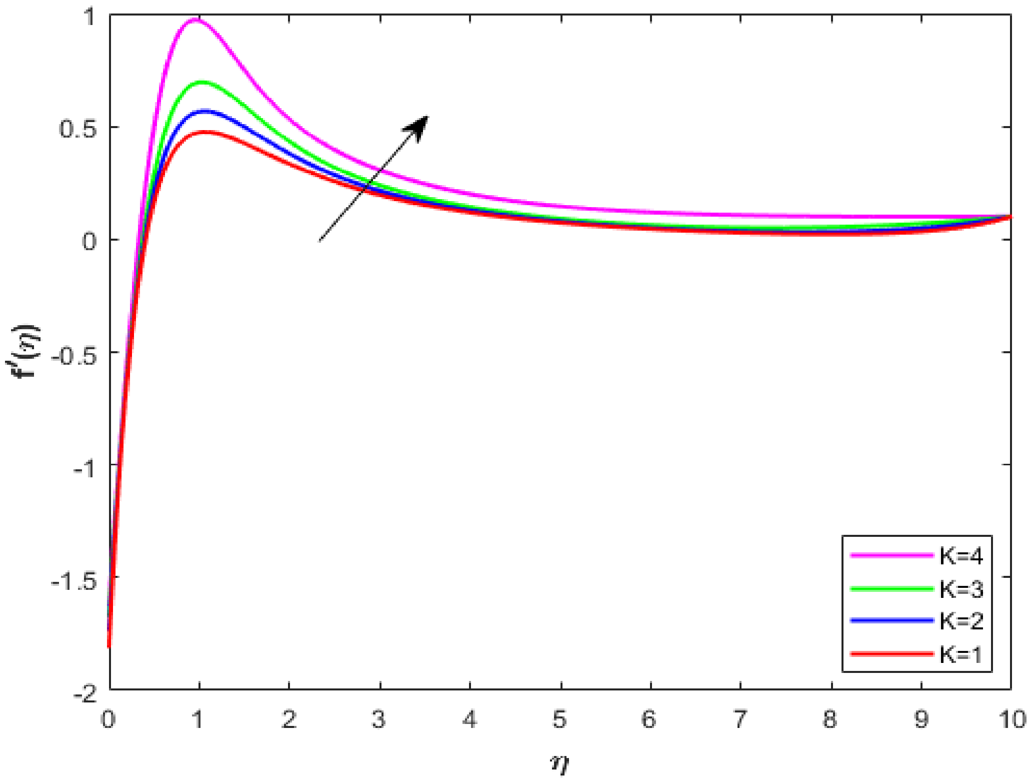

FIGURE 5.7: Effect of K on $f'(\eta)$ when $\omega = \delta = We = n = A = Q = Ec = \alpha = \Gamma = \chi = Sc = 0.1,\ \beta = Nt = Nb = 0.5,\ M = Rd = Pr = \gamma = Gc = 1,\ Gr = 2,\ \lambda = -1,\ S = 0.2$

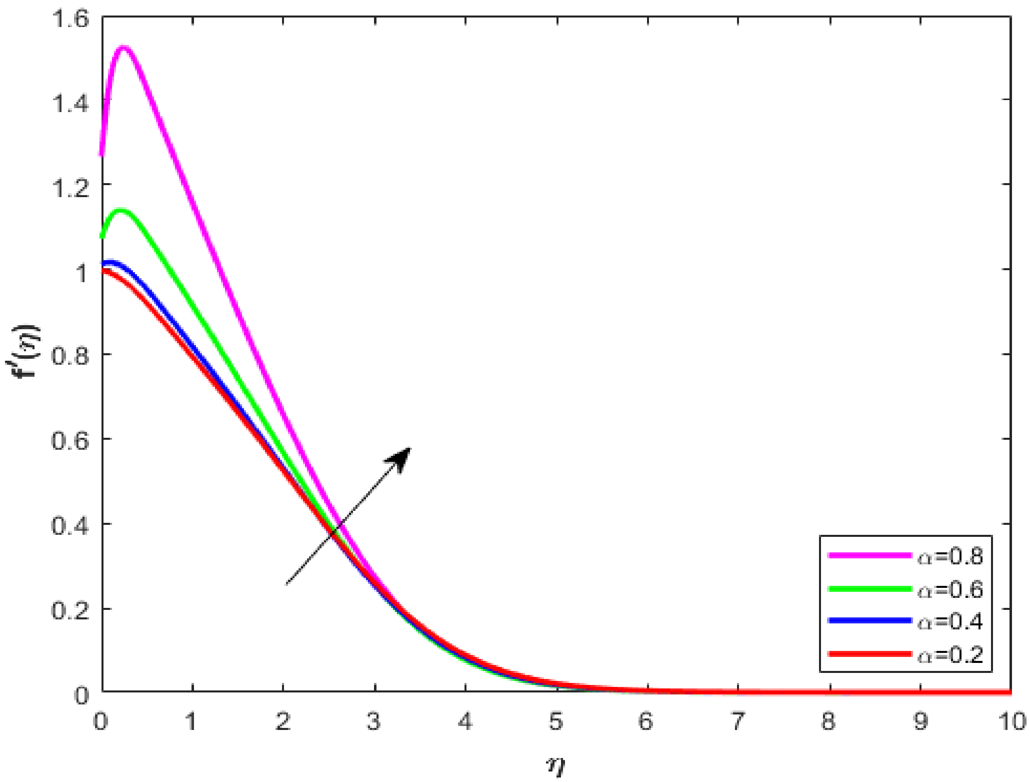

FIGURE 5.8: Effect of α on $f'(\eta)$ when $K = \omega = \delta = We = n = A = Q = Ec = \Gamma = \chi = Sc = 0.1,\ \beta = Nt = Nb = 0.5,\ M = Rd = Pr = \gamma = Gc = 1,\ Gr = 2,\ \lambda = -1,\ S = 0.2$

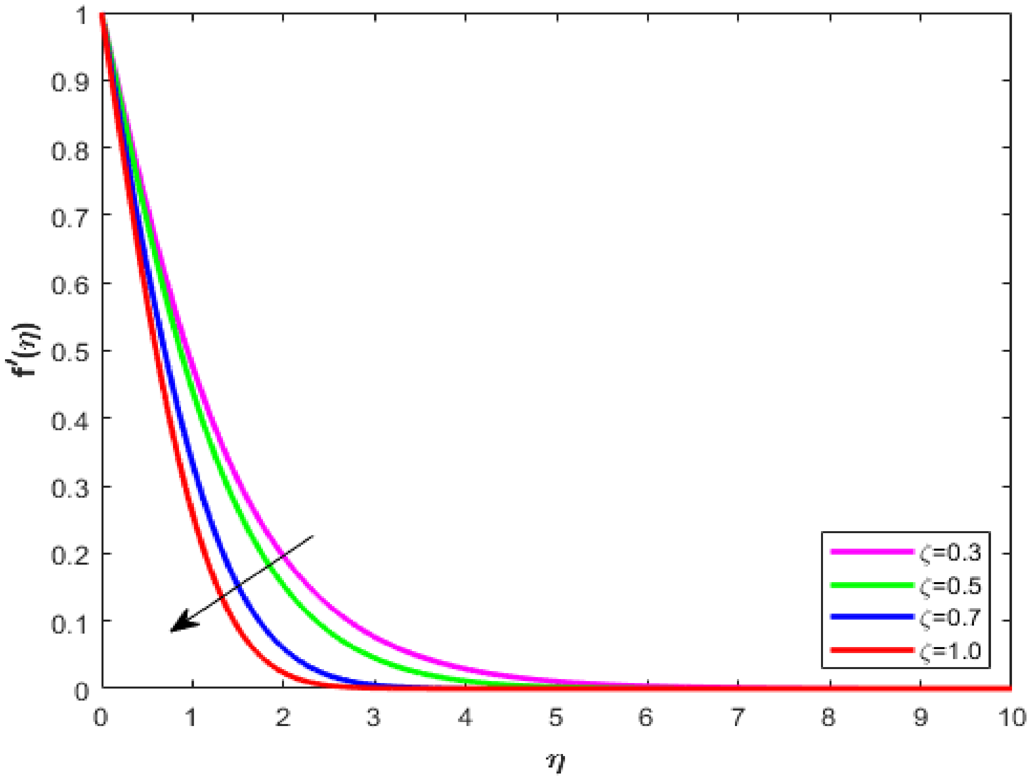

FIGURE 5.9: Effect of ζ on $f'(\eta)$ when $K = \omega = \delta = n = A = Q = Ec = \alpha = \Gamma = \chi = Sc = 0.1,\ Nt = Nb = 0.5,\ M = Rd = Pr = \gamma = Gc = 1,\ Gr = 2,\ \lambda = -1,\ S = 0.2$

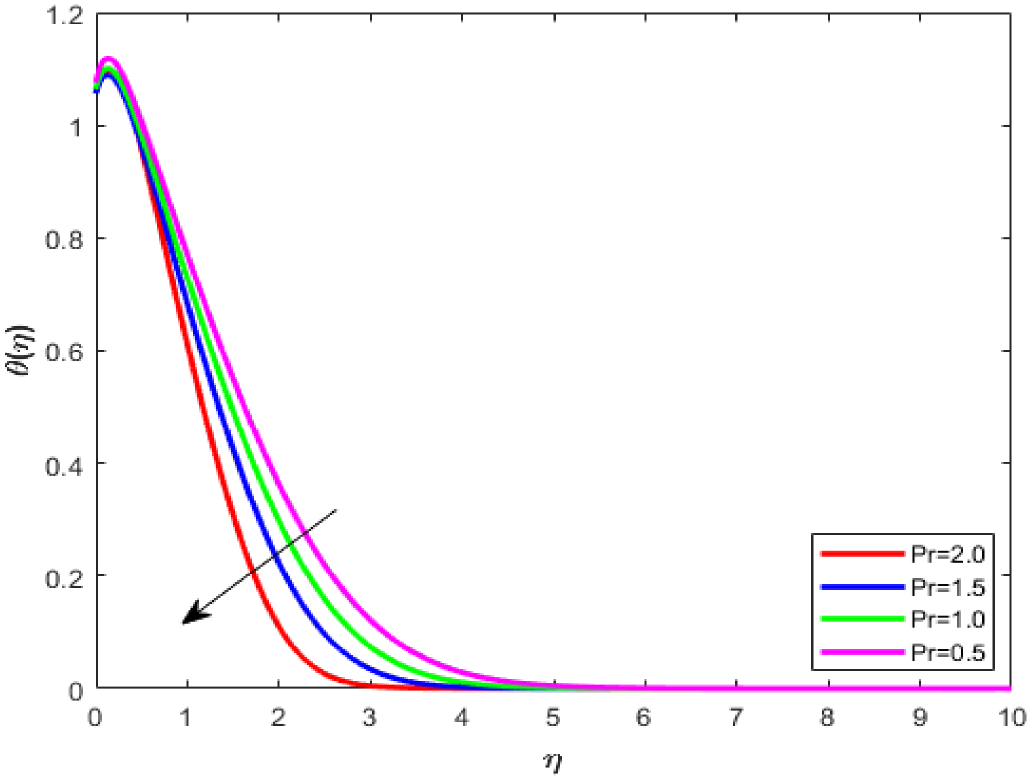

FIGURE 5.10: Effect of Pr on $\theta(\eta)$ when $K = \omega = \delta = We = n = A = Q = Ec = \alpha = \Gamma = \chi = Sc = 0.1,\ \beta = Nt = Nb = 0.5,\ M = Rd = \gamma = Gc = 1,\ Gr = 2,\ \lambda = -1,\ S = 0.2$

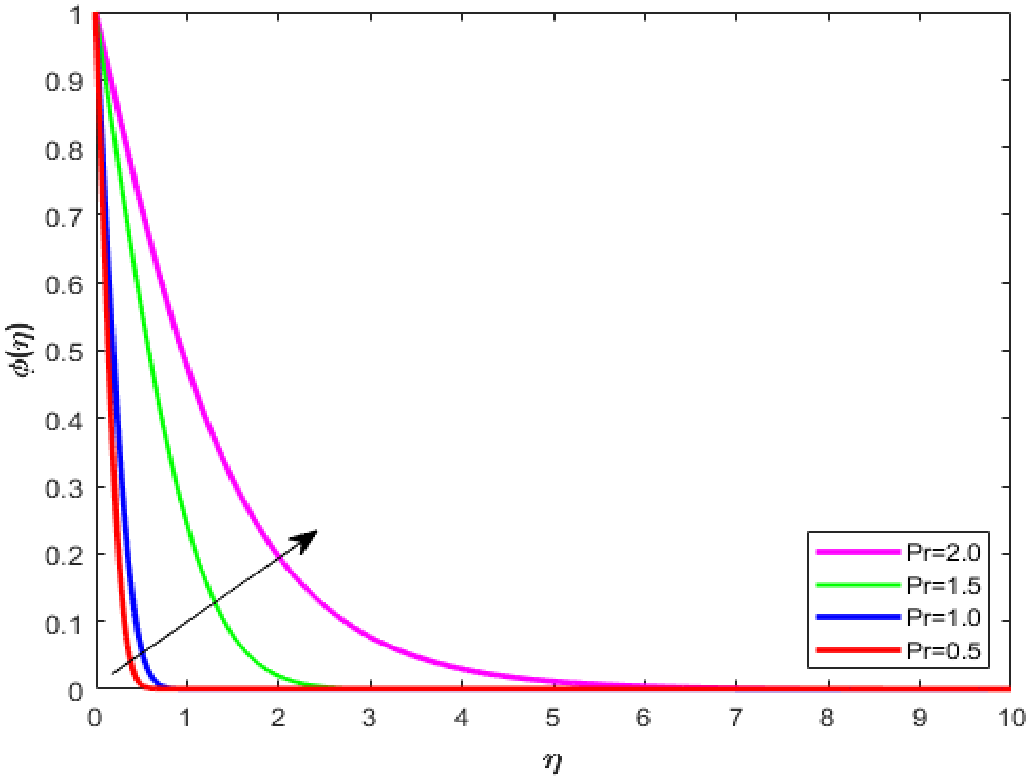

FIGURE 5.11: Effect of Pr on $\phi(\eta)$ when $K = \omega = \delta = We = n = A = Q = Ec = \alpha = \Gamma = \chi = Sc = 0.1,\ \beta = Nt = Nb = 0.5,\ M = Rd = \gamma = Gc = 1,\ Gr = 2,\ \lambda = -1,\ S = 0.2$

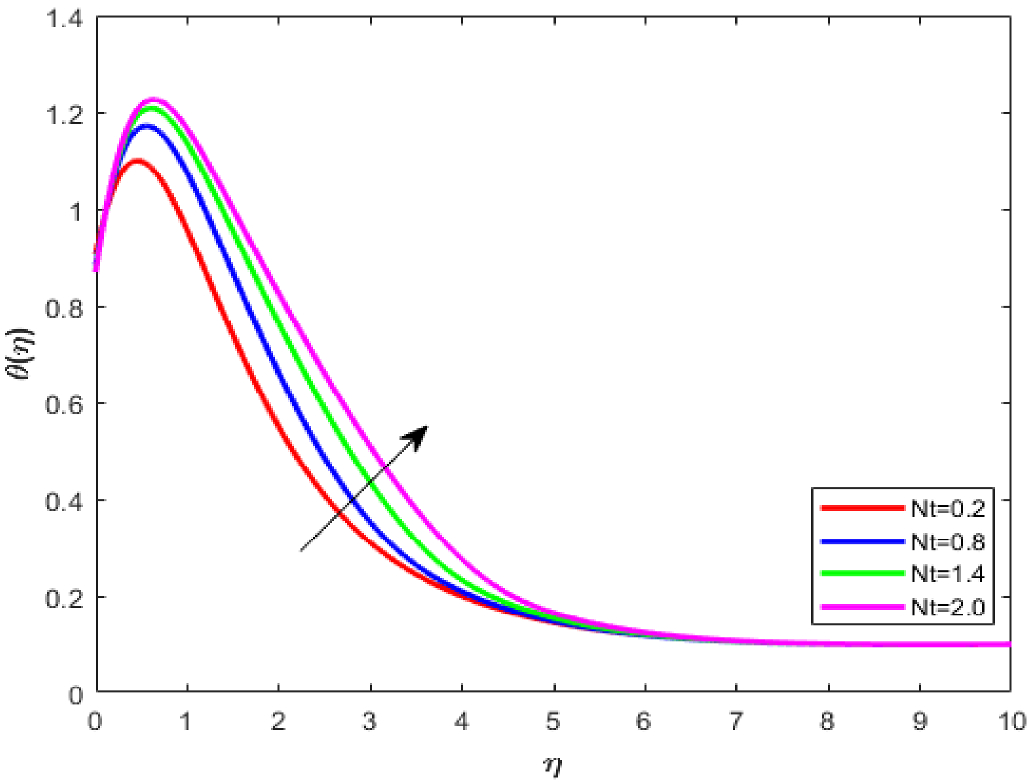

FIGURE 5.12: Effect of Nt on $\theta(\eta)$ when $K = \omega = \delta = We = n = A = Q = Ec = \alpha = \Gamma = \chi = Sc = 0.1,\ \beta = Nb = 0.5,\ M = Rd = Pr = \gamma = Gc = 1,\ Gr = 2,\ \lambda = -1,\ S = 0.2$

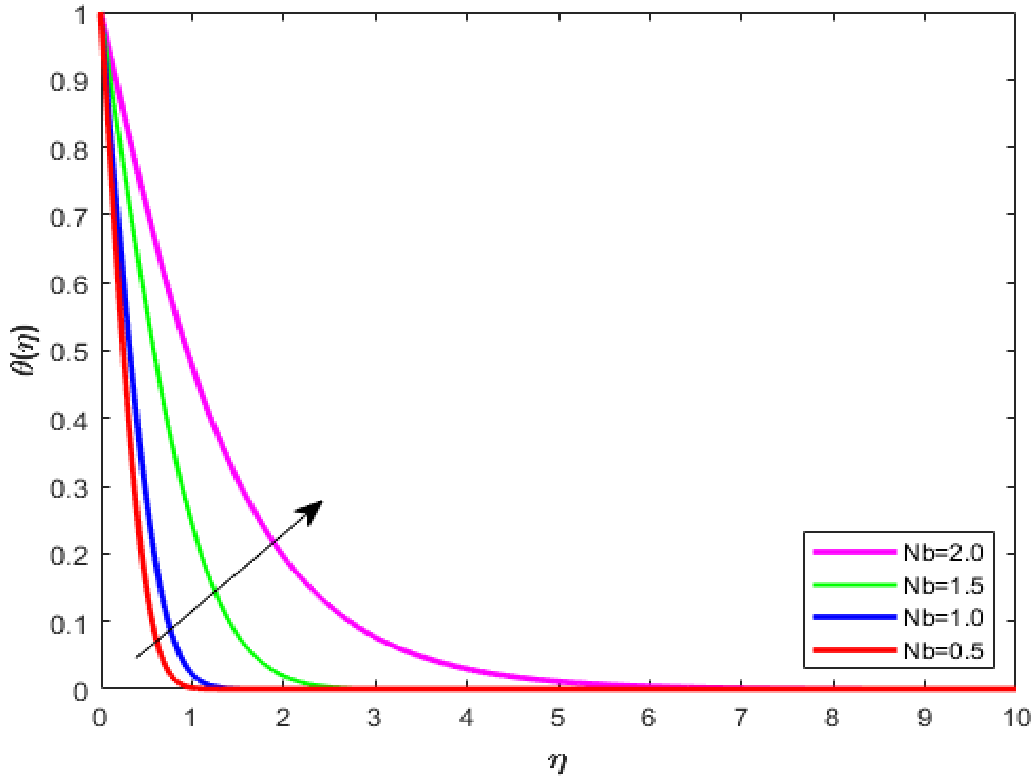

FIGURE 5.13: Effect of Nb on $\theta(\eta)$ when $K = \omega = \delta = We = n = A = Q = Ec = \alpha = \Gamma = \chi = Sc = 0.1,\ \beta = Nt = 0.5,\ M = Rd = Pr = \gamma = Gc = 1,\ Gr = 2,\ \lambda = -1,\ S = 0.2$

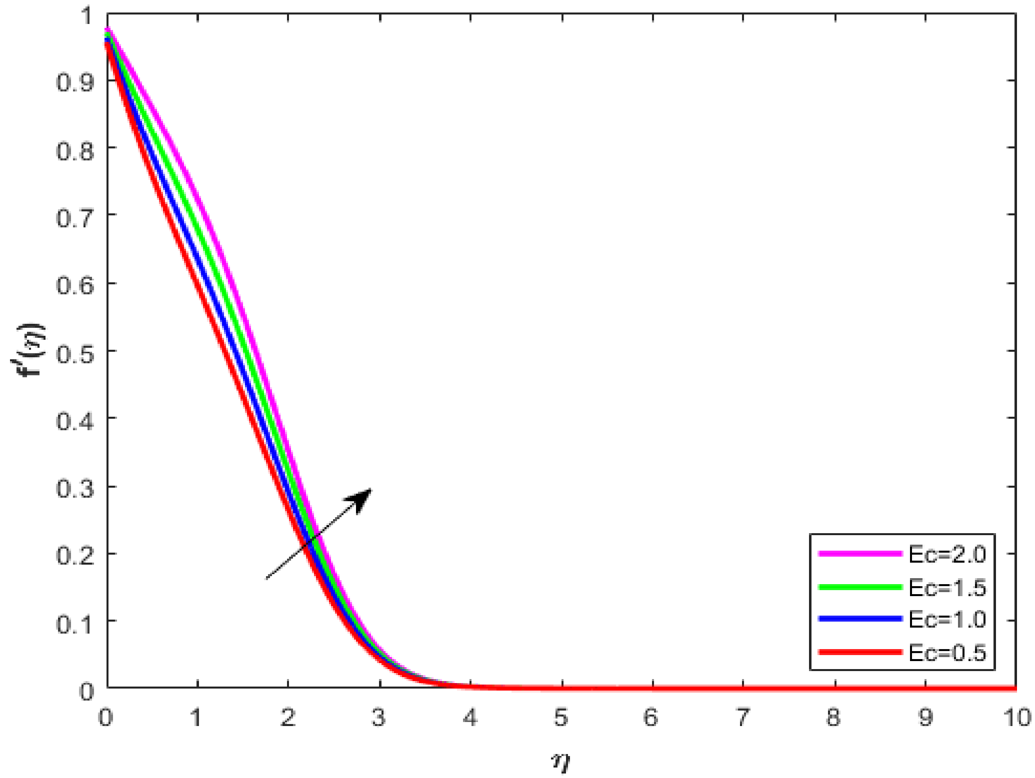

FIGURE 5.14: Effect of Ec on $f'(\eta)$ when $K = \omega = \delta = We = n = A = Q = \alpha = \Gamma = \chi = Sc = 0.1, \beta = Nt = Nb = 0.5,\ M = Rd = Pr = \gamma = Gc = 1,\ Gr = 2,\ \lambda = -1,\ S = 0.2$

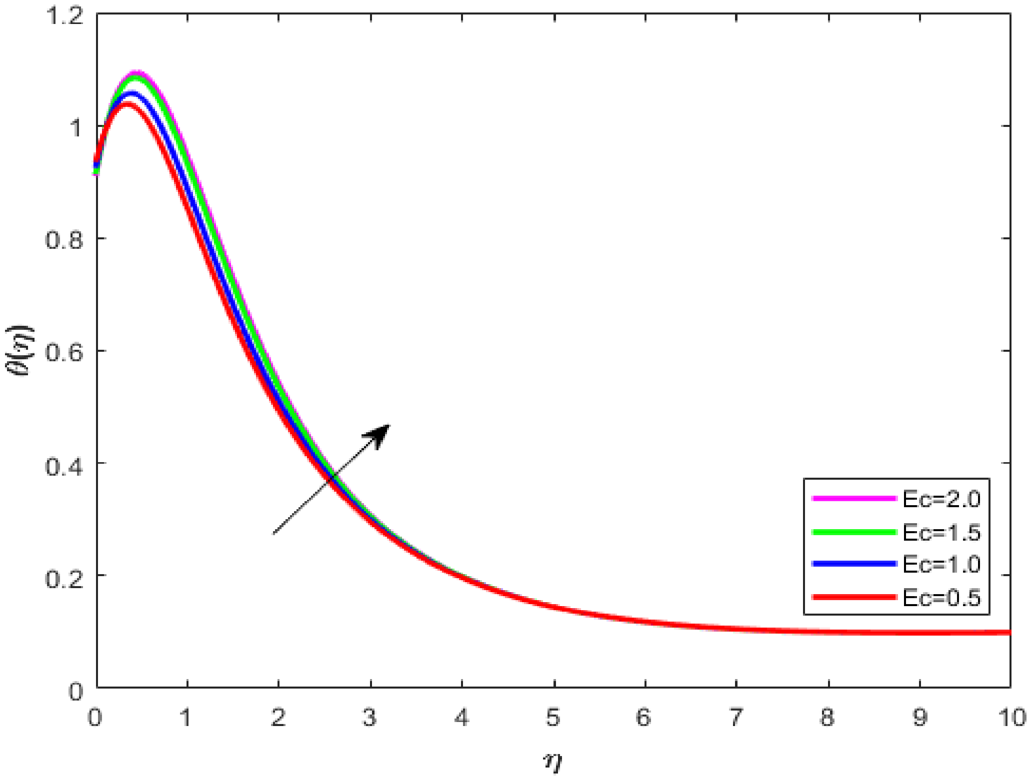

FIGURE 5.15: Effect of Ec on $\theta(\eta)$ when $K = \omega = \delta = We = n = A = Q = \alpha = \Gamma = \chi = Sc = 0.1,\ \beta = Nt = Nb = 0.5,\ M = Rd = Pr = \gamma = Gc = 1,\ Gr = 2,\ \lambda = -1,\ S = 0.2$

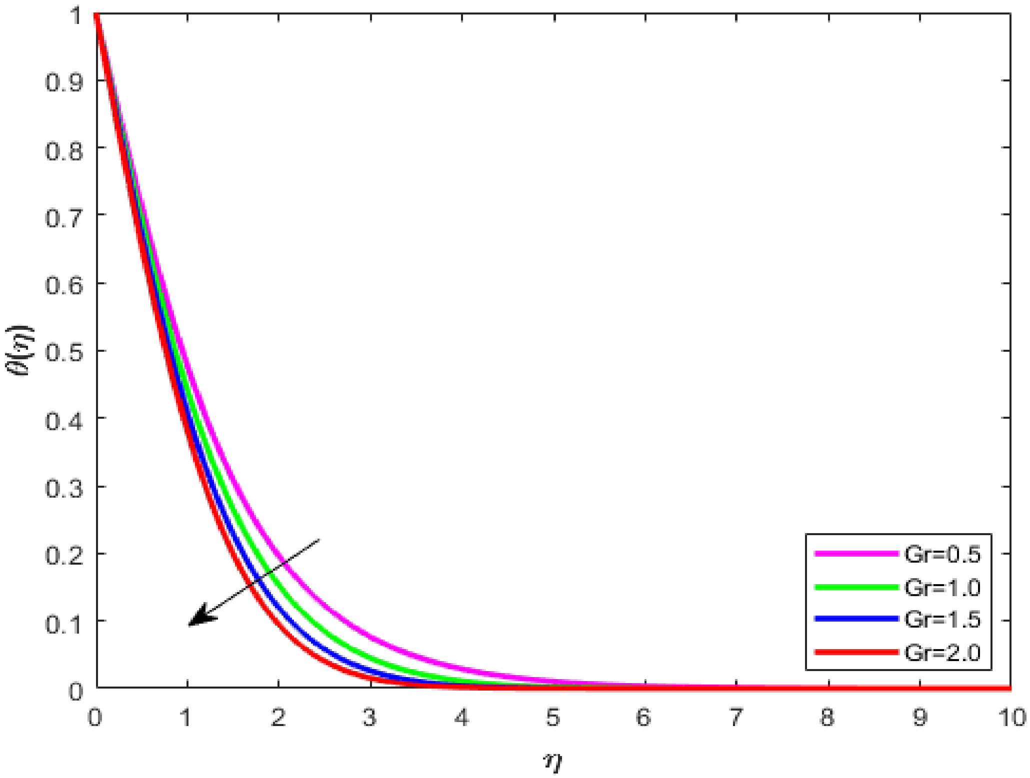

FIGURE 5.16: Effect of Gr on $\theta(\eta)$ when $K = \omega = \delta = We = n = A = Q = Ec = \alpha = \Gamma = \chi = Sc = 0.1,\ \beta = Nt = Nb = 0.5,\ M = Rd = Pr = \gamma = Gc = 1,\ \lambda = -1,\ S = 0.2$

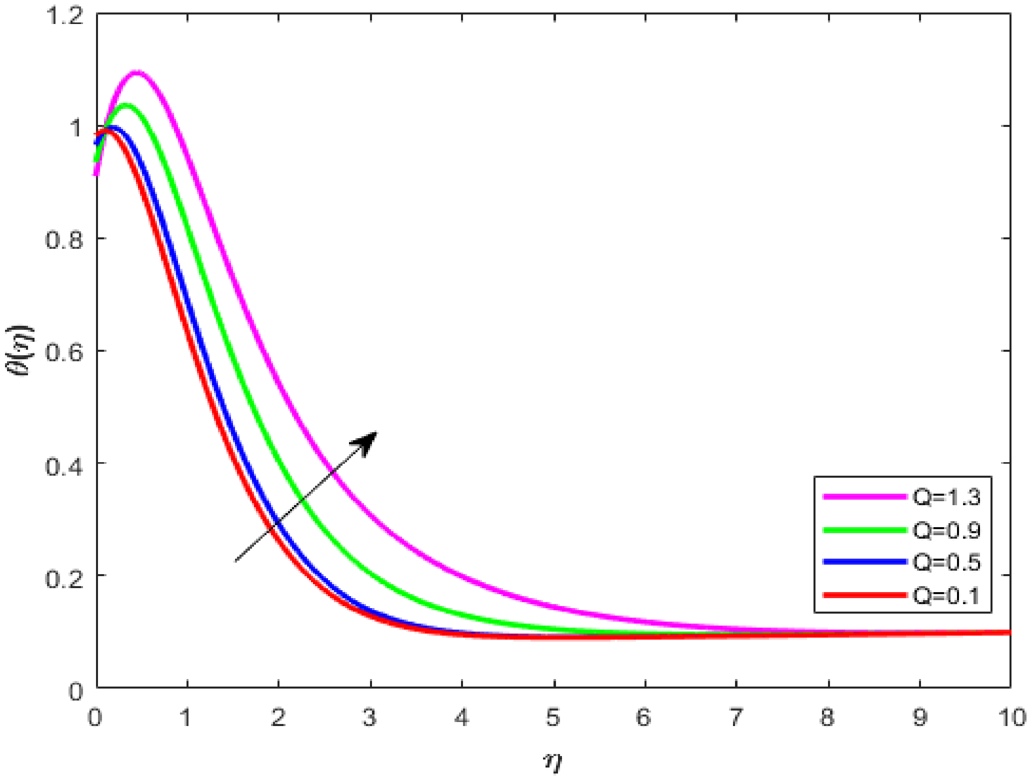

FIGURE 5.17: Effect of Q on $\theta(\eta)$ when $K = \omega = \delta = We = n = A = Ec = \alpha = \Gamma = \chi = Sc = 0.1,\ \beta = Nt = Nb = 0.5,\ M = Rd = Pr = \gamma = Gc = 1,\ Gr = 2,\ \lambda = -1,\ S = 0.2$

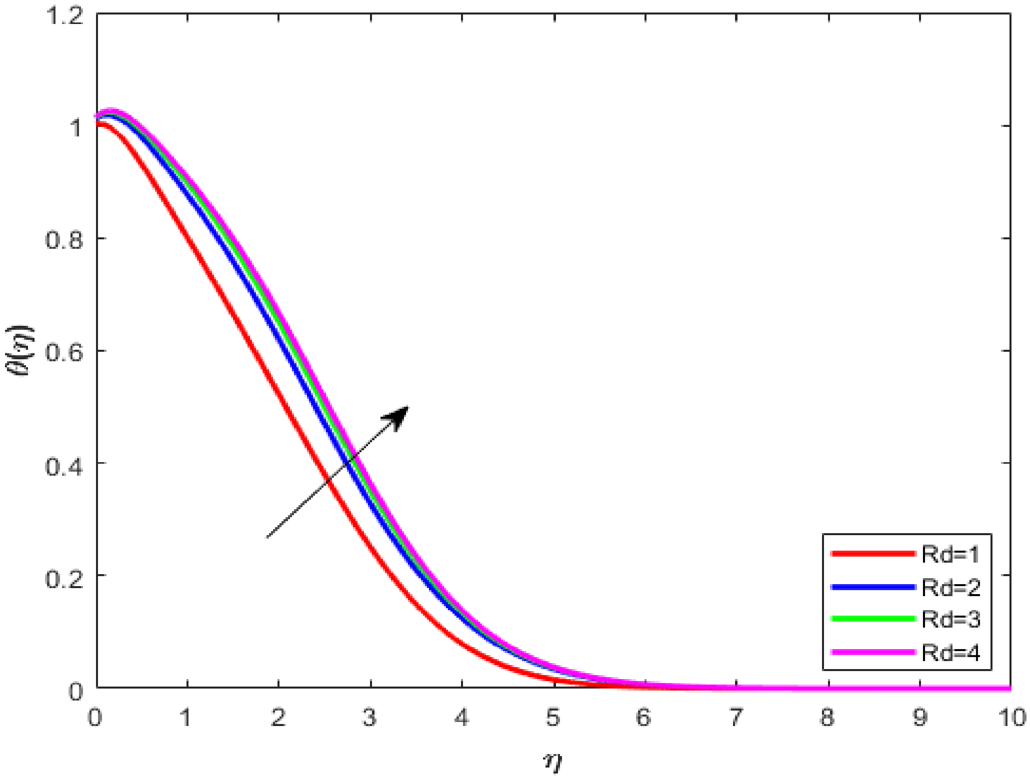

FIGURE 5.18: Effect of Rd on $\theta(\eta)$ when $K = \omega = \delta = We = n = A = Q = Ec = \alpha = \Gamma = \chi = Sc = 0.1,\ \beta = Nt = Nb = 0.5,\ M = Pr = \gamma = Gc = 1,\ Gr = 2,\ \lambda = -1,\ S = 0.2$

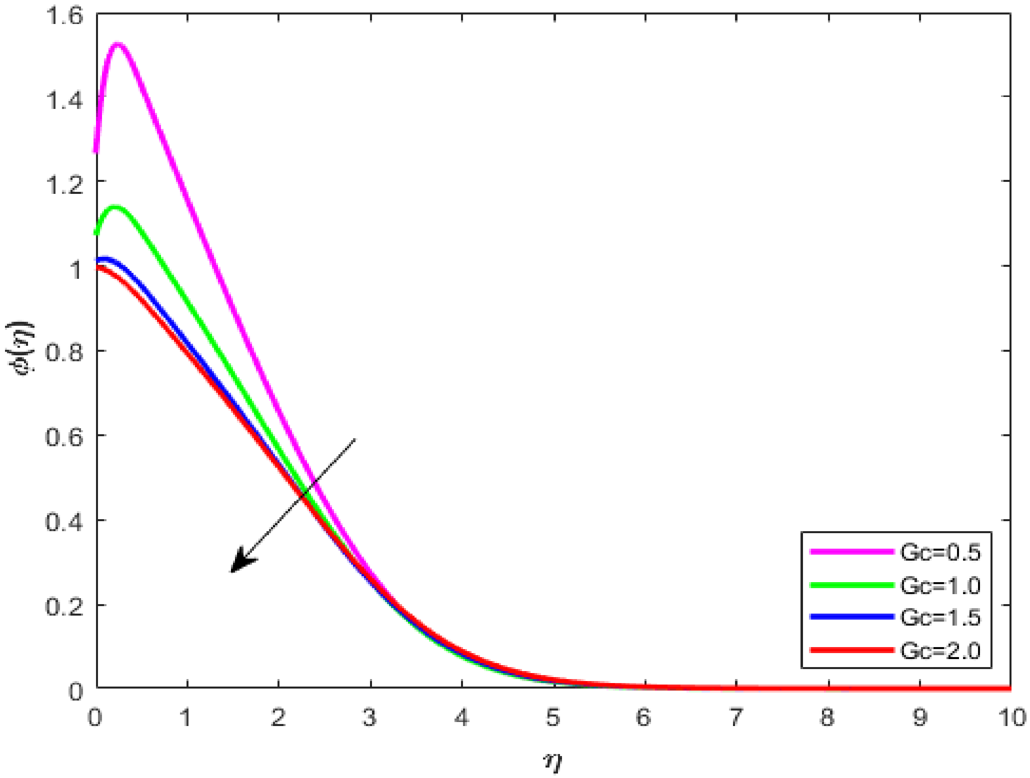

FIGURE 5.19: Effect of Gc on $\phi(\eta)$ when $K = \omega = \delta = We = n = A = Q = Ec = \alpha = \Gamma = \chi = Sc = 0.1,\ \beta = Nt = Nb = 0.5,\ Gr = 2,\ \lambda = -1,\ S = 0.2$

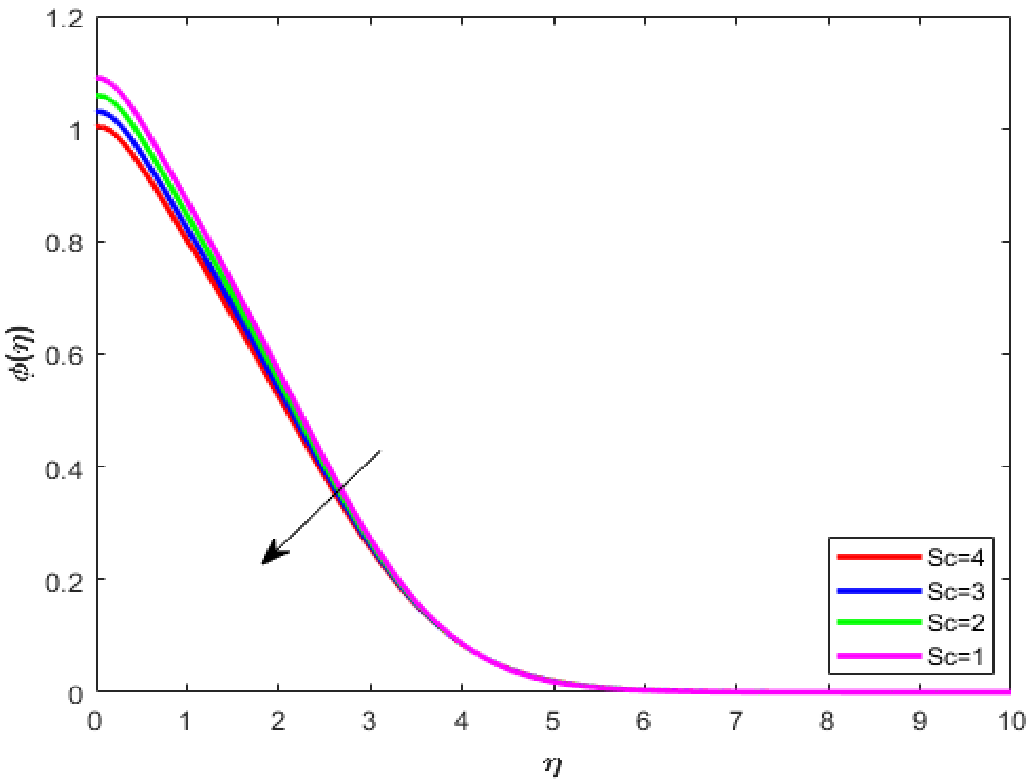

FIGURE 5.20: Effect of Sc on $\phi(\eta)$ when $K = \omega = \delta = We = n = A = Q = Ec = \alpha = \Gamma = \chi = 0.1,\ \beta = Nt = Nb = 0.5,\ M = Rd = Pr = \gamma = Gc = 1,\ Gr = 2,\ \lambda = -1,\ S = 0.2$

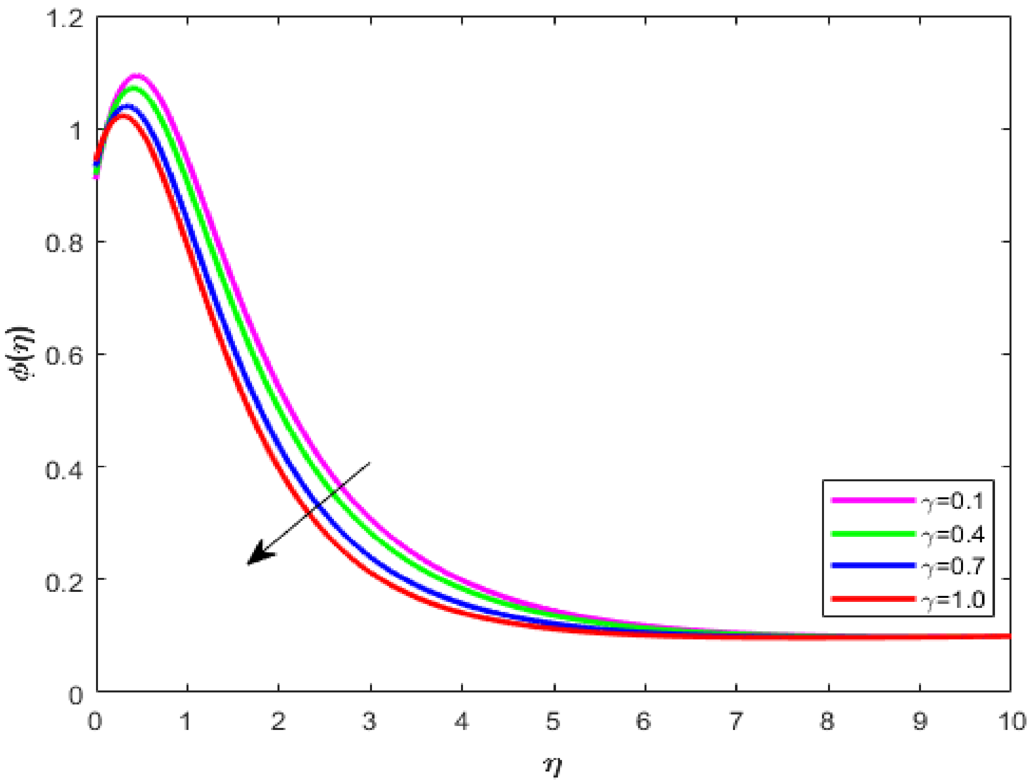

FIGURE 5.21: Effect of γ on $\phi(\eta)$ when $K = \omega = \delta = We = n = A = Q = Ec = \alpha = \Gamma = \chi = Sc = 0.1,\ \beta = Nt = Nb = 0.5,\ M = Rd = Pr = Gc = 1,\ Gr = 2,\ \lambda = -1,\ S = 0.2$

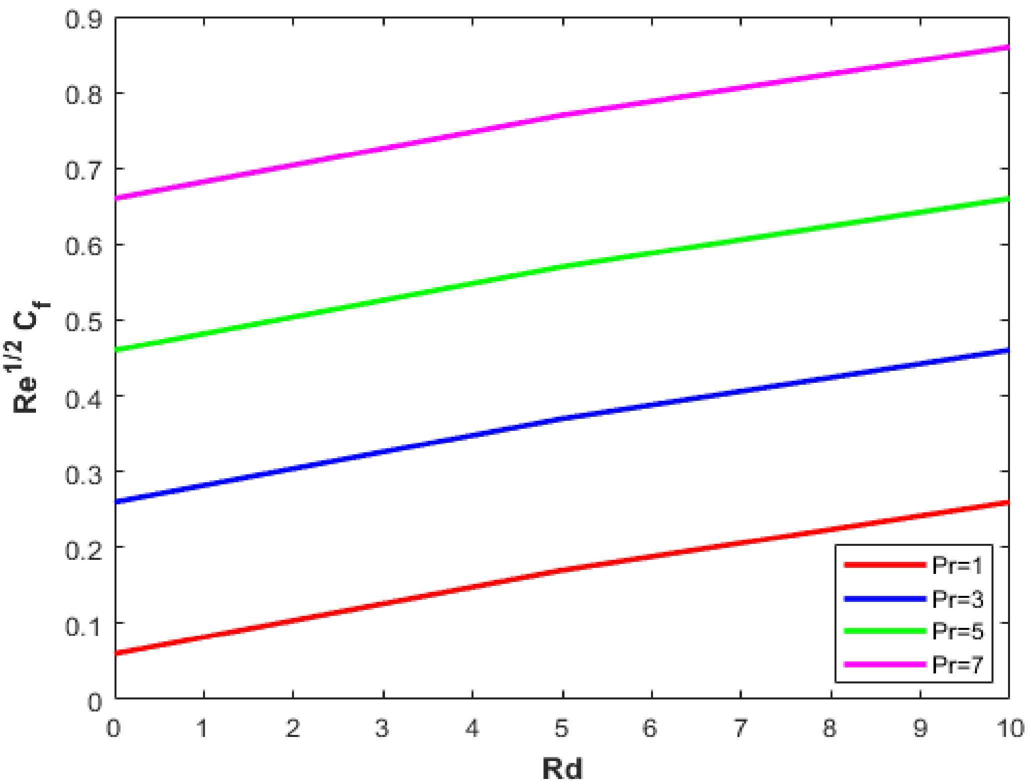

FIGURE 5.22: Effect of Rd and Pr on $Re^{\frac{1}{2}}C_f$ when $K = \omega = \delta = n = A = Q = Ec = \alpha = \Gamma = \chi = Sc = 0.1$, $Nt = Nb = 0.5$, $M = Rd = Pr = \gamma = Gc = 1$, $Gr = 2$, $\lambda = -1$, $S = 0.2$

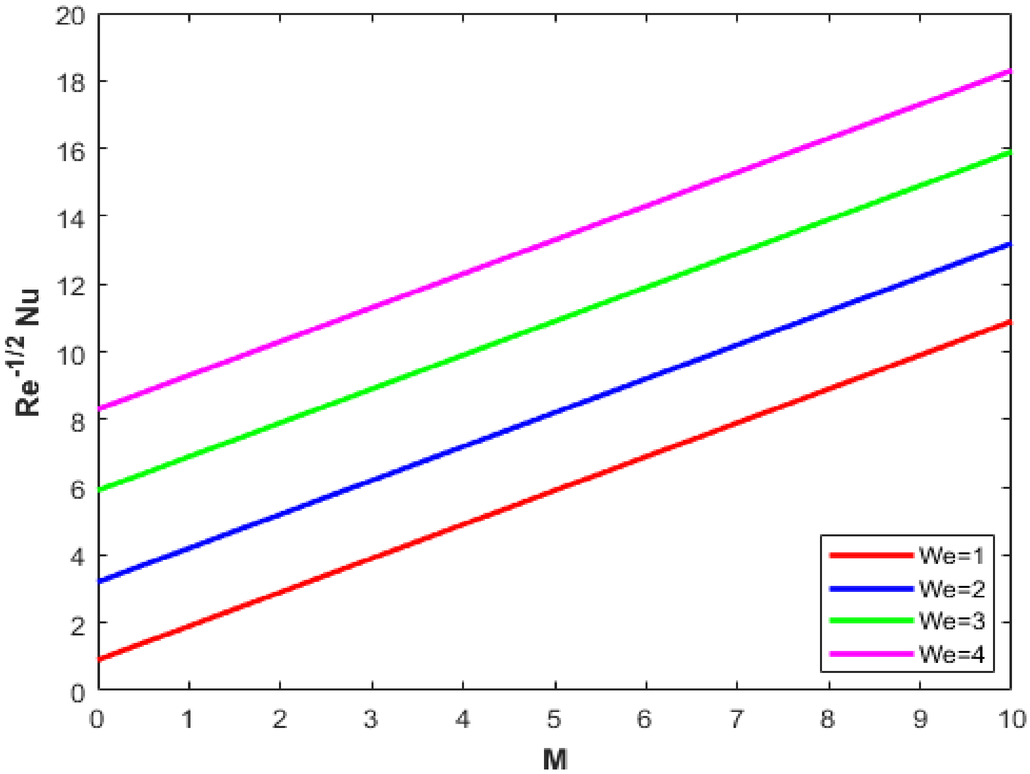

FIGURE 5.23: Effect of We and M on $Re^{-\frac{1}{2}}\ Nu$ when $K = \omega = \delta = n = A = Q = Ec = \alpha = \Gamma = \chi = Sc = 0.1$, $Nt = Nb = 0.5$, $M = Rd = Pr = \gamma = Gc = 1$, $Gr = 2$, $\lambda = -1$, $S = 0.2$

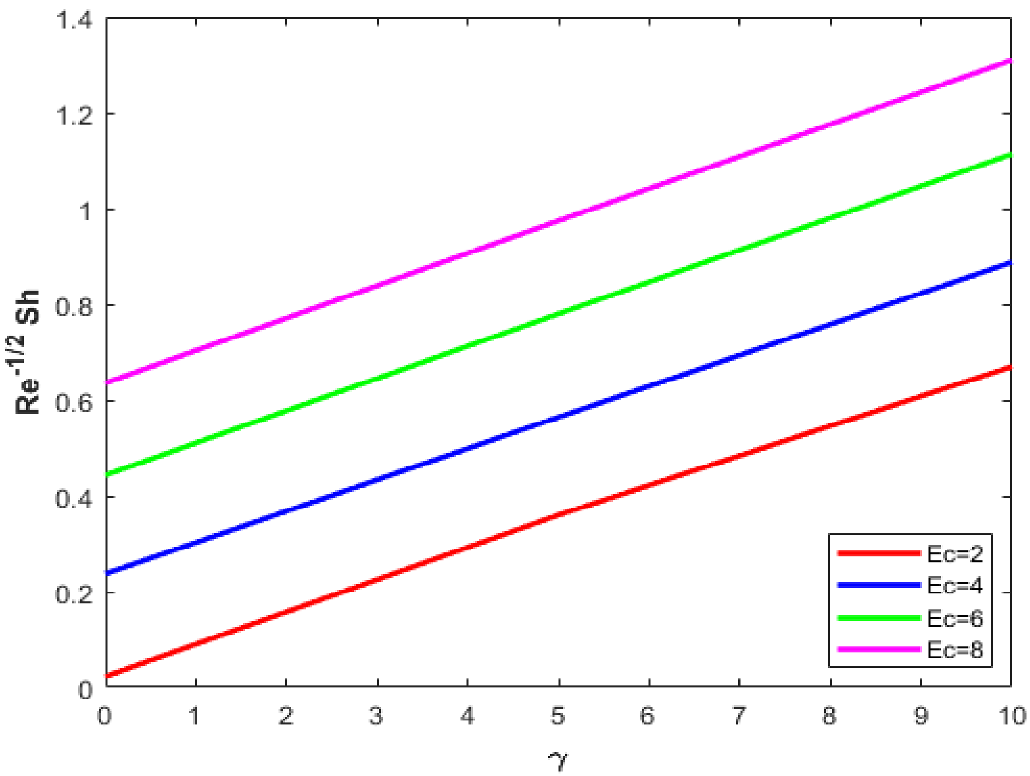

FIGURE 5.24: Effect of γ and Ec on $Re^{-\frac{1}{2}}Sh$ when $K = \omega = \delta = n = A = Q = Ec = \alpha = \Gamma = \chi = Sc = 0.1$, $Nt = Nb = 0.5$, $M = Rd = Pr = \gamma = Gc = 1$, $Gr = 2$, $\lambda = -1$, $S = 0.2$

Chapter 6

Transportation of Thermal and Mass Fluxes using Casson-Carreau Nanofluid

6.1 Introduction

The flow of Casson-Carreau nanofluids over a non-linear stretching sheet has been taken into account. The velocity of the sheet is supposed to be $\mathscr{U}_e = a\,(x+y)^m$, $\mathscr{V}_e = a\,(x+y)^m$, where $a, b \geq 0$. The flow is restrained in the neighborhood $z \geq 0$. The following crucial hypotheses have further been considered:

- compressible, steady and non-linear 3D-flow,
- boundary layer approximation,
- Cattaneo-Christov heat flux model,
- variable magnetic field, Brownian motion and thermophoresis.
- single phase nanofluid model.

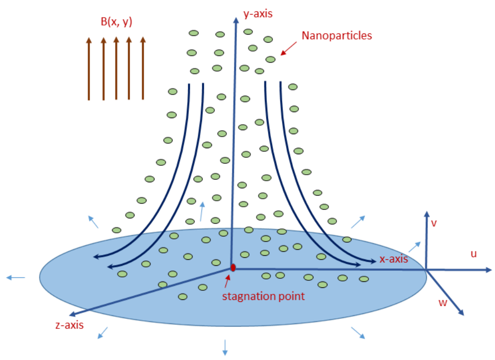

FIGURE 6.1: Schematic physical model

The mathematical formulation of the model takes the following form [75]:

$$\frac{\partial}{\partial x} + \frac{\partial}{\partial z} + \frac{\partial}{\partial y} = 0, \tag{6.1}$$

$$\begin{aligned}\frac{\partial}{\partial x} + \frac{\partial}{\partial y} + \frac{\partial}{\partial z} = \nu_f \left[\left(1 + \frac{1}{\beta}\right) + \left(1 + \Gamma^2 \left(\frac{\partial}{\partial z}\right)^2\right)^{\frac{n-1}{2}} \right] \frac{\partial^2}{\partial z^2} + \mathscr{U}_e \frac{d\mathscr{U}_e}{dx} - \frac{\nu_f}{k'} \\ + \nu_f (n-1) \Gamma^2 \frac{\partial^2}{\partial z^2} \left(\frac{\partial}{\partial z}\right)^2 \left[1 + \tau^2 \left(\frac{\partial}{\partial z}\right)^2\right]^{\frac{n-3}{2}} - \frac{\sigma B_o^2(x,y)}{\rho_f} \\ + g\beta_T(T - T_\infty) + g\beta_c(C - C_\infty),\end{aligned} \tag{6.2}$$

$$\begin{aligned}\frac{\partial}{\partial x} + \frac{\partial}{\partial y} + \frac{\partial}{\partial z} = \nu_f \left[\left(1 + \frac{1}{\beta}\right) + \left(1 + \Gamma^2 \left(\frac{\partial}{\partial z}\right)^2\right)^{\frac{n-1}{2}} \right] \frac{\partial^2}{\partial z^2} + \mathscr{V}_e \frac{d\mathscr{V}_e}{dy} - \frac{\nu_f}{k'} \\ + \nu_f (n-1) \Gamma^2 \frac{\partial^2}{\partial z^2} \left(\frac{\partial}{\partial z}\right)^2 \left[1 + \tau^2 \left(\frac{\partial}{\partial z}\right)^2\right]^{\frac{n-3}{2}} - \frac{\sigma B_o^2(x,y)}{\rho_f} \\ + g\beta_T(T - T_\infty) + g\beta_c(C - C_\infty),\end{aligned} \tag{6.3}$$

$$\begin{aligned}\frac{\partial T}{\partial x} + \frac{\partial T}{\partial y} + \frac{\partial T}{\partial z} + \lambda^* \Bigg[2 \frac{\partial^2 T}{\partial x \partial y} + 2 \frac{\partial^2 T}{\partial x \partial z} + 2 \frac{\partial^2 T}{\partial y \partial z} + {}^2 \frac{\partial^2 T}{\partial x^2} + {}^2 \frac{\partial^2 T}{\partial z^2} \\ + v^2 \frac{\partial^2 T}{\partial y^2} + \left(u \frac{\partial u}{\partial x} + v \frac{\partial u}{\partial y} + w \frac{\partial u}{\partial z}\right) T_x + \left(u \frac{\partial v}{\partial x} + v \frac{\partial v}{\partial y} + w \frac{\partial v}{\partial z}\right) T_y + \Big(u \frac{\partial w}{\partial x} \\ + v \frac{\partial w}{\partial y} + \frac{\partial}{\partial z}\Big) T_z \Bigg] = \alpha_f \frac{\partial^2 T}{\partial z^2} + \tau \left[D_B \frac{\partial C}{\partial z} \frac{\partial T}{\partial z} + \frac{D_T}{T_\infty} \left(\frac{\partial T}{\partial z}\right)^2 \right] + \frac{\sigma B_0^2(x,y)\left({}^2 + {}^2\right)}{(\rho c_p)_f} \\ + \frac{\nu_f}{c_p} \left(1 + \frac{1}{\beta}\right) \left[\left(\frac{\partial}{\partial z}\right)^2 + \left(\frac{\partial v}{\partial z}\right)^2 \right] + \frac{Q_0(T - T_\infty)}{(\rho c_p)_f},\end{aligned} \tag{6.4}$$

$$u \frac{\partial C}{\partial x} + v \frac{\partial C}{\partial y} + w \frac{\partial C}{\partial z} + \lambda^* \Bigg[2uv \frac{\partial^2 C}{\partial x \partial y} + 2uw \frac{\partial^2 C}{\partial x \partial z} + 2vw \frac{\partial^2 C}{\partial y \partial z} + u^2 \frac{\partial^2 C}{\partial x^2} + w^2 \frac{\partial^2 C}{\partial z^2}$$

$$+ v^2 \tfrac{\partial^2 C}{\partial y^2} + \left(u\tfrac{\partial u}{\partial x} + v\tfrac{\partial u}{\partial y} + w\tfrac{\partial u}{\partial z}\right)C_x + \left(u\tfrac{\partial v}{\partial x} + v\tfrac{\partial v}{\partial y} + W\tfrac{\partial v}{\partial z}\right)C_y + \left(u\tfrac{\partial w}{\partial x}\right.$$

$$\left. + v\tfrac{\partial w}{\partial y} + w\tfrac{\partial w}{\partial z}\right)C_z\Bigg] = D_B \tfrac{\partial^2 C}{\partial z^2} + \tfrac{D_T}{T_\infty}\tfrac{\partial^2 T}{\partial z^2} - C_r\left(C - C_\infty\right). \tag{6.5}$$

Furthermore, for the relevant boundary layers, the following boundary conditions have been focused:

$$u = U_w = ax, \quad v = V_w = by, \quad T = T_w, \quad C = C_w, \quad w = 0 \quad \text{at} \quad z = 0,$$

$$u \to 0, \quad v \to 0, \quad T \to T_\infty, \quad C \to C_\infty \quad \text{as} \quad z \to \infty. \tag{6.6}$$

For the transformation of the above model into the dimensionless form, the following similarity transformations have been taken into account:

$$u = a\left(x+y\right)^m f'\left(\eta\right), \quad v = b\left(x+y\right)^m g'\left(\eta\right), \quad \eta = \left(\tfrac{a}{\nu}\right)^{\frac{1}{2}} z(x+y)^{\frac{n-1}{2}},$$

$$w = -\left(av\right)^{\frac{1}{2}}\left(x+y\right)^{\frac{m-1}{2}}\left[\tfrac{m+1}{2}(f\left(\eta\right)+g\left(\eta\right)) + \eta\tfrac{m-1}{2}(f'\left(\eta\right)+g'\left(\eta\right))\right],$$

$$\theta\left(\eta\right) = \frac{T - T_\infty}{T_f - T_\infty}, \quad \phi\left(\eta\right) = \frac{C - C_\infty}{C_f - C_\infty}. \tag{6.7}$$

Upon incorporating the aforementioned similarity transformations, the ODEs describing the proposed flow problem take on the subsequent structure.

$$\left[\left(1 + nWe^2\left(''\right)^2\right)\left(1 + We^2\left(''\right)^2\right)^{\frac{n-3}{2}} + \left(1 + \tfrac{1}{\beta}\right)\right]''' + \left(\tfrac{m+1}{2}\right)\left('+'\right)''$$

$$- K' - m\left('+'\right)' - M' + Gr\theta + Gc\phi = 0, \tag{6.8}$$

$$\left[\left(1 + nWe^2\left(''\right)^2\right)\left(1 + We^2\left(''\right)^2\right)^{\frac{n-3}{2}} + \left(1 + \tfrac{1}{\beta}\right)\right]''' + \left(\tfrac{m+1}{2}\right)\left('+'\right)''$$

$$- K' - m\left('+'\right)' - M' + Gr\theta + Gc\phi = 0, \tag{6.9}$$

$$\tfrac{1}{Pr}\theta'' + Nb\theta'\phi' + Nt\theta'^2 + \left(\tfrac{m+1}{2}\right)\left(+\right)\theta' + Q\theta + \left(1 + \tfrac{1}{\beta}\right)Ec\left(''^2 + ''^2\right)$$

$$+ EcM^2\left('+'\right) - \sigma_a\left(\left(+\right)('+')\theta' + \left(+\right)^2\theta''\right) = 0, \tag{6.10}$$

$$\tfrac{1}{Sc}\phi'' + \frac{Nt}{Nb}\theta'' + \tfrac{n+1}{2}\left(+\right)\phi' - \sigma_b\left(\left(+\right)('+')\phi' + \left(+\right)^2\phi''\right)$$

$$+ \left(2\phi' - \gamma\phi\right) = 0. \tag{6.11}$$

The corresponding conditions prescribed at the boundary are as follows.

$$
\begin{aligned}
& f(0)=0,\ g(0)=0,\ f'(0)=1,\ g'(0)=\Gamma,\ \theta'(0)=-Bi_1(1-\theta(0)), \\
& \phi'(0)=-Bi_2(1-\phi(0)), \\
& {}'\to 0,\ {}'\to 0,\ \phi\to 0,\ \theta\to 0 \ \text{ as } \ \eta\to\infty. \qquad (6.12)
\end{aligned}
$$

The formulation of the non-dimensional quantities incorporated in the above equations takes the following form.

$$
\begin{aligned}
& Nb=\frac{\tau D_B(C_f-C_\infty)}{\nu_f},\ Pr=\frac{\nu_f}{\alpha_f},\ Nt=\frac{\tau D_T(T_f-T_\infty)}{\nu_f T_\infty},\ M^2=\frac{\sigma B_0^2}{\rho_f a}, \\
& Q=\frac{Q_0}{\rho_f c_p a},\ Ec=\frac{a^2(x+y)^2}{\alpha_f c_p(T_f-T_\infty)},\ A=\frac{b}{a},\ Sc=\frac{\nu_f}{D_B},\ We^2=\frac{\Gamma^2 a^3(x+y)^2}{\nu_f}, \\
& Gr=\frac{g\beta_T(T_f-T_\infty)}{a^2(x+y)},\quad Gc=\frac{g\beta_c(C_f-C_\infty)}{a^2(x+y)},\quad \gamma=\frac{C_r}{a}.
\end{aligned}
$$

Given below are the formulae for the drag coefficient, heat and mass transfer gradients in the original form.

$$
C_{fx}=\frac{\tau_{xz}}{\rho_f \mathscr{U}_w^2},\ C_{fy}=\frac{\tau_{yz}}{\rho_f \mathscr{U}_w^2},\ Nu=\frac{(x+y)N_w}{k_f(T_f-T_\infty)},\ Sh=\frac{(x+y)S_w}{D_B(C_f-C_\infty)}. \qquad (6.13)
$$

The formulation of τ_{xz}, N_w, S_w and τ_{yz} are as follows:

$$
\begin{aligned}
& \tau_{xz}=\mu\left(\frac{\partial}{\partial z}\right)_{z=0}\left[\left(1+\tfrac{1}{\beta}\right)+\left[1+\Gamma^2\left(\frac{\partial}{\partial z}\right)^2\right]_{z=0}^{\frac{n-1}{2}}\right],\quad N_w=-k_f\left[\left(\frac{\partial T}{\partial z}\right)\right]_{z=0}, \\
& S_m=-D_B\left(\frac{\partial C}{\partial z}\right)_{z=0},\quad \tau_{yz}=\mu\left(\frac{\partial}{\partial z}\right)_{z=0}\left[\left(1+\tfrac{1}{\beta}\right)+\left[1+\Gamma^2\left(\frac{\partial}{\partial z}\right)^2\right]_{z=0}^{\frac{n-1}{2}}\right].
\end{aligned}
\qquad (6.14)
$$

The non-dimensional form of the skin-friction coefficient, Nusselt number and Sherwood number obtained by incorporating the similarity variables is given by:

$$
\begin{aligned}
& Re^{\frac{1}{2}}C_{fx}=\left[\left(1+\tfrac{1}{\beta}\right)+\left(1+We^{2\prime\prime 2}(0)\right)^{\frac{n-1}{2}}\right]''(0),\ Re^{-\frac{1}{2}}Nu=-\theta'(0), \\
& Re^{\frac{1}{2}}C_{fy}=\left[\left(1+\tfrac{1}{\beta}\right)+\left(1+We^{2\prime\prime 2}(0)\right)^{\frac{n-1}{2}}\right]''(0),\ Re^{-\frac{1}{2}}Sh=-\phi'(0), \qquad (6.15)
\end{aligned}
$$

where $Re = \dfrac{(x+y)\mathscr{U}_w}{\nu_f}$ elucidates the local Reynolds number.

6.2 Solution Methodology

In order to acquire numerical results for the system of ODEs (6.8)-(6.11) along with the specified boundary conditions (6.12), the shooting method has been employed. The unknown initial conditions $F''(0)$, $G''(0)$, $\theta(0)$ and $\phi(0)$ have been represented by A, B, C and D, respectively. Prior to introducing the shooting technique, it is necessary to incorporate the following notations.

$$= y_1, ' = y_2, '' = y_3, \; = y_4, ' = y_5, '' = y_6, \theta = y_7, \theta' = y_8, \phi = y_9, \phi' = y_{10}. \tag{6.16}$$

Incorporating the above notations in equations (6.8)-(6.11) results in yielding the following first-order ODEs.

$$y_1' = y_2, \qquad y_1(0) = 0,$$

$$y_2' = y_3, \qquad y_2(0) = 1,$$

$$y_3' = \frac{-\left(\frac{m+1}{2}\right)(y_2+y_5)\,y_3 + Ky_2 + m\,(y_2+y_5)\,y_2 + My_2 - Gry_7 - Gcy_9}{\left[\left(1+nWe^2\,(y_3)^2\right)\left(1+We^2\,(y_3)^2\right)^{\frac{n-3}{2}} + \left(1+\frac{1}{\beta}\right)\right]},$$

$$y_3(0) = A,$$

$$y_4' = y_5, \qquad y_4(0) = 0,$$

$$y_5' = y_6, \qquad y_5(0) = 1,$$

$$y_6' = \frac{-\left(\frac{m+1}{2}\right)(y_2+y_5)\,y_6 + Ky_5 + m\,(y_2+y_5)\,y_5 + My_5 - Gry_7 - Gcy_9}{\left[\left(1+nWe^2\,(y_6)^2\right)\left(1+We^2\,(y_6)^2\right)^{\frac{n-3}{2}} + \left(1+\frac{1}{\beta}\right)\right]},$$

$$y_6(0) = B,$$

$$y_7' = y_8, \qquad y_7(0) = C,$$

$$\begin{aligned} y_8' = {} & \frac{-Pr}{1 - Pr\sigma_a\left((y_1+y_4)^2\right)}\Big(Nby_8y_{10} + Nty_8^2 + \left(\tfrac{m+1}{2}\right)(y_1+y_4)\,y_8 + Qy_7 \\ & + \left(1+\tfrac{1}{\beta}\right)Ec\left(y_3^2+y_6^2\right)^2 + EcM^2\,(y_2+y_4) - \sigma_a\left((y_1+y_4)(y_2+y_5)y_8\right), \end{aligned}$$

$$y_8(0) = -Bi_1(1 - y_7(0)),$$

$$y_9' = y_{10}, \qquad y_9(0) = D,$$

$$y_{10}' = \frac{-\frac{Nt}{Nb}y_8 - \frac{n+1}{2}(y_1 + y_4)y_9 + \sigma_b(y_1 + y_4)(y_2 + y_5)y_9 - (2y_1y_{10} - \gamma y_9)}{\frac{1}{Sc} - \sigma_b(y_1 + y_4)^2},$$

$$y_{10}(0) = -Bi_2(1 - y_9(0)).$$

In addition to this, the above equations are differentiated w.r.t. the variables A, B, C and D and the obtained IVP is solved with the aid of RK-4 technique. The computed values of the boundary conditions obtained at the right endpoint of the domain are then compared with the given conditions in equation (6.12). The refinement of the missing conditions is done by using Newton's method. Moreover, the step size is chosen to be 0.001 and accuracy to be 10^{-14} as the convergence criterion. In the current article, we find that using $\eta_\infty = 10$ serves as a suitable approximation for the right end of the domain in all the numerical results presented.

6.3 Results with Discussion

In this section, we have illustrated the numerical outcomes of the proposed flow model across various selections of relevant flow parameters. The remarkable numerical values of the skin-friction coefficient, Sherwood and Nusselt numbers against salient parameters have been delineated in the tabular format.

6.3.1 Skin-friction Coefficient, Nusselt and Sherwood Numbers

TABLE 6.1: Contrasting the current findings of $-\left(1+\frac{1}{\beta}\right)f''(0)$ with those reported in the existing literature.

	$\left(1+\frac{1}{\beta}\right)f''(0)$ with $\beta=\infty$	
M	Sohail et. al [77]	Present

0	1.998023	1.9980235189
0.5	2.087394	2.0873942814
1.0	2.241731	2.2417316102

The MATLAB code validation process involves reproducing the results for $-(1+\frac{1}{\beta})f''(0)$ as presented in the problem posed by Sohail et al. [77], using the shooting technique. As depicted in Table 1, the outcomes reveal a substantial agreement between the numerical results generated by the current code and the established ones.

Tables 6.2-6.4 are delineated to throw light on the numerical values of the drag coefficient coupled with the heat and mass transfer rates by fluctuating the values of various dimensionless parameters like n, Q, Nb, We, β, M, K, Gr, Gc, Pr, Nt, Ec, Sc, γ, Bi_1 and Bi_2.

The numerical results gathered after incorporating the shooting method give the picture of an increasing behavior of the skin friction coefficients, Nusselt and Sherwood numbers by assuming higher values of Gc, Ec, γ and Bi_1 whereas, an unlike trend has been seen in the case of We. Moreover, the rising values of n, K, Gr, Nb, Sc and Bi_2 depreciate the magnitude of the skin-friction coefficients and heat transfer rate and at the same time, the mass transfer rate climbs marginally, however, for the elevated magnitude of Nt, an opposite fashion is witnessed. More than that, an increase in the Prandtl number is noticed to escalate the heat and mass transfer rates and a considerable decay in the skin-friction coefficients.

Table 6.2: The numerical results of drag coefficients, heat and mass transfer gradients for $Nt = Nb = Bi_1 = Bi_2 = 0.5$, $Sc = Q = Ec = \gamma = Pr = 0.1, Gc = 1$.

n	We	β	K	M	Gr	$Re^{\frac{1}{2}}C_{fx}$	$Re^{\frac{1}{2}}C_{fy}$	$Re^{\frac{-1}{2}}Nu$	$Re^{\frac{-1}{2}}Sh$
0.1	0.1	0.5	0.1	0.1	2.0	-2.131845	-2.058362	0.485541	-0.089018
4.0						-3.115202	-5.214502	0.436748	0.016130
8.0						-4.041507	-7.086183	0.419741	0.047646

	0.5					-3.673575	-4.235685	0.474825	0.031231
	0.9					-3.982583	-4.674567	0.474558	0.030718
		10				-2.357785	-4.673451	0.452905	0.052141
		20				-9.949806	-7.521892	0.491321	0.628054
			1.1			1.366238	0.165423	0.228911	0.244571
			2.1			3.809156	5.578923	0.841718	0.203623
				3.0		-5.100607	-4.710924	0.560073	0.013248
				6.0		-9.381958	-8.178234	0.579562	0.023959
					4.0	-7.470140	-5.190235	0.444801	0.030264
					6.0	-9.959044	-7.470912	0.419098	0.068842

Table 6.3: The numerical results of drag coefficients, heat and mass transfer gradients for $n = We = K = M = Pr = 0.1, \beta = Bi_1 = Bi_2 = 0.5, Gc = 1, Gr = 2$.

Q	Nb	Nt	Ec	Sc	γ	$Re^{\frac{1}{2}}C_{fx}$	$Re^{\frac{1}{2}}C_{fy}$	$Re^{\frac{-1}{2}}Nu$	$Re^{\frac{-1}{2}}Sh$
0.1	0.5	0.5	0.1	0.1	0.1	-2.131845	-2.058362	0.485541	-0.089018
0.5						-4.841695	-3.154328	0.504292	-0.051981
0.9						-8.504382	-5.510344	0.507668	-0.028087
	1.0					-6.982959	-4.091842	0.484932	0.047658
	1.5					-7.030055	-9.102337	0.480047	0.054411
		1.5				-1.402637	0.234567	0.495219	-0.054312
		2.5				3.359015	2.784563	0.500532	-0.153411
			0.4			-1.008789	0.126543	0.498391	0.026510
			0.7			0.383623	4.132523	0.502994	0.026668
				3.0		-4.803264	-5.678452	0.550842	0.016014
				6.0		-6.024954	-7.746423	0.550763	0.040048
					0.5	1.520564	-8.465787	0.472800	0.117173
					0.9	5.501267	3.507568	0.863134	0.163103

TABLE 6.4: The numerical results of drag coefficients, heat and mass transfer gradients for $n = We = K = M = Pr = Sc = Q = Ec = \gamma = 0.1, \beta = 0.5, Gc = 1, Gr = 2, Nt = Nb = 0.5$.

Gc	Pr	Bi_1	Bi_2	$Re^{\frac{1}{2}}C_{fx}$	$Re^{\frac{1}{2}}C_{fy}$	$Re^{\frac{-1}{2}}Nu$	$Re^{\frac{-1}{2}}Sh$
1.0	0.1	0.5	0.5	-2.131845	-2.058362	0.485541	-0.089018
2.0				1.373889	4.023479	0.560031	0.035947
3.0				3.492228	8.409123	0.622090	0.048246
	0.3			-4.865814	-5.189023	1.141926	-0.061857
	0.5			-9.366462	-7.908653	9.940296	-1.985372
		1.5		2.388819	3.458781	0.636757	0.056573
		2.5		6.622202	6.986023	0.678925	0.071398
			1.5	4.865814	5.127654	0.141926	-0.061857
			2.5	8.640263	9.476529	0.093912	0.027374

Figures 6.2-6.7 illustrate the impact of n, We, and β on the velocity distribution. Increasing the values of these parameters leads to an increase in the velocity. Furthermore, when higher values of We are considered, an enhancement is observed in the thickness of the velocity boundary layer, while a sudden drop is seen in the case of larger β. Moreover, for the case of the parameter n, the velocity boundary layer of $f'(\eta)$ is enhanced whereas an unlike behaviour is observed for $f'(\eta)$.

Figures 6.8-6.11 are plotted to emphasize the effect of the magnetic parameter M on the velocity, temperature, and concentration profiles. As mentioned earlier, when a higher magnetic field is applied, an increase in temperature and concentration profiles is observed while the velocity profile decreases. As a consequence, a significant decrease in the momentum boundary layer thickness and a slight increase in the thickness of thermal and concentration boundary layers have been observed.

Figures 6.12-6.13 depict the influence of Pr on temperature and concentration profiles. Physically, Pr is defined as the ratio between the viscous diffusion rate and thermal diffusivity. As Pr increases, the thermal diffusion rate decreases, leading to a significant reduction in the fluid's temperature. Consequently, there is an observed declination in the thermal boundary layer thickness. Conversely, for the higher values of Pr, the fluid's concentration shows an increasing behaviour. Additionally, a sudden rise is observed in the thickness of the concentration boundary layer.

The impact of the thermophoresis parameter on the temperature and concentration gradients is portrayed in Figures 6.14-6.15. It can be remarked that both the magnitudes of temperature and concentration augment considerably by assuming the higher values of Nt. Moreover, an elevation in the associated thermal and concentration boundary layer thickness has been seen.

Figures 6.16-6.17 showcase the effect of the Brownian motion parameter on the temperature and concentration curves. The temperature profile exhibits a marginal elevation for higher magnitudes of Nb. This phenomenon can be attributed to the fact mentioned in the earlier chapters. An escalation in temperature and the thickness of the thermal boundary layer is sighted. Conversely, as Nb assumes higher values, the fluid concentration diminishes, accompanied by a reduction in the thickness of the concentration boundary layer.

The progression of the velocity and temperature profiles by amalgamating contrasting values of Bi_1 and Gr has been displayed in Figures 18-19. The figures demonstrate that the temperature cools down by accounting for greater magnitudes of Gr and henceforth, the depletion is observed in the thermal boundary layer thickness. In contrast, Bi_1 has displayed a divergent pattern.

Figures 20-21 are mapped out to spotlight the impact of Sc and Bi_2 on the concentration distribution. When the concentration Biot number increases, it results in a corresponding increase in the concentration of the fluid, which subsequently leads to an expansion in the thickness of the concentration boundary layer. Conversely, a contrasting pattern can be observed with the Schmidt number.

Figure 6.22 illustrates the influence of Ec and M on the skin-friction coefficient. Notably, the drag coefficient increases with the higher values of Ec and M. Additionally, Figure 6.23 underscores the significant effect of We and β on the skin-friction coefficient. As the values of β and We rise, the surface stress increases. The substantial impact of Pr and Sc on the Nusselt number is portrayed in Figure 6.24. For the larger Pr and Sc, the mass transfer rate diminishes drastically. The effect of Nb and Q on the Sherwood number is depicted in Figure 6.25. Clearly, for the higher Nb and Q, the mass transfer gradient experiences an increment in the magnitude.

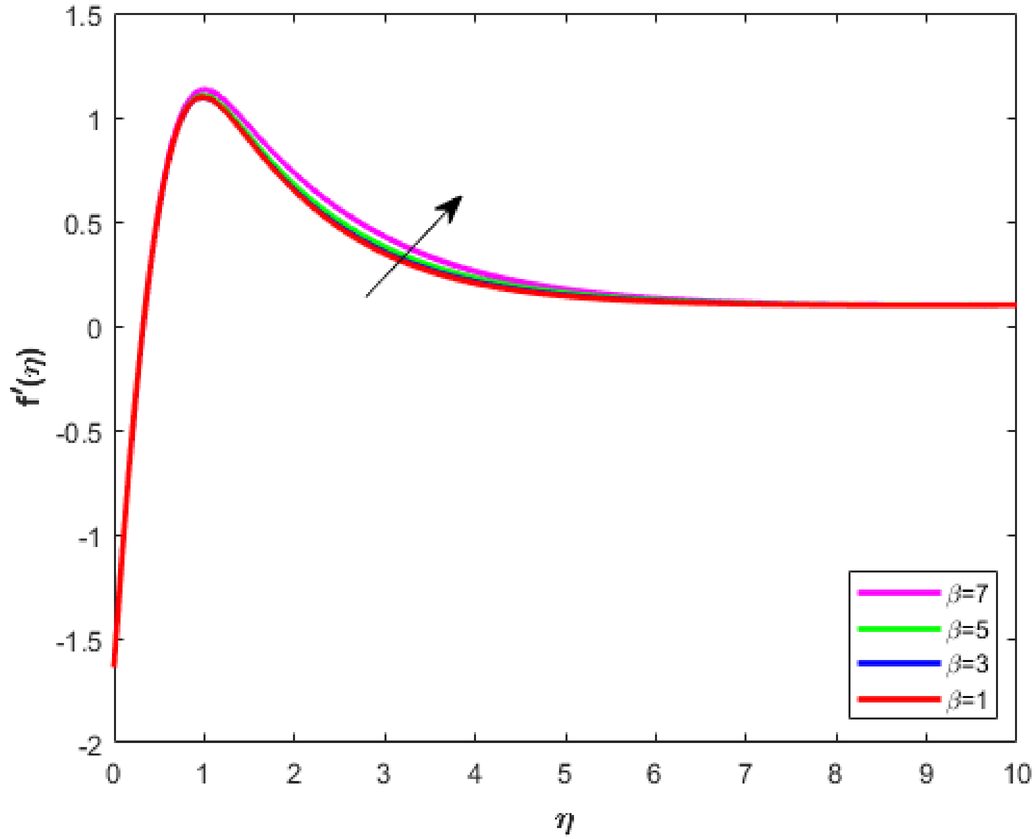

FIGURE 6.2: Effect of β on $f'(\eta)$ when $K = \sigma_a = We = n = A = Q = Ec = \alpha = \Gamma = \sigma_b = Sc = 0.1,\ Nt = Nb = B_{i1} = B_{i2} = 0.5,\ M = Rd = Pr = \gamma = Gc = 1,\ Gr = 2$

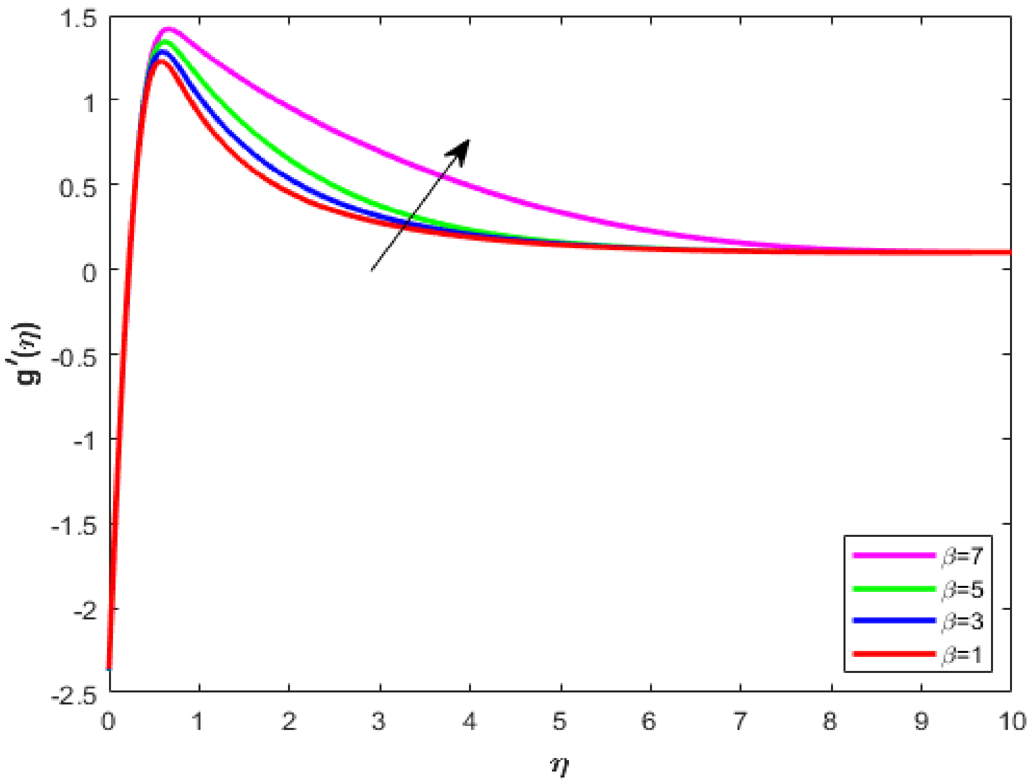

FIGURE 6.3: Effect of β on $g'(\eta)$ when $K = \sigma_a = We = n = A = Q = Ec = \alpha = \Gamma = \sigma_b = Sc = 0.1,\ Nt = Nb = B_{i1} = B_{i2} = 0.5,\ M = Rd = Pr = \gamma = Gc = 1,\ Gr = 2$

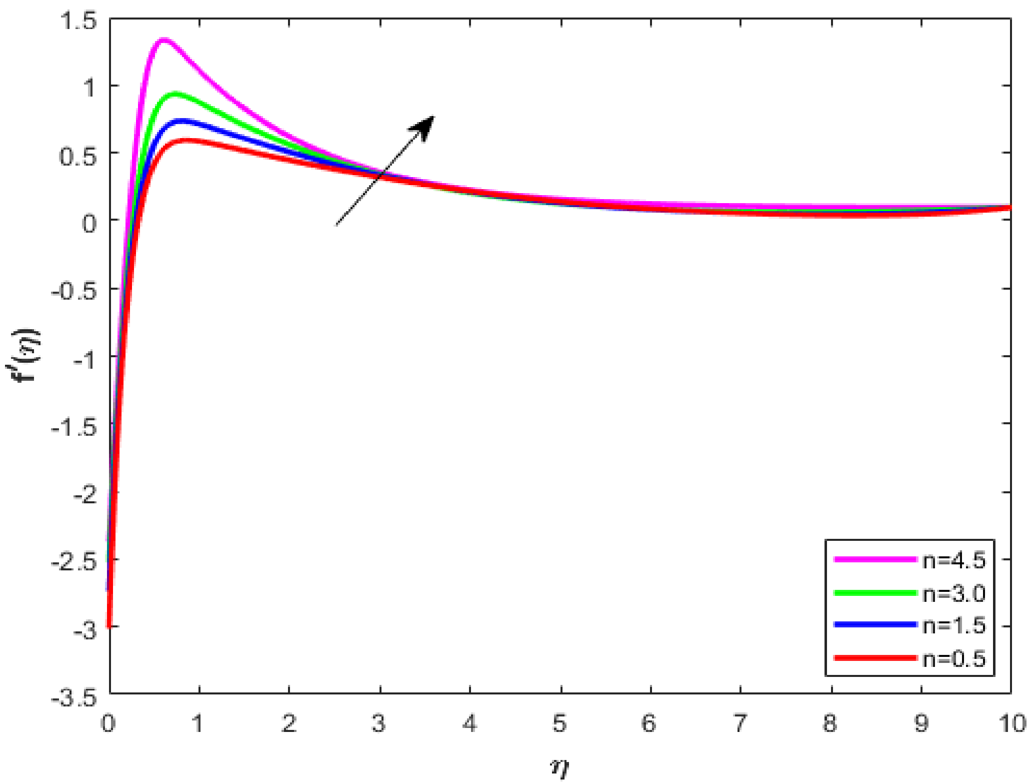

FIGURE 6.4: Effect of n on $f'(\eta)$ when $K = \sigma_a = We = A = Q = Ec = \alpha = \Gamma = \sigma_b = Sc = 0.1,\ \beta = Nt = Nb = B_{i1} = B_{i2} = 0.5,\ M = Rd = Pr = \gamma = Gc = 1,\ Gr = 2$

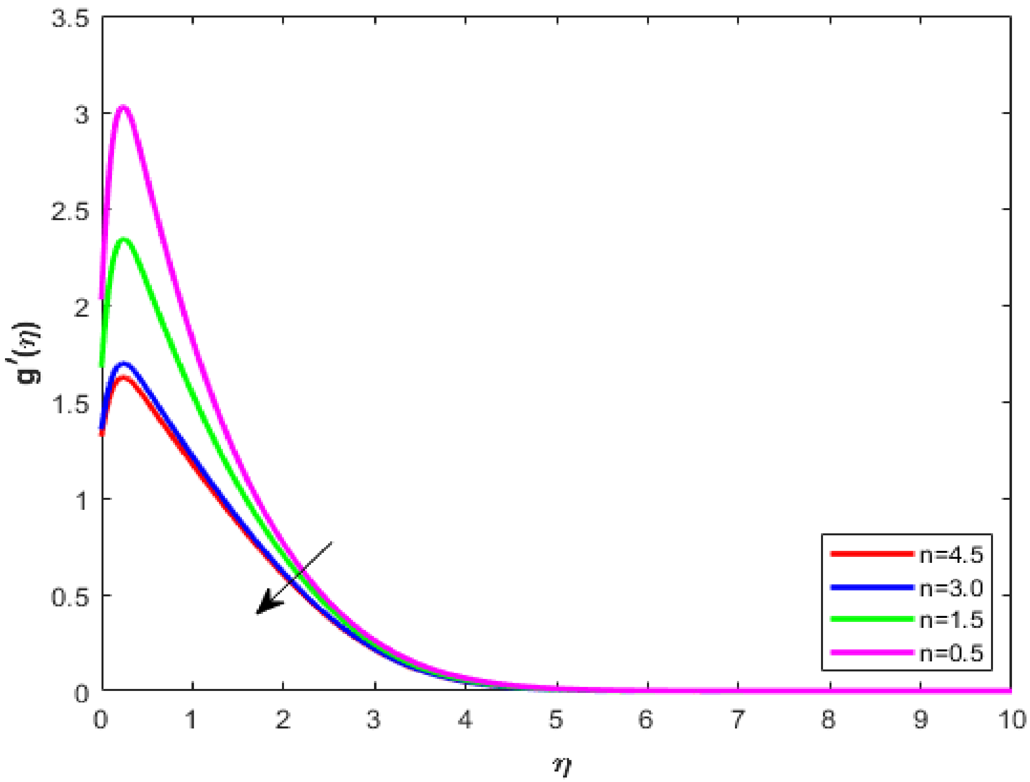

FIGURE 6.5: Effect of n on $g'(\eta)$ when $K = \sigma_a = We = A = Q = Ec = \alpha = \Gamma = \sigma_b = Sc = 0.1,\ \beta = Nt = Nb = B_{i1} = B_{i2} = 0.5,\ M = Rd = Pr = \gamma = Gc = 1,\ Gr = 2$

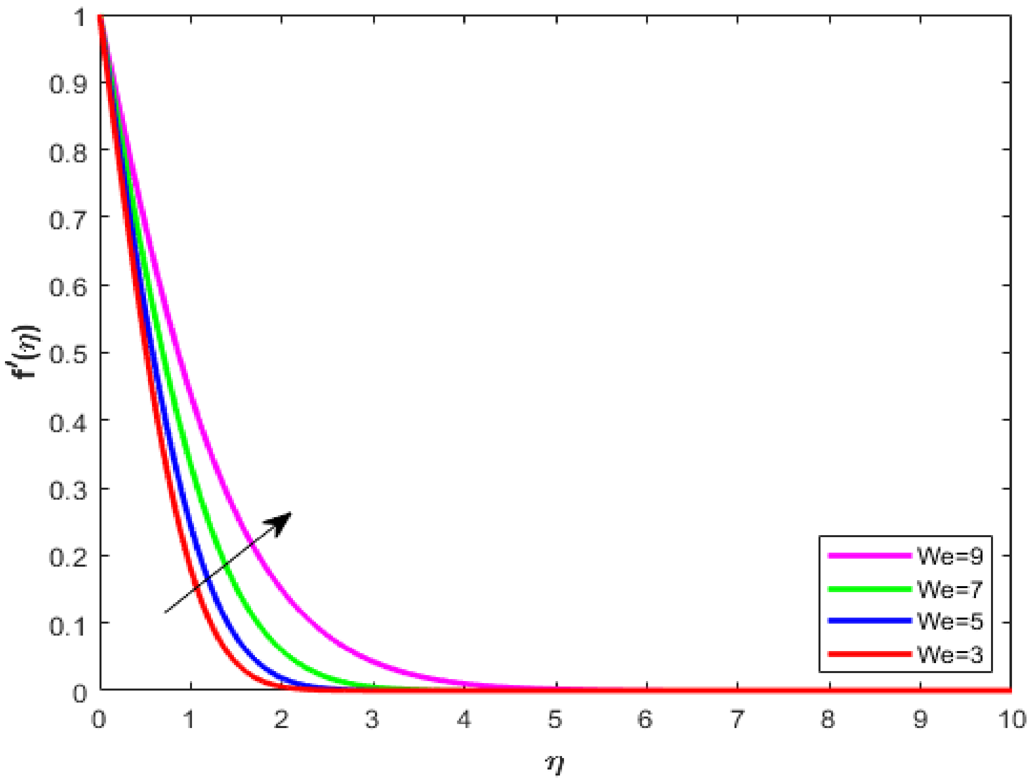

FIGURE 6.6: Effect of We on $f'(\eta)$ when $K = \sigma_a = n = A = Q = Ec = \alpha = \Gamma = \sigma_b = Sc = 0.1,\ \beta = Nt = Nb = B_{i1} = B_{i2} = 0.5,\ M = Rd = Pr = \gamma = Gc = 1,\ Gr = 2$

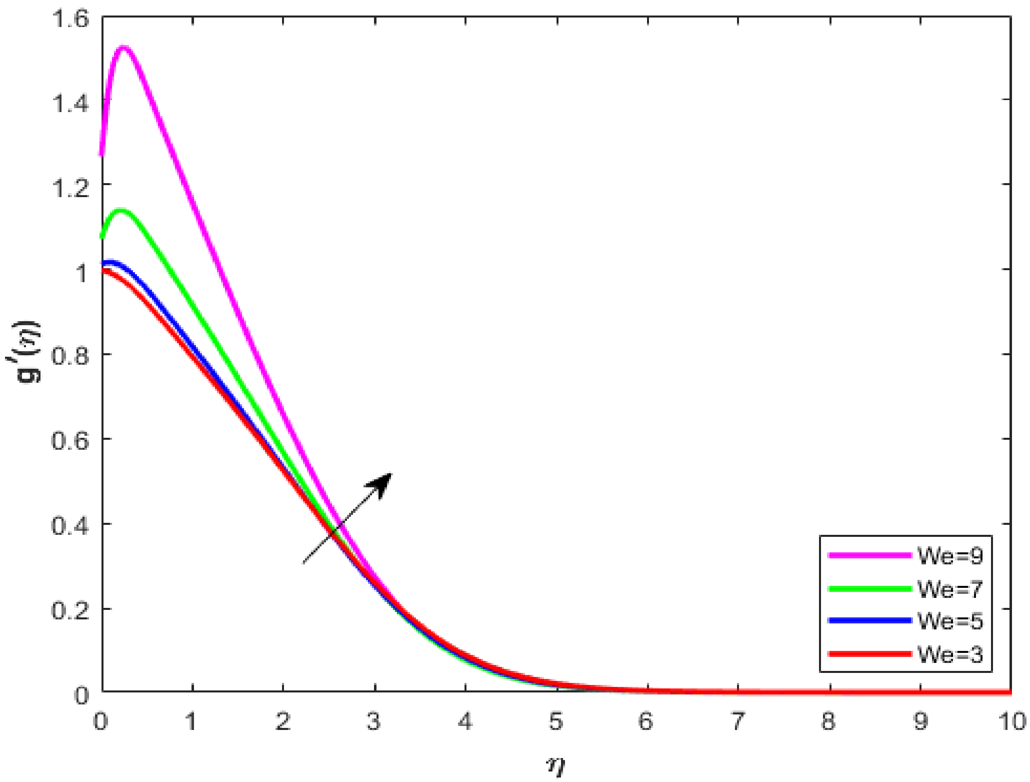

FIGURE 6.7: Effect of We on $g'(\eta)$ when $K = \sigma_a = n = A = Q = Ec = \alpha = \Gamma = \sigma_b = Sc = 0.1$, $\beta = Nt = Nb = B_{i1} = B_{i2} = 0.5$, $M = Rd = Pr = \gamma = Gc = 1$, $Gr = 2$

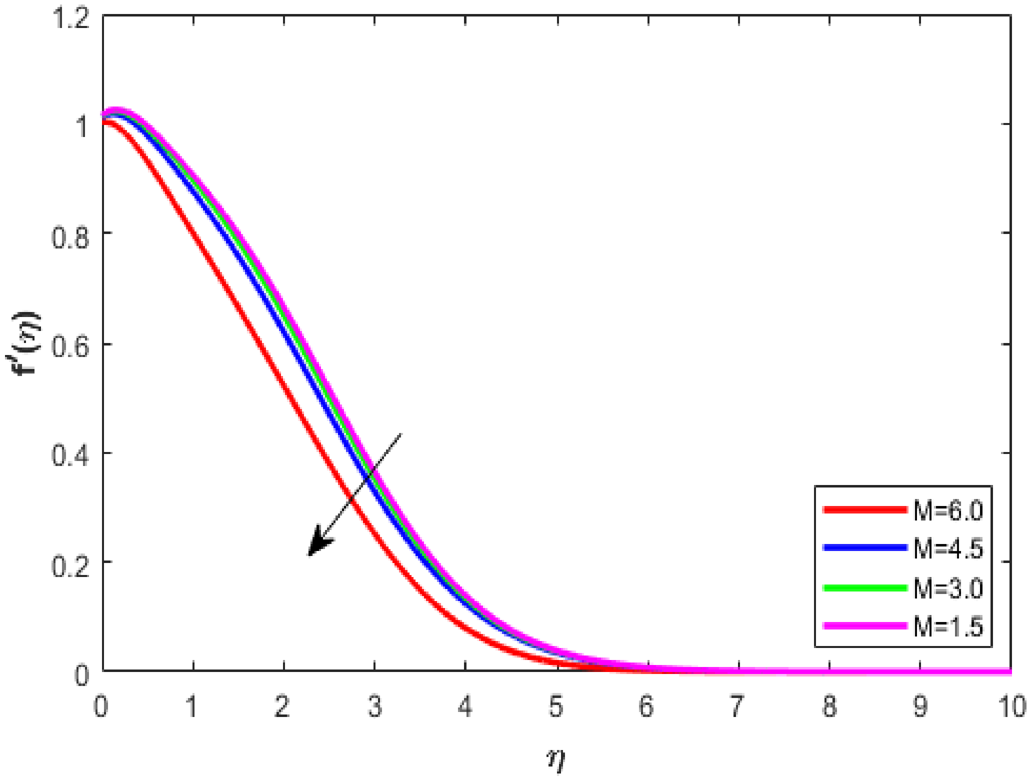

FIGURE 6.8: Effect of M on $f'(\eta)$ when $K = \sigma_a = We = n = A = Q = Ec = \alpha = \Gamma = \sigma_b = Sc = 0.1$, $\beta = Nt = Nb = B_{i1} = B_{i2} = 0.5$, $Rd = Pr = \gamma = Gc = 1$, $Gr = 2$

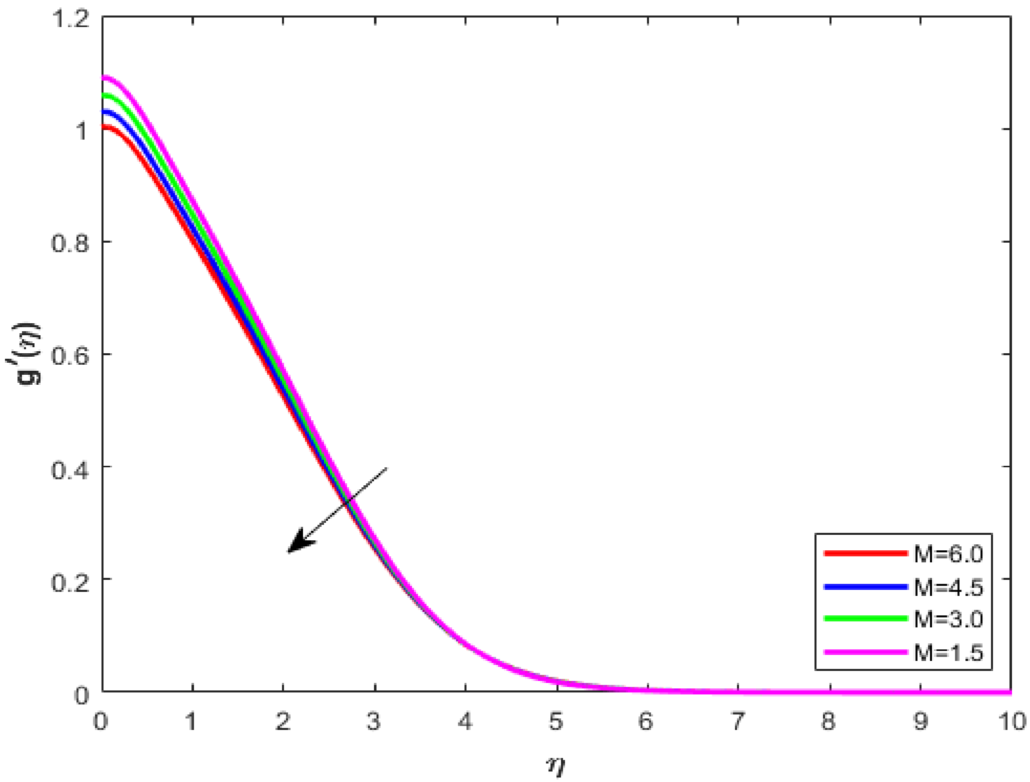

FIGURE 6.9: Effect of M on $g'(\eta)$ when $K = \sigma_a = We = n = A = Q = Ec = \alpha = \Gamma = \sigma_b = Sc = 0.1,\ \beta = Nt = Nb = B_{i1} = B_{i2} = 0.5,\ Rd = Pr = \gamma = Gc = 1,\ Gr = 2$

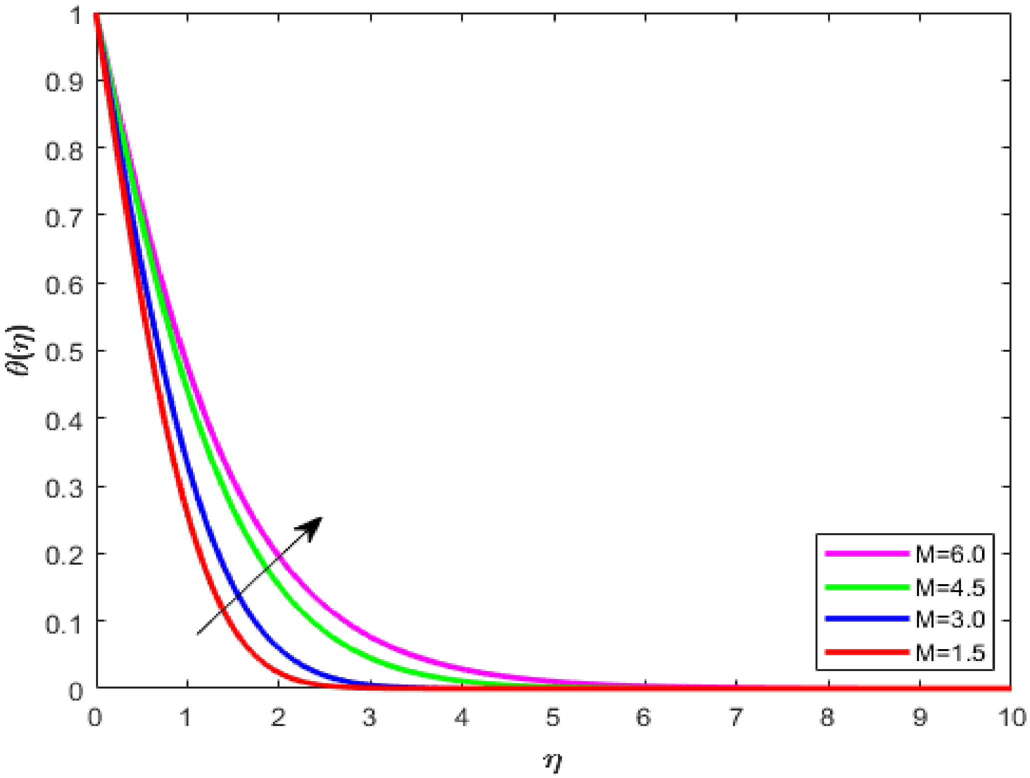

FIGURE 6.10: Effect of M on $\theta(\eta)$ when $K = \sigma_a = We = n = A = Q = Ec = \alpha = \Gamma = \sigma_b = Sc = 0.1,\ \beta = Nt = Nb = B_{i1} = B_{i2} = 0.5,\ Rd = Pr = \gamma = Gc = 1,\ Gr = 2$

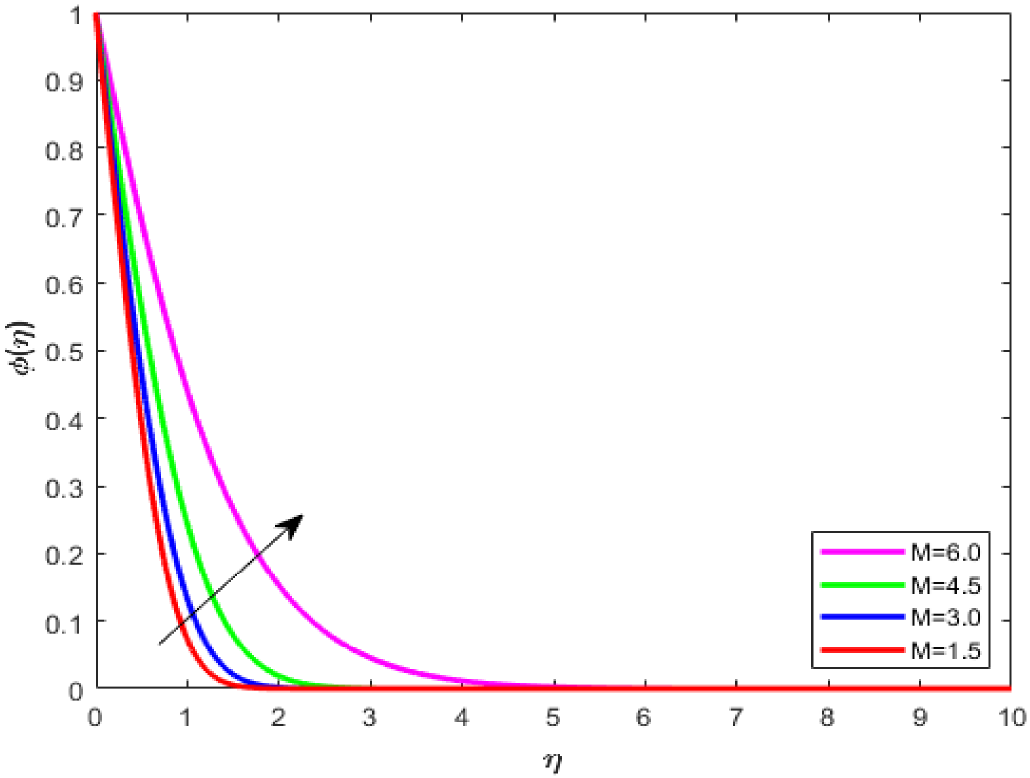

FIGURE 6.11: Effect of M on $\phi(\eta)$ when $K = \sigma_a = We = n = A = Q = Ec = \alpha = \Gamma = \sigma_b = Sc = 0.1,\ \beta = Nt = Nb = B_{i1} = B_{i2} = 0.5,\ Rd = Pr = \gamma = Gc = 1,\ Gr = 2$

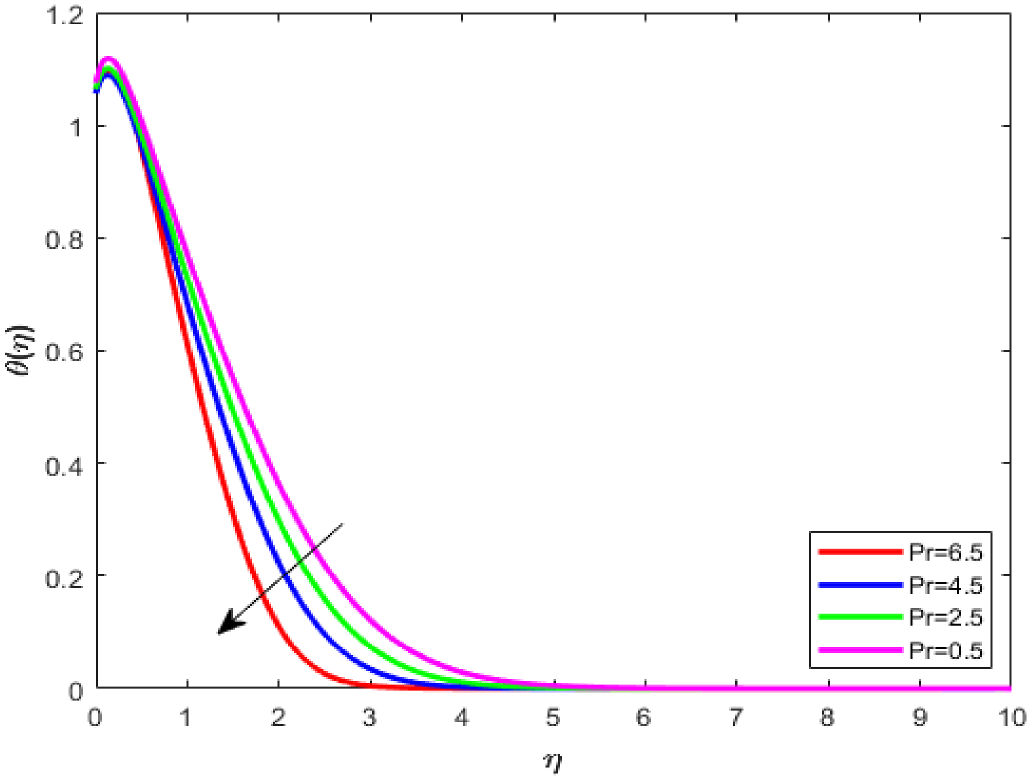

FIGURE 6.12: Effect of Pr on $\theta(\eta)$ when $K = \sigma_a = We = n = A = Q = Ec = \alpha = \Gamma = \sigma_b = Sc = 0.1,\ \beta = Nt = Nb = B_{i1} = B_{i2} = 0.5,\ M = Rd = \gamma = Gc = 1,\ Gr = 2$

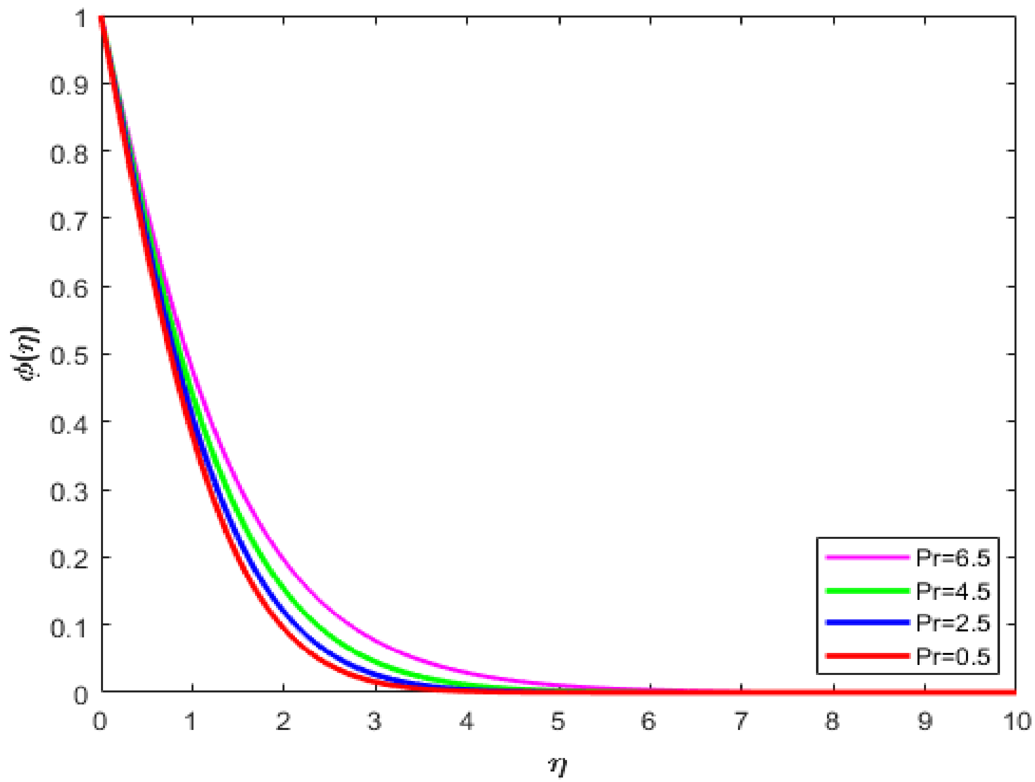

FIGURE 6.13: Effect of Pr on $\phi(\eta)$ when $K = \sigma_a = We = n = A = Q = Ec = \alpha = \Gamma = \sigma_b = Sc = 0.1,\ \beta = Nt = Nb = B_{i1} = B_{i2} = 0.5,\ M = Rd = \gamma = Gc = 1,\ Gr = 2$

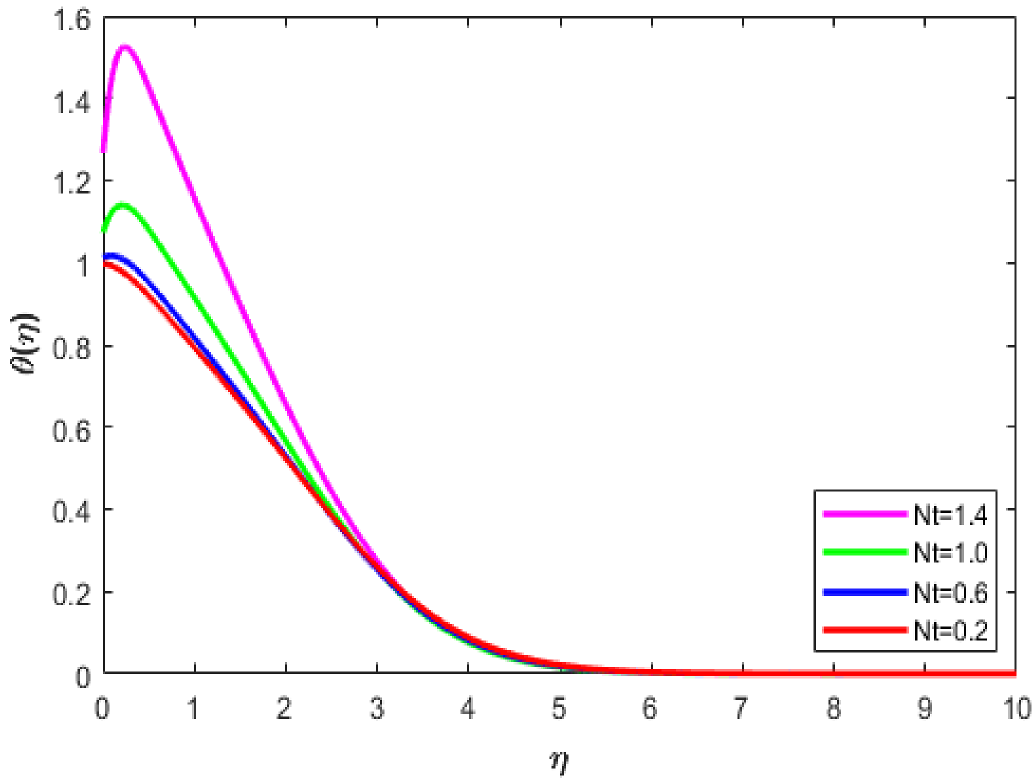

FIGURE 6.14: Effect of Nt on $\theta(\eta)$ when $K = \sigma_a = We = n = A = Q = Ec = \alpha = \Gamma = \sigma_b = Sc = 0.1,\ \beta = Nb = B_{i1} = B_{i2} = 0.5,\ M = Rd = \gamma = Gc = 1,\ Gr = 2$

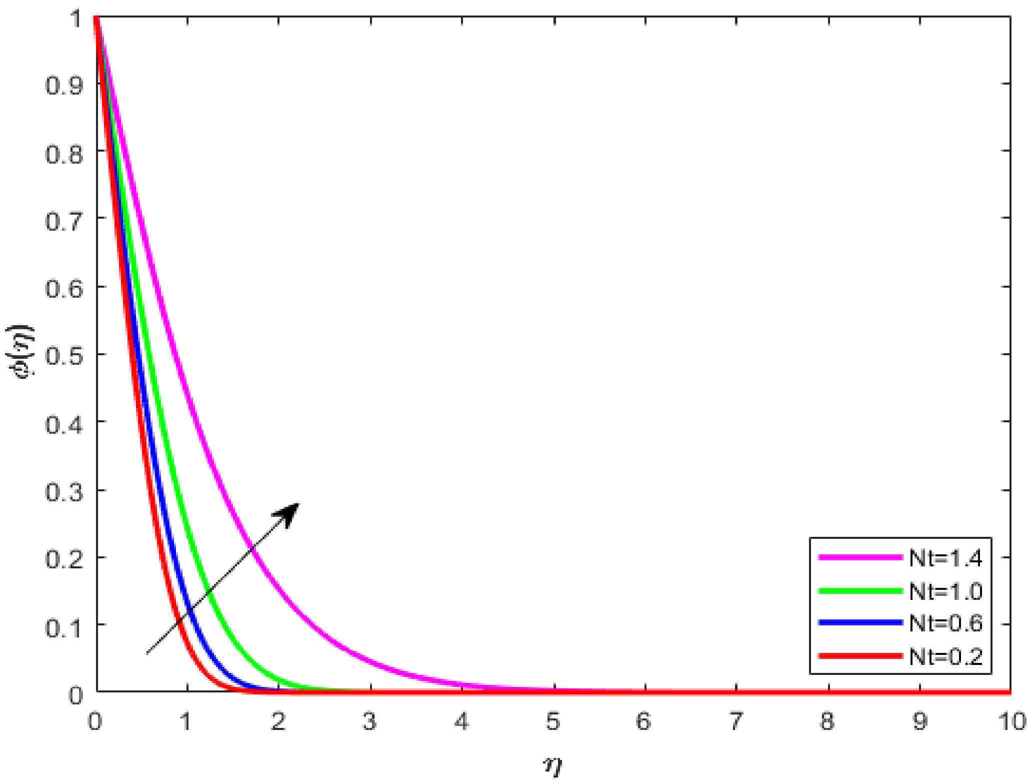

FIGURE 6.15: Effect of Nt on $\phi(\eta)$ when $K = \sigma_a = We = n = A = Q = Ec = \alpha = \Gamma = \sigma_b = Sc = 0.1,\ \beta = Nt = Nb = B_{i1} = B_{i2} = 0.5,\ M = Rd = \gamma = Gc = 1,\ Gr = 2$

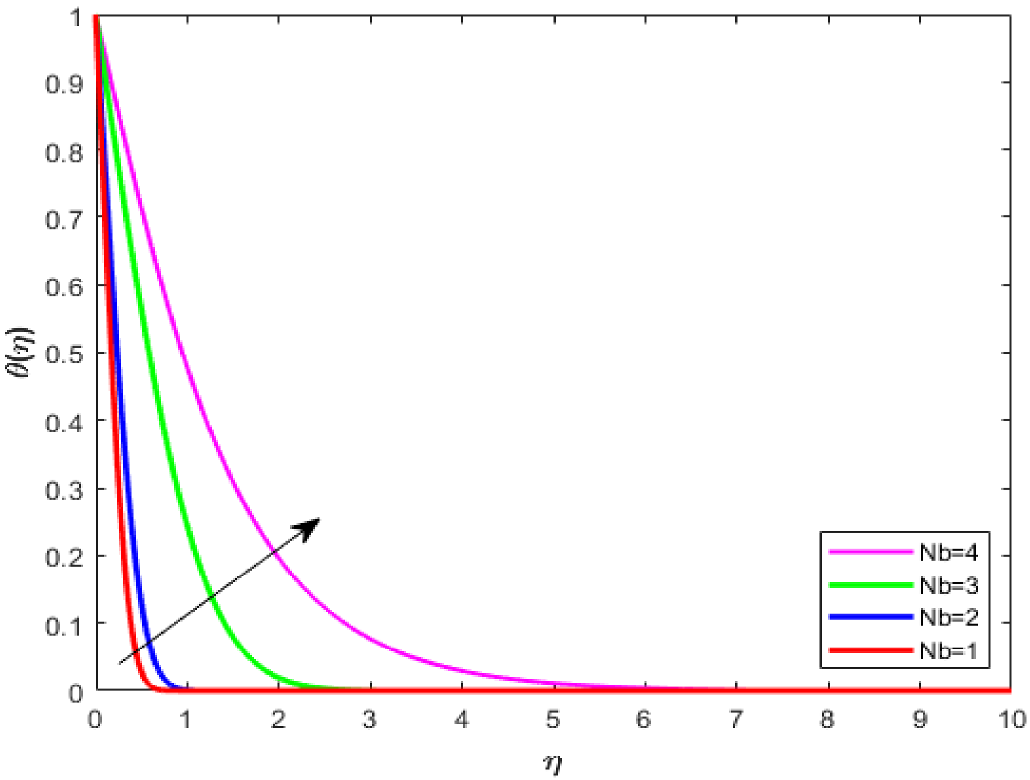

FIGURE 6.16: Effect of Nb on $\theta(\eta)$ when $K = \sigma_a = We = n = A = Q = Ec = \alpha = \Gamma = \sigma_b = Sc = 0.1,\ \beta = Nt = B_{i1} = B_{i2} = 0.5,\ M = Rd = Pr = \gamma = Gc = 1,\ Gr = 2$

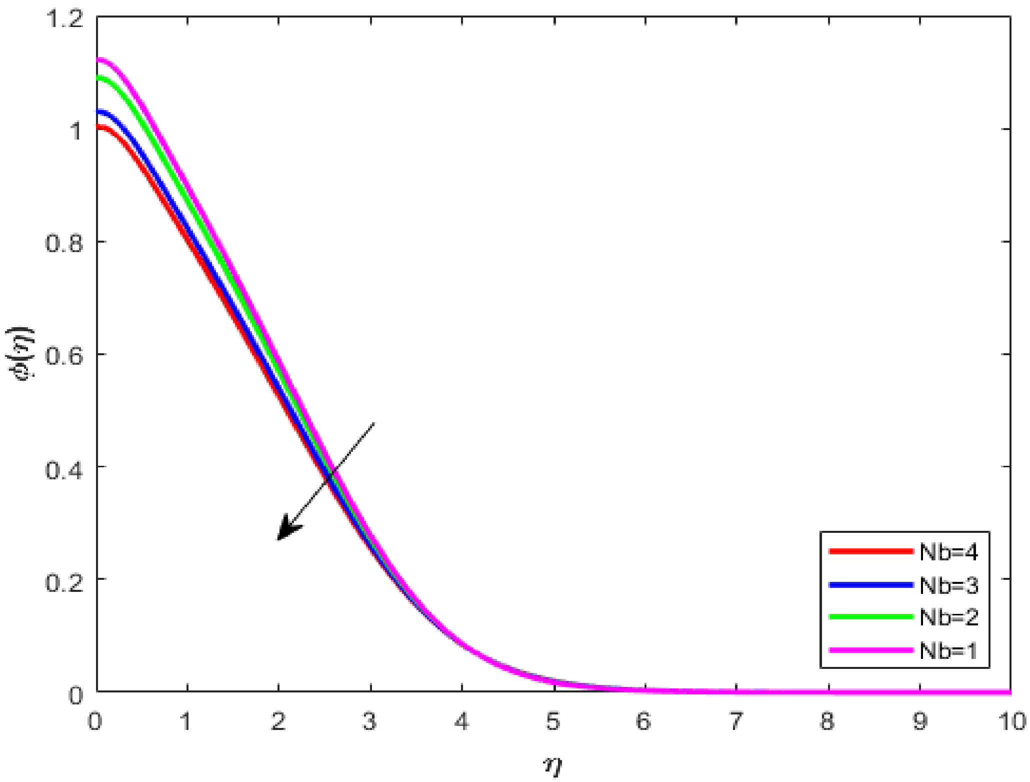

FIGURE 6.17: Effect of Nb on $\phi(\eta)$ when $K = \sigma_a = We = n = A = Q = Ec = \alpha = \Gamma = \sigma_b = Sc = 0.1,\ \beta = Nt = B_{i1} = B_{i2} = 0.5,\ M = Rd = Pr = \gamma = Gc = 1,\ Gr = 2$

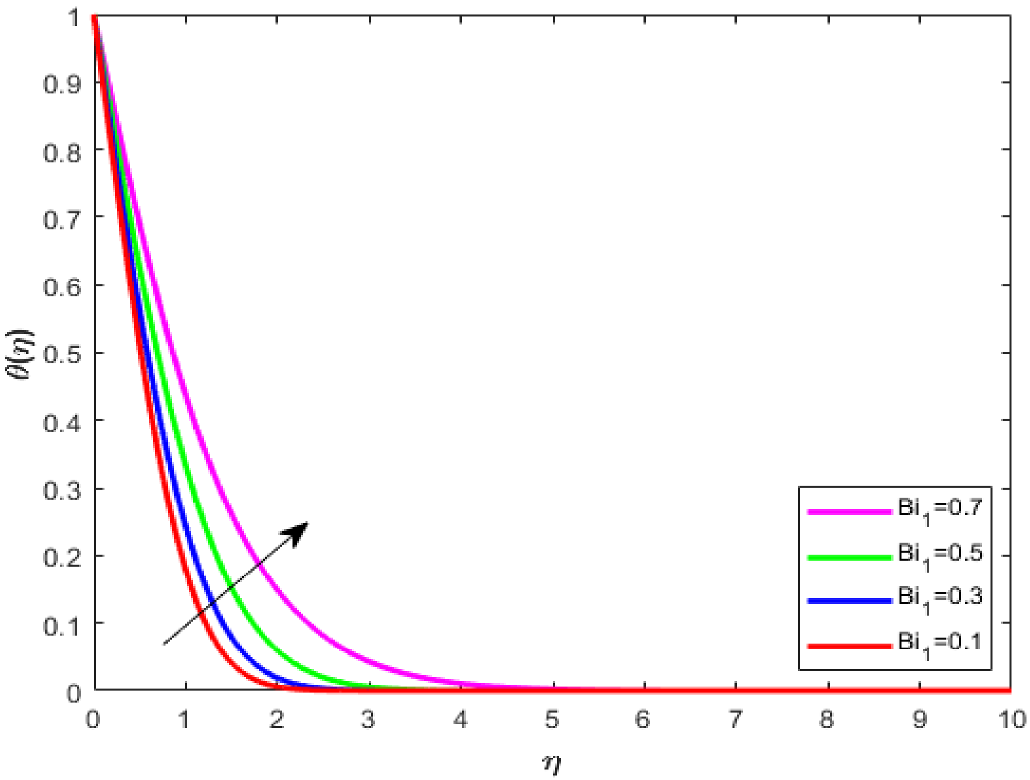

FIGURE 6.18: Effect of Bi_1 on $\theta(\eta)$ when $K = \sigma_a = We = n = A = Q = Ec = \alpha = \Gamma = \sigma_b = Sc = 0.1,\ \beta = Nt = Nb = B_{i2} = 0.5,\ M = Rd = Pr = \gamma = Gc = 1,\ Gr = 2$

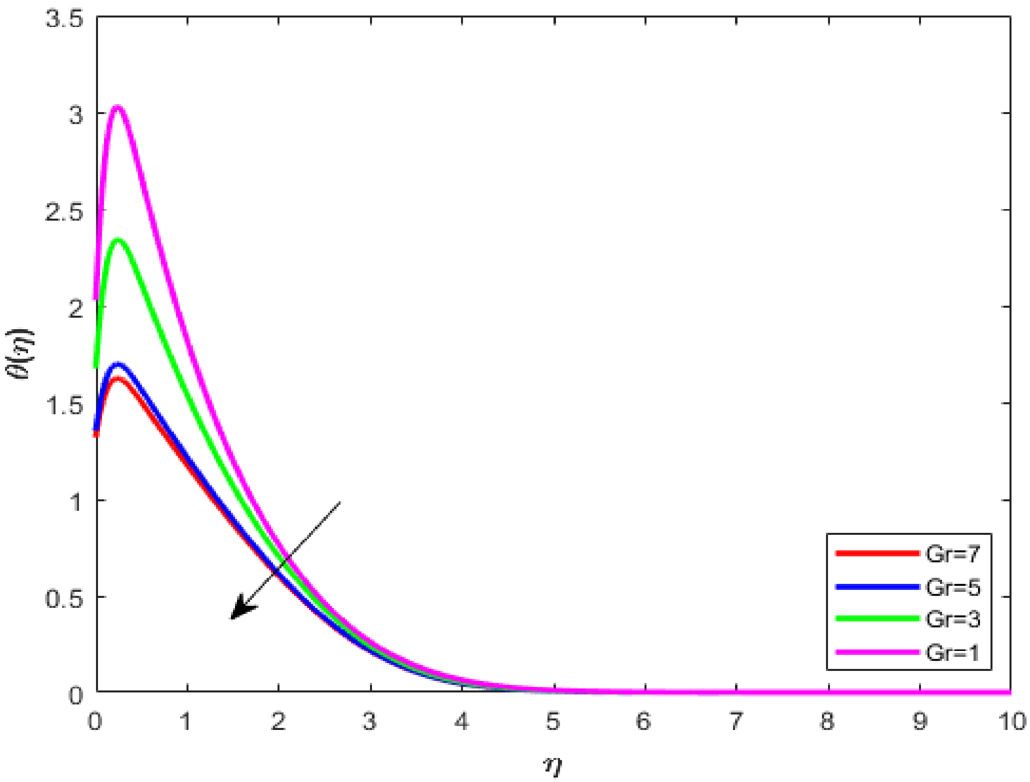

FIGURE 6.19: Effect of Gr on $\theta(\eta)$ when $K = \sigma_a = We = n = A = Q = Ec = \alpha = \Gamma = \sigma_b = Sc = 0.1,\ \beta = Nt = Nb = B_{i1} = B_{i2} = 0.5,\ M = Rd = Pr = \gamma = Gc = 1$

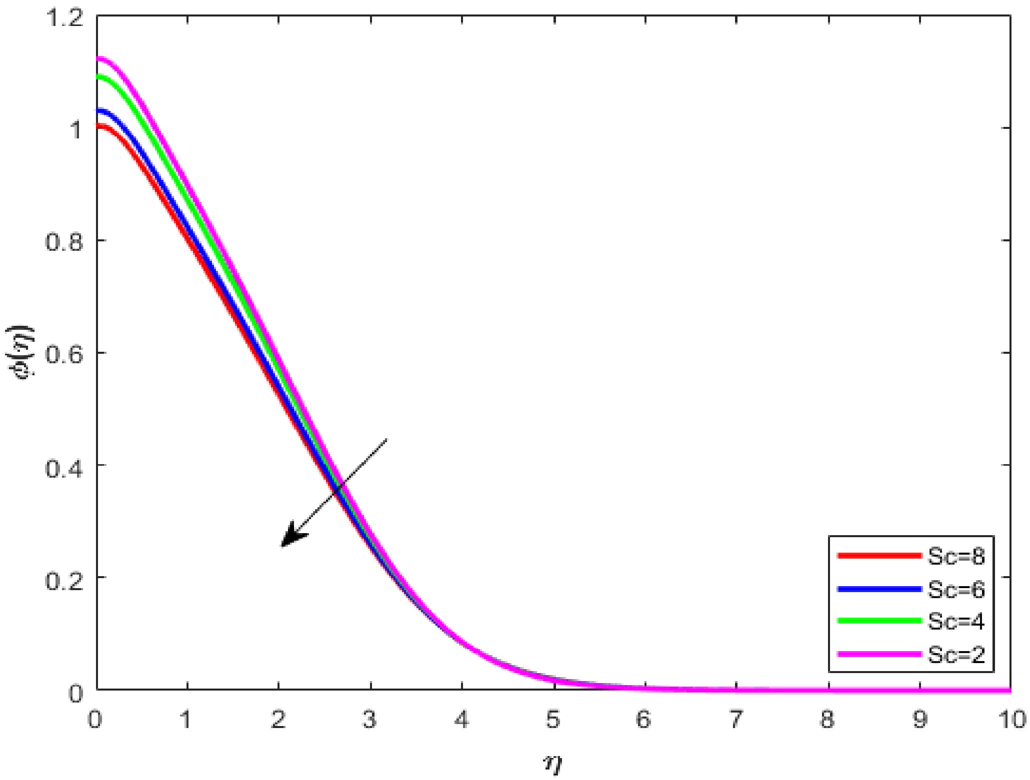

FIGURE 6.20: Effect of Sc on $\phi(\eta)$ when $K = \sigma_a = We = n = A = Q = Ec = \alpha = \Gamma = \sigma_b = 0.1,\ \beta = Nt = Nb = B_{i1} = B_{i2} = 0.5,\ M = Rd = Pr = \gamma = Gc = 1,\ Gr = 2$

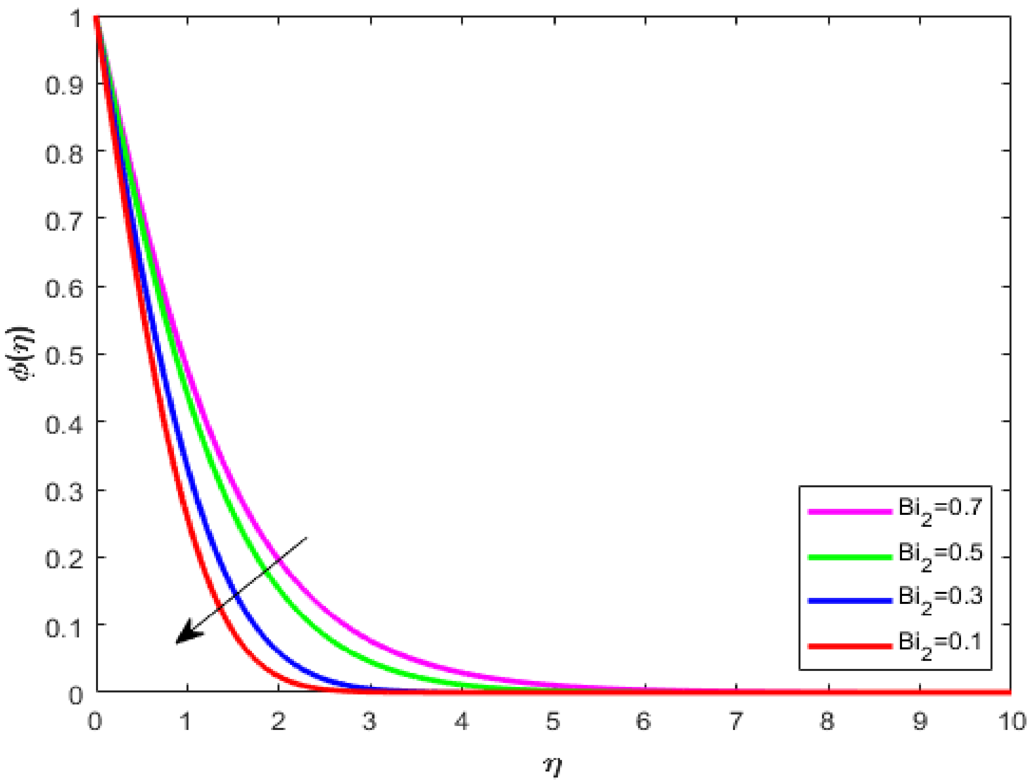

FIGURE 6.21: Effect of Bi_2 on $\phi(\eta)$ when $K = \sigma_a = We = n = A = Q = Ec = \alpha = \Gamma = \sigma_b = Sc = 0.1,\ \beta = Nt = Nb = B_{i1}0.5,\ M = Rd = Pr = \gamma = Gc = 1,\ Gr = 2$

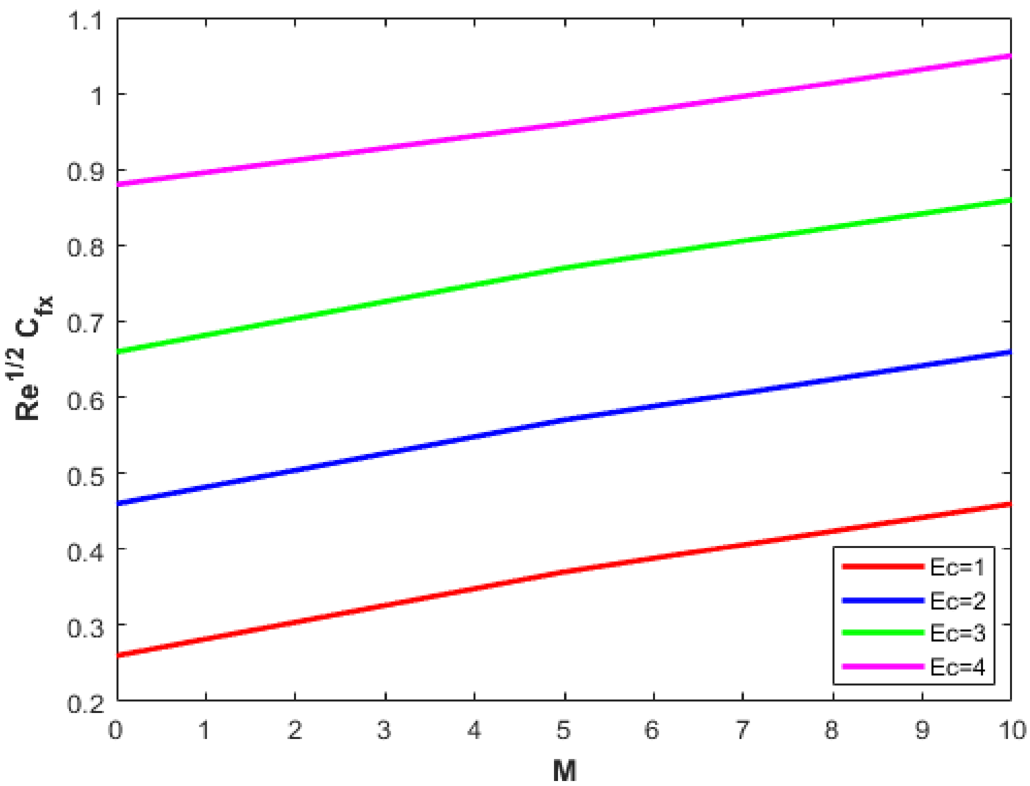

FIGURE 6.22: Effect of Ec and M on $Re^{\frac{1}{2}}\, C_{fx}$ when $K = \sigma_a = We = n = A = Q = \alpha = \Gamma = \sigma_b = Sc = 0.1, \beta = Nt = Nb = B_{i1} = B_{i2} = 0.5, \quad M = Rd = Pr = \gamma = Gc = 1, \quad Gr = 2$

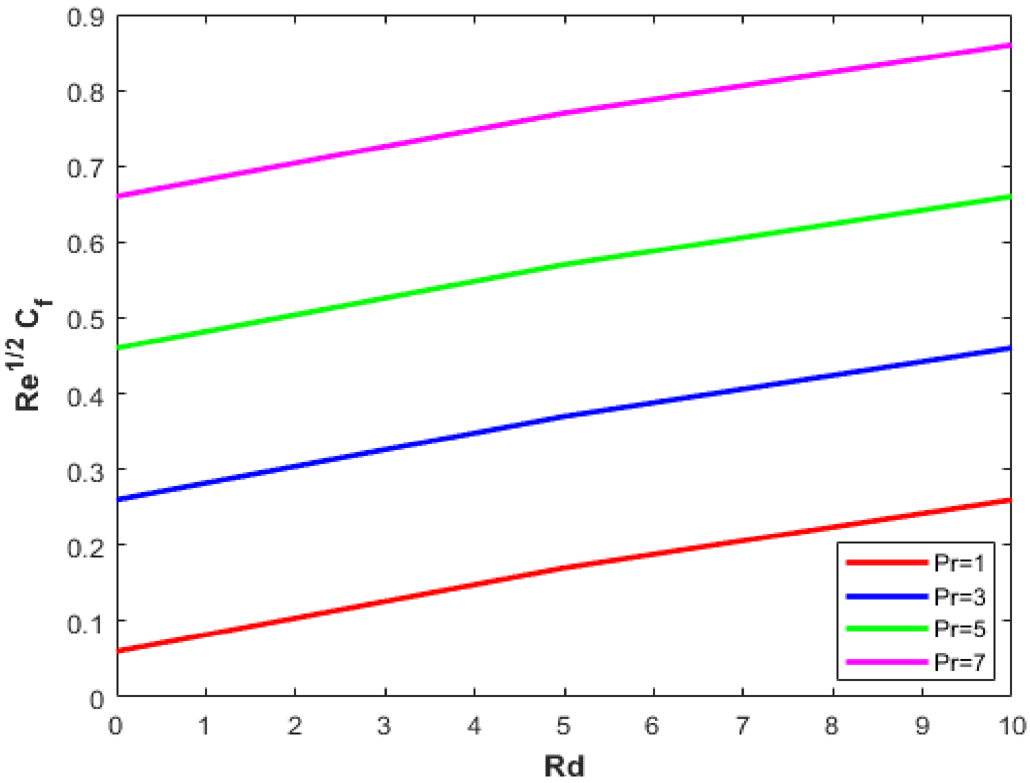

FIGURE 6.23: Effect of We and β on $Re^{\frac{1}{2}}\ C_{fy}$ when $K = \sigma_a = We = n = A = Q = \alpha = \Gamma = \sigma_b = Sc = 0.1, \beta = Nt = Nb = B_{i1} = B_{i2} = 0.5, \quad M = Rd = Pr = \gamma = Gc = 1, \quad Gr = 2$

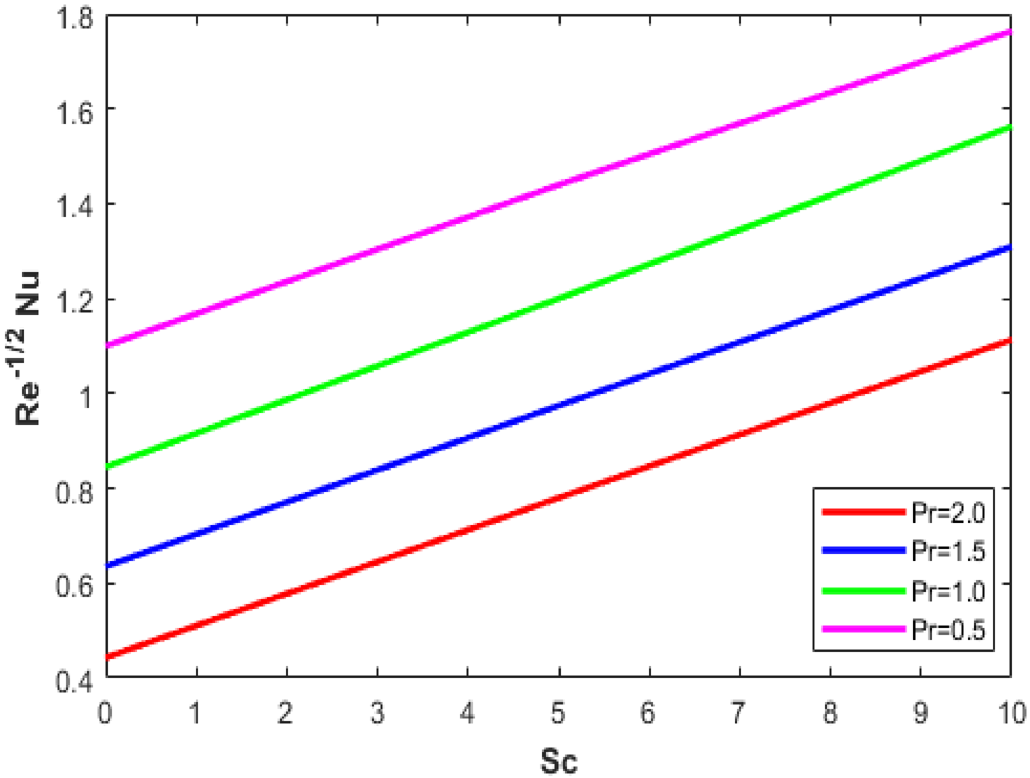

FIGURE 6.24: Effect of Sc and Pr on $Re^{-\frac{1}{2}}\ Nu$ when $K = \sigma_a = We = n = A = Q = \alpha = \Gamma = \sigma_b = Sc = 0.1, \beta = Nt = Nb = B_{i1} = B_{i2} = 0.5, \quad M = Rd = Pr = \gamma = Gc = 1, \quad Gr = 2$

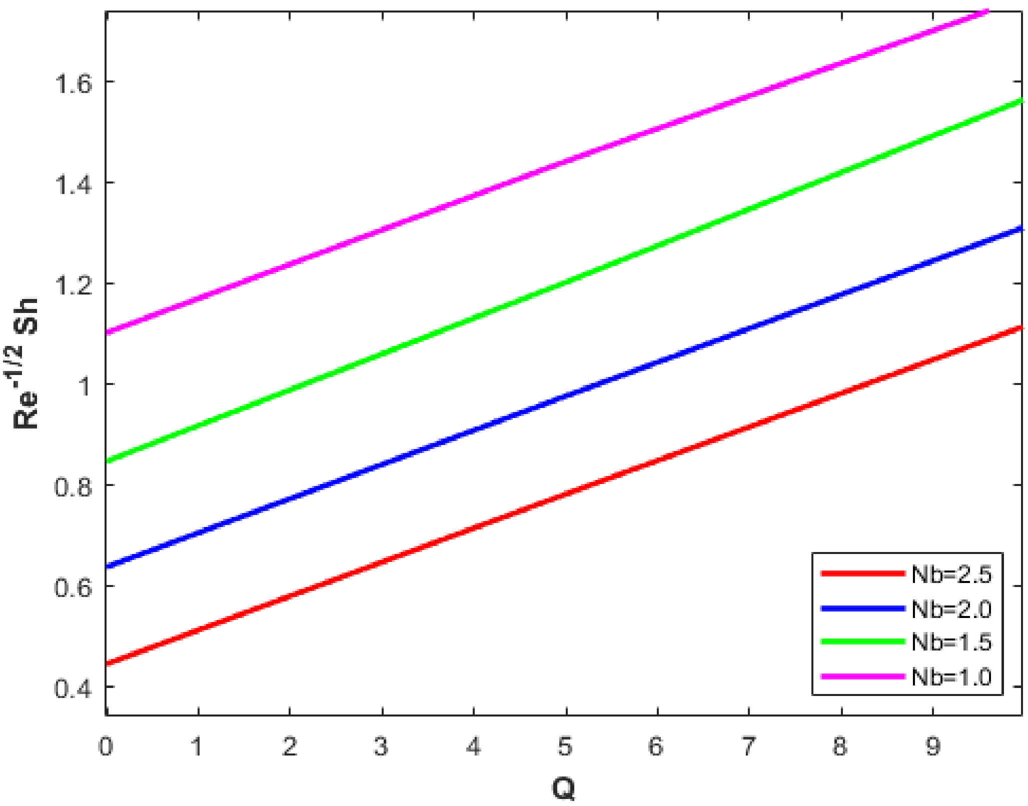

FIGURE 6.25: Effect of Q and Nb on $Re^{-\frac{1}{2}}\ Sh$ when $K = \sigma_a = We = n = A = Q = \alpha = \Gamma = \sigma_b = Sc = 0.1, \beta = Nt = Nb = B_{i1} = B_{i2} = 0.5, \quad M = Rd = Pr = \gamma = Gc = 1, \quad Gr = 2$

Chapter 7

Conclusion and Future Work

7.1 Conclusion

This dissertation thoroughly investigates the numerical analysis of the magnetohydrodynamic flow near a stagnation point over a stretching sheet by incorporating Casson and Carreau nanofluids. Irrespective of the choice of the nanofluid considered, in every study the effects of thermal radiation,inclined magnetic field, heat generation and absorption, Brownian motion and thermophoresis in the light of Cattaneo-Christov heat flux model. The conversion of non-linear partial differential equations describing the proposed flow problem into a set of ordinary differential equations is achieved through the use of appropriate similarity transformations. The numerical solution is obtained using the shooting method. The influence of significant flow parameters on the dimensionless velocity, temperature, and concentration profiles is demonstrated in both tabular and graphical representations. Furthermore, the numerical results showing the magnitude of Skin-friction coefficient, Nusselt and Sherwood numbers have been presented in via graphs and tables. The combined conclusions drawn from the numerical findings of each study are summarized as follows.

- An escalation in the magnitude of the thermal thermal Grashof number leads to the escalation in the mass transfer rate whereas an unlike trend has been seen for the heat transfer rate.

- The temperature cools down whereas the concentration increases by assuming the higher values of the Prandtl number.

- It has been noted that the higher the radiation parameter, the greater the concentration of the fluid.

- For the higher values of the solutal Grashof number, the magnitude of skin-friction coefficient and Sherwood numbers augments significantly.

- A rise in the temperature is noticed for the larger values of the heat generation parameter.

- The velocity profile and the skin-friction coefficient show an increasing behavior by escalating the Casson parameter.

- The thermopherosis parameter escalates the heat transfer for Carreau nanofluid by 29.7% whereas upto 31.03% is observed for the Casson nanofluid.

- The rise in the values of the permeability parameter calls forth a diminution in the heat transfer rate.

- The elevated values of chemical reaction parameter give rise to an increment in the magnitude of Nusselt and Sherwood numbers.

- The higher the Brownian motion parameter, the lesser the nanoparticle volume fraction of the fluid.

- The temperature as well as velocity increase significantly by taking into consideration the higher values of the Eckert number.

- For the Casson-Carreau nanofluids, the skin friction coefficient has an inverse relation with the Prandtl number, Schmidt number, Weissenberg number and Brownian motion parameter. However, an opposite behaviour has been sighted by taking into account the thermophoresis parameter.

- As the magnitude of the Weissenberg number heightens, the concentration distribution suddenly falls down.

- The magnetic parameter reduces the velocity while an inverse pattern is noted for the thermal and concentration fields.

- For the Casson fluid, an increased value of the Casson parameter enhances the velocity, temperature, and concentration contributions.

- The chemical reaction parameter amplifies the rate of mass transfer by 31.4% in the Carreau nanofluid, while an improvement reaching 34.06% is recorded in the Casson nanofluid.

Figure 7.1 demonstrates how the skin-friction coefficient, responds to changes in the rheological properties of non-Newtonian fluids governed by the Carreau and Casson models. As seen from the figure, an increase in the Casson parameter results in a reduction of the skin-friction coefficient. This behavior arises because the higher Casson parameter tends to make the fluid behave more like a Newtonian fluid, thereby reducing resistance and allowing smoother flow. Conversely, an increase in the effects of Carreau nanofluids leads to a rise in the skin-friction coefficient, particularly when the fluid retains some characteristics of a Casson nanofluid.

Figure 7.2 illustrates the effect of Casson and Carreau fluids on convective heat transfer. It is noteworthy that the presence of these non-Newtonian fluids contributes to a significant enhancement in heat transfer performance.w

The influence of the mass transfer rate, considering the combined effects of Casson and Carreau fluids, is illustrated in Figure 7.3. It can be observed from the figure that an increase in the parameters associated with Casson and Carreau fluids leads to a decrease in the magnitude of the Sherwood number, thereby indicating a reduction in the mass transfer rate.

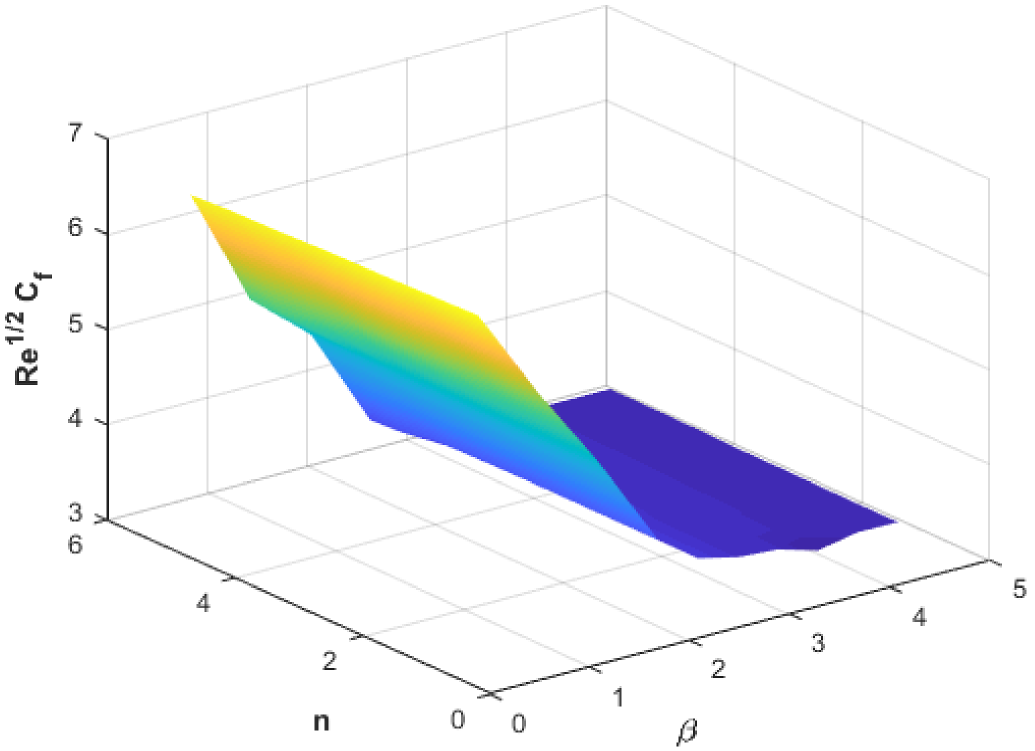

FIGURE 7.1: Effect of n and β on $Re^1/2C_f$ when $K = \omega = \delta = We = n = A = Q = Ec = \alpha = \Gamma = \chi = Sc = 0.1,\ Nt = Nb = 0.5,\ M = Pr = \gamma = Gc = 1,\ Gr = 2,\ \lambda = -1,\ S = 0.2$

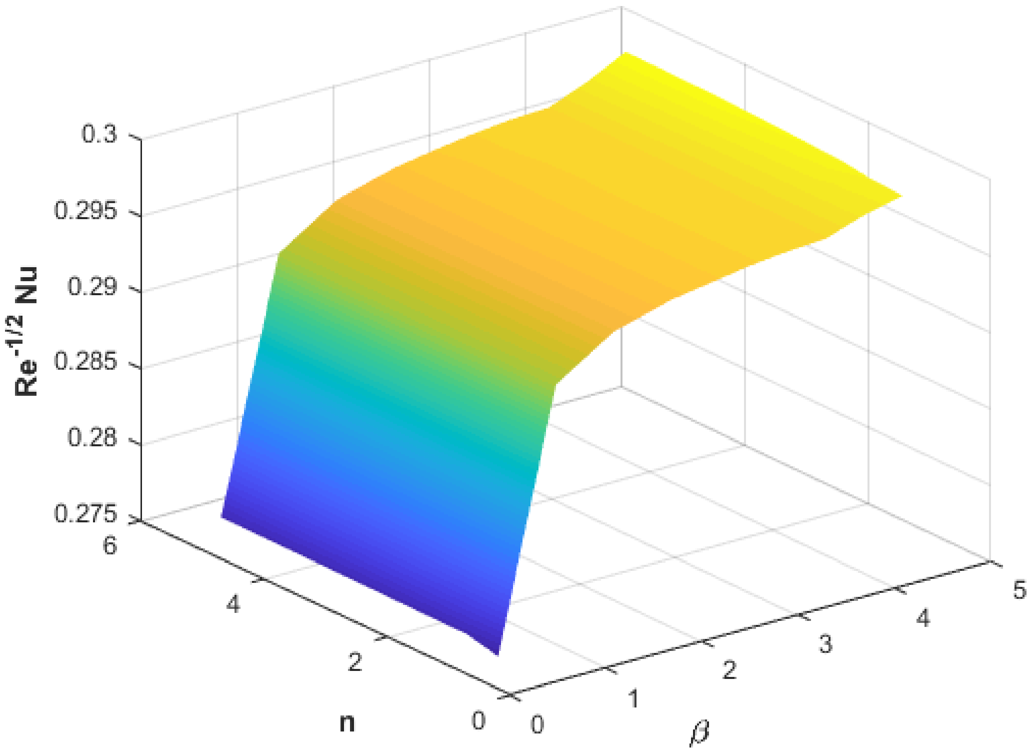

FIGURE 7.2: Effect of n and β on $Re^-1/2Nu$ when $K = \omega = \delta = We = n = A = Q = Ec = \alpha = \Gamma = \chi = Sc = 0.1,\ Nt = Nb = 0.5,\ M = Pr = \gamma = Gc = 1,\ Gr = 2,\ \lambda = -1,\ S = 0.2$

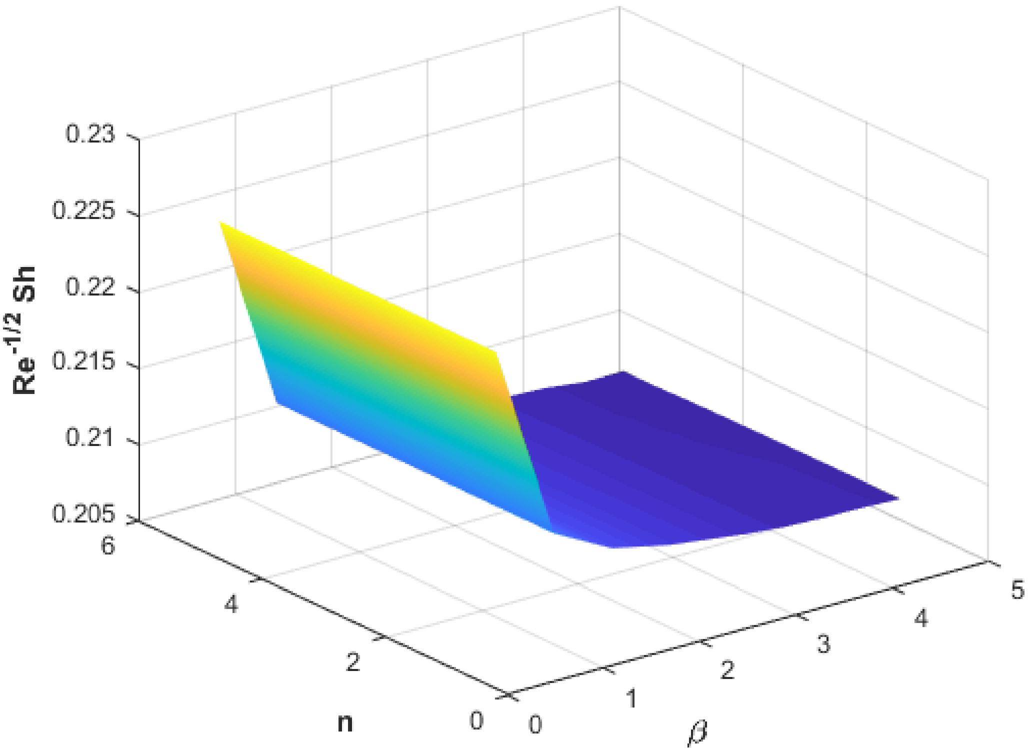

FIGURE 7.3: Effect of n and β on $Re^{-}1/2Sh$ when $K = \omega = \delta = We = n = A = Q = Ec = \alpha = \Gamma = \chi = Sc = 0.1,\ Nt = Nb = 0.5,\ M = Pr = \gamma = Gc = 1,\ Gr = 2,\ \lambda = -1,\ S = 0.2$

7.2 Future Work

The study of fluids provides an understanding of several everyday phenomena. The industrial significance of the Newtonian and non-Newtonian fluid models is discussed in the Introduction. In this dissertation, the primary objective is to shed light on the characteristics of Newtonian and non-Newtonian models with different physical effects. The presented study opens up several avenues for further exploration and can be extended in the following ways.

- The present study focuses on the exploration of the characteristics and heat and mass transfer of Casson and Carreau nanofluids. Different fluid models like Maxwell fluid model, hybrid fluid, Williamson fluid, hyperbolic tangent fluid, Jeffery fluid can also be incorporated to study the flow properties.

- The effects of Brownian motion, thermopherosis, heat generation/absorption and inclined magnetic field are studied in detail using the Casson and Careau nanofluids. Moreover, the impact of viscous dissipation, Hall effects, Joule heating and Soret and Dufour effects can also be taken into account.

- For examining the flow properties and the heat and mass transfer, the MHD flow near stagnation point using the Casson and Carreau nanofluids past a stretching sheet has been taken into account. In addition to this, radially, non- linearly or exponentially stretching sheet can also be considered.

- The flow characteristics and heat and mass transfer rates can be studied using the circular cylinder, wedge, microtubes and microchannels. Moreover, porous plate can also be utilized.

Bibliography

[1] E. Brujan, *Cavitation in Non-Newtonian fluids: with bio-medical and bio-engineering applications.* Springer Science & Business Media, 2010.

[2] P. Chaturani and R. P. Samy, "Pulsatile flow of Casson's fluid through stenosed arteries with applications to blood flow," *Biorheology*, vol. **23**, no. 5, pp. 499–511, 1986.

[3] V. Srivastava and M. Saxena, "Two-layered model of Casson fluid flow through stenotic blood vessels: applications to the cardiovascular system," *Journal of Biomechanics*, vol. **27**, no. 7, pp. 921–928, 1994.

[4] N. S. Akbar, "Influence of magnetic field on peristaltic flow of a Casson fluid in an asymmetric channel: application in crude oil refinement," *Journal of Magnetism and Magnetic Materials*, vol. **378**, pp. 463–468, 2015.

[5] K. A. Kumar, V. Sugunamma, and N. Sandeep, "Effect of thermal radiation on MHD Casson fluid flow over an exponentially stretching curved sheet," *Journal of Thermal Analysis and Calorimetry*, vol. 140, pp. 2377–2385, 2020.

[6] V. K. Verma and S. Mondal, "A brief review of numerical methods for heat and mass transfer of Casson fluids," *Partial Differential Equations in Applied Mathematics*, vol. 3, p. 100034, 2021.

[7] K. A. Khan, F. Jamil, J. Ali, I. Khan, N. Ahmed, M. Andualem, and M. Rafiq, "Analytical simulation of heat and mass transmission in Casson fluid flow across a stretching surface," *Mathematical Problems in Engineering*, vol. 2022, pp. 1–11, 2022.

[8] S. A. Lone, A. Anwar, S.and Saeed, and G. Bognár, "A stratified flow of a non-Newtonian Casson fluid comprising microorganisms on a stretching sheet with activation energy," *Scientific Reports*, vol. 13, no. 1, p. 11240, 2023.

[9] N. M. Hafez, A. M. Abd-Alla, and T. M. N. Metwaly, "Influences of rotation and mass and heat transfer on MHD peristaltic transport of Casson fluid through inclined plane," *Alexandria Engineering Journal*, vol. 68, pp. 665–692, 2023.

[10] R. Leelavathi, S. L. Vyakaranam, T. S. Rao, V. R. R. Gurrampati, and A. S. Oke, "MHD Casson fluid flow in stagnation point over an inclined porous surface," *CFD Letters*, vol. 16, no. 4, pp. 69–84, 2024.

[11] Q. Khan, M. Farooq, and S. Ahmad, "Generalized transport analysis on mixed convection squeeze flow of a Casson fluid over an inclined stretching sheet with viscous dissipation and double stratification," *Ain Shams Engineering Journal*, vol. 15, no. 1, p. 102253, 2024.

[12] A. M. Mohamad, D. Yadav, M. K. Awasthi, R. Ragoju, K. Bhattacharyya, and A. Mahajan, "Analytical and numerical examinations on the stability investigation of Casson nanofluid flow in a permeable layer controlled by vertical throughflow," *World Journal of Engineering*, 2024.

[13] M. A. Basit, M. Imran, A. Akgül, M. K. Hassani, and A. Alhushaybari, "Mathematical analysis of heat and mass transfer efficiency of bio-convective Casson nanofluid flow through conical gap among the rotating surfaces under the influences of thermal radiation and activation energy," *Results in Physics*, vol. 63, p. 107863, 2024.

[14] B. S. Bhadauria, A. Kumar, S. K. Rawat, M. Yaseen *et al.*, "Thermal instability of tri-hybrid Casson nanofluid with thermal radiation saturated porous medium in different enclosures," *Chinese Journal of Physics*, vol. 87, pp. 710–727, 2024.

[15] M. D. Shamshuddin, K. K. Asogwa, and M. J. N. H. T. Ferdows, "Thermo-solutal migrating heat producing and radiative Casson nanofluid flow via bidirectional stretching surface in the presence of bi-lateral reactions," *Numerical Heat Transfer, Part A: Applications*, vol. 85, no. 5, pp. 719–738, 2024.

[16] W. D. Alamirew, G. Awgichew, and E. Haile, "Mixed convection flow of MHD Casson nanofluid over a vertically extending sheet with effects of Hall, ion slip and non-linear thermal radiation," *International Journal of Thermofluids*, vol. 23, p. 100762, 2024.

[17] W. A. Khan, Z. Hussain, M. Ali, W. Ahmad, and S. Almutairi, "Thermo-dynamical analysis of bioconvective chemically reactive and magnetized thermal-radiative bi-directional Casson nanofluid flow with heat-sink-source aspects," *Journal of Radiation Research and Applied Sciences*, vol. 17, no. 4, p. 101138, 2024.

[18] M. Gayatri, K. J. Reddy, and M. J. Babu, "Slip flow of Carreau fluid over a slendering stretching sheet with viscous dissipation and Joule heating," *SN Applied Sciences*, vol. 2, pp. 1–11, 2020.

[19] T. Salahuddin, M. Awais, and Z. Salleh, "A flow study of Carreau fluid near the boundary layer region of paraboloid surface with viscous dissipation and variable fluid properties," *Journal of Materials Research and Technology*, vol. 14, pp. 901–909, 2021.

[20] S. M. Hussain, B. S. Goud, P. Madheshwaran, W. Jamshed, A. A. Pasha, R. Safdar, M. Arshad, R. W. Ibrahim, and M. K. Ahmad, "Effectiveness of non-uniform heat generation (sink) and thermal characterization of a Carreau fluid flowing across a non-linear elongating cylinder: A numerical study," *ACS omega*, vol. 7, no. 29, pp. 25 309–25 320, 2022.

[21] Y. Hou, X. Feng, M. Zahid, M. A. Rana, B. Souayeh *et al.*, "Theoretical and numerical investigation of the Carreau fluid model during a non-isothermal roll coating process: a comparative study," *Case Studies in Thermal Engineering*, vol. 51, p. 103503, 2023.

[22] H. A. Nabwey, T. Shabbir, M. Mushtaq, M. Ashraf, A. M. Rashad, S. M. M. EL-Kabeir, H. A. EL-Mky, and L. F. Seddek, "Numerical study of Carreau fluid flow along an exponential curved stretching surface," *Special Topics & Reviews in Porous Media: An International Journal*, vol. 15, no. 2, 2024.

[23] F. Ullah and M. B. Ashraf, "Numerical heat transfer analysis of Carreau nanofluid flow over curved stretched surface with non-linear effects and viscous dissipation," *International Journal of Thermofluids*, vol. 24, p. 100914, 2024.

[24] S. Z. H. Shah, Z. Sabir, A. Ayub, A. Rashid, R. Sadat, and M. R. Ali, "An efficient numerical scheme for solving the melting transportation of energy with time dependent Carreau nanofluid," *South African Journal of Chemical Engineering*, vol. 47, pp. 345–356, 2024.

[25] U. Farooq, M. A. Basit, S. Noreen, N. Fatima, A. Alhushaybari, S. M. El Din, M. Imran, and A. Akgül, "Recent progress in Cattaneo-Christov heat and mass fluxes for bioconvectional Carreau nanofluid with motile microorganisms and activation energy passing through a non-linear stretching cylinder," *Ain Shams Engineering Journal*, vol. 15, no. 1, p. 102316, 2024.

[26] O. K. Koriko, K. S. Adegbie, N. A. Shah, I. L. Animasaun, and M. A. Olotu, "Numerical solutions of the partial differential equations for investigating the significance of partial slip due to lateral velocity and viscous dissipation: the case of blood-gold Carreau nanofluid and dusty fluid," *Numerical methods for partial differential equations*, vol. 40, no. 2, p. e22754, 2024.

[27] S. Bilal, I. A. Shah, M. Rashid, and I. Khan, "Impact of activation energy on carreau nanofluid flow over non-linear stretching surface," *Heliyon*, vol. 10, no. 1, 2024.

[28] J.-H. He, G. M. Moatimid, M. A. Mohamed, and K. Elagamy, "A stretching cylindrical Carreau nanofluid border layer movement with motile microorganisms and variable thermal characteristics," *International Journal of Modern Physics B*, vol. 38, no. 17, p. 2450223, 2024.

[29] B. Ali, G. Rasool, S. Hussain, D. Baleanu, and S. Bano, “Finite element study of MHD and activation energy in Darcy-Forchheimer rotating flow of Casson-Carreau nanofluid,” *Processes*, vol. 8, no. 9, p. 1185, 2020.

[30] S. Shaw, A. Patra, A. Misra, M. K. Nayak, and A. J. Chamkha, “A numerical approach to the modeling of Thomson and Troian slip on non-linear radiative microrotation of Casson-Carreau nanomaterials in MHD,” *Journal of Nanofluids*, vol. 10, no. 3, pp. 305–315, 2021.

[31] K. V. Reddy, G. V. R. Reddy, and A. J. Chamkha, “Effects of viscous dissipation and thermal radiation on an electrically conducting Casson-Carreau nanofluids flow with Cattaneo-Christov heat flux model,” *Journal of Nanofluids*, vol. 11, no. 2, pp. 214–226, 2022.

[32] G. M. Sobamowo, S. A. Oladosu, and R. O. Kuku, “Computational analysis of MHD flow behaviour and heat transfer characteristics of dissipative Casson-Carreau nanofluid over a stretching sheet with internal heat generation,” *Journal of Complex Flow*, vol. 5, no. 2, pp. 25–33, 2023.

[33] V. Seethamahalakshmi, L. Rekapalli, T. S. Rao, P. N. Santoshi, G. V. R. Reddy, and A. S. Oke, “MHD slip flow of upper-convected Casson and Maxwell nanofluid over a porous stretched sheet: Impacts of heat and mass transfer,” *CFD Letters*, vol. 16, no. 3, pp. 96–111, 2024.

[34] M. Saleem and M. Hussain, “Numerical comparison of non-linear thermal radiation and chemically reactive bio-convection flow of Casson-Carreau nanoliquid with gyro-tactic microorganisms: Lie group theoretic approach,” *Heliyon*, 2024.

[35] F. Almeida, P. Kumar, A. R. Ajaykumar, and B. Nagaraja, “Implementation of artificial neural network using levenberg marquardt algorithm for Casson–Carreau nanofluid flow over exponentially stretching curved surface,” *Neural Computing and Applications*, vol. 36, no. 31, pp. 19 393–19 415, 2024.

[36] Faisal, A. R., and N. A. Shah, "Dynamic simulation of unsteady Casson–Carreau fluid flow considering temperature-dependent variable-properties and thermo-solutal mixed convection over flat and slendering sheets," *Numerical Heat Transfer, Part A: Applications*, pp. 1–21, 2024.

[37] N. Sandeep, P. Nanda, C. Sulochana, and G. P. Ashwinkumar, "Dynamics of Casson/Carreau hybrid nanofluid flow over a wedge with thermophoresis and Brownian motion effects," *International Journal of Modelling and Simulation*, pp. 1–12, 2024.

[38] J. B. J. Fourier, "Théorie analytique de la chaleur, cambridge library collection(2009)," 1822.

[39] C. Cattaneo, "Sulla conduzione del calore," *Atti Sem. Mat. Fis. Univ. Modena*, vol. **3**, pp. 83–101, 1948.

[40] C. I. Christov, "On frame indifferent formulation of the Maxwell-Cattaneo model of finite-speed heat conduction," *Mechanics Research Communications*, vol. **36**, no. 4, pp. 481–486, 2009.

[41] U. Nazir, S. Saleem, M. Nawaz, M. A. Sadiq, and A. A. Alderremy, "Study of transport phenomenon in Carreau fluid using Cattaneo–Christov heat flux model with temperature dependent diffusion coefficients," *Physica A: Statistical Mechanics and its Applications*, vol. 554, p. 123921, 2020.

[42] R. J. P. Gowda, R. N. Kumar, R. Kumar, and B. C. Prasannakumara, "3D coupled flow and heat transfer in non-Newtonian magnetic nanofluid: An application of Cattaneo-Christov heat flux model," *Journal of Magnetism and Magnetic Materials*, vol. 567, p. 170329, 2023.

[43] N. Fatima, A. Majeed, N. Ijaz, R. Ghodhbani, and N. Saleem, "Thermal performance of Cattaneo-Christov heat flux model on 3-D micropolar fluid with motile microbes across a permeable surface," *BioNanoScience*, vol. 14, no. 3, pp. 2419–2434, 2024.

[44] F. Shah, D. Zhang, and G. Linlin, "Non-similar analysis of two-phase hybrid nano-fluid flow with Cattaneo-Christov heat flux model: a computational study," *Engineering Applications of Computational Fluid Mechanics*, vol. 18, no. 1, p. 2380800, 2024.

[45] M. Gentile and B. Straughan, "Thermal convection with a Cattaneo heat flux model," *Proceedings of the Royal Society A*, vol. 480, no. 2282, p. 20230771, 2024.

[46] T. Oreyeni, A. O. Akindele, A. M. Obalalu, S. O. Salawu, and K. Ramesh, "Thermal performance of radiative MHD Oldroyd-B hybrid nanofluid with Cattaneo–Christov heat flux model: Solar-powered ship application," *Numerical Heat Transfer, Part A: Applications*, vol. 85, no. 12, pp. 1954–1972, 2024.

[47] N. Muhammad, S. Nadeem, U. Khan, E. S. M. Sherif, and A. Issakhov, "Insight into the significance of Richardson number on two-phase flow of ethylene glycol-silver nanofluid due to Cattaneo-Christov heat flux," *Waves in Random and Complex Media*, vol. 34, no. 6, pp. 5624–5642, 2024.

[48] R. Ullah, M. I. U. Rehman, A. Hamid, S. Arooj, and W. A. Khan, "Heat and mass transport aspect on magnetised Jeffery fluid flow over a stretching cylinder with the Cattaneo–Christov heat flux model," *Molecular Physics*, vol. 122, no. 11, p. e2288701, 2024.

[49] P. Soni, K. Sharma, H. Berrehal, and K. Jat, "Effect of Cattaneo–Christov heat flux model and elastic deformation on Walters' B viscoelastic fluid flow with porosity," *International Journal of Thermofluids*, vol. 24, p. 100825, 2024.

[50] J. A. Khan, M. Mustafa, T. Hayat, and A. Alsaedi, "3D flow of nanofluid over a non-linearly stretching sheet: An application to solar energy," *International Journal of Heat and Mass Transfer*, vol. 86, pp. 158–164, 2015.

[51] L. J. Crane, "Flow past a stretching plate," *Zeitschrift für Angewandte Mathematik und Physik ZAMP*, vol. 21, no. 4, pp. 645–647, 1970.

[52] M. Qayyum, T. Abbas, S. Afzal, S. T. Saeed, A. Akgül, M. Inc, K. H. Mahmoud, and A. S. Alsubaie, “Heat transfer analysis of unsteady MHD Carreau fluid flow over a stretching/shrinking sheet,” *Coatings*, vol. 12, no. 11, p. 1661, 2022.

[53] R. Kumar, S. Khan, D. Kumar *et al.*, “Heat and mass transfer on 3D radiative MHD Casson fluid flow over a stretching permeable sheet with chemical reaction and heat source/sink.” *Journal of Computational Analysis & Applications*, vol. 33, no. 1, 2024.

[54] M. Alammari, “Numerical framework of magnetized thermal Casson nanoliquid flow with time-dependent stretching channel enclosing chemical reaction effect and variable fluid properties: A particle swarm optimization with stability,” *Modern Physics Letters B*, vol. 38, no. 15, p. 2450109, 2024.

[55] F. Almeida, P. K. NagarajaBasavarajappa, and A. A. Ramakrishnappa, “Irreversibility analysis of non-linear mixed convective time-based flow analysis of Casson-Williamson nanofluid accelerated by curved stretching surface,” *Computational Thermal Sciences*, vol. 16, no. 5, pp. 15–41, 2024.

[56] M. Adel, M. M. Khader, and H. Ahmad, “MHD nanofluid flow and heat transfer caused by a stretching sheet that is heated convectively: an approximate solution using ADM,” *Case Studies in Thermal Engineering*, vol. 60, p. 104683, 2024.

[57] M. Khan, T. Salahuddin, M. Awais, and B. A. Alwan, “An entropy analysis in a slip condition flow over a linear stretching sheet,” *Chinese Journal of Physics*, vol. 89, pp. 801–809, 2024.

[58] P. Agarwal, R. Jain, and K. Loganathan, “Thermally radiative flow of MHD Powell-Eyring nanofluid over an exponential stretching sheet with swimming microorganisms and viscous dissipation: A numerical computation,” *International Journal of Thermofluids*, vol. 23, p. 100773, 2024.

[59] B. Nayak, M. Panda, and S. R. Mishra, “Analysis of Brownian motion and thermophoresis effects with chemical reaction on Williamson nanofluid flow

over permeable stretching sheet," *Partial Differential Equations in Applied Mathematics*, vol. 11, p. 100908, 2024.

[60] M. Y. Ali, M. Rahman, M. M. Ali, S. F. Ahmmed, and S. Haque, "Data analysis of non-linear radiative electro-periodic mhd flow past a stretching sheet with activation energy impact," *International Communications in Heat and Mass Transfer*, vol. 155, p. 107572, 2024.

[61] Y. A. Cengel and J. M. Cimbala, "Fluid mechanics," p. 931, 2006.

[62] S. Molokov, R. Moreau, and H. K. Moffatt, "Magnetohydrodynamics, historical evolution and trends," *Book*, p. p 407, 2006.

[63] J. Kunes., "Dimensionless physical quantities in science and engineering," *Book*, p. p 441, 2012.

[64] G. K. Ramesh, B. J. Gireesha, A. Shehzad, S, and F. M. Abbasi, "Analysis of heat transfer phenomenon in MHD Casson fluid flow through Cattaneo-Christov heat diffusion theory," *Communications in Theoretical Physics*, vol. 68, no. 1, p. 91, 2017.

[65] J. Raza, "Thermal radiation and slip effects on MHD stagnation point flow of Casson fluid over a convective stretching sheet," *Propulsion and Power Research*, vol. 8, no. 2, pp. 138–146, 2019.

[66] A. Asghar, A. F. Chandio, Z. Shah, N. Vrinceanu, W. Deebani, M. Shutaywi, and L. A. Lund, "Magnetized mixed convection hybrid nanofluid with effect of heat generation/absorption and velocity slip condition," *Heliyon*, vol. 9, no. 2, 2023.

[67] W. A. Khan and I. Pop, "Boundary layer flow of a nanofluid past a stretching sheet," *International journal of heat and mass transfer*, vol. 53, no. 11-12, pp. 2477–2483, 2010.

[68] S. Arulmozhi, K. Sukkiramathi, S. S. Santra, R. Edwan, U. F. Gamiz, and S. Noeiaghdam, "Heat and mass transfer analysis of radiative and chemical

reactive effects on MHD nanofluid over an infinite moving vertical plate," *Results in Engineering*, vol. 14, p. 100394, 2022.

[69] J. V. Tawade, C. N. Guled, S. Noeiaghdam, U. F. Gamiz, V. Govindan, and S. Balamuralitharan, "Effects of thermophoresis and Brownian motion for thermal and chemically reacting Casson nanofluid flow over a linearly stretching sheet," *Results in Engineering*, vol. 15, p. 100448, 2022.

[70] H. Sardar, L. Ahmad, M. Khan, and A. S. Alshomrani, "Investigation of mixed convection flow of Carreau nanofluid over a wedge in the presence of Soret and Dufour effects," *International Journal of Heat and Mass Transfer*, vol. 137, pp. 809–822, 2019.

[71] M. Irfan, M. S. Anwar, I. Kebail, and W. A. Khan, "Thermal study on the performance of Joule heating and Sour-Dufour influence on non-linear mixed convection radiative flow of Carreau nanofluid," *Tribology International*, vol. 188, p. 108789, 2023.

[72] K. K. Ganesh, G. K. Ramesh, B. J. Gireesha, and A. M. Rashad, "On stretched magnetic flow of Carreau nanofluid with slip effects and non-linear thermal radiation," *Non-linear Engineering*, vol. 8, no. 1, pp. 340–349, 2019.

[73] R. Cortell, "A note on MHD flow of a power-law fluid over a stretching sheet," *Applied Mathematics and Computation*, vol. 168, no. 1, pp. 557–566, 2005.

[74] P. N. Santoshi, G. V. R. Reddy, and P. Padma, "Numerical scrutinization of three dimensional Casson-Carreau nanofluid flow," *Journal of Applied and Computational Mechanics*, vol. 6, no. 3, pp. 531–542, 2020.

[75] A. Fatima, M. Sagheer, and S. Hussain, "A study of inclined magnetically driven Casson nanofluid using the Cattaneo-Christov heat flux model with multiple slips towards a chemically reacting radially stretching sheet," *Journal of Central South University*, vol. 30, no. 11, pp. 3721–3736, 2023.

[76] S. Nadeem, R. U. Haq, N. S. Akbar, and Z. H. Khan, "MHD three-dimensional Casson fluid flow past a porous linearly stretching sheet," *Alexandria Engineering Journal*, vol. 52, no. 4, pp. 577–582, 2013.

[77] M. Sohail, U. Ali, F. T. Zohra, W. Al-Kouz, Y. M. Chu, and P. Thounthong, "Utilization of updated version of heat flux model for the radiative flow of a non-Newtonian material under Joul heating: OHAM application," *Open Physics*, vol. **19**, no. 1, pp. 100–110, 2021.